frontiers | Research Topics

Machine learning and deep learning applications in pathogenic microbiome research

Edited by
Gang Ye, Ujjal Bhawal, Jianguo Tang and Wenle Li

Published in
Frontiers in Cellular and Infection Microbiology

ISSN 1664-8714
ISBN 978-2-8325-4956-8
DOI 10.3389/978-2-8325-4956-8

About Frontiers

Frontiers is more than just an open access publisher of scholarly articles: it is a pioneering approach to the world of academia, radically improving the way scholarly research is managed. The grand vision of Frontiers is a world where all people have an equal opportunity to seek, share and generate knowledge. Frontiers provides immediate and permanent online open access to all its publications, but this alone is not enough to realize our grand goals.

Frontiers journal series

The Frontiers journal series is a multi-tier and interdisciplinary set of open-access, online journals, promising a paradigm shift from the current review, selection and dissemination processes in academic publishing. All Frontiers journals are driven by researchers for researchers; therefore, they constitute a service to the scholarly community. At the same time, the *Frontiers journal series* operates on a revolutionary invention, the tiered publishing system, initially addressing specific communities of scholars, and gradually climbing up to broader public understanding, thus serving the interests of the lay society, too.

Dedication to quality

Each Frontiers article is a landmark of the highest quality, thanks to genuinely collaborative interactions between authors and review editors, who include some of the world's best academicians. Research must be certified by peers before entering a stream of knowledge that may eventually reach the public - and shape society; therefore, Frontiers only applies the most rigorous and unbiased reviews. Frontiers revolutionizes research publishing by freely delivering the most outstanding research, evaluated with no bias from both the academic and social point of view. By applying the most advanced information technologies, Frontiers is catapulting scholarly publishing into a new generation.

What are Frontiers Research Topics?

Frontiers Research Topics are very popular trademarks of the *Frontiers journals series*: they are collections of at least ten articles, all centered on a particular subject. With their unique mix of varied contributions from Original Research to Review Articles, Frontiers Research Topics unify the most influential researchers, the latest key findings and historical advances in a hot research area.

Find out more on how to host your own Frontiers Research Topic or contribute to one as an author by contacting the Frontiers editorial office: frontiersin.org/about/contact

Machine learning and deep learning applications in pathogenic microbiome research

Topic editors

Gang Ye — Sichuan Agricultural University, China
Ujjal Bhawal — Nihon University, Japan
Jianguo Tang — Fudan University, China
Wenle Li — Xiamen University, China

Citation

Ye, G., Bhawal, U., Tang, J., Li, W., eds. (2024). *Machine learning and deep learning applications in pathogenic microbiome research*. Lausanne: Frontiers Media SA. doi: 10.3389/978-2-8325-4956-8

Table of contents

05 Editorial: Machine learning and deep learning applications in pathogenic microbiome research
An-Tian Chen, Xinyan Wu, Gang Ye and Wenle Li

08 Alteration and clinical potential in gut microbiota in patients with cerebral small vessel disease
Yachen Shi, En Zhao, Lei Li, Songyun Zhao, Haixia Mao, Jingyu Deng, Wei Ji, Yang Li, Qianqian Gao, Siyuan Zeng, Lin Ma, Guangjun Xi, Yiping You, Junfei Shao, Xiangming Fang and Feng Wang

21 Gut microbiota landscape and potential biomarker identification in female patients with systemic lupus erythematosus using machine learning
Wenzhu Song, Feng Wu, Yan Yan, Yaheng Li, Qian Wang, Xueli Hu and Yafeng Li

34 The effect and mechanism of Fushen Granule on gut microbiome in the prevention and treatment of chronic renal failure
Lin Wang, Ao Xu, Jinxiang Wang, Guorong Fan, Ruiqi Liu, Lijuan Wei and Ming Pei

54 Gut microbiome-based noninvasive diagnostic model to predict acute coronary syndromes
Jincheng Wang, Zhao Hu, Qiuyue Xu, Yunke Shi, Xingyu Cao, Yiming Ma, Mingqiang Wang, Chaoyue Zhang, Xiang Luo, Fanru Lin, Xianbin Li, Yong Duan and Hongyan Cai

71 Construction and validation of a machine learning model for the diagnosis of juvenile idiopathic arthritis based on fecal microbiota
Jun-Bo Tu, Wei-Jie Liao, Si-Ping Long, Meng-Pan Li and Xing-Hua Gao

81 Exploring blood lipids-immunity associations following HBV vaccination: evidence from a large cross-sectional study
Qian Yang, Benhua Li, Tiankuo Luan, Xiaoyu Wang, Bixia Duan, Chengcheng Wei and Shi Chen

92 Exploring the impact of pathogenic microbiome in orthopedic diseases: machine learning and deep learning approaches
Zhuce Shao, Huanshen Gao, Benlong Wang and Shenqi Zhang

100 Comprehensive assessment of HF-rTMS treatment mechanism for post-stroke dysphagia in rats by integration of fecal metabolomics and 16S rRNA sequencing
Fei Zhao, Jiemei Chen, Yilong Shan, Jiena Hong, Qiuping Ye, Yong Dai, Jiahui Hu, Jiantao Zhang, Chao Li and Hongmei Wen

115 Integrating machine learning algorithms and single-cell analysis to identify gut microbiota-related macrophage biomarkers in atherosclerotic plaques
Yin Ke, Jian Yue, Jiaming He and Guojing Liu

127 The impact of Sangju Qingjie Decoction on the pulmonary microbiota in the prevention and treatment of chronic obstructive pulmonary disease
Zheng Liu, Ying Huang, Chao Hu and Xiang Liu

137 Comparative characterization of supragingival plaque microbiomes in malocclusion adult female patients undergoing orthodontic treatment with removable aligners or fixed appliances: a descriptive cross-sectional study
Jiajia Zheng, Xiujing Wang, Ting Zhang, Jiuhui Jiang and Jiaqi Wu

149 Traditional Chinese herbal formulas modulate gut microbiome and improve insomnia in patients with distinct syndrome types: insights from an interventional clinical study
Huimei Zeng, Jia Xu, Liming Zheng, Zhi Zhan, Zenan Fang, Yunxi Li, Chunyi Zhao, Rong Xiao, Zhuanfang Zheng, Yan Li and Lingling Yang

frontiers | Frontiers in Cellular and Infection Microbiology

TYPE Editorial
PUBLISHED 20 June 2024
DOI 10.3389/fcimb.2024.1429197

OPEN ACCESS

EDITED AND REVIEWED BY
Shira Lynn Broschat,
Washington State University, United States

*CORRESPONDENCE
Wenle Li
drlee0910@163.com

RECEIVED 07 May 2024
ACCEPTED 10 June 2024
PUBLISHED 20 June 2024

CITATION
Chen AT, Wu X, Ye G and Li W (2024) Editorial: Machine learning and deep learning applications in pathogenic microbiome research.
Front. Cell. Infect. Microbiol. 14:1429197.
doi: 10.3389/fcimb.2024.1429197

Editorial: Machine learning and deep learning applications in pathogenic microbiome research

An-Tian Chen[1,2], Xinyan Wu[3], Gang Ye[3] and Wenle Li[4]*

[1]Department of Cardiology, State Key Laboratory of Cardiovascular Disease, Fuwai Hospital, Chinese Academy of Medical Sciences & Peking Union Medical College/National Center for Cardiovascular Diseases, Beijing, China, [2]Department of Computer Science, College of Natural Sciences, The University of Texas at Austin, Austin, TX, United States, [3]College of Veterinary Medicine, Sichuan Agricultural University, Chengdu, China, [4]State Key Laboratory of Molecular Vaccinology and Molecular Diagnostics & Center for Molecular Imaging and Translational Medicine, School of Public Health, Xiamen University, Xiamen, China

KEYWORDS

machine learning, application, predictive model, pathogenic microbiome, gut microbiota

Editorial on the Research Topic
Machine learning and deep learning applications in pathogenic microbiome research

Artificial intelligence has established a solid basis for deep learning (DL), especially with the introduction of the Transformer architecture, which has gained much attention from researchers in multiple disciplines. Machine learning (ML) and DL, branches of artificial intelligence, have increasingly transformed research in various fields. One area notably impacted is microbiology (Obermeyer and Emanuel, 2016). In particular, the complexity and diversity of microbiomes and infectious diseases make them ideal candidates for novel ML and DL techniques.

In this Research Topic, titled "*Machine Learning and Deep Learning Applications in Pathogenic Microbiome Research*", we have gathered a collection of 11 manuscripts that embody the application of ML and DL in the research field of pathogenic microbiomes. These collected manuscripts are mostly original articles that provide an understanding of how ML and DL can be used to further insights into research on pathogenic microbiomes. Currently, ML is widely used in the development of predictive models (Collins and Moon, 2019). By integrating ML or DL approaches with predictive models, the manuscripts in this Research Topic highlight the importance of interdisciplinary integration in understanding diseases associated with pathogenic microbiomes and promoting better health and the well-being of both humans and ecosystems.

In this Research Topic, Shao et al. dive into the complex interactions between pathogenic microorganisms and various orthopedic conditions in the mini-review "*Exploring the impact of pathogenic microbiome in orthopedic diseases: machine learning and deep learning approaches*". By analyzing datasets on microbiota and the interactions with the host, they highlight how ML and DL can enhance the understanding, diagnosis, and treatment of diseases such as osteoporosis and arthritis.

Gut microbiota impact human health and disease (Lynch and Pedersen, 2016). By utilizing ML and DL, relationships between microbiota and diseases can be established and understood, enhancing overall health and contributing to the management of diseases. In their manuscript entitled "*Gut microbiota landscape and potential biomarker identification in female patients with systemic lupus erythematosus using machine learning*", Song et al. explore the relationship between gut microbiota and the autoimmune disease systemic lupus erythematosus (SLE) and aim to identify biomarkers for SLE by analyzing the gut microbiota in female patients using machine learning techniques. The article "*Gut microbiome-based noninvasive diagnostic model to predict acute coronary syndromes*" presents a study by Wang et al. on the potential of using a gut microbiome profile as a noninvasive diagnostic tool for acute coronary syndromes. "*Construction and validation of a machine learning model for the diagnosis of juvenile idiopathic arthritis based on fecal microbiota*", by Tu et al., discusses the use of fecal microbiome profiling in developing a diagnostic tool for juvenile idiopathic arthritis, leading to development of the XGBoost model.

Chronic diseases are also closely linked to gut microbiota. The article by Wang et al., "*The effect and mechanism of Fushen Granule on gut microbiome in the prevention and treatment of chronic renal failure*", examines the impact of Fushen Granule, a Traditional Chinese Medicine (TCM), on the gut microbiome and its therapeutic effects on chronic renal failure. For further study concerning TCM, Zeng et al. discuss the impacts of two Chinese herbal formulas on insomnia treatment via gut microbiome modulation in their research paper "*Traditional Chinese herbal formulas modulate gut microbiome and improve insomnia in patients with distinct syndrome types: insights from an interventional clinical study*", enhancing our understanding of the gut-brain axis and supporting strategies for using TCM for insomnia. The study, "*Alteration and clinical potential in gut microbiota in patients with cerebral small vessel Disease*", by Shi et al. examines changes in the gut microbiota of patients with cerebral small vessel disease and the potential clinical implications.

Apart from gut microbiota, microbiomes located in other parts of the body can also impact health. "*The impact of Sangju Qingjie Decoction on the pulmonary microbiota in the prevention and treatment of chronic obstructive pulmonary disease*" by Liu et al. examines the effects of Sangju Qingjie Decoction (SJQJD) on the pulmonary microbiota of COPD rats, finding that SJQJD improves lung structure, reduces inflammation, and enhances the diversity and abundance of lung microbiota. The study by Zheng et al. titled "*Comparative characterization of supragingival plaque microbiomes in malocclusion adult female patients undergoing orthodontic treatment with removable aligners or fixed appliances: a descriptive cross-sectional study*" investigates the effects of different orthodontic appliances on the oral microbiome. The study found that fixed appliances are associated with increased anaerobic and Gram-negative bacteria compared to clear aligners and could lead to the development of better cleaning techniques and materials. The authors emphasized the need for tailored oral hygiene practices for individuals undergoing orthodontic treatment.

In addition to studies related to human health, the collection of papers in this Research Topic includes content on animal experiments and single-cell analysis. In the original article, "*Comprehensive assessment of HF-rTMS treatment mechanism for post-stroke dysphagia in rats by integration of fecal metabolomics and 16S rRNA sequencing*", Zhao et al. explore the effects of high-frequency repetitive transcranial magnetic stimulation (HF-rTMS) on swallowing dysfunction in post-stroke rats and reveal that HF-rTMS can improve swallowing function and modify gut microbiota composition. The study titled "*Integrating machine learning algorithms and single-cell analysis to identify gut microbiota-related macrophage biomarkers in atherosclerotic plaques*" by Ke et al. focuses on identifying macrophage biomarkers linked to gut microbiota that are influential in the development of atherosclerotic plaques, combining machine learning techniques and single-cell analysis.

In conclusion, the Research Topic "*Machine Learning and Deep Learning Applications in Pathogenic Microbiome Research*" encompasses 11 valuable manuscripts that integrate ML and DL into innovative microbiome research. The Research Topic features interdisciplinary applications ranging from diagnostic models to interactions between microbiomes and various diseases, highlighting the significance of understanding and managing health through the view of microbiota. We are thankful to the editorial team and authors for their significant contributions which have been instrumental to the success of this Research Topic.

Author contributions

A-TC: Writing – original draft. XW: Writing – review & editing. GY: Writing – review & editing. WL: Writing – review & editing.

Conflict of interest

The authors declare that the research was conducted in the absence of any commercial or financial relationships that could be construed as a potential conflict of interest.

Publisher's note

References

Collins, G. S., and Moons, K. G. M. (2019). Reporting of artificial intelligence prediction models. *Lancet* 393, 1577–1579. doi: 10.1016/S0140-6736(19)30037-6

Lynch, S. V., and Pedersen, O. (2016). The human intestinal microbiome in health and disease. *N Engl. J. Med.* 375, 2369–2379. doi: 10.1056/NEJMra1600266

Obermeyer, Z., and Emanuel, E. J. (2016). Predicting the future - big data, machine learning, and clinical medicine. *N Engl. J. Med.* 375, 1216–1219. doi: 10.1056/NEJMp1606181

frontiers | Frontiers in Cellular and Infection Microbiology

TYPE Original Research
PUBLISHED 11 July 2023
DOI 10.3389/fcimb.2023.1231541

OPEN ACCESS

EDITED BY
Jianguo Tang,
Fudan University, China

REVIEWED BY
Le Kai,
The First Affiliated Hospital of Nanchang University, China
Zan Wang,
Southeast University, China

*CORRESPONDENCE
Yachen Shi
yachen_shi@163.com
Xiangming Fang
xiangming_fang@njmu.edu.cn
Feng Wang
wangfeng_njmu@163.com

†These authors have contributed equally to this work and share first authorship

RECEIVED 30 May 2023
ACCEPTED 27 June 2023
PUBLISHED 11 July 2023

CITATION
Shi Y, Zhao E, Li L, Zhao S, Mao H, Deng J, Ji W, Li Y, Gao Q, Zeng S, Ma L, Xi G, You Y, Shao J, Fang X and Wang F (2023) Alteration and clinical potential in gut microbiota in patients with cerebral small vessel disease.
Front. Cell. Infect. Microbiol. 13:1231541.
doi: 10.3389/fcimb.2023.1231541

Alteration and clinical potential in gut microbiota in patients with cerebral small vessel disease

Yachen Shi[1,2*†], En Zhao[3†], Lei Li[1,2†], Songyun Zhao[4†], Haixia Mao[5], Jingyu Deng[1,2], Wei Ji[4,6], Yang Li[1,2], Qianqian Gao[5], Siyuan Zeng[5], Lin Ma[5], Guangjun Xi[1,2], Yiping You[1,6], Junfei Shao[4], Xiangming Fang[5*] and Feng Wang[1,2*]

[1]Department of Neurology, the Affiliated Wuxi People's Hospital of Nanjing Medical University, Wuxi People's Hospital, Wuxi Medical Center, Nanjing Medical University, Wuxi, China, [2]Department of Interventional Neurology, the Affiliated Wuxi People's Hospital of Nanjing Medical University, Wuxi People's Hospital, Wuxi Medical Center, Nanjing Medical University, Wuxi, China, [3]Department of Gastroenterology, Xishan People's Hospital of Wuxi City, Wuxi, China, [4]Department of Neurosurgery, the Affiliated Wuxi People's Hospital of Nanjing Medical University, Wuxi People's Hospital, Wuxi Medical Center, Nanjing Medical University, Wuxi, China, [5]Department of Radiology, the Affiliated Wuxi People's Hospital of Nanjing Medical University, Wuxi People's Hospital, Wuxi Medical Center, Nanjing Medical University, Wuxi, China, [6]Department of Functional Neurology, the Affiliated Wuxi People's Hospital of Nanjing Medical University, Wuxi People's Hospital, Wuxi Medical Center, Nanjing Medical University, Wuxi, China

Background: Cerebral small vessel disease (CSVD) is a cluster of microvascular disorders with unclear pathological mechanisms. The microbiota-gut-brain axis is an essential regulatory mechanism between gut microbes and their host. Therefore, the compositional and functional gut microbiota alterations lead to cerebrovascular disease pathogenesis. The current study aims to determine the alteration and clinical value of the gut microbiota in CSVD patients.

Methods: Sixty-four CSVD patients and 18 matched healthy controls (HCs) were included in our study. All the participants underwent neuropsychological tests, and the multi-modal magnetic resonance imaging depicted the changes in brain structure and function. Plasma samples were collected, and the fecal samples were analyzed with 16S rRNA gene sequencing.

Results: Based on the alpha diversity analysis, the CSVD group had significantly decreased Shannon and enhanced Simpson compared to the HC group. At the genus level, there was a significant increase in the relative abundances of Parasutterella, Anaeroglobus, Megasphaera, Akkermansia, Collinsella, and Veillonella in the CSVD group. Moreover, these genera with significant differences in CSVD patients revealed significant correlations with cognitive assessments, plasma levels of the blood-brain barrier-/inflammation-related indexes, and structural/functional magnetic resonance imaging changes. Functional prediction demonstrated that lipoic acid metabolism was significantly higher in CSVD patients than HCs. Additionally, a composite biomarker depending on six gut microbiota at the genus level displayed an area under the curve of 0.834 to distinguish CSVD patients from HCs using the least absolute shrinkage and selection operator (LASSO) algorithm.

Conclusion: The evident changes in gut microbiota composition in CSVD patients were correlated with clinical features and pathological changes of CSVD. Combining these gut microbiota using the LASSO algorithm helped identify CSVD accurately.

KEYWORDS

cerebral small vessel disease, gut microbiota, cognitive function, magnetic resonance imaging, least absolute shrinkage and selection operator algorithm

Introduction

Cerebral small vessel disease (CSVD) is a prevalent neuropathological process in clinical practice and is vital in dementia, stroke, depression, and gait disturbances among elderly patients (Cannistraro et al., 2019; Markus and Erik De Leeuw, 2023). Disrupting the blood-brain barrier (BBB), neuroinflammation, and impaired neurovascular coupling can cause CSVD (Ungvari et al., 2021). However, the underlying pathogenesis remains poorly understood. Currently, the clinical diagnosis of CSVD is based on brain magnetic resonance imaging (MRI) features, such as recent small subcortical infarcts, white matter hyperintensities (WMH), lacunar infarcts (Lis), cerebral microbleeds (CMBs), and enlarged perivascular spaces (EPVS) (Chen et al., 2019b; Van Den Brink et al., 2023). Additionally, various circulating blood indexes are considered potential biomarkers to identify and reflect the pathological changes in CSVD. These include matrix metalloproteinase-9 (MMP-9) in BBB integrality (Li et al., 2022), neurofilament light in axonal injury (Qu et al., 2021), and tumor necrosis factor-alpha (TNF-α) in inflammatory response (Wan et al., 2023). Meanwhile, advanced imaging also provides new insight into CSVD pathophysiology. Resting-state functional MRI depicts the association between altered brain function in the sensorimotor and frontoparietal networks and gait disorders (Zhou et al., 2020) and the underlying mechanism of aberrant spontaneous brain activity within the default mode network, leading to cognitive decline in CSVD (Li et al., 2021).

Gut microbes can develop neuroactive compounds and regulate neuronal function, vital in gut-brain interactions (Ascher and Reinhardt, 2018; Pluta et al., 2021). The gut-brain axis is necessary for the onset and progression of cerebrovascular disease through complex signaling pathways. These involve vagus nerves within the enteric nervous system, the neuronal-glial-endothelial interactions, and activating gut inflammatory and immune cells induced by cytokines (Arya and Hu, 2018). The microbial-derived metabolites (*e.g.*, short-chain fatty acids, trimethylamines, amino acid metabolites) play an essential role in metabolic and signaling functions of BBB and brain neurons to protect from the pathology and inflammation asstociated with disease (Parker et al., 2020; Hoyles et al., 2021). However, the intestinal ecological imbalance can affect the global immune system and alter the production of neuroprotective intestinal metabolites (Huang and Xia, 2021; Nelson et al., 2021). This causes aggravation of neuroinflammation and BBB dysfunction. Previous studies have demonstrated that stroke patients have reduced gut microbiome diversity, and several microbial taxa, such as *Streptococcus*, *Lactobacillus*, *Escherichia*, *Eubacterium*, and *Roseburia*, could be risk indicators of ischemic stroke (Peh et al., 2022; Zou et al., 2022). Cai et al. recently observed that gut microbiota could up-regulate interleukin-17A production in neutrophils by activating RORγt signaling to induce CSVD occurrence (Cai et al., 2021). Cerebral autosomal dominant arteriopathy with subcortical infarcts and leukoencephalopathy also depicts significant changes in gut microbiota abundance at the genus level, and this could lead to the onset and progression of hereditary CSVD (Matsuura et al., 2019). Since these findings are in the initial stage, the underlying association of gut microbiota with CSVD should be investigated. Therefore, recognizing the implication of the gut microbiota in CSVD pathophysiology and identifying beneficial gut bacteria are crucial as early warning CSVD biomarkers.

The current study aimed to determine the gut microbiota alteration and underlying pathological mechanisms in CSVD patients. Additionally, the relationship between the clinical features of CSVD and the expression of the gut microbiota was thoroughly investigated. Meanwhile, machine learning helped build a composite biomarker depending on the gut microbiota in CSVD. The current study also assessed the diagnostic potential of the gut microbiota to identify CSVD early.

Materials and methods

Participants

64 CSVD patients were recruited from the Affiliated Wuxi People's Hospital of Nanjing Medical University, and 18 matched healthy controls (HCs) were included in the present study through community health screening. All participants were Chinese Han. Neuropsychological assessments including Mini-Mental State Examination (MMSE), and Montreal Cognitive Assessment (MoCA), and 17-Item Hamilton Depression Rating Scale (HAMD-17), were carried out on all the recruited participants. Moreover, National Institutes of Health Stroke Scale (NIHSS) was also used for evaluate the symptom of stroke. Furthermore, the multi-modal MRI including the structural MRI and functional MRI, were conducted in all the participants.

All the participants provided a written informed consent. The Ethics Committee of the Affiliated Wuxi People's Hospital of Nanjing Medical University approved the present study (approval number: KY2112).

Inclusion and exclusion criteria

The inclusion criteria for all the participants were: (1) aged 50-80 years old; (2) ≥ six years of education; and (3) no contraindication in MRI scan.

CSVD patients were diagnosed according to the established diagnostic criteria (Chen et al., 2019b) using MRI evidence of vascular changes. Participants were found as the CSVD patients with the following features: (1) total number of lacunar infarcts (Lis) were counted, and ≥ 2 Lis were considered as the presence of lacunes; (2) periventricular and deep WMH was quantified using the Fazekas scale (overall score of 3), and a score ≥ 1 was considered as displaying WMH; (3) the total number of CMBs were counted, and ≥ 1 CMBs was considered as a positive; or (4) the total number of EPVS were counted, and ≥ 10 EPVS was considered as a threshold. Additionally, all the matched HCs had not any stroke performance, as reflected by no imaging changes (Table 1).

The exclusion criteria for each participant were: (1) clinical evidence supporting cerebrovascular disorders with large intracranial vascular lesions; (2) any severe psychiatric disorders (*e.g.*, schizophrenia); (3) abuse or alcohol or drugs dependence; (4) brain trauma or other neurologic diseases (*e.g.*, Parkinson's disease); and (5) any significant medical problems (*e.g.*, tumor, significantly impaired liver or kidney functions).

Functional MRI data acquisition and preprocessing

The imaging data preprocessing was performed using the Data Processing Assistant for Resting-State functional MRI (DPARSFA 2.3) toolbox (Chao-Gan and Yu-Feng, 2010). The amplitude of low-frequency fluctuation (ALFF) estimates the local spontaneous neuronal activity (Chen et al., 2022; Shi et al., 2023a). The REST

TABLE 1 Comparison of demographic and clinical characteristics of subjects between the CSVD and HC groups.

	CSVD (n = 64)	HC (n = 18)	*P-value*
Age (years)	69.15 ± 5.73	66.17 ± 5.49	0.052*
Sex (male/female)	32/32	7/11	0.437[&]
Education years	8.83 ± 2.43	8.89 ± 2.42	0.782[#]
Hypertension (yes/no)	38/26	9/9	0.592[&]
Diabetes (yes/no)	16/48	2/16	0.335[&]
NIHSS scores	0.48 ± 0.73	0	–
MMSE scores	27.59 ± 2.20	28.67 ± 1.24	0.032[#]
MoCA scores	24.52 ± 4.27	27.00 ± 2.09	0.023[#]
HAMD-17 scores	3.48 ± 3.98	2.33 ± 3.24	0.214[#]
Plasma S100β (pg/ml)	96.25 ± 26.03	71.07 ± 27.03	0.001*
Plasma MMP-9 (ng/ml)	25.42 ± 12.04	21.41 ± 5.48	0.538[#]
Plasma NSE (ng/ml)	49.85 ± 22.41	13.70 ± 9.16	< 0.001*
Plasma TNF-α (pg/ml)	8.15 ± 2.07	6.20 ± 1.64	< 0.001*
Structural MRI features			
Periventricular WMH Fazekas scores	1.80 ± 0.67	0	–
Deep WMH Fazekas scores	0.89 ± 0.89	0	–
Total WMH Fazekas scores	2.69 ± 1.38	0	–
Number of EPVS	4.45 ± 5.37	0	–
Number of CMBs	2.84 ± 3.53	0	–
Number of Lis	10.41 ± 8.49	0	–

CSVD, cerebral small vessel disease; HC, healthy control; NIHSS, National Institutes of Health Stroke Scale; MMSE, Mini-mental State Examination; MoCA, Montreal Cognitive Assessment; HAMD-17, 17-Item Hamilton Depression Rating Scale; S100β, S100beta protein; MMP-9, matrix metalloproteinase-9; NSE, neuron-specific enolase; TNF-α, tumor necrosis factor-alpha; MRI, magnetic resonance imaging; WMH, white matter hyperintensities; EPVS, enlarged perivascular spaces; CMBs, cerebral microbleeds; Lis, lacunar infarcts.
*P-values were obtained by Independent-Samples T test.
[#]P-values were obtained by Mann-Whitney U test.
[&]P-values were obtained by Chi-square test.
"-" means no statistic analysis was performed.

software was used to calculate ALFF values and help perform the statistical analysis between the two groups (Alphasim multiple comparison correction $p < 0.05$). The brain regions with significant ALFF values were displayed using the BrainNet Viewer software. More details were displayed in Supplementary Materials and could be found in our previous studies (Shi et al., 2021a; Shi et al., 2021b; Shi et al., 2022).

Collection of fecal samples and 16S rRNA gene sequencing

After overnight fasting, the fecal sample was collected (7:00-9:00 AM) after participant's defecation using stool collection tubes with stool DNA stabilizer (Genstone Biotech, Beijing, China), and then stored at - 80°C.

The DNA extractions of fecal samples using FastDNA Spin Kit For Soil (MP Biomedicals, Santa Ana, CA) and compositional analysis of gut microbiota were performed by Genesky Biotechnologies Inc. (Shanghai, China). Details of sequencing and data analysis were provided in Supplementary Materials and previous study (Xu et al., 2022).

Collection of plasma samples and detection of plasma indexes

Peripheral venous blood was collected using EDTA-coated tubes after the collection of fecal samples immediately. Then, the plasma samples were obtained by centrifugation at 2000 × g at 4°C for 10 minutes, and further were stored at -80°C until use.

Four plasma indexes, S100beta protein (S100β) (Cao et al., 2022), MMP-9 (Rempe et al., 2016), neuron-specific enolase (NSE) (Yun et al., 2022), and TNF-α (Zelová and Hošek, 2013), were detected using commercial enzyme-linked immunosorbent assays kit (FineTest, Wuhan, China; Catalog Number: EH0543 for S100β, EH0238 for MMP-9, EH0370-HS for NSE, and EH0302 for TNF-α). The levels of these indexes were measured in triplicate and the inter- and intra-assay coefficients of variation were < 5%.

Statistical analyses

The data analyses were conducted using SPSS version 22.0 (SPSS Inc. Chicago, IL, USA) and R software package (version 4.2.1).

The diversity analysis of gut microbiota was comprised of alpha and beta diversity analyses. The alpha-diversity included Observed species, Chao1, and ACE indicators for the community richness and Shannon, Simpson, and Coverage for the community diversity. Beta diversity is used to indicate differences in the composition of gut microbiota using Partial Least Squares-Discriminant Analysis. Linear Discriminant Analysis (LDA) Effect Size (LEfSe) was conducted to identify the markers to interpret the difference between groups where the threshold score of LDA was two. The functions of species in the gut microbiota of both the groups were predicted using PICRUSt2 analysis tool and Kyoto Encyclopedia of Genes and Genomes database (https://www.genome.jp/kegg/pathway.html).

The Kolmogorov-Smirnov test was used to evaluate the normal distribution of the data. The continuous variables were shown as mean ± standard deviation and were analyzed using the Mann-Whitney U test for non-normal distribution, or the Student's t-test for normal distribution. The categorical variables were analyzed using the chi-square test. Pearson correlation analysis was used to determine the correlation between the taxonomies of gut microbiota and clinical data and MRI data. Furthermore, to identify the potential diagnostic biomarker of gut microbiota for CSVD, least absolute shrinkage and selection operator (LASSO) algorithm was used to construct a composite biomarker based on the gut microbiota with significant difference between the groups (Ji et al., 2021; Shi et al., 2023b). Receiver operating characteristic (ROC) curves were utilized to compute the area under the curve (AUC) for determining the diagnostic accuracy of the biomarkers. The Youden index was used to estimate optimal values of sensitivity and specificity. The statistically significant differences were considered as P-value < 0.05.

Results

Characteristics of participants

Table 1 represents no difference in age, sex, education years and complications (hypertension and diabetes) between the CSVD and HC groups. CSVD patients had significantly increased NIHSS, MMSE, and MoCA scores when compared to HCs. However, there was no significant difference in HAMD-17 scores between the two groups.

Additionally, the plasma levels of S100β, NSE, and TNF-α were significant higher in CSVD patients than HCs, however, plasma MMP-9 exhibited a similar level between the two groups (Table 1).

Compositional analysis of gut microbiota in CSVD and HC groups

A total 5,357,333 sequences were obtained from 82 samples, including 4,160,196 sequences in the CSVD group, and 1,197,137 sequences in the HC group, after the quality filtration, noise reduction, splicing, and de-chimerism of data using QIIME2 software (SRA accession number: PRJNA985039).

The operational taxonomic units were assigned with a 95% sequence similarity threshold. The CSVD group exhibited a higher number of operational taxonomic units than the HC group (3463 vs. 1560), including 901 similar operational taxonomic units (Supplementary Figure 1A). All the samples' curves in the rarefaction curves based on the amplicon sequence variant reached saturation plateau at the depth of 52,000 reads, indicating that the sequencing depths were sufficient to represent the majority of microbe species, and the number of samples was reasonable (Supplementary Figure 1B).

Diversity analysis of gut microbiota between two groups

Alpha diversity analysis

Six α-diversity indicators, *i.e.*, Observed species, Chao1, ACE, Shannon, Simpson, and Coverage, were analyzed in the present study (Supplementary Figure 2A). Except for Coverage scores, significant reduced Shannon scores and significant elevated Simpson scores were found in the CSVD group when compared to the HC group, suggesting lower species diversity in the gut microbiota of the CSVD group. Meanwhile, compared with the HC group, Observed, Chao 1, and ACE scores displayed reduced trends in the CSVD group, which suggested lower species richness in the gut microbiota of the CSVD group.

Beta diversity analysis

The β-diversity was calculated using Partial Least Squares-Discriminant Analysis, a supervised discriminant analysis, for the reduction of the impact of intergroup differences (Supplementary Figure 2B). The results of β-diversity suggested that the overall composition of gut microbiota in the CSVD group patients was different from that of the HC group.

Compositional analysis of gut microbiota at genus level levels between two groups

The top four most dominant bacterial genera with the highest relative abundances in both the two groups were consistent, *i.e.*, *Bacteroidetes*, *Faecalibacterium*, *Prevotella*, and *Lachnospiracea_incertae_sedis* (Figures 1A, B). Except for *Bacteroidetes* with the same highest abundances between the groups, the second highest abundance was that of *Faecalibacterium* (6.36%), followed by *Lachnospiracea_incertae_sedis* (5.57%) and *Prevotella* (5.68%) in the CSVD group, however, in HCs, *Faecalibacterium* (9.74%) accounted for the second highest relative abundance, followed by *Prevotella* (9.48%) and *Lachnospiracea_incertae_sedis* (5.39%) (Figure 1C).

The MetaStats analysis represented six genera with significant differences in their relative abundances between the two groups (Figure 2A). *Parasutterella*, *Anaeroglobus*, *Megasphaera*, *Akkermansia*, *Collinsella*, and *Veillonella* significantly increased in the CSVD group as compared to the HC group.

LEfSe analysis

Using the LEfSe analysis, there were 17 taxa identified with LDA scores of > 2 and p-value of < 0.05. Supplementary Figure 3A showed a cladogram for all the taxonomic levels abundance, and Supplementary Figure 3B showed the top 10 taxa with the highest LDA scores in each group. At the genus level, the CSVD group had significantly increased relative abundance of *Parasutterella*, *Enterobacter*, *Terrisporobacter*, *Ezakiella*, and *Anaerostipes* as compared to the HC group, and the HC group had increased relative abundance of *Bacteroides*, *Coprococcus*, *Pseudomonas*, *Dorea*, *Parabacteroides*, and *Phascolarctobacterium* than the CSVD group.

Correlation analysis of environmental factors in CSVD patients

Neuropsychological assessments

As shown in Figures 2B, C, the MMSE and MoCA scores were negatively correlated with the relative abundance of *Parasutterella*. However, there was no correlation between the MMSE and MoCA scores and others gut microbiota at genus level levels.

Plasma indexes

The relative abundance of *Parasutterella* was positively correlated with plasma levels of S100β (Figure 2D). Moreover, a positive correlation was also found between the relative abundance of *Collinsella* and plasma levels of TNF-α (Figure 2E).

MRI features

The total Fazekas scores and periventricular WMH Fazekas scores were positively correlated with the relative abundance of *Collinsella*, and the number of Lis was positively correlated with the relative abundance of *Veillonella* (Figure 3A).

In addition, compared with HCs, CSVD patients exhibited decreased ALFF values in the left supplementary motor area and left median cingulate and paracingulate gyri, and increased ALFF values in the bilateral middle frontal gyrus, bilateral calcarine fissure and surrounding cortex, right superior occipital gyrus, right paracentral lobule (Figure 3B, AlphaSim corrected $p < 0.05$, number of voxels: 70). Further correlation analyses in CSVD patients revealed that the ALFF values in the bilateral middle frontal gyrus were positively correlated with the relative abundance of *Parasutterella*, the ALFF values in the bilateral calcarine fissure and surrounding cortex were positively correlated with the relative abundance of *Veillonella*, and the ALFF values in the right paracentral lobule were positively correlated with the relative abundance of *Akkermansia* (Figure 3C).

Functional predictions for gut microbiota in the two groups

Using the PICRUSt2 analysis tool, the species' functions in the gut microbiota of both the groups were predicted and annotated based on the Kyoto Encyclopedia of Genes and Genomes database. The relative abundances of the functional genes in gut microbiota responsible for the "biosynthesis of ansamycins", "biosynthesis of vancomycin group antibiotics", "valine, leucine and isoleucine biosynthesis", "glycan degradation", and "D-Glutamine and D-glutamate metabolism" were high (Figure 4A). Meanwhile, the differences in the functional

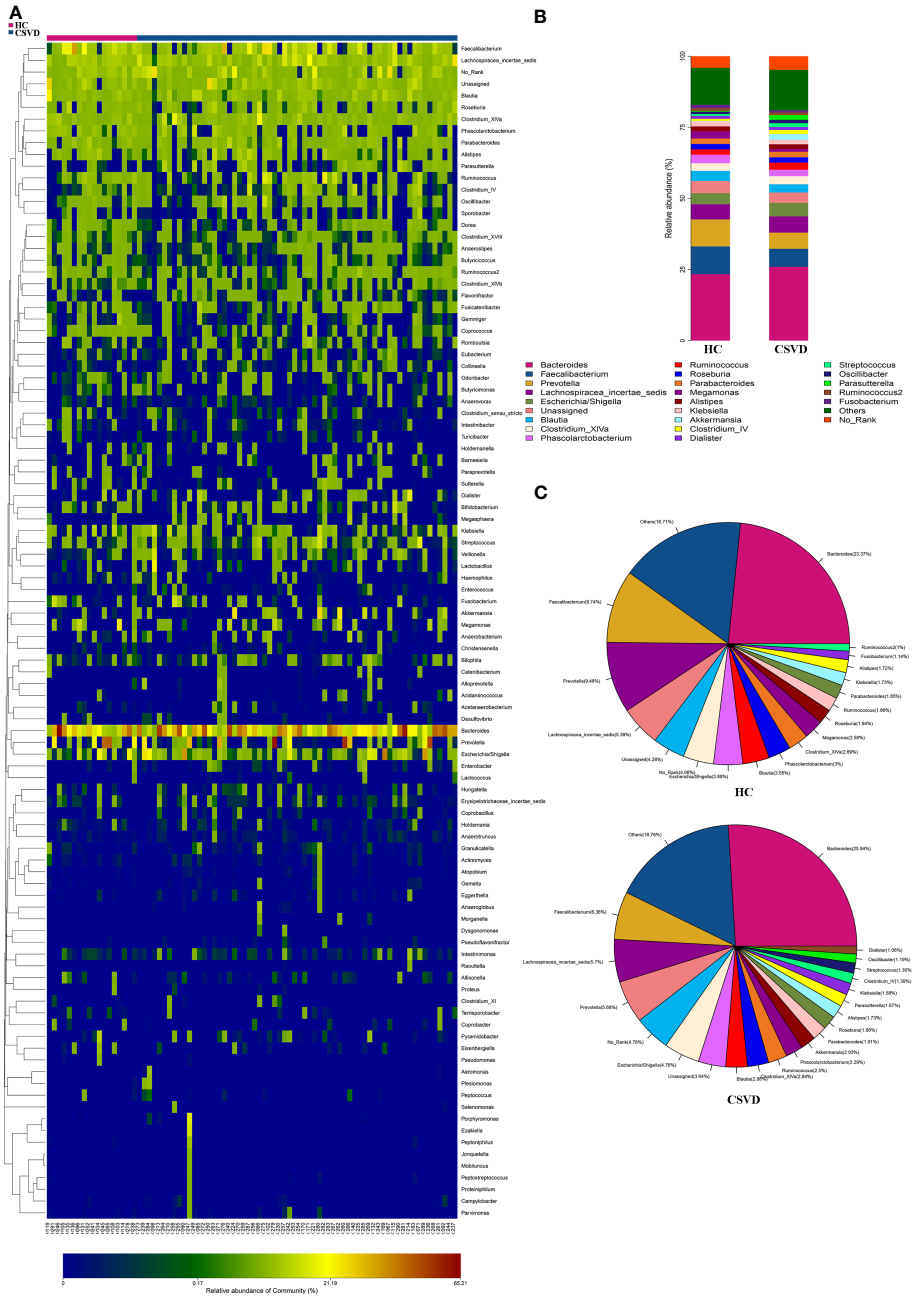

FIGURE 1
Relative abundances at genus level between CSVD and HC groups. **(A)** Heat-map analysis at genus. Abscissa is the sample and ordinate is the taxa at genus level. The colors in heat-map represent the species abundance, and the gradual change of color from blue to red indicates that the species abundance changed from small to large. **(B)** Bar plots of the relative abundances of two groups at genus level. **(C)** Pieplots of the distribution of the relative abundances of two groups at genus level. CSVD, cerebral small vessel disease; HC, healthy control.

prediction between the two groups were analyzed further using Welch's t-test. The pathway of "lipoic acid metabolism" in the CSVD group was significantly higher than the HC group (Figure 4B).

Diagnostic performance of gut microbiota for CSVD

Using the machine learning, a composite biomarker was built based on the gut microbiota at genus level with significant differences between the groups. The composite biomarker of the LASSO model was calculated as follows: *composite biomarker = the relative abundance of Parasutterella × 3.8879931 + the relative abundance of Anaeroglobus × 1.9590061 + the relative abundance of Megasphaera × 3.5400764 + the relative abundance of Akkermansia × 0.6387538 + the relative abundance of Collinsella × 24.9083996 + the relative abundance of Veillonella × 2.3311538 + 0.6438699* (Figures 5A, B).

There was the significant difference in the relative levels of the composite biomarker between the CSVD and HC groups (Figure 5C). ROC curve indicated that the composite biomarker had an AUC value

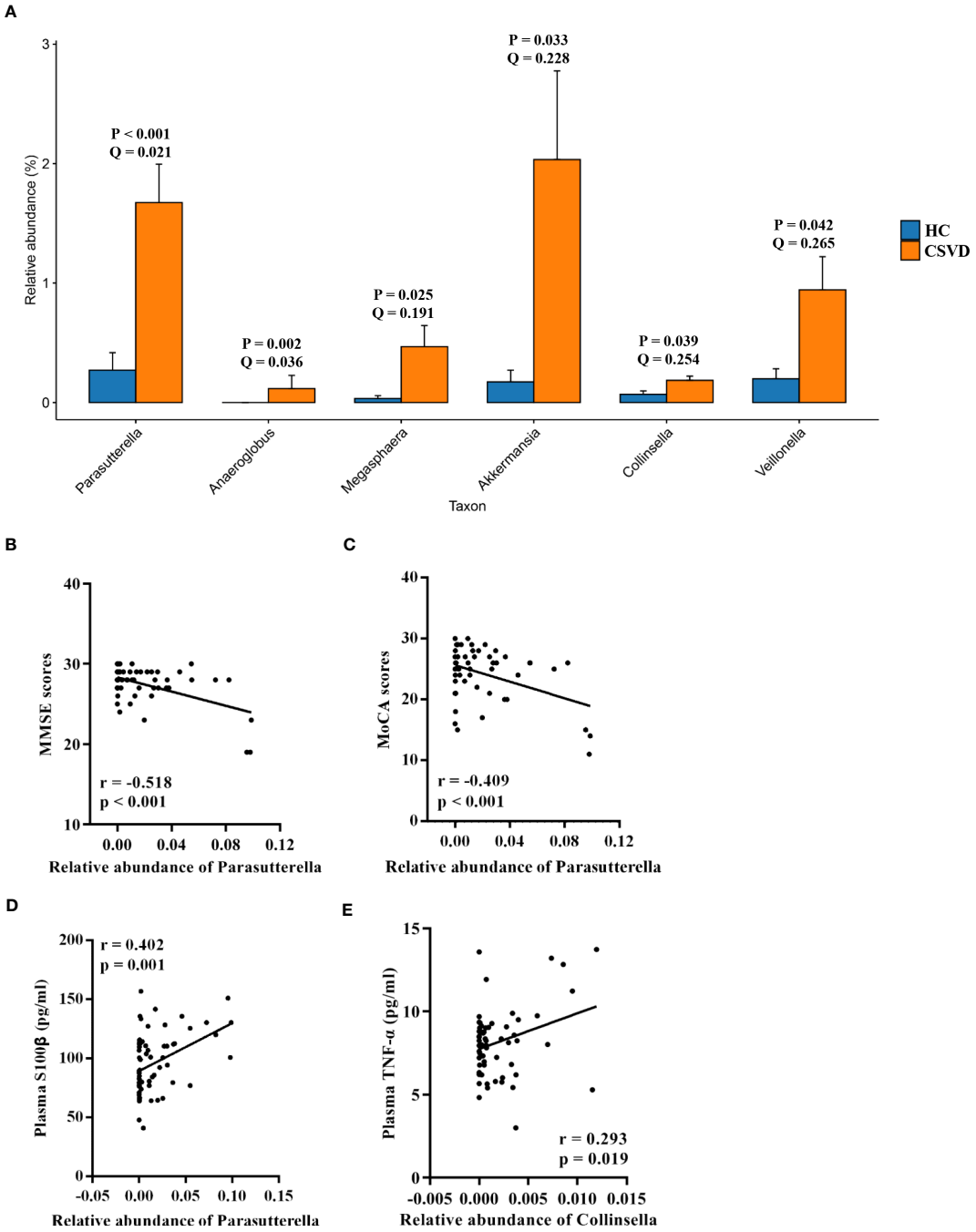

FIGURE 2
Analysis of taxa with significant differences at genus level. **(A)** Taxa with significant differences at genus level between the CSVD and HC groups. P-value was obtained using Metastats analysis, and Q-value was obtained using FDR correction. **(B, C)** Correlation analysis of MMSE and MoCA scores with taxa with significant differences at genus level in CSVD patients. **(D, E)** Correlation analysis of plasma levels of S100β and TNF-α with taxa with significant differences at genus level in CSVD patients. CSVD, cerebral small vessel disease; HC, healthy control; NIHSS, National Institutes of Health Stroke Scale; MMSE, Mini-mental State Examination; MoCA, Montreal Cognitive Assessment; S100β, S100beta protein; TNF-α, tumor necrosis factor-alpha.

of 0.834 to identifying CSVD patients from HCs (sensitivity = 76.56%, specificity = 77.78%), which was the higher than other single index of gut microbiota (Figures 5D, E; Supplementary Table 1).

Discussion

The main findings of the present study were: (1) The CSVD group had significantly lower species diversity and richness in the gut microbiota than the HC group. (2) CSVD patients showed significantly higher genus-level relative abundances of *Parasutterella*, *Anaeroglobus*, *Megasphaera*, *Akkermansia*, *Collinsella*, and *Veillonella* than HCs. (3) Significant associations could be seen between the gut microbiota and cognitive assessments, BBB-/inflammation-related indexes, and structural/functional MRI changes in CSVD patients. (4) Lipoic acid metabolism was involved in CSVD pathogenesis. (5) A composite

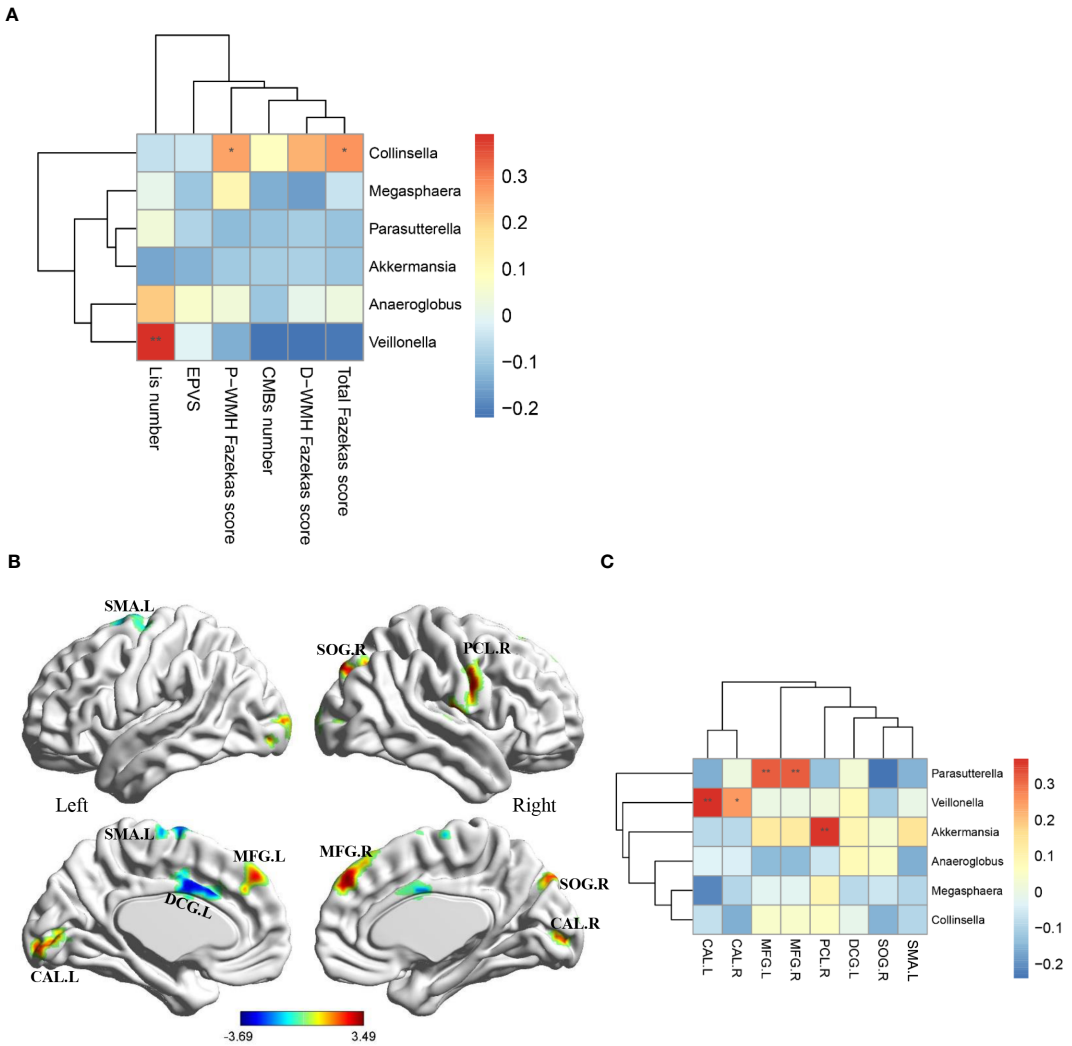

FIGURE 3
Associations of MRI features with gut microbiota at genus level. **(A)** Heatmap shows the correlation coefficient between structural MRI features and gut microbiota at genus level. **(B)** Eight region with significantly differential ALFF in CSVD patients compared with HCs ($p < 0.05$, Alphasim multiple comparison correction, voxel number: 70). Covariates were age, gender and years of education. **(C)** Heatmap shows the correlation coefficient between ALFF values in eight brain regions and gut microbiota at genus level. MRI, magnetic resonance imaging; CSVD, cerebral small vessel disease; HC, healthy control; P-WMH, periventricular white matter hyperintensities; D-WMH, deep white matter hyperintensities; EPVS, enlarged perivascular spaces; CMBs, cerebral microbleeds; Lis, lacunar infarcts; ALFF, amplitude of low-frequency fluctuation; SMA, supplementary motor area; DCG, median cingulate and paracingulate gyri; MFG, middle frontal gyrus; CAL, calcarine fissure and surrounding cortex; SOG, superior occipital gyrus; PCL, paracentral lobule. *P-value < 0.05; **P-value < 0.01.

biomarker of intestinal bacteria revealed the optimal diagnostic power for distinguishing CSVD from HCs. Therefore, the gut microbiota is vital in CSVD pathogenesis (Figure 6), with great potential as a clinical biomarker for CSVD diagnosis.

The present study analyzed diversity and potential function in the gut microbiota of CSVD patients. Meanwhile, environmental factors, such as clinical symptoms, peripheral molecular indexes, and brain imaging features, helped comprehensively estimate the association between gut microbiota and CSVD. Furthermore, a machine learning LASSO model was used to build a composite biomarker depending on the gut microbiota at the genus level to improve the CSVD identification accuracy. The rigorous study design and findings strongly support the significance of gut microbiota in CSVD pathological changes. Therefore, we first proposed ideal biomarkers of the gut microbiota for CSVD clinical application.

The *Parasutterella* genus is a core component of the human gut microbiota and is associated with bile acid maintenance and cholesterol metabolism (Ju et al., 2019). Recently, Akash et al. observed that Alzheimer's disease rat model had an age-related enhancement of *Parasutterella* (Nagarajan et al., 2023). Additionally, a neuroprotective drug, resveratrol, can effectively improve cognitive impairment and increase the abundance of *Parasutterella* in Alzheimer's disease mice (Yang et al., 2023). Similarly, in our study, CSVD patients had significantly elevated relative abundances compared with HCs. Moreover, significant

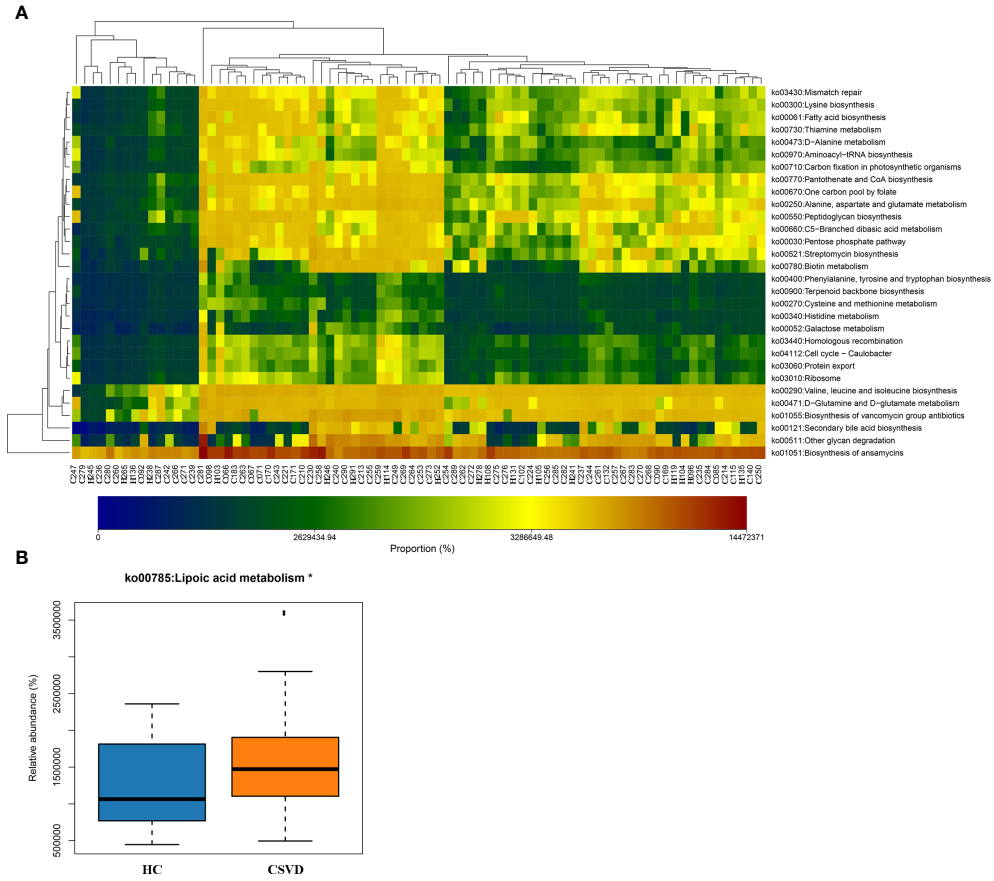

FIGURE 4
Functional predictions of the gut microbiota. **(A)** Heat-map of functional genes in gut microbiota of all participants, showing top. 30 genes with maximum relative abundances. The Abscissa stands for the samples, and the ordinate is functional genes. The colors represent the abundance of function, and the gradual change in color from light to deep indicates the relative abundance of function from low to high. **(B)** Significant difference in Kyoto Encyclopedia of Genes and Genomes pathways for gut microbiota in CSVD and HC groups. *P-value < 0.05. CSVD, cerebral small vessel disease; HC, healthy control.

correlations were observed in CSVD patients between relative abundances of *Parasutterella* and specific clinical features (*e.g.*, MMSE and MoCA scores and the ALFF values of bilateral middle frontal gyrus). Thus, the *Parasutterella*-mediated pathological mechanism may affect cognitive decline (Liang et al., 2022). Furthermore, there was a significantly positive correlation between the relative abundance of *Parasutterella* in CSVD patients and S100β plasma levels, a peripheral BBB function marker (Thelin et al., 2017; Solarz et al., 2021), which suggested that *Parasutterella* may be associated with disrupted BBB integrality in CSVD. Previous studies indicated that high-density lipoproteins protected endothelial function and BBB integrity (Tran-Dinh et al., 2013). However, increased high cholesterol ingestion could exacerbate BBB disruption and affect cognitive function (De Oliveira et al., 2020). Therefore, *Parasutterella* may control the cholesterol metabolism to affect the BBB function, leading to cognitive impairment in CSVD patients.

The relative abundances of *Collinsella* were significantly increased in some psychiatry disorders [*e.g.*, schizophrenia (Li et al., 2020) and autism spectrum disorders (Ding et al., 2020)] compared to HCs in the published studies, indicating that *Collinsella* could affect the normal function of the central nervous system. However, only one study on cerebrovascular disease revealed that combining Puerariae Lobatae Radix and Chuanxiong Rhizoma can enhance intestinal Collinsella disturbances in ischemic stroke (Chen et al., 2019a). The present study observed significantly elevated *Collinsella* levels and a positive correlation with the WMH scores in CSVD patients. This indicated that the relative abundance of *Collinsella* may reflect the CSVD severity. Additionally, *Ruiz-Limón et al.* demonstrated that the increase of the genus *Collinsella* was related to cumulative inflammatory activity (Ruiz-Limón et al., 2022). A significant association was observed in our study between *Collinsella* and plasma TNF-α levels in CSVD patients. Hence, *Collinsella*-mediated inflammation response could have an effect on the CSVD white matter lesions.

A previous study identified more *Akkermansia* in cerebral ischemic stroke patients than HCs (Li et al., 2019). However, another study described contrary results in stroke patients (Chang et al., 2021). In our study, CSVD patients had significantly elevated

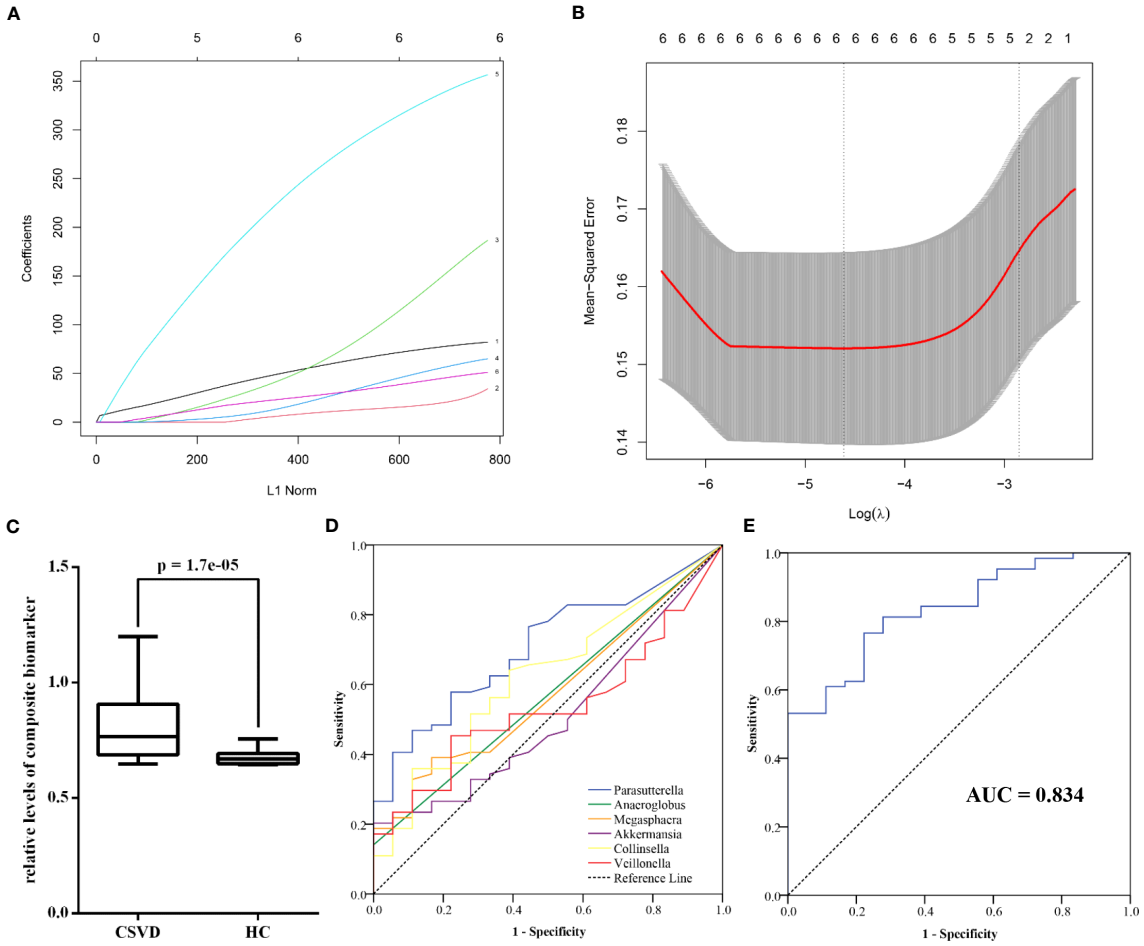

FIGURE 5
Diagnostic performance of gut microbiota at genus level for CSVD. **(A)** The coefficients of each gut microbiota in the LASSO model (1 = *Parasutterella*, 2 = *Anaeroglobus*, 3 = *Megasphaera*, 4 = *Akkermansia*, 5 = *Collinsella*, 6 = *Veillonella*). **(B)** The mean-squared error of LASSO model. **(C)** The significant difference in the relative levels of the composite biomarker between CSVD patients and HCs. **(D)** ROC curve of six gut microbiota at genus level for identifying CSVD. **(E)** ROC curve of the composite biomarker for identifying CSVD. CSVD, cerebral small vessel disease; HC, healthy control; LASSO, least absolute shrinkage and selection operator; ROC, receiver operating characteristic.

Akkermansia levels compared to HCs. Moreover, *Akkermansia* levels were positively associated with the ALFF values in the right paracentral lobule. Due to lower paracentral lobule activity being negatively associated with the total small vessel disease burden (Xu et al., 2018), *Akkermansia* as a probiotic (Zhang et al., 2019) may protect CSVD.

Furthermore, CSVD patients showed a significantly higher relative abundance of *Veillonella*, *Megasphaera*, and *Veillonella* than HCs. Among them, elevated *Megasphaera* was also observed in stroke patients (Wang et al., 2021), but other gut microbiota were proposed firstly by us in patients with cerebrovascular disease. The present study revealed that significantly increased *Veillonella* exhibited positive correlations with the number of Lis and the ALFF values in the bilateral calcarine fissure and surrounding cortex among CSVD patients. Therefore, *Veillonella* could be associated with CSVD occurrence by affecting brain activity in bilateral calcarine fissure and surrounding cortex. However, the underlying mechanism of these gut microbiota in CSVD pathology remains unknown.

A combined biomarker using the LASSO model showed better diagnostic performance in identifying CSVD than the single gut microbiota biomarker. Thus, using machine learning contributes to elevating the differential power for CSVD.

The present study had some limitations. (1) The number of HCs was less than the CSVD group. A sample size calculator was used (https://sample-size.net/), which indicated the acceptability of the current sample size. The sample size will be increased in subsequent studies to verify the obtained results. (2) Since CSVD patients possess various clinical symptoms, the different clinical subtypes of CSVD may possess distinct performances of gut microbiota. We did not analyze the differences in gut microbiota among CSVD patients with cognitive impairment, depression, or gait disturbances. (3) The independent present composite biomarker verification of gut microbiota is absent in the present study. (4) Animal study is

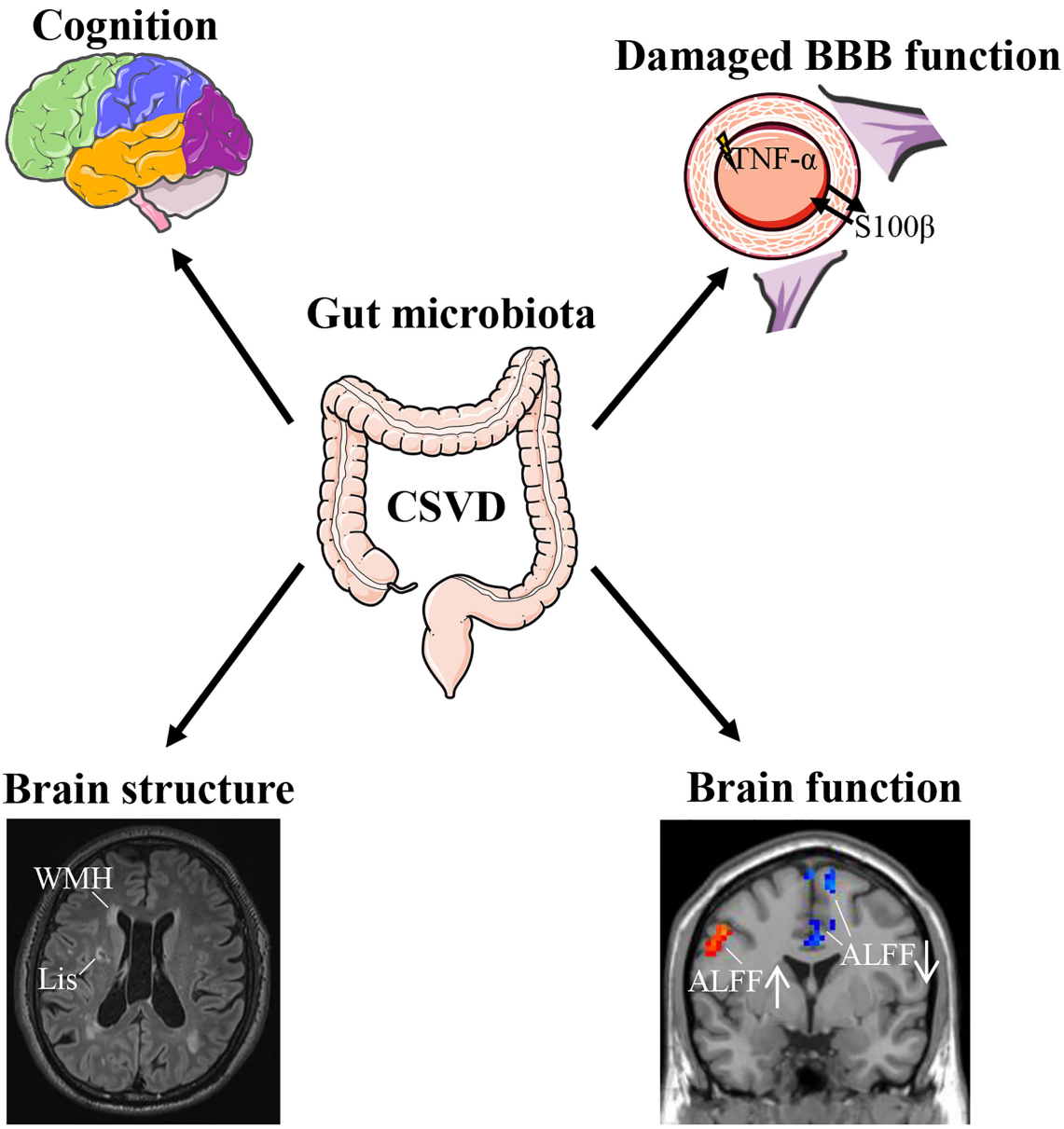

FIGURE 6
Association of gut microbiota with CSVD. CSVD, cerebral small vessel disease; BBB, blood-brain barrier; WMH, white matter hyperintensities; Lis, lacunar infarcts; ALFF, amplitude of low-frequency fluctuation.

absent in the present study. We will conduct the animal study to determine the association between the gut microbiota and CSVD pathological mechanisms in the following study. Therefore, a multi-center study should be conducted to validate the current findings.

Conclusion

The present study demonstrated the composition of gut microbiota composition in patients with CSVD and found several microbes correlated with cognitive decline, BBB integrality, and brain MRI changes, which might expound the underlying pathogenesis of CSVD. Meanwhile, a composite biomarker of gut microbiota using LASSO model will contribute to identifying CSVD conveniently and accurately.

Data availability statement

The datasets presented in this study can be found in online repositories. The names of the repository/repositories and accession number(s) can be found below: The sequencing data can be obtained from GEO database (SRA accession number: PRJNA985039; https://www.ncbi.nlm.nih.gov/bioproject/PRJNA985039).

Ethics statement

The studies involving human participants were reviewed and approved by the Ethics Committee of the Affiliated Wuxi People's Hospital of Nanjing Medical University (approval number: KY2112). The patients/participants provided their written informed consent to participate in this study. Written informed consent was obtained from the individual(s) for the publication of any potentially identifiable images or data included in this article.

Author contributions

YS, XF, and FW designed the study. YS and EZ draft the manuscript. HM, QG, SiZ, and LM collected the image data. LL, JD, YL, GX, and YY recruited the participants, completed the neuropsychological assessments, and collected the blood samples. LL and SoZ analyzed the data. JS contributed to the discussion. XF and FW contributed to the discussion and revised the manuscript. All authors contributed to the article and approved the submitted version.

Funding

This study was funded by the WuXi Municipal Health Commission (No. Q202222), the Jiangsu Province Natural Science Foundation (No. BK20191143), the Medical Expert Team Program of Wuxi Taihu Talent Plan 2021 (2021THRC-TF-YXYXK), and Wuxi Taihu Lake Talent Plan, Supports for Leading Talents in Medical and Health Profession (2020THRC-DJ-SNW).

Acknowledgments

The authors would like to thank all participants in the present study for their cooperation and relevant medical staff (*e.g.*, Mr. Kefei Chen, Mrs. Ping He, Miss. Mengjia Pu, Miss. Qinyu Han, and Mrs. Yan Han) from the Neurology Department of the Affiliated Wuxi People's Hospital of Nanjing Medical University for their assistance in this work. The authors would like to thank Mr. Lingbin Sun for his technical assistance from Genesky Biotechnologies Inc. (Shanghai, China).

Conflict of interest

The authors declare that the research was conducted in the absence of any commercial or financial relationships that could be construed as a potential conflict of interest.

Publisher's note

All claims expressed in this article are solely those of the authors and do not necessarily represent those of their affiliated organizations, or those of the publisher, the editors and the reviewers. Any product that may be evaluated in this article, or claim that may be made by its manufacturer, is not guaranteed or endorsed by the publisher.

Supplementary material

The Supplementary Material for this article can be found online at: https://www.frontiersin.org/articles/10.3389/fcimb.2023.1231541/full#supplementary-material

References

Arya, A. K., and Hu, B. (2018). Brain-gut axis after stroke. *Brain Circ.* 4 (4), 165–173. doi: 10.4103/bc.bc_32_18

Ascher, S., and Reinhardt, C. (2018). The gut microbiota: an emerging risk factor for cardiovascular and cerebrovascular disease. *Eur. J. Immunol.* 48 (4), 564–575. doi: 10.1002/eji.201646879

Cai, W. C. X., Men, X., Ruan, H., Hu, M., Liu, S., Lu, T., et al. (2021). Gut microbiota from patients with arteriosclerotic CSVD induces higher IL-17A production in neutrophils via activating RORγt. *Sci. Adv.* 7 (4), eabe4827. doi: 10.1126/sciadv.abe4827

Cannistraro, R. J., Badi, M., Eidelman, B. H., Dickson, D. W., Middlebrooks, E. H., and Meschia, J. F. (2019). CNS small vessel disease: a clinical review. *Neurology* 92 (24), 1146–1156. doi: 10.1212/WNL.0000000000007654

Cao, M. C., Cawston, E. E., Chen, G., Brooks, C., Douwes, J., Mclean, D., et al. (2022). Serum biomarkers of neuroinflammation and blood-brain barrier leakage in amyotrophic lateral sclerosis. *BMC Neurol.* 22 (1), 216. doi: 10.1186/s12883-022-02730-1

Chang, Y., Woo, H. G., Jeong, J. H., Kim, G. H., Park, K. D., and Song, T. J. (2021). Microbiota dysbiosis and functional outcome in acute ischemic stroke patients. *Sci. Rep.* 11 (1), 10977. doi: 10.1038/s41598-021-90463-5

Chao-Gan, Y., and Yu-Feng, Z. (2010). DPARSF: a MATLAB toolbox for "Pipeline" data analysis of resting-state fMRI. *Front. Syst. Neurosci.* 4, 13. doi: 10.3389/fnsys.2010.00013

Chen, F., Wang, L., and Ding, Z. (2022). Alteration of whole-brain amplitude of low-frequency fluctuation and degree centrality in patients with mild to moderate depression: a resting-state functional magnetic resonance imaging study. *Front. Psychiatry* 13, 1061359. doi: 10.3389/fpsyt.2022.1061359

Chen, X., Wang, J., Shan, Y., Cai, W., Liu, S., Hu, M., et al. (2019b). Cerebral small vessel disease: neuroimaging markers and clinical implication. *J. Neurol.* 266 (10), 2347–2362. doi: 10.1007/s00415-018-9077-3

Chen, R., Wu, P., Cai, Z., Fang, Y., Zhou, H., Lasanajak, Y., et al. (2019a). Puerariae lobatae radix with chuanxiong rhizoma for treatment of cerebral ischemic stroke by remodeling gut microbiota to regulate the brain-gut barriers. *J. Nutr. Biochem.* 65, 101–114. doi: 10.1016/j.jnutbio.2018.12.004

De Oliveira, J., Engel, D. F., De Paula, G. C., Dos Santos, D. B., Lopes, J. B., Farina, M., et al. (2020). High cholesterol diet exacerbates blood-brain barrier disruption in LDLr-/- mice: impact on cognitive function. *J. Alzheimers Dis.* 78 (1), 97–115. doi: 10.3233/JAD-200541

Ding, X., Xu, Y., Zhang, X., Zhang, L., Duan, G., Song, C., et al. (2020). Gut microbiota changes in patients with autism spectrum disorders. *J. Psychiatr. Res.* 129, 149–159. doi: 10.1016/j.jpsychires.2020.06.032

Hoyles, L., Pontifex, M. G., Rodriguez-Ramiro, I., Anis-Alavi, M. A., Jelane, K. S., Snelling, T., et al. (2021). Regulation of blood-brain barrier integrity by microbiome-associated methylamines and cognition by trimethylamine n-oxide. *Microbiome* 9 (1), 235. doi: 10.1186/s40168-021-01181-z

Huang, Q., and Xia, J. (2021). Influence of the gut microbiome on inflammatory and immune response after stroke. *Neurol. Sci.* 42 (12), 4937–4951. doi: 10.1007/s10072-021-05603-6

Ji, W., Liu, Y., Xu, B., Mei, J., Cheng, C., Xiao, Y., et al. (2021). Bioinformatics analysis of expression profiles and prognostic values of the signal transducer and activator of transcription family genes in glioma. *Front. Genet.* 12, 625234. doi: 10.3389/fgene.2021.625234

Ju, T., Kong, J. Y., Stothard, P., and Willing, B. P. (2019). Defining the role of parasutterella, a previously uncharacterized member of the core gut microbiota. *Isme J.* 13 (6), 1520–1534. doi: 10.1038/s41396-019-0364-5

Li, H., Jia, X., Li, Y., Jia, X., and Yang, Q. (2021). Aberrant amplitude of low-frequency fluctuation and degree centrality within the default mode network in patients with vascular mild cognitive impairment. *Brain Sci.* 11 (11), 1534. doi: 10.3390/brainsci11111534

Li, M., Sun, H., Shen, T., Xue, S., Zhao, Y., Leng, B., et al. (2022). Increased serum levels of cyclophilin a and matrix metalloproteinase-9 are associated with cognitive impairment in patients with obstructive sleep apnea. *Sleep Med.* 93, 75–83. doi: 10.1016/j.sleep.2021.10.009

Li, N., Wang, X., Sun, C., Wu, X., Lu, M., Si, Y., et al. (2019). Change of intestinal microbiota in cerebral ischemic stroke patients. *BMC Microbiol.* 19 (1), 191. doi: 10.1186/s12866-019-1552-1

Li, S., Zhuo, M., Huang, X., Huang, Y., Zhou, J., Xiong, D., et al. (2020). Altered gut microbiota associated with symptom severity in schizophrenia. *PeerJ* 8, e9574. doi: 10.7717/peerj.9574

Liang, X., Yuan, Q., Xue, C., Qi, W., Ge, H., Yan, Z., et al. (2022). Convergent functional changes of the episodic memory impairment in mild cognitive impairment: an ALE meta-analysis. *Front. Aging Neurosci.* 14, 919859. doi: 10.3389/fnagi.2022.919859

Markus, H. S., and Erik De Leeuw, F. (2023). Cerebral small vessel disease: recent advances and future directions. *Int. J. Stroke* 18 (1), 4–14. doi: 10.1177/17474930221144911

Matsuura, J., Inoue, R., Takagi, T., Wada, S., Watanabe, A., Koizumi, T., et al. (2019). Analysis of gut microbiota in patients with cerebral autosomal dominant arteriopathy with subcortical infarcts and leukoencephalopathy (CADASIL). *J. Clin. Biochem. Nutr.* 65 (3), 240–244. doi: 10.3164/jcbn.19-22

Nagarajan, A., Srivastava, H., Morrow, C. D., and Sun, L. Y. (2023). Characterizing the gut microbiome changes with aging in a novel alzheimer's disease rat model. *Aging (Albany NY)* 15 (2), 459–471. doi: 10.18632/aging.204484

Nelson, J. W., Phillips, S. C., Ganesh, B. P., Petrosino, J. F., Durgan, D. J., and Bryan, R. M. (2021). The gut microbiome contributes to blood-brain barrier disruption in spontaneously hypertensive stroke prone rats. *FASEB J.* 35 (2), e21201. doi: 10.1096/fj.202001117R

Parker, A., Fonseca, S., and Carding, S. R. (2020). Gut microbes and metabolites as modulators of blood-brain barrier integrity and brain health. *Gut Microbes* 11 (2), 135–157. doi: 10.1080/19490976.2019.1638722

Peh, A., O'donnell, J. A., Broughton, B. R. S., and Marques, F. Z. (2022). Gut microbiota and their metabolites in stroke: a double-edged sword. *Stroke* 53 (5), 1788–1801. doi: 10.1161/STROKEAHA.121.036800

Pluta, R., Januszewski, S., and Czuczwar, S. J. (2021). The role of gut microbiota in an ischemic stroke. *Int. J. Mol. Sci.* 22 (2), 915. doi: 10.3390/ijms22020915

Qu, Y., Tan, C. C., Shen, X. N., Li, H. Q., Cui, M., Tan, L., et al. (2021). Association of plasma neurofilament light with small vessel disease burden in nondemented elderly: a longitudinal study. *Stroke* 52 (3), 896–904. doi: 10.1161/STROKEAHA.120.030302

Rempe, R. G., Hartz, A. M. S., and Bauer, B. (2016). Matrix metalloproteinases in the brain and blood-brain barrier: versatile breakers and makers. *J. Cereb. Blood Flow Metab.* 36 (9), 1481–1507. doi: 10.1177/0271678X16655551

Ruiz-Limón, P., Mena-Vázquez, N., Moreno-Indias, I., Manrique-Arija, S., Lisbona-Montañez, J. M., Cano-García, L., et al. (2022). Collinsella is associated with cumulative inflammatory burden in an established rheumatoid arthritis cohort. *Biomed. Pharmacother.* 153, 113518. doi: 10.1016/j.biopha.2022.113518

Shi, Y., Mao, H., Gao, Q., Xi, G., Zeng, S., Ma, L., et al. (2022). Potential of brain age in identifying early cognitive impairment in subcortical small-vessel disease patients. *Front. Aging Neurosci.* 14, 973054. doi: 10.3389/fnagi.2022.973054

Shi, Y., Song, R., Wang, Z., Zhang, H., Zhu, J., Yue, Y., et al. (2021a). Potential clinical value of circular RNAs as peripheral biomarkers for the diagnosis and treatment of major depressive disorder. *EBioMedicine* 66, 103337. doi: 10.1016/j.ebiom.2021.103337

Shi, Y., Wang, Z., Chen, P., Cheng, P., Zhao, K., Zhang, H., et al. (2023a). Episodic memory-related imaging features as valuable biomarkers for the diagnosis of alzheimer's disease: a multicenter study based on machine learning. *Biol. Psychiatry Cognit. Neurosci. Neuroimaging* 8 (2), 171–180. doi: 10.1016/j.bpsc.2020.12.007

Shi, Y., Xuan, C., Ji, W., Wang, F., Huang, J., Li, L., et al. (2023b). Combination of platelet-to-lymphocyte ratio and d-dimer for the identification of cardiogenic cerebral embolism in non-valvular atrial fibrillation. *Front. Neurol.* 14, 1069261. doi: 10.3389/fneur.2023.1069261

Shi, Y., Zhang, L., Wang, Z., Lu, X., Wang, T., Zhou, D., et al. (2021b). Multivariate machine learning analyses in identification of major depressive disorder using resting-state functional connectivity: a multicentral study. *ACS Chem. Neurosci.* 12 (15), 2878–2886. doi: 10.1021/acschemneuro.1c00256

Solarz, A., Majcher-Maślanka, I., and Chocyk, A. (2021). Effects of early-life stress and sex on blood-brain barrier permeability and integrity in juvenile and adult rats. *Dev. Neurobiol.* 81 (7), 861–876. doi: 10.1002/dneu.22846

Thelin, E. P., Nelson, D. W., and Bellander, B. M. (2017). A review of the clinical utility of serum S100B protein levels in the assessment of traumatic brain injury. *Acta Neurochirurgica* 159 (2), 209–225. doi: 10.1007/s00701-016-3046-3

Tran-Dinh, A., Diallo, D., Delbosc, S., Varela-Perez, L. M., Dang, Q. B., Lapergue, B., et al. (2013). HDL and endothelial protection. *Br. J. Pharmacol.* 169 (3), 493–511. doi: 10.1111/bph.12174

Ungvari, Z., Toth, P., Tarantini, S., Prodan, C. I., Sorond, F., Merkely, B., et al. (2021). Hypertension-induced cognitive impairment: from pathophysiology to public health. *Nat. Rev. Nephrol.* 17 (10), 639–654. doi: 10.1038/s41581-021-00430-6

Van Den Brink, H., Doubal, F. N., and Duering, M. (2023). Advanced MRI in cerebral small vessel disease *Int. J. Stroke* 18 (1), 28–35. doi: 10.1177/17474930221091879

Wan, S., Dandu, C., Han, G., Guo, Y., Ding, Y., Song, H., et al. (2023). Plasma inflammatory biomarkers in cerebral small vessel disease: a review *CNS Neurosci Ther.* 29, 2, 498–515. doi: 10.1111/cns.14047

Wang, Z., Xu, K., and Zhou, H. (2021). [Characteristics of gut virome and microbiome in patients with stroke]. nan fang yi ke da xue xue bao. *J. South. Med. Univ.* 41 (6), 862–869. doi: 10.12122/j.issn.1673-4254.2021.06.08

Xu, X., Lau, K. K., Wong, Y. K., Mak, H. K. F., and Hui, E. S. (2018). The effect of the total small vessel disease burden on the structural brain network. *Sci. Rep.* 8 (1), 7442. doi: 10.1038/s41598-018-25917-4

Xu, Y., Shao, M., Fang, X., Tang, W., Zhou, C., Hu, X., et al. (2022). Antipsychotic-induced gastrointestinal hypomotility and the alteration in gut microbiota in patients with schizophrenia. *Brain Behav. Immun.* 99, 119–129. doi: 10.1016/j.bbi.2021.09.014

Yang, L., Wang, Y., Li, Z., Wu, X., Mei, J., and Zheng, G. (2023). Brain targeted peptide-functionalized chitosan nanoparticles for resveratrol delivery: impact on insulin resistance and gut microbiota in obesity-related alzheimer's disease. *Carbohydr. Polym.* 310, 120714. doi: 10.1016/j.carbpol.2023.120714

Yun, G. S., In, Y. N., Kang, C., Park, J. S., You, Y., Min, J. H., et al. (2022). Development of a strategy for assessing blood-brain barrier disruption using serum S100 calcium-binding protein b and neuron-specific enolase in early stage of neuroemergencies: a preliminary study. *Med. (Baltimore)* 101 (28), e29644. doi: 10.1097/MD.0000000000029644

Zelová, H., and Hošek, J. (2013). TNF-α signalling and inflammation: interactions between old acquaintances. *Inflammation Res.* 62 (7), 641–651. doi: 10.1007/s00011-013-0633-0

Zhang, T., Li, Q., Cheng, L., Buch, H., and Zhang, F. (2019). Akkermansia muciniphila is a promising probiotic. *Microb. Biotechnol.* 12 (6), 1109–1125. doi: 10.1111/1751-7915.13410

Zhou, X., Zhang, C., Li, L., Zhang, Y., Zhang, W., Yin, W., et al. (2020). Altered brain function in cerebral small vessel disease patients with gait disorders: a resting-state functional MRI study. *Front. Aging Neurosci.* 12, 234. doi: 10.3389/fnagi.2020.00234

Zou, X., Wang, L., Xiao, L., Wang, S., and Zhang, L. (2022). Gut microbes in cerebrovascular diseases: gut flora imbalance, potential impact mechanisms and promising treatment strategies. *Front. Immunol.* 13, 975921. doi: 10.3389/fimmu.2022.975921

frontiers | Frontiers in Cellular and Infection Microbiology

TYPE Original Research
PUBLISHED 19 December 2023
DOI 10.3389/fcimb.2023.1289124

OPEN ACCESS

EDITED BY
Jianguo Tang,
Fudan University, China

REVIEWED BY
Shenghui Li,
Puensum Genetech Institute, China
Yotsawat Pomyen,
Chulabhorn Research Institute, Thailand

*CORRESPONDENCE
Yafeng Li
dr.yafengli@gmail.com

RECEIVED 05 September 2023
ACCEPTED 28 November 2023
PUBLISHED 19 December 2023

CITATION
Song W, Wu F, Yan Y, Li Y, Wang Q, Hu X and Li Y (2023) Gut microbiota landscape and potential biomarker identification in female patients with systemic lupus erythematosus using machine learning. *Front. Cell. Infect. Microbiol.* 13:1289124. doi: 10.3389/fcimb.2023.1289124

Gut microbiota landscape and potential biomarker identification in female patients with systemic lupus erythematosus using machine learning

Wenzhu Song[1], Feng Wu[2], Yan Yan[2], Yaheng Li[3], Qian Wang[3], Xueli Hu[4] and Yafeng Li[2,3,5,6]*

[1]School of Public Health, Shanxi Medical University, Taiyuan, Shanxi, China, [2]Department of Nephrology, Shanxi Provincial People's Hospital (Fifth Hospital) of Shanxi Medical University, Taiyuan, China, [3]Shanxi Provincial Key Laboratory of Kidney Disease, Taiyuan, Shanxiuan, China, [4]Department of Nephrology, Hejin People's Hospital, Yuncheng, Shanxi, China, [5]Core Laboratory, Shanxi Provincial People's Hospital (Fifth Hospital) of Shanxi Medical University, Taiyuan, China, [6]Academy of Microbial Ecology, Shanxi Medical University, Taiyuan, China

Objectives: Systemic Lupus Erythematosus (SLE) is a complex autoimmune disease that disproportionately affects women. Early diagnosis and prevention are crucial for women's health, and the gut microbiota has been found to be strongly associated with SLE. This study aimed to identify potential biomarkers for SLE by characterizing the gut microbiota landscape using feature selection and exploring the use of machine learning (ML) algorithms with significantly dysregulated microbiotas (SDMs) for early identification of SLE patients. Additionally, we used the SHapley Additive exPlanations (SHAP) interpretability framework to visualize the impact of SDMs on the risk of developing SLE in females.

Methods: Stool samples were collected from 54 SLE patients and 55 Negative Controls (NC) for microbiota analysis using 16S rRNA sequencing. Feature selection was performed using Elastic Net and Boruta on species-level taxonomy. Subsequently, four ML algorithms, namely logistic regression (LR), Adaptive Boosting (AdaBoost), Random Forest (RF), and eXtreme gradient boosting (XGBoost), were used to achieve early identification of SLE with SDMs. Finally, the best-performing algorithm was combined with SHAP to explore how SDMs affect the risk of developing SLE in females.

Results: Both alpha and beta diversity were found to be different in SLE group. Following feature selection, 68 and 21 microbiota were retained in Elastic Net and Boruta, respectively, with 16 microbiota overlapping between the two, i.e., SDMs for SLE. The four ML algorithms with SDMs could effectively identify SLE patients, with XGBoost performing the best, achieving Accuracy, Sensitivity, Specificity, Positive Predictive Value, Negative Predictive Value, and AUC values of 0.844, 0.750, 0.938, 0.923, 0.790, and 0.930, respectively. The SHAP interpretability framework showed a complex non-linear relationship between the relative abundance of SDMs and the risk of SLE, with *Escherichia_fergusonii* having the largest SHAP value.

Conclusions: This study revealed dysbiosis in the gut microbiota of female SLE patients. ML classifiers combined with SDMs can facilitate early identification of female patients with SLE, particularly XGBoost. The SHAP interpretability framework provides insight into the impact of SDMs on the risk of SLE and may inform future scientific treatment for SLE.

KEYWORDS

systemic lupus erythematosus, machine learning, elastic net, Boruta, gut microbiota

Introduction

Advancements in medical technology and increasing awareness of health issues have brought a growing focus on women's health, given their unique physiological structure and functions (Qiao et al., 2021). Systemic lupus erythematosus (SLE) is a chronic autoimmune disease with high incidence, frequent relapses, and a generally poor prognosis, particularly affecting women between the ages of 20 and 40 (Tsang and Bultink, 2021; Lazar and Kahlenberg, 2023). It exhibits a wide range of clinical manifestations, ranging from mild cutaneous issues to severe organ failure and complications during pregnancy (Barber et al., 2021). Besides, individuals with SLE face an increased risk of conditions like atherosclerosis, thrombosis, arterial inflammation, and vascular spasms compared to the general population (Samuelsson et al., 2021).Tragically, SLE ranks among the leading causes of death in young women (Yen and Singh, 2018), with a significantly elevated mortality rate.

In the USA, a meta-analysis of over 26,000 female SLE patients revealed a mortality rate 2.6 times higher than the general population (Lee et al., 2016). In Asia, the annual incidence ranges from 2.8 to 8.6 cases per 100,000 person-years, with a prevalence varying from 26.5 to 103 cases per 100,000 individuals (Chiu and Lai, 2010; Zou et al., 2014; Barber et al., 2021). The current treatment for SLE primarily involves glucocorticoids and immunosuppressants. While standard therapy is effective to some extent, it comes with severe side effects and is not suitable for long-term use (Golder and Tsang, 2020). Also, until now, the diagnosis of SLE is primarily based on clinical assessment, although there are a few instances where serologic tests show negative results. There are no specific diagnostic criteria for SLE, and diagnosis is frequently made using classification criteria, albeit with notable limitations (Fanouriakis et al., 2021). Since women with SLE often experience more severe symptoms and organ damage than men, early diagnosis and prevention are essential for women's health, and identifying new biomarkers associated with SLE is of great clinical significance.

Studies have shown a close relationship between intestinal flora and the occurrence of SLE, with significant differences in gut microbiota composition and metabolites in SLE patients compared to healthy individuals (Hevia et al., 2014). A study found that the *Firmicutes*/*Bacteroidetes* ratio in SLE patients was significantly lower than that in healthy subjects, which was confirmed by quantitative PCR analysis. Besides, another study showed that *Proteobacteria* increased and *Ruminococcaceae* decreased in SLE patients in different regions of Heilongjiang (Wei et al., 2019). Additionally, there are significant differences in the levels of metabolites in the gut microbiota of SLE patients compared to healthy individuals, especially aromatic amino acids and phosphatidylinositol (Robinson et al., 2021).

Given the close relationship, constructing a model with significantly dysregulated microbiotas (SDMs) for SLE would make its early identification possible. Yet, traditional regression models, which are determined by maximum likelihood estimation, have not made much progress in disease auxiliary diagnosis (Song et al., 2022). Notably, machine learning (ML), a research hotspot in the field of life sciences, gains ground in various diseases, including cardiovascular and cerebrovascular diseases (Zheng et al., 2021), kidney diseases (Belur Nagaraj et al., 2020), tumours (Sammut et al., 2022), neurological diseases (Boutet et al., 2021), immune diseases (Chen et al., 2021). Therefore, the utilization of ML techniques for the diagnosis of SLE based on gut microbiota is of great interest. However, there is currently a relative lack of research on this topic. Thus, ML could be adopted to identify crucial microbiota that may be intimately associated with the onset and progression of SLE. Building multiple algorithms utilizing these significant microbiotas as predictive factors to recognize SLE may potentially offer novel insights and value for the microbiota perspective of SLE diagnosis. Furthermore, interpretability serves as a critical supplement to ML decisions, and by integrating interpretable techniques with the most effective ML algorithms and presenting the diagnostic rationale of the model to physicians through visualization methods, it could greatly facilitate the treatment of SLE, which helps promote women's health.

Considering the mounting evidence linking gut microbiota dysbiosis to SLE, there is a growing interest in exploring the potential of using gut microbiota as a predictive indicator for early identification and prevention of SLE in female patients. To this end, the present study aimed to characterize the gut microbiota landscape using feature selection approaches, develop and validate ML algorithms for early identification of SLE in female patients. Additionally, we aimed to use interpretability techniques to visualize the predictive factor mechanism, shedding light on the complex relationships between gut microbiota and SLE risk

occurrence, and providing a reference for the future scientific treatment of SLE.

Materials and methods

Participants

This is a cross-sectional study conducted between December 2018 and August 2019, in which 54 patients diagnosed with systemic lupus erythematosus (SLE) at the Second Hospital of Shanxi Medical University were enrolled. Additionally, 55 negative controls (NC) who had no history of rheumatic immune diseases or family history were also recruited at the Physical Examination Centre of Shanxi Provincial People's Hospital. The inclusion criteria for the study were as follows: patients with primary SLE diagnosed by a rheumatologist and who met the 1997 classification criteria for SLE as revised by the American College of Rheumatology (Hochberg, 1997). Exclusion criteria included patients with other autoimmune diseases, those who had received immunosuppressant or antibiotic therapy in the past 2 months, those with incomplete clinical data, those who were pregnant, those with special dietary habits, and those with severe hepatic and renal insufficiency.

Ethics approval for the study was obtained from the Ethics Committee of the Second Hospital of Shanxi Medical University (Ethics No.: 2019-YX-107), and all patients provided informed consent. The study workflow is illustrated in Figure 1.

Sample collection and experiments

Demographic information, including age and gender, was collected from study participants before the experiment. Stool samples were collected from both the SLE and NC groups after defecation during admission or health examination, and stored at -80°C in a protective solution using sterile cotton swabs for subsequent sequencing. The detection of microorganisms in the intestinal flora is based on the Illumina MiSeq sequencing platform, which employs bipartite sequencing technology to construct sequence libraries of small fragments that can be analyzed by sequencing. By splicing and filtering the Reads, clustering or noise reduction to obtain the Operational Taxonomic Unit (OTU), and then annotating and analyzing the abundance of the species, the species composition of the intestinal flora of the research object can be revealed.

The experiment procedures consist of DNA extraction and Illumina sequencing, Operational taxonomic unit (OTU) cluster analysis and species annotation and Bioinformatics analysis, as previously described (Xin et al., 2022).

According to the manufacturer's instructions, we first removed the fecal specimens adsorbed with enteric flora from the cannula and extracted the total DNA of the microorganisms in the samples using the MagMAX^{TM} Nucleic Acid Separation Kit; we tested the DNA quality of the samples by agar gel electrophoresis, NanoDrop One and Qubit 4 (Thermo Fisher Scientific); we extracted the DNA, and analyzed it by Phanta EVO Ultra The DNA was extracted and amplified by Phanta EVO Ultra Fidelity DNA Polymerase (Vazyme) to amplify the highly variable region of V3-V4 of the microbial 16S rRNA gene. The product was purified and recovered by FC magnetic bead kit (enlightenment). After purification, the concentration of the purified product was detected by Qubit 4, and its length distribution was detected on a Qsep100 Bioanalyzer, and the fragment length was basically in the range of 350-400 bp. Each PCR product was mixed homogeneously at the same final concentration and sequenced 75 bp bipartite using the Illumina MiSeq platform using MiSeq V2 reagent.

Pairs of raw data were acquired by sequencing using the Illumina Miseq platform, followed by preprocessing of the raw data, i.e., quality control, including low-quality filtering, and length filtering, to obtain high-quality sequences. When the single-end sequencing Read was less than 50 bp, the pair of Paired Reads was deleted.When the single-end sequence read contained bases (Q value< 5) less than 50% of the read length, the read was deleted.The above steps were performed in Fastp software.

In addition, host genes were deleted using Bowtie2 software, i.e., comparing them with the host sequence and filtering out reads that may be of host origin.Finally, quality-controlled Clean Reads were compared with microbial databases using Kraken2 software to obtain microbial data. In order to study the diversity information of microbial composition of the samples, the valid sequences of all samples were clustered into OTUs using Vsearch 2.4.4 with 97% similarity (Hu et al., 2022). The representative sequences were then analyzed by Silva128 database (http://www.arb-silva.de/) for species annotation and taxonomy.

Also, we discuss the α diversity and β diversity between the two groups. As for the β diversity, both Principal Co-ordinates Analysis (PCoA) based on the Bray-Curtis distance matrix and Permutation-based Multivariate Analysis of Variance (PERMANOVA) and Non-metric multidimensional scaling (NMDS) were employed to determine the significance of the difference (Franklin et al., 2022).

Feature selection

Feature selection is a crucial step in data mining, which eliminates irrelevant and redundant features while preserving the original data's value. It improves the data quality and reduces computational costs, enhancing the model's generalization ability (Abbasi Mesrabadi et al., 2023). In the analysis of intestinal microbiota in SLE patients, characterizing microbiota data at the taxonomic level and removing redundant and irrelevant features is necessary to reduce noise. ML algorithms offer three feature selection methods: filtering, packaging, and embedding (Saha et al., 2022). This study uses embedded-based Elastic Net and packaging-based Boruta algorithms due to the differences in the subset of features selected by different methods.

The Elastic Net algorithm is a linear regression model that utilizes L1 and L2 regularization matrices. It inherits the sparsity of

10.3389/fcimb.2023.1289124

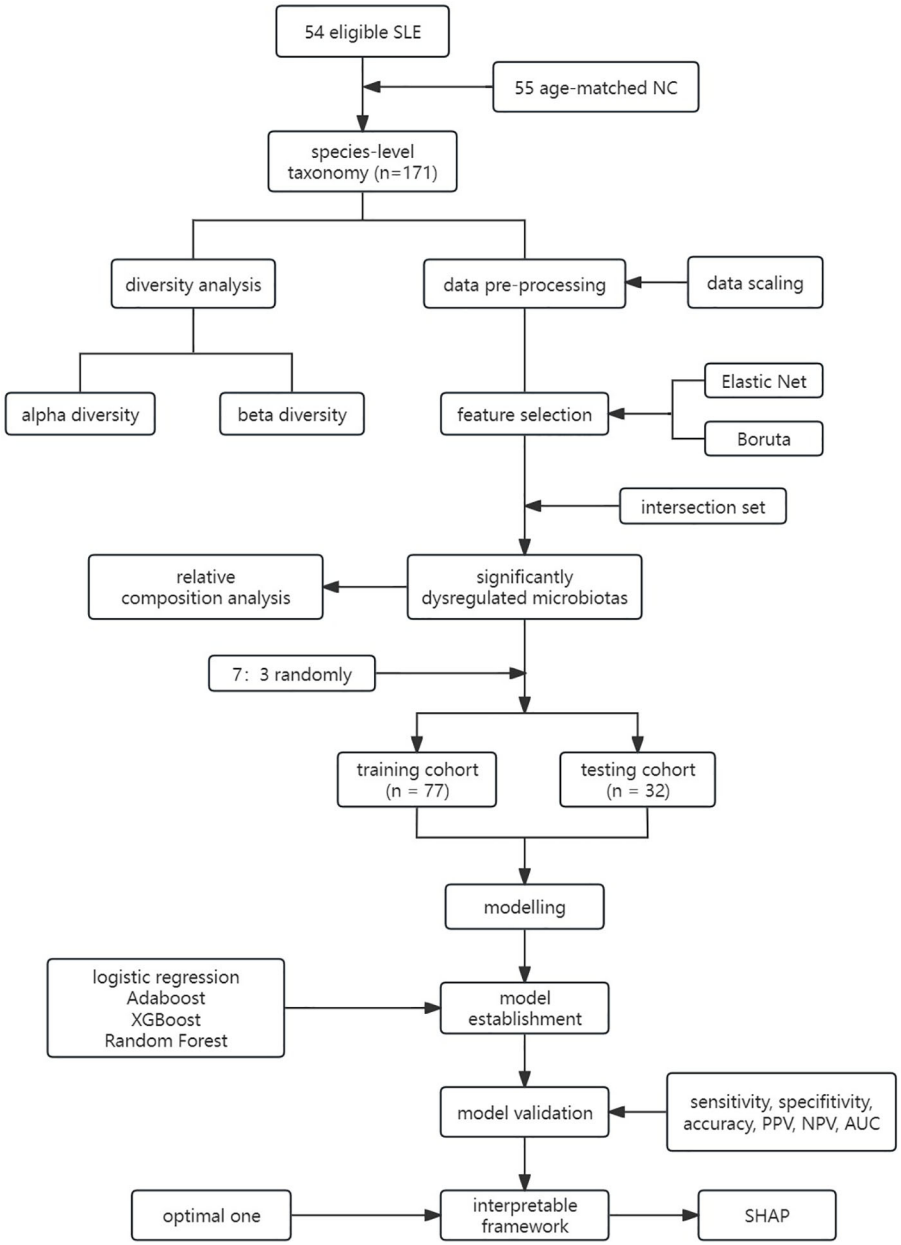

FIGURE 1
Workflow of this study. LR, Logistic Regression; LASSO, Least Absolute Shrinkage and Selection Operator; CART, Classification and Regression Tree; Adaboost, Adaptive Boosting; XGBoost, Extreme Gradient Boosting; RF, Random Forest; PPV, Positive Predicted Value; NPV, Negative Predicted Value; AUC, Area Under the Curve.

the LASSO method and the stability of the ridge regression L2 regularization. Elastic Net combines the two to obtain an optimal sparse model when cross-validating feature selection while compensating for the correlation between observed variables. Most feature selection methods seek the feature set that minimizes the model's loss function. In contrast, Boruta selects a set of features relevant to the outcome. It is a wrapping algorithm for all relevant feature selections and identifies all features related to classification in the candidate features, determining the optimal subset of features (Kursa and Rudnicki, 2010; Kursa and Rudnicki, 2010).

Model construction

To investigate the potential of the intestinal significantly dysregulated microbiota as a biomarker for SLE, four ML algorithms were utilized to establish the relationship between 16 SDMs and SLE. These algorithms include logistic regression (LR), adaptive boosting (AdaBoost), eXtreme gradient boosting (XGBoost), and Random Forest (RF).

LR is a generalized linear model that assumes a Bernoulli distribution for the dependent variable y. Logistic regression introduces the Sigmoid function to better handle nonlinear

classification problems, unlike linear regression, which assumes a Gaussian distribution for y (LaValley, 2008; Meurer and Tolles, 2017). AdaBoost is a fundamental ML algorithm that assigns different weights to the bit error rate of the weak classifier to create a strong classifier (Sevinç, 2022). XGBoost is an enhanced algorithm that combines individual learners to efficiently construct parallel operations on the augmented tree (Davagdorj et al., 2020). By adding regular terms to the original function, it reduces the possibility of overfitting and accelerates the convergence speed (Ogunleye and Wang, 2020). RF is an ensemble learning algorithm that constructs multiple classification trees based on autonomously sampled training data. It selects independent variables to achieve decorrelation between trees, which in turn reduces the model variance. The final classification result is obtained by aggregating the results of multiple trees (Liu et al., 2022).

In summary, these algorithms were chosen for their ability to handle nonlinear classification problems, reduce overfitting, and achieve strong generalization ability.

Model evaluation

This study employs various performance evaluation metrics for ML algorithm models, including Accuracy, Sensitivity, Specificity, Positive Predictive Value (PPV), Negative Predictive Value (NPV), and the receiver operating characteristic curve (ROC curve) with Area under the Curve (AUC).

SHAP interpretability framework

SHAP is an additivity interpretation framework developed by Lundberg et al. and is based on the ideas of game theory (Li et al., 2023). For any individual, the prediction model outputs a prediction, and the SHAP framework assumes that each feature is a "contributor" to the target prediction and assigns Shapley values to them. The sum of the cumulative Shapley value of the target prediction and the average prediction value gives the contribution of all features of the individual.

The shapley value for a particular feature x_j represents the average marginal contribution of that feature to the prediction. The difference between the predictions with and without feature x_j is obtained by calculating the difference between the predictions with and without feature x_j for all possible combinations, specifically by weighted summation with all possible combinations of features:

EQUATION 1

$$\Phi_j(val) = \sum_{S \subseteq \{x_1,\ldots,x_p\} \setminus \{x_j\}} \frac{|S|!\,(p-|S|-1)!}{p!} \left(val(S \cup \{x_j\}) - val(S)\right) \quad (1)$$

EQUATION 2

$$val(S) = \int \hat{f}(x_1,\ldots,x_p) d\mathbb{P}_{x \notin S} - E_x\left(\hat{f}(X)\right) \quad (2)$$

x represents the feature value of the individual to be interpreted, $S \subseteq \{x_1,\ldots,x_p\} \setminus \{x_j\}$ is the subset of all features excluding $\{x_j\}$, p is the number of features in the subset, $val(S \cup \{x_j\})$ denotes the prediction of all features in the subset that contains $\{x_j\}$, $val(S)$ is the prediction of the subset S that does not contain $\{x_j\}$ of all feature, $E_x(\hat{f}(X))$is the predicted expectation of all features, where $\frac{|S|!\,(p-|S|-1)!}{p!}$ is the weight of the subset S. For the understanding of the weights of subset S: p features have p!possibilities under any ordering, and after determining the subset S, p features have $|S|!\,(p-|S|-1)!$ kinds of possibilities, so $\frac{|S|!\,(p-|S|-1)!}{p!}$ is the possible share of feature combinations for subset S.

Positive SHAP values (>0) indicate a feature positively affects the predicted value, while negative SHAP values (<0) indicate an adverse impact (Jiang et al., 2021). SHAP provides both global and local explanations. Global explanations calculate the average SHAP value of each feature on the entire dataset, while local explanations determine the SHAP value of each feature for a single sample. The SHAP framework is useful in understanding the mechanism behind predictive models and making informed decisions.

Statistical analysis

The statistical analysis in this study was performed using R software (version 4.2.0). Continuous variables with normal distributions were reported as Mean ± Standard Deviation, while skewed variables were presented as median (interquartile range). Two-sample t-tests or Wilcoxon's rank sum tests were utilized to draw statistical inferences. To build the ML models, random sampling was employed to split the dataset into training sets (70%) and test sets (30%), respectively. The level of significance was set at $P< 0.05$.

Results

Baseline characteristics

This study enrolled a total of 54 female patients diagnosed with SLE and 55 healthy women in the NC group. The mean age of SLE patients was 39.0 (32.0, 50.0) years, while the mean age of the NC group was 34.0 (28.0 to 53.0) years. The age difference was not statistically significant (P = 0.111), as shown in Table 1.

Diversity analysis

This study employed alpha diversity to assess the richness and evenness of intestinal microbiota in SLE patients. The findings indicated that the Chao1 and Richness indices of the SLE group were significantly lower than those of the NC group (P< 0.001), indicating reduced bacterial Richness in the SLE group (Figures 2A, B).

TABLE 1 Comparision of age in two groups.

Variable	NC (N=55)	SLE (N=54)	p
age	39.00 (32.00 to 50.00)	34.00 (28.00 to 53.00)	0.111

10.3389/fcimb.2023.1289124

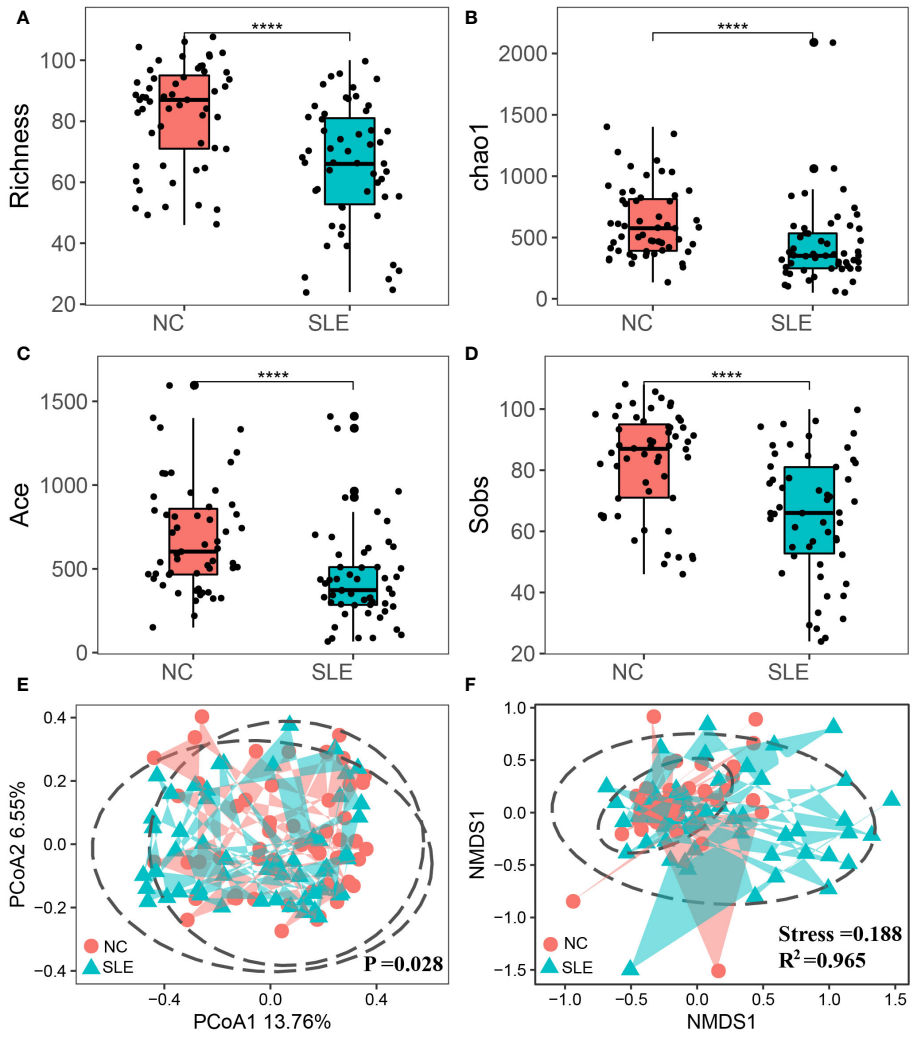

FIGURE 2
Comparison of alpha and beta diversity between SLE and NC groups. The points in the figure represent samples; *P<0.0001; **(A)** chao1 index; **(B)** Richness index; **(C)** Sobs index; **(D)** Shannon index; **(E)** Principal Co-ordinates Analysis; the closer the distance between samples, the more similar the species; **(F)** Non-metric multi-dimensional scale analysis, the closer the distance between samples, the higher the similarity between samples; Stress value<0.2 indicated that NMDS could explain the similarity of sample structure to some extent; The R^2 was defined as the ratio of variance to the total variance of each group, and higher R^2 values indicated a higher degree of explanation for sample differences between different groups.

Furthermore, the Ace and Sobs indices of the SLE group were also significantly lower than those of the NC group (P< 0.05), suggesting an abnormal Evenness in the SLE group (Figures 2C, D).

Beta diversity was utilized to assess the structural composition similarity of intestinal flora. PCoA analysis revealed that Coordinate 1 accounted for 13.76% and Coordinate 2 occupied 6.55%. Also, the PERMANOVA analysis demonstrated that there were significant structural differences between the two groups (P = 0.028). Additionally, NMDS analysis indicated dissimilarity of species composition between the two groups, as demonstrated in Figures 2E, F.

Feature selection

In total, there were 171 microbial species, which were considered for feature selection. To obtain a subset of highly correlated and non-redundant flora, Elastic Net and Boruta were utilized for feature selection. The parameters of Elastic Net for α equals 0.3 and for $Lambda_{min}$ equals 0.085. Besides, the parameters employed for Boruta were as follows: doTrace=1, ntree=500, and maxRuns=350. The resulting flora subsets consisted of 68 and 21 features in Elastic Net and Boruta, respectively (Figures 3A, B). Among these subsets, 16 SDMs were identified (Figure 3C).

Among them, the abundance of *Faecalibacterium_prausnitzii*, *Eubacterium_eligens*, *Dialister_succitiphilus*, and *Roseburia_intestilis*, while *Roseburia_inulinivorans*, *Vallitalea_pronyensi*, *Pseudobutyrivibrio_ruminis*, *Papillibacter_cinmivorans*, and *Clostridium_asparagiforme* were comparatively higher in SLE group, while the abundance of *Escherichia_fergusonii* and *Bacteroides_fragilis* were higher in the SLE group, with *Blautia_wexlerae*, *Eubacterium_hallii*, *Blautia_faecis*, *Clostridium_aldenense*, and *Dorea_longicate* showing a slightly higher abundance in the SLE group as well (Figure 3D).

10.3389/fcimb.2023.1289124

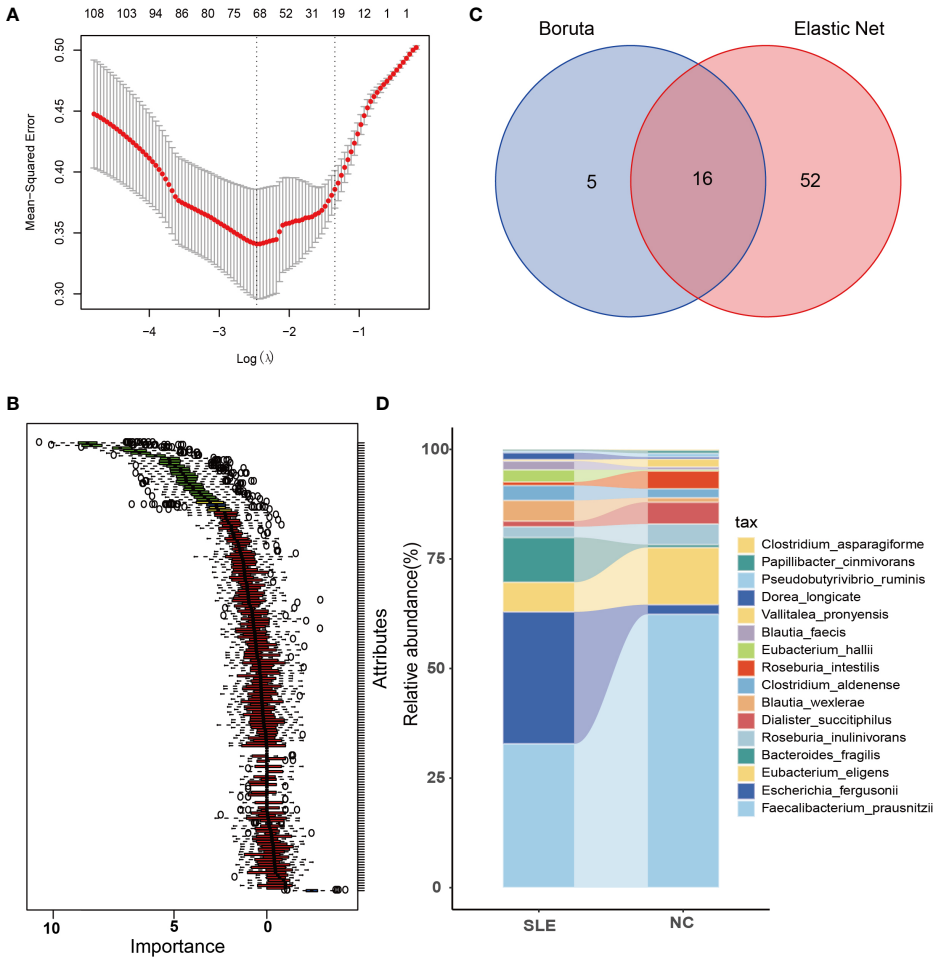

FIGURE 3
Feature selection and comparison of SDMs between the two groups. **(A)** When Log (Lamda) is taken the smallest, there are 68 bacteria left after using Elastic Net for feature selection; **(B)** There are 21 bacteria left after using Boruta for feature selection, the red part in the figure is the eliminated intestinal flora, and the green part is the remaining ones; **(C)** the intersected bacteria by using Elastic Net and Boruta, a total of 16, i.e. significantly dysregulated microbiotas (SDMs). **(D)** comparison of 16 SDMs in the two groups.

Comparison of SDMs in training and test sets

This study randomly allocate the training and testing sets, achieving a balanced ratio of 39:38 for NC and SLE in the training set, and 16:16 in the testing set. This balanced ratio of 1:1 was implemented to mitigate any adverse impact on model training arising from class imbalance. Additionally, a rank sum test was conducted to ensure the comparability of microbiota in both sets and to facilitate an accurate evaluation of model performance. The findings revealed no statistically significant difference ($P > 0.05$) in the 16 SDMs between the groups in both sets, as demonstrated in Figure 4.

Model evaluation

In this study, model performance evaluation was conducted using Accuracy, Sensitivity, Specificity, PPV, NPV and AUC. As shown in Table 2, all four ML algorithms showed commendable classification performance, with values exceeding 0.750 for all metrics. Specifically, LR achieved a value of 0.750 for each metric. AdaBoost achieved an Accuracy, Sensitivity, Specificity, PPV, and NPV of 0.844, 0.875, 0.813, 0.824, and 0.867, respectively. XGBoost exhibited metrics of 0.844, 0.750, 0.938, 0.923 and 0.930, while RF achieved metrics of 0.875, 0.750, 1.000, 1.000, and 0.800. AUC values were ranked as follows: XGBoost (0.930), RF (0.875), AdaBoost (0.844), and LR (0.750), demonstrating the high performance of the models.

XGBoost-SHAP interpretable framework

This study employed the XGBoost algorithm in combination with the SHAP interpretability framework, owing to the former's superior performance compared to other models. The SHAP values of 16 SDMs were outputted to obtain global and partial dependence plots for the SLE risk of disease. The SHAP global dependency plot in Figure 5 ranks the importance of XGBoost algorithm variables

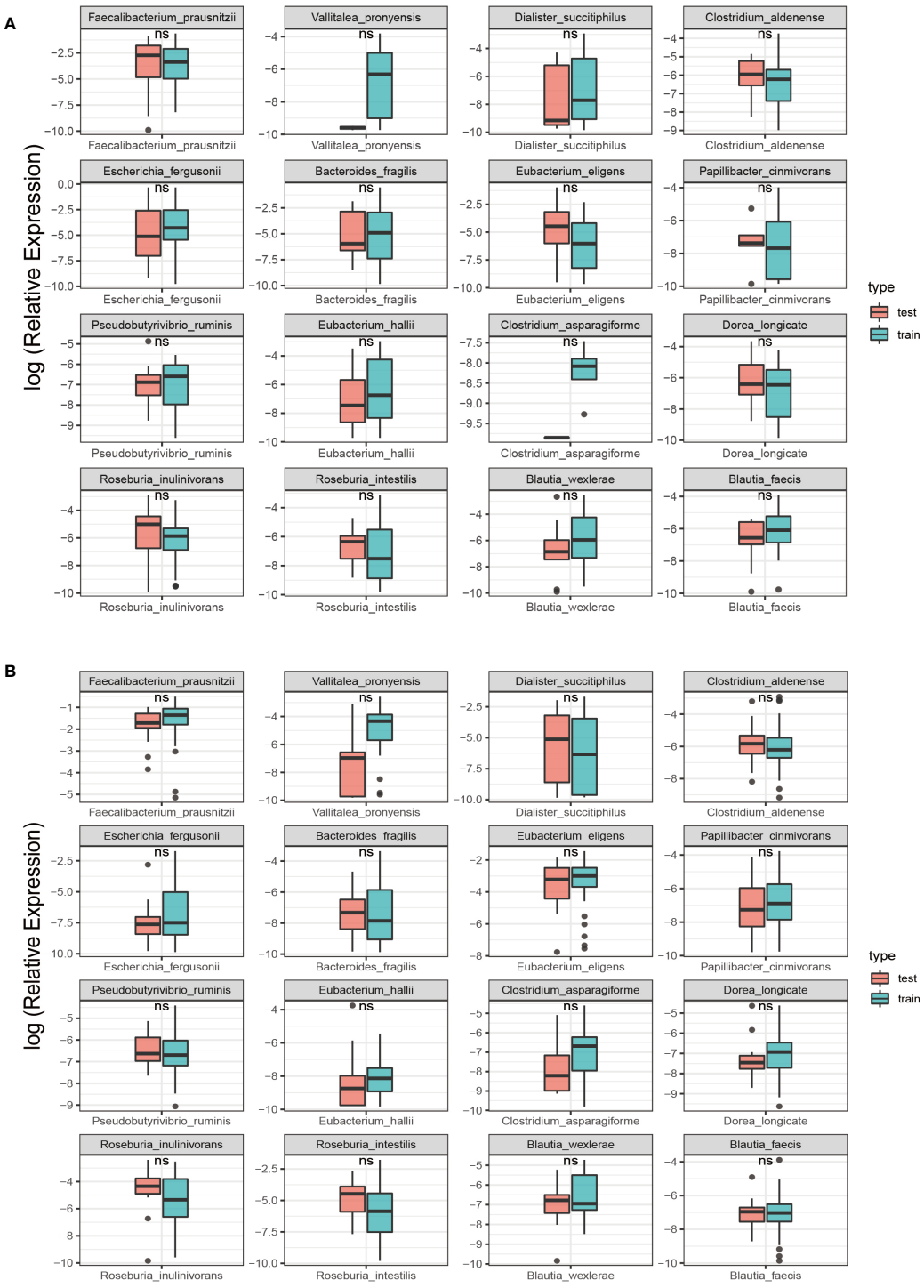

FIGURE 4
Comparison of SDMs between the training and test sets in the two groups. Red represents the testing set; Green represents the training set; ns, non-significant, P > 0.05; **: P< 0.01. **(A)** SLE group; **(B)** NC group.

and their respective positive and negative effects on SLE. The top 10 bacteria in terms of importance are *Escherichia_fergusonii*, *Faecalibacterium_prausnitzii*, *Eubacterium_eligens*, *Clostridium_aldenense*, *Vallitalea_pronyensis*, *Dorea_longicate*, *Blautia_faecis*, *Roseburia_intestilis*, *Roseburia_inulinivorans*, and *Papillibacter_cinmivorans*. The colour gradient from low to high represents the feature value from small to large, while the positive and negative SHAP values denote the correlation between the feature and the prediction result. For instance, a negative value for *Eubacterium_eligens* in a sample with a large value suggests a reduced risk of SLE. The SHAP value is mainly concentrated in the region with a positive SHAP value in the lower half of the colour gradient in the figure, indicating that the higher the relative expression of *Roseburia_intestilis*, the lower the risk of SLE.

TABLE 2 Model performance evaluation of four algorithms.

Algorithms	Accuracy	Sensitivity	Specificity	PPV	NPV	AUC
LR	0.750	0.750	0.750	0.750	0.750	0.750
Adaboost	0.844	0.875	0.813	0.824	0.867	0.844
XGBoost	0.844	0.750	0.938	0.923	0.790	0.930
RF	0.875	0.750	1.000	1.000	0.800	0.875

PPV, Positive Predicted Value; NPV, Negative Predicted Value.

However, the SHAP global dependency plot is limited in its ability to accurately reveal the relationship between each feature and SLE. Therefore, we analyzed the SHAP partial dependency plot to better comprehend the impact of feature samples on SLE, as depicted in Figure 6. Each point in the plot represents the sample value of that feature, where the abscissa denotes the magnitude of the feature value and the ordinate represents the SHAP value of the corresponding feature. For *Faecalibacterium_prausnitzii*, the SHAP value indicates a trend of first decreasing and then rising, implying that the relative expression of the bacterium and the risk of SLE exhibit a complex nonlinear relationship, with a lower risk first and higher risk afterwards.

Discussion

Women's health is a crucial issue in contemporary society, and research indicates that gut microbiota plays a vital role in women's health. However, the aetiology of SLE, a female-dominated immune disease, remains incompletely understood. This study aimed to explore the dysregulation of gut microbiota in SLE patients and identify significantly dysregulated microbiota in SLE patients in comparison with NC using ML algorithms.

In this study, we found significant differences in alpha and beta diversity between the SLE and NC groups, indicating gut microbiota dysregulation in SLE patients, which is consistent with prior findings in related immune diseases, such as autoimmune hepatitis (Wei et al., 2020), rheumatoid arthritis (Qiao et al., 2022), and primary dry syndrome (Siddiqui et al., 2016). The investigation identified 16 significantly dysregulated microbial taxa in SLE patients using Elastic Net and Boruta. We also revealed a complex relationship between the relative abundance of each bacterium and the risk of SLE using the SHAP interpretability framework.

Feature selection (Açıkoğlu and Tuncer, 2020) is a common data preprocessing method used in ML modelling. It reduces model

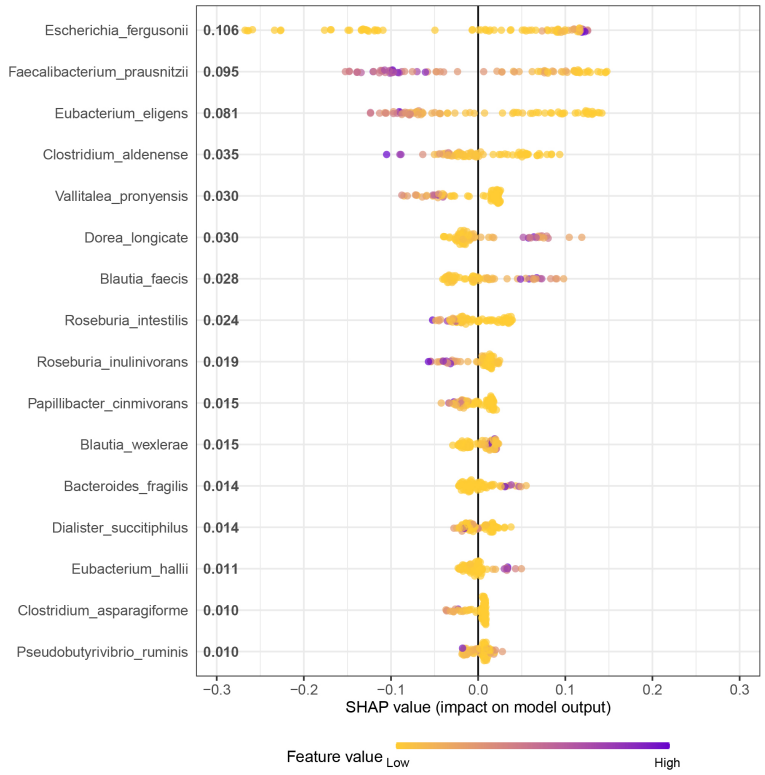

FIGURE 5
XGBoost-SHAP partial dependency plot Analysis for Distribution of Feature Importance in SLE occurrence risk.

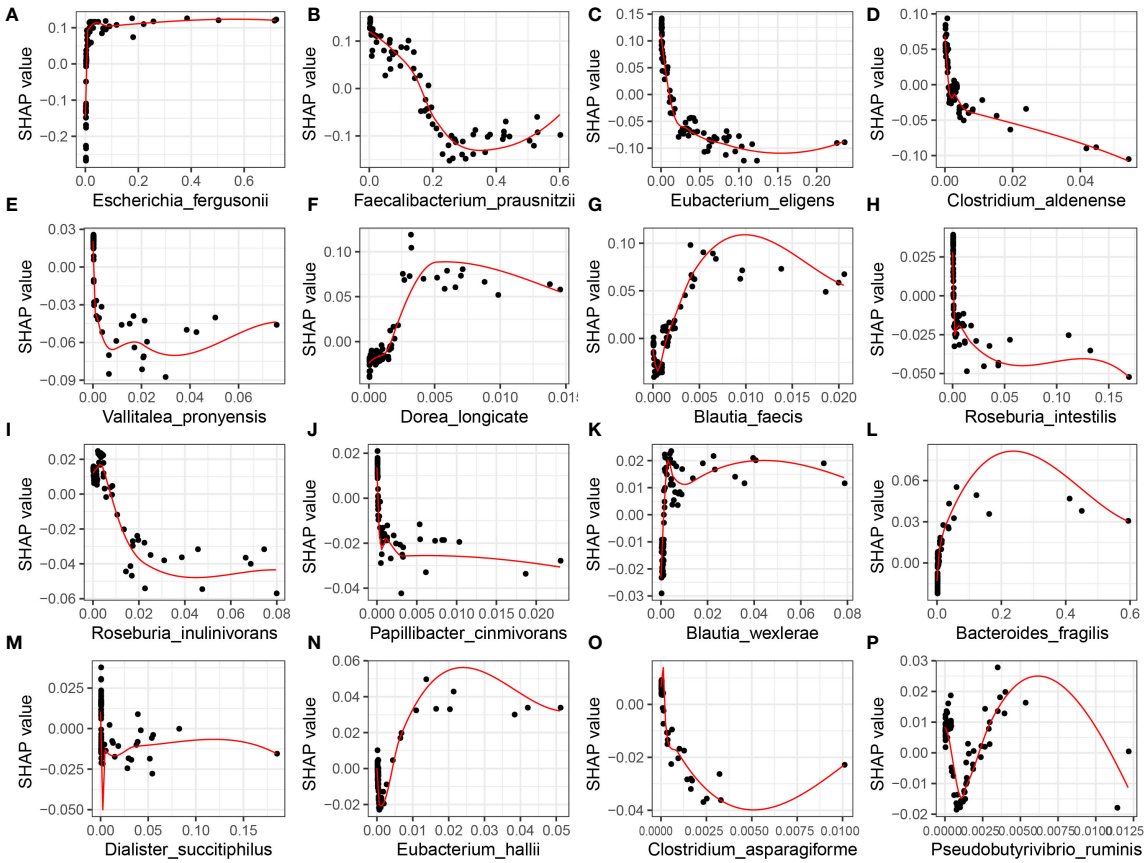

FIGURE 6
XGBoost-SHAP Global Dependence Plot Analysis for Distribution of Feature Importance in SLE occurrence risk. The distribution of the impact of each feature on the model is displayed in the figure, where each point corresponds to a sample and the colour of the point represents the magnitude of the variable value. The variable values are colour-coded from yellow to purple, corresponding to a high-to-low gradient. The x-axis represents relative abundance. **(A)** *Escherichia_fergusonii*; **(B)** *Faecalibacterium_prausnitzii*; **(C)** *Eubacterium_eligens*; **(D)** *Clostridium_aldenense*; **(E)** *Vallitalea_pronyensis*; **(F)** *Dorea_longicate*; **(G)** *Blautia_faecis*; **(H)** *Roseburia_intestilis*; **(I)** *Roseburia_inulinivorans*; **(J)** *Papillibacter_cinmivorans*; **(K)** *Blautia_wexlerae*; **(L)** *Bacteroides_fragilis*; **(M)** *Dialister_succitiphilus*; **(N)** *Eubacterium_hallii*; **(O)** *Clostridium_asparagiforme*; **(P)** *Pseudobutyrivibrio_ruminis*.

complexity and improves accuracy by selecting a subset of features with strong discriminatory power. Among the significantly dysregulated microbial taxa, *Faecalibacterium_prausnitzii*, *Eubacterium_eligens*, and *Roseburia_intestilis* were found to be more abundant in the NC group, while *Escherichia_fergusonii* and *Bacteroides_fragilis* were more abundant in the SLE group. These microbial taxa are associated with gut health, systemic inflammation, and immune diseases. *Roseburia_intestilis* is a butyrate-producing bacterium that maintains gut health and alleviates systemic inflammation through the production of metabolites. It has the potential to improve atherosclerosis (Kasahara et al., 2018; Nie et al., 2021). *Faecalibacterium_prausnitzii* is one of the most common gut bacteria in healthy adults. Changes in its abundance may lead to the occurrence of immune diseases (Miquel et al., 2013; Lopez-Siles et al., 2017). *Eubacterium_eligens* plays an important role in intestinal inflammation. Studies have shown that its abundance is significantly reduced in patients with atherosclerosis (Liu et al., 2020) and hypertension (Nakai et al., 2021). *Escherichia_fergusonii* is a pathogenic bacterium that causes infections in humans and animals (Gaastra et al., 2014) and is overexpressed in the gut of non-alcoholic fatty liver disease patients (Xin et al., 2022). An increase in its abundance may contribute to the development of SLE. Previous studies have shown that the abundance of *Proteobacteria* increases, while *Ruminococcaceae* decreases in the gut microbiome of SLE patients (Hevia et al., 2014; Wei et al., 2019). This is not consistent with this study, which may be caused by regional differences.

The nonlinearity between gut microbiota and SLE has not been adequately modelled due to high dimensionality and significant inter-individual variability of gut microbiota (Qutrio Baloch et al., 2020). Recent advancements in artificial intelligence and big data have led to the emergence of data-driven ML algorithms in medical research (Ngiam and Khor, 2019). In this study, we divided the gut microbiota data into training and testing sets, with a 7:3 ratio, respectively. The feasibility of this approach was confirmed by the non-statistically significant differences of the 16 SDMs between the two datasets and a 1:1 SLE to NC ratio.

In this study, XGBoost showed the best performance, followed by RF. RF is a classifier that can be trained and used for prediction through multiple decision trees (Zhang et al., 2023). It is capable of adapting to complex datasets and improves the richness, generalizability, stability, and accuracy of the results by using random sampling (Yu and Zeng,

2022). This method can effectively avoid overfitting, and therefore, the overall performance of the RF was better than other algorithms, second only to XGBoost. Boosting is an effective ML technique that transforms basic weak classifiers into strong classifiers using ensemble algorithm theory to achieve better classification performance (Davagdorj et al., 2020). XGBoost demonstrated robustness and improved the model's accuracy, avoiding overfitting and being less constrained by linear, collinear, and other issues compared to traditional models (Liang et al., 2021). Therefore, the performance of XGBoost was better than that of other algorithms.

Although sophisticated algorithms can potentially benefit patients by improving accuracy in clinical decision-making, their ambiguous decision-making processes create a "black box" dilemma. To address this issue, SHAP feature attribution analysis was employed to determine the influence of each attribute on the final model output, thereby improving the model's interpretability. This study is the first to use SHAP to explore the impact of microbiota on SLE, revealing how changes in the relative abundance of SDMs affect the risk of SLE. For example, an increase in the relative abundance of *Escherichia_fergusonii* was found to increase the risk of SLE, while the relationship between *Faecalibacterium_prausnitzii* and SLE risk was complex and non-linear. However, the risk of SLE increased after a certain reduction in the relative abundance of *Faecalibacterium_prausnitzii*, suggesting that intestinal flora can be used as a dynamic detection index for SLE to identify high-risk groups. Clinical trials are necessary to validate the model and guide clinicians in conducting reasonable interventions on the flora that increase the risk of SLE, thus providing a new direction for individualized treatment of SLE.

While there is a large body of research exploring the relationship between the gut microbiota and SLE (Chen et al., 2022; Mohd et al., 2023; Toumi et al., 2023), it is important to note that our study focused specifically on female participants. This thoughtful choice was made due to the higher prevalence of SLE in women, making our study more gender-specific and relevant to the population most affected by the disease. This unique approach allowed us to gain insight into how SLE manifests itself in more common groups. In addition, our study first introduced ML-based SHAP to investigate how specific microbial communities influence the occurrence of SLE. This innovative approach provides a more detailed understanding of the key microbial factors contributing to the development of SLE, allowing us to analyze the complex relationship between gut microbiota and SLE more comprehensively.

The study has several limitations. Firstly, the sample size was small, and the data were collected from only one hospital in Shanxi province, which may limit the generalizability of the results. To enhance the robustness of our findings, future studies should aim to include larger sample sizes from different regions to more fully control for potential confounders and to improve the external validity of the results. Additionally, the study only controlled for age, and other confounders may have affected the results. Future research should include larger sample sizes from multiple regions to better control for other confounders and to verify the reliability of the findings. Furthermore, the study did not analyze the metabolic pathways of the SDMs, making it challenging to speculate whether the SDMs contributed to inflammation and immune responses leading to disease. Future studies may benefit from metabolomic analyses to elucidate these potential mechanistic links. Lastly, the SHAP results were not experimentally validated, limiting the study's conclusions. Further studies should aim to experimentally validate the SHAP results and improve the credibility of our findings and their applicability in clinical practice.

Conclusion

By comparing the composition of intestinal flora in SLE and NC groups, this study showed that the alpha and beta diversity of intestinal flora in SLE patients were significantly different from that of NC individuals, which suggests dysregulation of intestinal flora in SLE patients. Additionally, this study revealed the characteristics of the intestinal microbiota in SLE patients. ML algorithms combined with SDMs can be used to identify SLE individuals, especially the XGBoost algorithm, which facilitates SLE prediction and provide a reference for clinical decision-making. Moreover, SHAP analysis helps to identify the relationship between SDMs and the risk of SLE, which provides valuable information for improving scientific treatment for SLE in the future.

Data availability statement

The data presented in the study are deposited in the NCBI repository, accession number PRJNA1045348.

Author contributions

WS: Writing – original draft, Conceptualization. FW: Formal analysis, Writing – review & editing. YY: Writing – review & editing. YHL: Supervision, Writing – review & editing. QW: Validation, Writing – review & editing. XH: Methodology, Writing – review & editing. YFL: Funding acquisition, Investigation, Supervision, Writing – review & editing.

Funding

The author(s) declare financial support was received for the research, authorship, and/or publication of this article. This work was supported by the National Natural Science Foundation of China (Grant No. 82170716).

Acknowledgments

We appreciate all the authors and patients participating in this study. We're also indebted to those who helped us a lot during our writing.

Conflict of interest

The authors declare that the research was conducted in the absence of any commercial or financial relationships that could be construed as a potential conflict of interest.

Publisher's note

References

Abbasi Mesrabadi, H., Faez, K., and Pirgazi, J. (2023). Drug-target interaction prediction based on protein features, using wrapper feature selection *Sci Rep.* 13 (1), 3594. doi: 10.1038/s41598-023-30026-y

Açıkoğlu, M., and Tuncer, S. A. (2020). Incorporating feature selection methods into a machine learning-based neonatal seizure diagnosis. *Med. Hypotheses* 135, 109464. doi: 10.1016/j.mehy.2019.109464

Barber, M. R. W., Drenkard, C., Falasinnu, T., Hoi, A., Mak, A., Kow, N. Y., et al. (2021). Global epidemiology of systemic lupus erythematosus. *Nat. Rev. Rheumatol.* 17 (9), 515–532. doi: 10.1038/s41584-021-00668-1

Belur Nagaraj, S., Pena, M. J., Ju, W., and Heerspink, H. L. (2020). Machine-learning-based early prediction of end-stage renal disease in patients with diabetic kidney disease using clinical trials data. *Diabetes Obes. Metab.* 22 (12), 2479–2486. doi: 10.1111/dom.14178

Boutet, A., Madhavan, R., Elias, G. J. B., Joel, S. E., Gramer, R., Ranjan, M., et al. (2021). Predicting optimal deep brain stimulation parameters for Parkinson's disease using functional MRI and machine learning. *Nat. Commun.* 12 (1), 3043. doi: 10.1038/s41467-021-23311-9

Chen, Y., Liao, R., Yao, Y., Wang, Q., and Fu, L. (2021). Machine learning to identify immune-related biomarkers of rheumatoid arthritis based on WGCNA network. *Clin. Rheumatol.* 41 (4), 1057-1068. doi: 10.1007/s10067-021-05960-9

Chen, Y., Lin, J., Xiao, L., Zhang, X., Zhao, L., Wang, M., et al. (2022). Gut microbiota in systemic lupus erythematosus: A fuse and a solution. *J. Autoimmunity.* 132, 102867. doi: 10.1016/j.jaut.2022.102867

Chiu, Y. M., and Lai, C. H. (2010). Nationwide population-based epidemiologic study of systemic lupus erythematosus in Taiwan. *Lupus* 19 (10), 1250–1255. doi: 10.1177/0961203310373780

Davagdorj, K., Pham, V. H., Theera-Umpon, N., and Ryu, K. H. (2020). XGBoost-based framework for smoking-induced noncommunicable disease prediction. *Int. J. Environ. Res. Public Health* 17 (18), 6513. doi: 10.3390/ijerph17186513

Fanouriakis, A., Tziolos, N., Bertsias, G., and Boumpas, D. T. (2021). Update on the diagnosis and management of systemic lupus erythematosus. *Ann. Rheum. Dis.* 80 (1), 14–25. doi: 10.1136/annrheumdis-2020-218272

Franklin, S., Aitken, S. L., Shi, Y., Sahasrabhojane, P. V., Robinson, S., Peterson, C. B., et al. (2022). Oral and stool microbiome coalescence and its association with antibiotic exposure in acute leukemia patients. *Front. Cell. Infect. Microbiol.* 12, 848580. doi: 10.3389/fcimb.2022.848580

Gaastra, W., Kusters, J. G., van Duijkeren, E., and Lipman, L. J. (2014). Escherichia fergusonii. *Veterinary Microbiol.* 172 (1-2), 7–12. doi: 10.1016/j.vetmic.2014.04.016

Golder, V., and Tsang, ASMWP. (2020). Treatment targets in SLE: remission and low disease activity state. *Rheumatol. (Oxford England)* 59 (Suppl5), v19–v28. doi: 10.1093/rheumatology/keaa420

Hevia, A., Milani, C., López, P., Cuervo, A., Arboleya, S., Duranti, S., et al. (2014). Intestinal dysbiosis associated with systemic lupus erythematosus. *mBio* 5 (5), e01548–e01514. doi: 10.1128/mBio.01548-14

Hochberg, M. C. (1997). Updating the American College of Rheumatology revised criteria for the classification of systemic lupus erythematosus. *Arthritis Rheum.* 40 (9), 1725. doi: 10.1002/art.1780400928

Hu, X., Fan, R., Song, W., Qing, J., Yan, X., Li, Y., et al. (2022). Landscape of intestinal microbiota in patients with IgA nephropathy, IgA vasculitis and Kawasaki disease. *Front. Cell. Infect. Microbiol.* 12, 1061629. doi: 10.3389/fcimb.2022.1061629

Jiang, Z., Bo, L., Xu, Z., Song, Y., Wang, J., Wen, P., et al. (2021). An explainable machine learning algorithm for risk factor analysis of in-hospital mortality in sepsis survivors with ICU readmission. *Comput. Methods Programs Biomed.* 204, 106040. doi: 10.1016/j.cmpb.2021.106040

Kasahara, K., Krautkramer, K. A., Org, E., Romano, K. A., Kerby, R. L., Vivas, E. I., et al. (2018). Interactions between Roseburia intestinalis and diet modulate atherogenesis in a murine model. *Nat. Microbiol.* 3 (12), 1461–1471. doi: 10.1038/s41564-018-0272-x

Kursa, M., and Rudnicki, W. (2010). Feature selection with boruta package. *J. Stat. Softw.* 36, 1–13. doi: 10.18637/jss.v036.i11

Kursa, M. B., and Rudnicki, W. R. (2010). Feature selection with the boruta package. *J. Stat. Softw.* 36, 1–13. doi: 10.18637/jss.v036.i11

LaValley, M. P. (2008). Logistic regression. *Circulation* 117 (18), 2395–2399. doi: 10.1161/CIRCULATIONAHA.106.682658

Lazar, S., and Kahlenberg, J. M. (2023). Systemic lupus erythematosus: new diagnostic and therapeutic approaches. *Annu. Rev. Med.* 74, 339–352. doi: 10.1146/annurev-med-043021-032611

Lee, Y. H., Choi, S. J., Ji, J. D., and Song, G. G. (2016). Overall and cause-specific mortality in systemic lupus erythematosus: an updated meta-analysis. *Lupus* 25 (7), 727–734. doi: 10.1177/0961203315627202

Li, X., Zhao, Y., Zhang, D., Kuang, L., Huang, H., Chen, W., et al. (2023). Development of an interpretable machine learning model associated with heavy metals' exposure to identify coronary heart disease among US adults via SHAP: Findings of the US NHANES from 2003 to 2018. *Chemosphere* 311 (Pt 1), 137039. doi: 10.1016/j.chemosphere.2022.137039

Liang, H., Jiang, K., Yan, T. A., and Chen, G. H. (2021). XGBoost: an optimal machine learning model with just structural features to discover MOF adsorbents of Xe/Kr. *ACS Omega* 6 (13), 9066–9076. doi: 10.1021/acsomega.1c00100

Liu, Y. H., Jin, J., and Liu, Y. J. (2022). Machine learning-based random forest for predicting decreased quality of life in thyroid cancer patients after thyroidectomy. *Supportive Care Cancer* 30 (3), 2507–2513. doi: 10.1007/s00520-021-06657-0

Liu, S., Zhao, W., Liu, X., and Cheng, L. (2020). Metagenomic analysis of the gut microbiome in atherosclerosis patients identify cross-cohort microbial signatures and potential therapeutic target. *FASEB J.* 34 (11), 14166–14181. doi: 10.1096/fj.202000622R

Lopez-Siles, M., Duncan, S. H., Garcia-Gil, L. J., and Martinez-Medina, M. (2017). Faecalibacterium prausnitzii: from microbiology to diagnostics and prognostics. *ISME J.* 11 (4), 841–852. doi: 10.1038/ismej.2016.176

Meurer, W. J., and Tolles, J. (2017). Logistic regression diagnostics: understanding how well a model predicts outcomes. *JAMA* 317 (10), 1068–1069. doi: 10.1001/jama.2016.20441

Miquel, S., Martín, R., Rossi, O., Bermúdez-Humarán, L. G., Chatel, J. M., Sokol, H., et al. (2013). Faecalibacterium prausnitzii and human intestinal health. *Curr. Opin. Microbiol.* 16 (3), 255–261. doi: 10.1016/j.mib.2013.06.003

Mohd, R., Chin, S. F., Shaharir, S. S., and Cham, Q. S. (2023). Involvement of gut microbiota in SLE and lupus nephritis. *Biomedicines* 11 (3), 653. doi: 10.3390/biomedicines11030653

Nakai, M., Ribeiro, R. V., Stevens, B. R., Gill, P., Muralitharan, R. R., Yiallourou, S., et al. (2021). Essential hypertension is associated with changes in gut microbial metabolic pathways: A multisite analysis of ambulatory blood pressure. *Hypertension (Dallas Tex 1979).* 78 (3), 804–815. doi: 10.1161/HYPERTENSIONAHA.121.17288

Ngiam, K. Y., and Khor, I. W. (2019). Big data and machine learning algorithms for health-care delivery. *Lancet Oncol.* 20 (5), e262–ee73. doi: 10.1016/S1470-2045(19)30149-4

Nie, K., Ma, K., Luo, W., Shen, Z., Yang, Z., Xiao, M., et al. (2021). Roseburia intestinalis: A beneficial gut organism from the discoveries in genus and species. *Front. Cell. Infect. Microbiol.* 11, 757718. doi: 10.3389/fcimb.2021.757718

Ogunleye, A., and Wang, Q. G. (2020). XGBoost model for chronic kidney disease diagnosis. *IEEE/ACM Trans. Comput. Biol. Bioinf.* 17 (6), 2131–2140. doi: 10.1109/TCBB.2019.2911071

Qiao, J., Wang, Y., Li, X., Jiang, F., Zhang, Y., Ma, J., et al. (2021). A Lancet Commission on 70 years of women's reproductive, maternal, newborn, child, and adolescent health in China. *Lancet (London England)* 397 (10293), 2497–2536. doi: 10.1016/S0140-6736(20)32708-2

Qiao, J., Zhang, S. X., Chang, M. J., Cheng, T., Zhang, J. Q., Zhao, R., et al. (2022). Specific enterotype of gut microbiota predicted clinical effect of methotrexate in patients with rheumatoid arthritis. *Rheumatol. (Oxford England)* 62 (3), 1087-1096. doi: 10.1093/rheumatology/keac458

Qutrio Baloch, Z., Raza, S. A., Pathak, R., Marone, L., and Ali, A. (2020). Machine learning confirms nonlinear relationship between severity of peripheral arterial disease, functional limitation and symptom severity. *Diagnostics (Basel Switzerland)* 10 (8), 515. doi: 10.3390/diagnostics10080515

Robinson, G. A., Waddington, K. E., Coelewij, L., Peng, J., Naja, M., Wincup, C., et al. (2021). Increased apolipoprotein-B:A1 ratio predicts cardiometabolic risk in patients with juvenile onset SLE. *EBioMedicine* 65, 103243. doi: 10.1016/j.ebiom.2021.103243

Saha, S., Priyoti, A. T., Sharma, A., and Haque, A. (2022). Towards an optimized ensemble feature selection for DDoS detection using both supervised and unsupervised method. *Sensors (Basel Switzerland)* 22 (23), 9144. doi: 10.3390/s22239144

Sammut, S. J., Crispin-Ortuzar, M., Chin, S. F., Provenzano, E., Bardwell, H. A., Ma, W., et al. (2022). Multi-omic machine learning predictor of breast cancer therapy response. *Nature* 601 (7894), 623–629. doi: 10.1038/s41586-021-04278-5

Samuelsson, I., Parodis, I., Gunnarsson, I., Zickert, A., Hofman-Bang, C., Wallén, H., et al. (2021). Myocardial infarctions, subtypes and coronary atherosclerosis in SLE: a case-control study. *Lupus Sci. Med.* 8 (1), e000515. doi: 10.1136/lupus-2021-000515

Sevinç, E. (2022). An empowered AdaBoost algorithm implementation: A COVID-19 dataset study. *Comput. Ind. Eng.* 165, 107912. doi: 10.1016/j.cie.2021.107912

Siddiqui, H., Chen, T., Aliko, A., Mydel, P. M., Jonsson, R., and Olsen, I. (2016). Microbiological and bioinformatics analysis of primary Sjogren's syndrome patients with normal salivation. *J. Oral. Microbiol.* 8, 31119. doi: 10.3402/jom.v8.31119

Song, W., Zhou, X., Duan, Q., Wang, Q., Li, Y., Li, A., et al. (2022). Using random forest algorithm for glomerular and tubular injury diagnosis. *Front. Med.* 9, 911737. doi: 10.3389/fmed.2022.911737

Toumi, E., Mezouar, S., Plauzolles, A., Chiche, L., Bardin, N., Halfon, P., et al. (2023). Gut microbiota in SLE: from animal models to clinical evidence and pharmacological perspectives. *Lupus Sci. Med.* 10 (1), e000776. doi: 10.1136/lupus-2022-000776

Tsang, ASMWP, and Bultink, I. E. M. (2021). New developments in systemic lupus erythematosus. *Rheumatol. (Oxford England)* 60 (Suppl 6), vi21–vvi8. doi: 10.1093/rheumatology/keab498

Wei, Y., Li, Y., Yan, L., Sun, C., Miao, Q., Wang, Q., et al. (2020). Alterations of gut microbiome in autoimmune hepatitis. *Gut* 69 (3), 569–577. doi: 10.1136/gutjnl-2018-317836

Wei, F., Xu, H., Yan, C., Rong, C., Liu, B., and Zhou, H. (2019). Changes of intestinal flora in patients with systemic lupus erythematosus in northeast China. *PloS One* 14 (3), e0213063. doi: 10.1371/journal.pone.0213063

Xin, X., Wang, Q., Qing, J., Song, W., Gui, Y., Li, X., et al. (2022). Th17 cells in primary Sjögren's syndrome negatively correlate with increased Roseburia and Coprococcus. *Front. Immunol.* 13, 974648. doi: 10.3389/fimmu.2022.974648

Xin, F. Z., Zhao, Z. H., Liu, X. L., Pan, Q., Wang, Z. X., Zeng, L., et al. (2022). Escherichia fergusonii Promotes Nonobese Nonalcoholic Fatty Liver Disease by Interfering With Host Hepatic Lipid Metabolism Through Its Own msRNA 23487. *Cell. Mol. Gastroenterol. Hepatol.* 13 (3), 827–841. doi: 10.1016/j.jcmgh.2021.12.003

Yen, E. Y., and Singh, R. R. (2018). Brief report: lupus-an unrecognized leading cause of death in young females: A population-based study using nationwide death certificates, 2000-2015. *Arthritis Rheumatol. (Hoboken NJ)* 70 (8), 1251–1255. doi: 10.1002/art.40512

Yu, X., and Zeng, Q. (2022). Random forest algorithm-based classification model of pesticide aquatic toxicity to fishes. *Aquat. Toxicol. (Amsterdam Netherlands)* 251, 106265. doi: 10.1016/j.aquatox.2022.106265

Zhang, H., Chi, M., Su, D., Xiong, Y., Wei, H., Yu, Y., et al. (2023). A random forest-based metabolic risk model to assess the prognosis and metabolism-related drug targets in ovarian cancer. *Comput. Biol. Med.* 153, 106432. doi: 10.1016/j.compbiomed.2022.106432

Zheng, X., Wang, F., Zhang, J., Cui, X., Jiang, F., Chen, N., et al. (2021). Using machine learning to predict atrial fibrillation diagnosed after ischemic stroke. *Int. J. Cardiol.* 347, 21-27. doi: 10.1016/j.ijcard.2021.11.005

Zou, Y. F., Feng, C. C., Zhu, J. M., Tao, J. H., Chen, G. M., Ye, Q. L., et al. (2014). Prevalence of systemic lupus erythematosus and risk factors in rural areas of Anhui Province. *Rheumatol. Int.* 34 (3), 347–356. doi: 10.1007/s00296-013-2902-1

frontiers | Frontiers in Cellular and Infection Microbiology

TYPE Original Research
PUBLISHED 11 January 2024
DOI 10.3389/fcimb.2023.1334213

OPEN ACCESS

EDITED BY
Gang Ye,
Sichuan Agricultural University, China

REVIEWED BY
Xingxing Yuan,
Heilongjiang Academy of Traditional Chinese Medicine, China
Hao Chi,
Macau University of Science and Technology, Macao SAR, China

*CORRESPONDENCE
Ming Pei
tjtcmpeiming@126.com

†These authors have contributed equally to this work and share first authorship

RECEIVED 06 November 2023
ACCEPTED 14 December 2023
PUBLISHED 11 January 2024

CITATION
Wang L, Xu A, Wang J, Fan G, Liu R, Wei L and Pei M (2024) The effect and mechanism of Fushen Granule on gut microbiome in the prevention and treatment of chronic renal failure. *Front. Cell. Infect. Microbiol.* 13:1334213. doi: 10.3389/fcimb.2023.1334213

The effect and mechanism of Fushen Granule on gut microbiome in the prevention and treatment of chronic renal failure

Lin Wang[1,2†], Ao Xu[1,2†], Jinxiang Wang[3†], Guorong Fan[1,2], Ruiqi Liu[4], Lijuan Wei[1,2] and Ming Pei[1,2*]

[1]Nephrology Department, First Teaching Hospital of Tianjin University of Traditional Chinese Medicine, Tianjin, China, [2]Graduate School, Tianjin University of Traditional Chinese Medicine, Tianjin, China, [3]Guangdong Provincial Key Laboratory of Digestive Cancer Research, Precision Medicine Center, Scientific Research Center, The Seventh Affiliated Hospital, Sun Yat-Sen University, Shenzhen, China, [4]Nephrology Department, Tianjin Academy of Traditional Chinese Medicine Affiliated Hospital, Tianjin, China

Background: Fushen Granule is an improved granule based on the classic formula Fushen Formula, which is used for the treatment of peritoneal dialysis-related intestinal dysfunction in patients with end-stage renal disease. However, the effect and mechanism of this granule on the prevention and treatment of chronic renal failure have not been fully elucidated.

Methods: A 5/6 nephrectomy model of CRF was induced and Fushen Granule was administered at low and high doses to observe its effects on renal function, D-lactate, serum endotoxin, and intestinal-derived metabolic toxins. The 16SrRNA sequencing method was used to analyze the abundance and structure of the intestinal flora of CRF rats. A FMT assay was also used to evaluate the effects of transplantation of Fushen Granule fecal bacteria on renal-related functional parameters and metabolic toxins in CRF rats.

Results: Gavage administration of Fushen Granule at low and high doses down-regulated creatinine, urea nitrogen, 24-h urine microalbumin, D-lactate, endotoxin, and the intestinal-derived toxins indophenol sulphateand p-cresol sulphate in CRF rats. Compared with the sham-operated group in the same period, CRF rats had a decreased abundance of the firmicutes phylum and an increased abundance of the bacteroidetes phylum at the phylum level, and a decreasing trend of the lactobacillus genus at the genus level. Fushen Granule intervention increased the abundance of the firmicutes phylum, decreased the abundance of the bacteroidetes phylum, and increased the abundance of the lactobacillus genus. The transplantation of Fushen Granule fecal bacteria significantly reduced creatinine(Cr), blood urea nitrogen(Bun), uric acid(UA), 24-h urinary microalbumin, D-lactate, serum endotoxin, and enterogenic metabolic toxins in CRF rats. Compared with the sham-operated group, the transplantation of Fushen Granule fecal bacteria modulated the Firmicutes and Bacteroidetes phyla and the Lactobacillus genus.

Conclusion: Fushen Granule improved renal function and intestinal barrier function by regulating intestinal flora, inhibiting renal fibrosis, and delaying the progression of chronic renal failure.

KEYWORDS

chronic renal failure, intestinal microecology, fecal microbiota transplantation, renal-intestinal axis, Fushen Granule

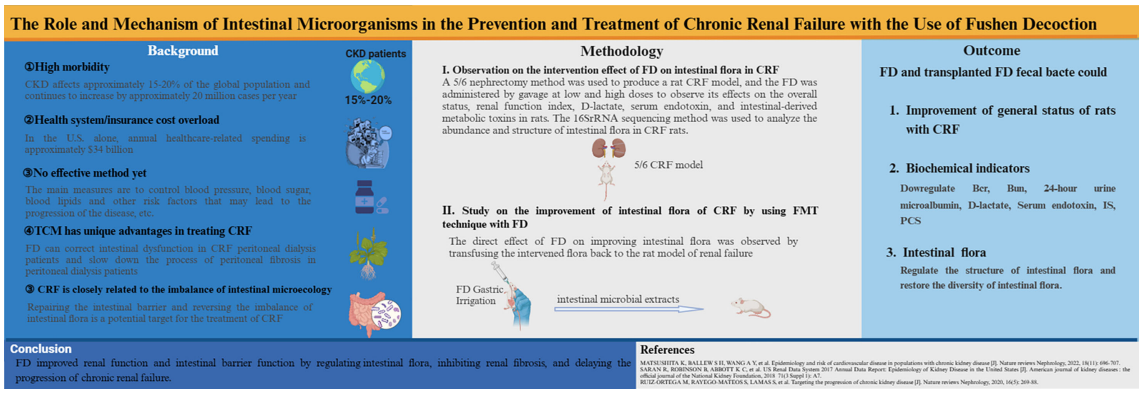

GRAPHICAL ABSTRACT

1 Introduction

Chronic renal failure (CRF) is a progressive disease resulting from various chronic kidney diseases (CKD), leading to abnormalities in kidney tissue structure and function until eventual failure (Fang et al., 2023). Its development into the final stage, end-stage renal disease (ESRD), poses a significant threat to human health and consumes considerable health resources(Wouters et al., 2015) (Dai et al., 2021; Wouk, 2021). Statistics show that CKD affects approximately 15-20% of the global population (Matsushita et al., 2022), with the number of cases increasing by about 20 million per year. The prevalence of CRF stands at 15.1% among adults in the US and 10.8% in China (Wang et al., 2021). As a late complication of CKD (Webster et al., 2017), ESRD is a major disease with high morbidity and mortality rates worldwide (Zhang et al., 2012; Liyanage et al., 2015). The cost of treating ESRD is currently staggering; in the US alone, it is estimated to be around US$34 billion per year (Saran et al., 2018). The burden of CRF on healthcare systems and health insurance costs has become a tremendous challenge for public health systems worldwide. Therefore, determining how to delay the disease process and improve patients' quality of life during the chronic kidney failure phase is a crucial issue in preventing and treating chronic kidney disease and end-stage renal disease.

The treatment of CRF still has no specific method in the international medical community, mainly to control protein intake, anti-oxidative stress, blood pressure, blood glucose and lipid control and other risk factors that may lead to the progression of the disease to slow down the deterioration (Ruiz-Ortega et al., 2020; Faria and de Pinho, 2021); Although there has been great progress in the study of molecular mechanisms and related markers, the clinical translation is poor. In recent years, more and more studies have demonstrated that the development of CRF is closely related to the imbalance of intestinal microecology, and that disorders of intestinal flora and disruption of intestinal barrier structure and function play an important role in disease progression (Yang et al., 2018; Pluznick, 2020). Intestinal dysfunction can be seen in the early stages of CRF, mainly in the form of digestive symptoms such as impaired digestion and absorption in the intestine, as well as varying degrees of impairment of intestinal barrier function. The presence of the intestinal barrier prevents bacteria, pathogens and other harmful substances in the intestinal lumen from entering the bloodstream to maintain the stability of the internal environment. After the intestinal barrier is damaged, endotoxins and intestinal flora can enter the blood circulation, resulting in enterogenic endotoxemia, which aggravates the micro-inflammatory state of the body. CRF and peritoneal dialysis patients are

Abbreviations: BUN, Blood urea nitrogen; CKD, Chronic kidney diseases; CR, Creatinine; CRF, Chronic renal failure; ESRD, End-stage renal disease; FMT, Fecal microbiota transplantation; IS, Indophenol sulphate; NMDS, Non-metric Multidimensional Scaling Analysis; PCA, Principal Component Analysis; PCoA, Principal Coordinate Analysis; PCS, P-cresol sulphate; SPF, Specific pathogen-free; TCM, Traditional Chinese medicine; UA, Uric acid.

combined with varying degrees of endotoxemia (Gonçalves et al., 2006; Szeto et al., 2008; Feroze et al., 2012), and uremic rats are more prone to lateral translocation of intestinal bacteria (de Almeida Duarte et al., 2004), this is a reflection of the impaired intestinal barrier in CRF. In addition, the accumulation of intestinal proteins in CRF alters the structure of the intestinal flora and increases the number of enteric proteolytic bacteria. Tryptophan is fermented in the intestine to produce indole, which is absorbed into the blood via the intestine and converted to IS in the liver; tyrosine and phenylalanine are fermented in the intestine to produce p-cresol, which is converted to PCS in the intestinal epithelium (Liabeuf et al., 2011). The latter is converted to PCS in the intestinal epithelium. Since IS and PCS are bound to albumin in the blood and cannot be excreted through dialysis, their accumulation in the body can accelerate the progression of renal failure by aggravating glomerulosclerosis and interstitial fibrosis (Miyazaki et al., 1997; Gelasco and Raymond, 2006; Watanabe et al., 2013). Therefore, repairing the intestinal barrier and reversing the imbalance of intestinal flora are considered as potential therapeutic targets and new targets for intervention in the treatment of CRF.

Traditional Chinese medicine (TCM) holds a unique advantage in the treatment of CRF. CRF involves a complex interplay among various organs, with a particularly intricate relationship between the spleen and kidney systems in TCM. The fundamental mechanism underlying CRF is often described as "deficiency of the spleen and kidney, accumulation of turbid toxins." Guided by this medical principle, the Department of Nephrology at the First Affiliated Hospital of Tianjin University of Traditional Chinese Medicine has tailored its approach to the pathogenic patterns of CRF. Draw upon extensive clinical practice and years of specialized case data, and referencing the optimized compilation and efficacy validation of nationwide TCM protocols for CRF, this has ultimately evolved into the "Fushen Formula." This formula serves as the basis for a corresponding composite herbal preparation named "Fushen Granule." The granule preparation has received hospital formulation approval (Batch Number: 140928) and is primarily employed to treat intestinal dysfunctions related to peritoneal dialysis in ESRD patients. It has been shown to achieve definite therapeutic effects in clinical practice. In clinical application, the treatment group receiving Fushen Granule demonstrated superior improvement in renal function and reduction in blood creatinine (BCR) and blood urea nitrogen(BUN) levels compared to the control group, with no adverse reactions observed (Sun and Liu, 2010). Among elderly CKD stage 4 patients, oral administration of Fushen Granule significantly enhanced kidney function and nutritional status, ameliorated symptoms, and elevated quality of life (Yang and Yang, 2015). Another study revealed that the combination of blood purification and oral administration of Fushen Granule for treating CRF significantly improved kidney function and quality of life, reduced hospitalization time, lowered mortality rates, and alleviated economic burdens (Lei, 2016). Furthermore, the comprehensive efficacy of oral administration of Fushen Granule combined with acupuncture at specific points was found to surpass that of conventional acupuncture alone in CKD stage 4 patients (Zhang and Yang, 2016). Building upon clinical practice, fundamental research on Fushen Granule has also been initiated. Results from basic experiments demonstrate that Fushen Granule can slow down the progression of renal function impairment in a rat model of CRF. It reduces the expression of mild inflammatory factors (such as hs-CRP, IL-6, and TNF-α), lowers blood urea nitrogen (BUN) and blood creatinine(BCR) levels, thereby improving kidney function and delaying the progression of renal deterioration (Zhang and Yang, 2018a; Zhang and Yang, 2018b). Fushen Granules are not only suitable for patients with CRF, but also for conditions such as peritoneal dialysis in CRF and renal interstitial fibrosis (Zhao et al., 2022). A multicenter clinical study involving 240 peritoneal dialysis patients over a 6-month period demonstrated significant enhancements attributed to Fushen Granules. These enhancements include improved TCM syndromes, enhanced dialysis efficiency, increased removal of toxins and excess water, slowed decline of residual kidney function, and an overall improvement in quality of life (Yang et al., 2012a; Yang et al., 2013). Additionally, Fushen Granules exhibited positive effects on the prognosis of peritonitis (Jiang et al., 2020a), gastrointestinal function in peritoneal dialysis patients (Chen, 2016), and maintenance of protein nutritional status (Yang et al., 2014; Lei and Yang, 2018; Lei et al., 2018a). In peritoneal dialysis rats, research reveals that Fushen Granules improve renal function damage through multiple pathways, including modulating Glo-1 expression levels and reducing serum AGEs accumulation, thereby safeguarding residual kidney function(Tang et al., 2017; Tang et al., 2018b). Furthermore, it alleviates ultrafiltration volume and glucose transport, enhancing peritoneal dialysis efficacy(Yang et al., 2021b). Fundamental research also indicates that Fushen Granules regulate Dcn, inhibit activation of the TGF-β pathway, disrupt extracellular matrix accumulation, modulate glucose and lipid metabolism, suppress expression of fibrosis-promoting factors (such as TGF-β1, TGF-βRII, CTGF, IL-6, CTGF, VEGF), and elevate expression of anti-fibrotic factors (HGF, BMP-7), thereby restraining peritoneal collagen formation and inhibiting mesothelial cell transdifferentiation. As a result, it slows the progression of peritoneal fibrosis (Yang et al., 2012b; Dou, 2015; Lei et al., 2018b; Lei et al., 2018c; Jiang et al., 2020b; Li et al., 2020; Yang et al., 2021a). Additionally, Fushen Granules reduce the accumulation of pro-oxidative factors like MG and MDA, upregulate the expression of the antioxidant GSH, subsequently ameliorating anemic conditions in CRF peritoneal dialysis rats (Tang et al., 2018a).

Fecal microbiota transplantation (FMT) has recently gained renewed clinical interest as a long-established therapy for rebuilding the intestinal flora. FMT, i.e. the isolation of functional donor or autologous intestinal flora and transplantation into the patient's gut, has been applied to treat a range of gastrointestinal/non-gastrointestinal disorders associated with intestinal flora and is a breakthrough medical advance in recent years (Cui et al., 2016). In addition, FMT is also used in the renal field for kidney transplantation (Ahmad and Bromberg, 2016). Although the correlation between intestinal flora and CKD/CRF is currently a hot topic of research, the use of FMT in the treatment of CKD/CRF has not yet been reported. Therefore, within the scope of affirming Fushen Granules' ability to retard peritoneal fibrosis progression, enhance dialysis efficacy, and improve quality of life for peritoneal dialysis patients—particularly in ameliorating intestinal functional

disorders—we have integrated Fushen Granules with FMT. This integration enables a more profound and direct impact of post-intervention microbiota reinfusion on intestinal microbiota dynamics. From this perspective, the pivotal role and significance of gut microbiota in CRF are harnessed, establishing novel avenues and intervention targets for preventing and treating CRF progression.

2 Materials and methods

2.1 Preparation of the experimental drug, Fushen Granule

Fushen Granules (Batch number: 140928) were provided by the First Teaching Hospital of Tianjin University of Traditional Chinese Medicine (Tianjin, China) in strict compliance with the Good Manufacturing Practice and Good Laboratory Practice guidelines for Pharmaceutical Manufacturers. Fushen Granules are primarily composed of eight different herbal ingredients. The names of these herbs have been revision in the plant list (http://www.theplantlist.org), and the details can be found in Table 1. Through UPLC/Q-TOF analysis, the main active components of the Fushen Granules were characterized. We have preliminarily identified 55 different compounds in FSG, as detailed in the attached document. The granules were dissolved in distilled water, and the dosage for rats was adjusted based on the body surface area of humans, with equal amounts administered as low doses and 10 times the amount given as high doses.

2.2 Laboratory animals

Specific pathogen-free (SPF) healthy male Sprague-Dawley (SD) rats (weight 180 ± 20g) were purchased from the Experimental Animal Centre of the Chinese People's Liberation Army Academy of Military Medical Sciences. They were housed in the Experimental Animal Centre of Tianjin University of Chinese Medicine. Throughout the experiment, the rats were fed normal chow (no yeast, no probiotics) and had ad libitum access to water. All animal procedures were conducted in accordance with the NIH Guide for the Care and Use of Laboratory Animals and the Chinese Laboratory Animal Management Methods. The ethical approval for this study was No. IRM-DWLL-2020100.

2.3 Experimental reagents and apparatus

The following reagents and apparatus were used in the study: Rat Indoxyl Sulfate (IS) ELISA Kit (Jianglai Bio, JL44174), Rat P-Cresol Sulfate (PCS) ELISA Kit (Jianglai Bio, JL48836), Lactate Test Kit (Nanjing Jiancheng, A019-2-1), Endotoxin Assay Kit (Xiamen Horseshoe Crab Bio, EC80545), Urea Nitrogen Assay Kit (Changchun Huili, C010), Creatinine Assay Kit (Changchun Huili, C074), Uric Acid Assay Kit (Changchun Huili, C075), and DNA Isolation Kit (MoBio, Carlsbad, CA, USA). An Illumina HiSeq platform was provided by Novogene Bioinformatics Co. Ltd., Beijing, China.

Equipment used in the study included a vertical refrigerated display cabinet (Star), a horizontal freezer (Meiling), an electronic balance (Mettler-Toledo Instruments (Shanghai) Co., Ltd.), a high-speed tissue grinder (Servicebio), a benchtop high-speed frozen centrifuge (ThermoFisher), and an enzyme-linked immunosorbent assay (BioTek).

3 Methods

3.1 Chronic renal failure rat model construction and sample collection

In this study, a 5/6 nephrectomy was performed to establish a chronic renal failure(CRF) model in rats. The left kidney was initially resected by 5/6 nephrectomy, and after a 1-week recovery period, the right kidney was completely resected. Blood and urine biochemical tests were conducted at the end of the modeling period. Fresh feces from each group were collected in sterile lyophilized tubes, immediately placed in liquid nitrogen, and then stored at -80°C.

TABLE 1 The constituents of Fushen Granule.

Num	Scientific name	Material	Latin name	Chinese name	Mass Ratio
1	Astragalus membranaceus	Root	*Hedysarum Multijugum* Maxim	Huangqi	15g
2	Angelica sinensis	Root	*Angelica sinensis* (Oliv.) Diels	Danggui	10g
3	Epimedium brevicornu Maxim	Root	*Epimedium brevicornu* Maxim	Xianlingpi	15g
4	Citrus reticulata Blanco	outer pericarp	*Citrus reticulata* Blanco	Chenpi	10g
5	Pinellia ternata	Roots and rootstalk	*Pinellia ternata* (Thunb.) Makino	Banxia	15g
6	Salvia miltiorrhiza Bunge	Roots and rootstalk	*Salvia miltiorrhiza* Bunge	Danshen	30g
7	Rheum	Roots and rootstalk	*Rheum palmatum* L.	Dahuang	10g
8	Siebold	Winged shoots or branch wings	*Euonymus alatus* (Thunb.) Siebold	Guijianyu	30g

3.2 Observation on the intervention effect of Fushen Granule on intestinal flora in CRF

For *in vivo* studies, 150 specific pathogen-free (SPF) healthy male Sprague-Dawley (SD) rats were acclimatized for 1 week. The rats were randomly divided into the following groups: 30 rats in the sham-operated group (Group A), 30 rats in the sham-operated Chinese medicine group (Group B), and 90 rats in the modeling group. The modeling group was further divided into a low-dose Chinese medicine group (Group C), a high-dose Chinese medicine group (Group D), and a control model group (Group E), with 30 animals in each group. Groups B and C received a low dose of Fushen Granule via gavage; Group D received 10 times the high dose of Fushen Granule via gavage; Groups A and E were given 2ml·d-1 distilled water via gavage. Six animals from each group were euthanized for examination at the beginning of drug intervention, at the end of the second week, and at the end of the fourth week. All remaining animals were euthanized at the end of the sixth week.

3.3 Fecal microbiota transplant experiment

After 1 week of acclimatization, 55 specific pathogen-free (SPF) healthy male Sprague-Dawley (SD) rats were randomly divided into a 5/6 nephrectomized kidney failure rat model recipient group (15 x 3) and a donor rat group (5 x 2, approximately 1/3 the number of the recipient group). The donor group was further divided into the Fushen Granule donor group and the normal donor group, while the recipient group was divided into the model group + Fushen Granule donor FMT group, the model group + normal donor FMT group, and the model group + saline sham operation group. In the Fushen Granule donor group, a low dose of Fushen Granule was administered for 6 weeks from the first day of right nephrectomy, based on the effect of the previous experimental intervention. No intervention was made in the normal donor group. Fresh, uncontaminated feces were collected daily, and intestinal microbial extracts were prepared in saline. Fecal microbiota transplantation(FMT) was completed within 4 hours of feces collection. The recipient groups, model group + Fushen Granule donor and model group + normal donor, underwent FMT with intestinal microbial extracts from the Fushen Granule donor group and the normal donor group, after determining successful modeling through dynamic observation of kidney function. The model group + saline sham group underwent a procedure with an equal amount of saline equivalent as the control group.

3.4 Observation indicators

The animals were dynamically observed, and their body weight was assessed every 5 days. The focus was on the general status of the rats at the beginning of drug intervention and at the end of the 2nd, 4th, and 6th weeks (general status in terms of behavioral activity, body weight, phenotypic signs, and survival rate), renal function indicators (Cr, BUN, UA, eGFR, and urinary microalbumin), serum endotoxin, D-lactate, metabolic toxins of intestinal origin (IS, PCS), and analysis of intestinal bacterial diversity.

3.5 Analysis of intestinal bacterial diversity

In this study, 16S rRNA was used to assess intestinal bacterial diversity, but the timing of fecal sample collection differed between the two experiments. Fresh fecal samples were collected at around 10 am at the beginning of the intervention and at the end of the second, fourth, and sixth weeks. Fecal samples were collected from the three model groups at two time points: before the start of the FMT experiment and 15 days after the transplantation (Note: The feces were collected for the same amount of time each instance). Fresh fecal samples collected were immediately frozen in liquid nitrogen for 5 minutes and then stored at -80°C. DNA was extracted from feces using the Power Fecal DNA Isolation Kit (MoBio, Carlsbad, CA, USA). DNA was recovered using 30 mL of the buffer included in the kit. Sequencing principles were used for synthetic sequencing with the Illumina HiSeq platform (Novogene Bioinformatics Co., Beijing, China). Taxonomic composition of the flora was analyzed to evaluate bacterial abundance and compositional diversity, using phylum, order, family, and genus classifications.

3.6 Statistical analysis

SPSS 19.0 for Windows statistical software was used for data analysis. Data were expressed as mean ± SEM relative to the number of samples in each group (n). Analysis of variance (ANOVA), Wilcoxon rank-sum test, Tukey's t-test, and Student's t-test were used to determine statistical significance between multiple treatment groups. The Kaplan-Meier survival test was used to analyze survival rates. Results with $p< 0.05$ were considered statistically significant.

4 Results

4.1 Effect of Fushen Granule on the status of rats with CRF

4.1.1 General state

During the modeling phase, rats in the model group typically exhibited irritability, emotional instability, and agitated reactions when injected or given the drug via gavage. Over time, rats in the sham-operated group gained weight, appeared in good spirits, moved freely, were responsive, and had well-groomed, moisturized fur. In contrast, rats in the model group gradually lost weight, ate less than the sham-operated group, appeared more depressed, squinted, were less active, less responsive, and had

disheveled and unkempt fur. Rats in the drug intervention group demonstrated better performance in terms of mental status, body weight, activity, responsiveness, and fur appearance after treatment, but still showed slight differences compared to the sham-operated group.

4.1.2 Observation of renal function indicators

Compared with the sham-operated group, the model group showed a statistically significant increase in Cr, BUN, and 24-h urinary microalbumin at weeks 2, 4, and 6 (P< 0.01), indicating successful modeling of renal failure (see Table 2). UA also tended to increase, but the difference was not statistically significant. Compared with the model group, the 24-h urine microalbumin in the Chinese medicine low-dose group decreased significantly at weeks 2 and 4 (P< 0.001), BUN decreased significantly at week 4 (P< 0.05), and Cr decreased significantly at week 6 (P< 0.05). The Chinese medicine high-dose group showed significant decreases in Cr and 24-h urine microalbumin at weeks 2, 4, and 6 (P< 0.01), and BUN at week 4 (P< 0.05) (Table 2). In conclusion, the herbal intervention group had a positive effect on the renal function indices of rats with CRF, and the efficacy of the high-dose herbal group was better.

4.1.3 Observation of serum endotoxins and metabolic toxin-like indicators of enteric origin

Compared with the sham-operated group, rats in the model group showed significantly higher IS, PCS, D-lactic acid, and endotoxin levels at weeks 2, 4, and 6 (P< 0.05), indicating successful modeling of renal failure. Compared with the model group, the Chinese medicine low-dose group showed significant decreases in IS, PCS, D-lactate, and endotoxin at weeks 2, 4, and 6 (P< 0.05). The high-dose group of Chinese medicine showed a significant decrease in PCS (P< 0.01) at the beginning of the drug intervention and in IS, PCS, D-lactic acid, and endotoxin at weeks 2, 4, and 6 (P< 0.05) (Table 3). This indicates that both the low and high dose groups of Chinese medicine demonstrated improvement in D-lactate, endotoxin, and enteric-derived metabolic toxin-like indicators. Compared with the low-dose group, the high-dose group generally had a better effect on D-lactate, endotoxin, and intestinal-derived metabolic toxins.

4.1.4 Analysis of intestinal bacterial diversity

4.1.4.1 Sequencing data quality and OTU analysis

The IonS5TMXL sequencing platform was utilized to analyze the diversity of intestinal bacteria. Using a single-end sequencing

TABLE 2 Indicators of kidney function.

Group	Point in time	Cr (mmol/L)	BUN (μmol/l)	UA (μmol/l)	24-h urine microalbumin (mg/L)
Sham-operated Group A	Initial	48.25 ± 4.28	18.29 ± 2.15	108.35 ± 4.79	23.28 ± 4.82
	2 weeks	42.45 ± 3.35	14.28 ± 2.23	104.22 ± 16.38	26.75 ± 3.24
	4 weeks	65.59 ± 10.07	16.58 ± 0.61	107.53 ± 20.37	29.36 ± 4.91
	6 weeks	74.31 ± 5.05	38.66 ± 1.07	117.16 ± 12.77	25.18 ± 3.52
Fushen Granule low dose control (Group B)	Initial	50.23 ± 5.97	20.34 ± 2.46	110.25 ± 5.32	25.17 ± 3.34
	2 weeks	55.9 ± 5.23	13.98 ± 2.80	121.00 ± 20.57	25.37 ± 5.82
	4 weeks	65.72 ± 9.82**	16.04 ± 1.16	109.29 ± 14.96	27.54 ± 3.26
	6 weeks	72.34 ± 8.14	38.47 ± 0.67	139.85 ± 40.34	24.34 ± 2.84
Model (Group E)	Initial	47.93 ± 4.74	19.23 ± 2.73	115.32 ± 5.28	27.43 ± 3.44
	2 weeks	109.23 ± 4.56***	50.24 ± 4.56***	110.25 ± 11.39	128.37 ± 12.37***
	4 weeks	103.75 ± 2.57**	45.47 ± 0.95**	104.42 ± 16.04	379.85 ± 28.37***
	6 weeks	107.79 ± 12.37**	44.33 ± 2.1**	127.40 ± 18.15	583.92 ± 45.29***
Fushen Granule at low doses (Group C)	Initial	51.2 ± 5.22	20.12 ± 1.94	109.73 ± 4.91	24.82 ± 4.19
	2 weeks	106.78 ± 1.25	45.91 ± 3.12	108.13 ± 26.28	88.24 ± 6.74###
	4 weeks	96.46 ± 3.67**	25.48 ± 2.63#	107.68 ± 24.15	128.49 ± 18.58###
	6 weeks	95.41 ± 3.91**#	44.63 ± 1.45**	136 ± 34.74	73.95 ± 10.28###
Fushen Granule at high doses (Group D)	Initial	49.37 ± 4.60	18.32 ± 2.31	111.20 ± 4.83	26.37 ± 2.58
	2 weeks	95.24 ± 3.13##	44.15 ± 4.50	103.67 ± 30.12	75.63 ± 6.53###
	4 weeks	85.1 ± 9.7**##	41.69 ± 0.9**#	120.97 ± 24.09	102.53 ± 13.45###
	6 weeks	90.41 ± 9.77**##	44.03 ± 2.24**	119.87 ± 15.49	58.24 ± 8.94###

Compared to the sham-operated group: * indicates p< 0.05, ** indicates p< 0.01, *** indicates p< 0.001; compared to the model group, # indicates p< 0.05, ## indicates p< 0.01, ### p< 0.001.

10.3389/fcimb.2023.1334213

TABLE 3 Indicators for D-lactate, endotoxin and enteric-derived metabolic toxin categories.

Group	Point in time	Metabolic toxins of enteric origin		Serum endotoxin	
		IS (μg/ml)	PCS (μg/ml)	D-Lactic acid (μg/ml)	Endotoxin (EU/ml)
Sham-operated (Group A)	Initial	1.02 ± 0.12	0.03 ± 0.01	7.68 ± 0.27	0.019 ± 0.003
	2 weeks	1.35 ± 0.34	0.05 ± 0.01	7.59 ± 0.31	0.029 ± 0.004
	4 weeks	1.66 ± 1.12	0.08 ± 0.01	7.51 ± 0.21	0.027 ± 0.002
	6 weeks	1.71 ± 0.47	0.13 ± 0.07	7.66 ± 0.30	0.032 ± 0.004
Fushen Granule low dose control (Group B)	Initial	0.85 ± 0.23	0.02 ± 0.01	7.52 ± 0.31	0.021 ± 0.002
	2 weeks	0.90 ± 0.11	0.04 ± 0.01	7.45 ± 0.36	0.025 ± 0.003
	4 weeks	0.96 ± 0.47	0.07 ± 0.01	7.22 ± 0.25	0.026 ± 0.006
	6 weeks	3.04 ± 0.6	0.06 ± 0.02	7.82 ± 0.48	0.021 ± 0.001
Model (Group E)	Initial	1.05 ± 0.19	0.05 ± 0.01*	7.61 ± 0.27	0.023 ± 0.003
	2 weeks	3.67 ± 0.65***	0.43 ± 0.11***	15.92 ± 0.28***	0.316 ± 0.027***
	4 weeks	6.02 ± 1.58**	0.58 ± 0.38**	20.31 ± 0.48***	0.429 ± 0.031***
	6 weeks	6.35 ± 2.24**	1.74 ± 0.34*	14.76 ± 0.34***	0.496 ± 0.038***
Fushen Granule at low doses (Group C)	Initial	0.98 ± 0.10	0.04 ± 0.01	7.76 ± 0.24	0.026 ± 0.003
	2 weeks	2.59 ± 0.35##	0.20 ± 0.04###	10.22 ± 0.47###	0.209 ± 0.023###
	4 weeks	3.89 ± 0.78**##	0.26 ± 0.1	9.03 ± 1.02###	0.297 ± 0.027###
	6 weeks	3.54 ± 1.97#	0.3 ± 0.23#	11.76 ± 0.13###	0.234 ± 0.025###
Fushen Granule at high doses (Group D)	Initial	0.95 ± 0.15	0.02 ± 0.01##	7.53 ± 0.25	0.025 ± 0.001
	2 weeks	2.48 ± 0.32##	0.13 ± 0.02###	9.84 ± 0.52###	0.174 ± 0.018###
	4 weeks	3.55 ± 0.79*##	0.15 ± 0.04#	10.79 ± 0.63###	0.216 ± 0.023###
	6 weeks	3.19 ± 1.56#	0.39 ± 0.24#	12.01 ± 0.44###	0.183 ± 0.017###

Compared to the sham-operated group: * indicates p< 0.05, ** indicates p< 0.01, *** indicates p< 0.001; compared to the model group, # indicates p< 0.05, ## indicates p< 0.01, ### p< 0.001.

method, an average of 83,925 reads per sample were measured by shear filtering of Reads, and an average of 78,965 valid data were obtained after quality control, with a quality control efficiency of 94.15%. The sequences were clustered into OTUs (Operational Taxonomic Units) with 97% agreement, yielding a total of 4,955 OTUs. The OTUs sequences were then analyzed against the Silva132 database for species annotation to understand the composition and differences between intestinal flora. A total of 4,955 OTUs were counted according to different taxonomic levels, of which the number of OTUs that could be annotated to the database was 4,954 (99.98%). Dilution curves were constructed by the number of OTUs detected at each sequencing depth of the experimental data, and it was found that as the sequencing depth gradually increased, the sparsity curve also gradually smoothed out, indicating that the current sequencing depth is essentially sufficient to reflect the microbial diversity contained in this community sample (Figures 1A, B). The smoothness of the Rank Abundance curve reflects the uniformity of the species distribution, and from the figure (Figure 1C), it can be observed that the distribution of microbial species contained in this sequenced sample was poorly distributed. Species accumulation box plots were used for sample size and diversity analysis of the biota. As seen in the box line plot (Figure 1D), the box positions no longer rose sharply but leveled off as the sample size expanded, indicating that the current sample size was abundant and adequate, and largely representative of the community's flora characteristics.

By clustering, sequences can be grouped into various categories based on their similarity to each other, with each category representing a taxonomic OTU. OTUs with a 97% similarity level are typically analyzed for bioinformatic statistics. In this study, we analyzed intestinal bacterial diversity in 5/6 nephrectomized rats. The results showed that the number of OTUs shared between the model and sham-operated groups was highest at week 0 (1465). However, the number of OTUs shared by the five groups gradually decreased at weeks 2 and 4, with 1197 and 541, respectively. This indicates that 5/6 nephrectomy can cause a decrease in the number of OTUs in the group. In terms of unique OTUs, the model group had 247, 186, and 66 unique OTUs at weeks 2, 4, and 6, respectively. The Chinese medicine high-dose treatment group had 393, 357, and 821 unique OTUs, while the low-dose treatment group had 87, 177, and 55 unique OTUs in that order. These findings suggest that Fushen Granule may alleviate intestinal flora damage and increase

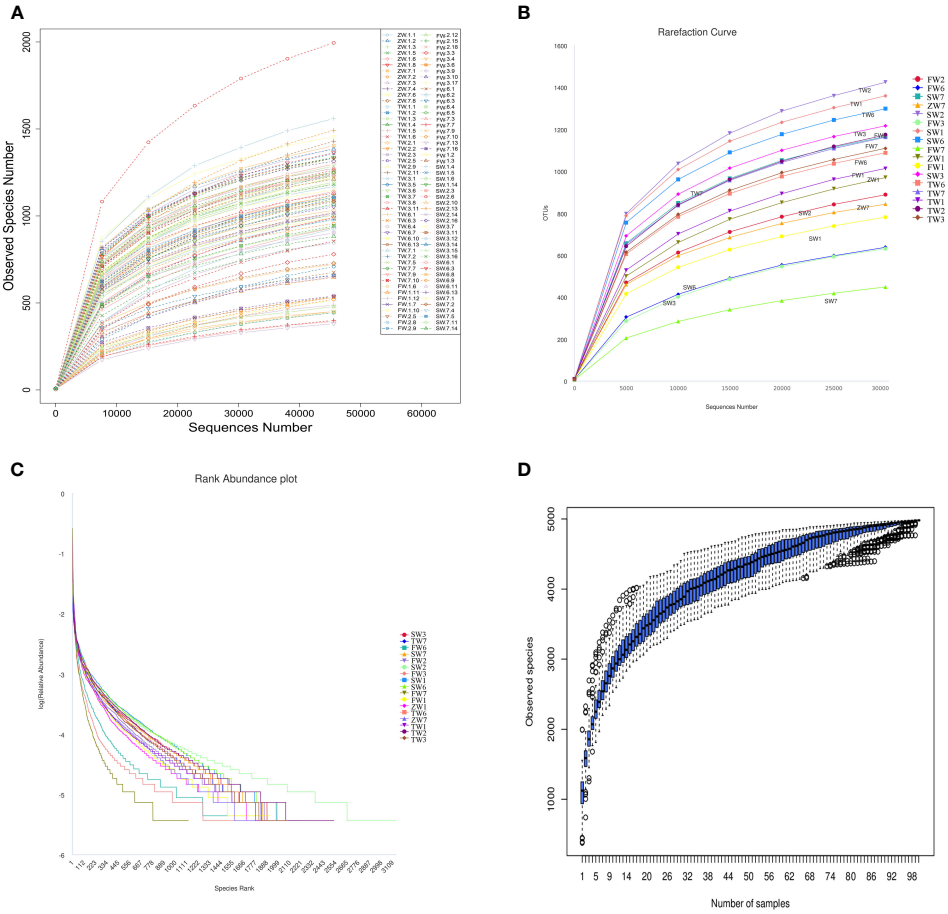

FIGURE 1
Analysis of intestinal bacterial diversity. **(A, B)** Sparsity curve of the sample to be tested; **(C)** Rank Abundance curve; **(D)** Cumulative box plot of species.

the number of OTUs in rats with 5/6 nephrectomy to some extent. Compared with the same time points, the herbal high-dose treatment groups at weeks 2, 4, and 6 contained the highest number of unique OTUs. This indicates that the Chinese medicine high-dose group was more effective in restoring intestinal flora diversity in 5/6 nephrectomized rats than the low-dose treatment group (Figure 2).

4.1.4.2 Species annotation and taxonomic analysis

Species abundance tables at different taxonomic levels were generated using QIIME software, and then mapped into community structure at each taxonomic level of the samples using R language tools. The results showed that the dominant species at the phylum level were Firmicutes, Bacteroidetes, and Proteobacteria; at the genus level, the dominant species were Lactobacillus, Enterococcus, and Stenotrophomonas. The phylum Firmicutes and the phylum Bacteroidetes are the most abundant bacterial phyla in the intestinal flora, accounting for more than 90% of all bacteria. An analysis of the relative abundance of the intestinal flora at the phylum and genus taxonomic levels is shown in Figure 3A, B. In the sham-operated group, the levels of the two bacteria, Phylum Firmicutes and Phylum Bacteroidetes, were relatively stable and did not change over time. The relative abundance of Phylum Firmicutes was 70%, 69%, 68%, and 63%, and the relative abundance of Phylum Bacteroidetes bacteria was 24%, 24%, 22%, and 30% at the four time points of 0, 2, 4, and 6 weeks, respectively. The ratio of Phylum Firmicutes to Phylum Bacteroidetes bacteria remained roughly between 2 and 3. In contrast, in the 5/6 nephrectomy model group, the relative abundance of the Firmicutes phylum decreased, and the relative abundance of the Bacteroidetes increased, resulting in a decrease in the Firmicutes phylum/Bacteroidetes phylum ratio. Compared to the sham-operated group during the same period, the relative abundance of Firmicutes phylum bacteria in the model group decreased from 81% at week 0 to 54% at week 6, while the relative abundance of Bacteroidetes phylum increased from 10% at week 0 to nearly 40% at week 6, with a decreasing trend in the ratio of the two contents (Table 4). Compared with the model group, the Chinese medicine low-dose and Chinese medicine high-dose groups could differently reduce this alteration to some extent and restore the Firmicutes phylum and Bacteroidetes phylum composition ratio. For example, at the second week, the Firmicutes phylum and Bacteroidetes phylum ratio was 2.88 in the sham-operated group, and the ratio was 1.1, 2.27, and 1.88 in the

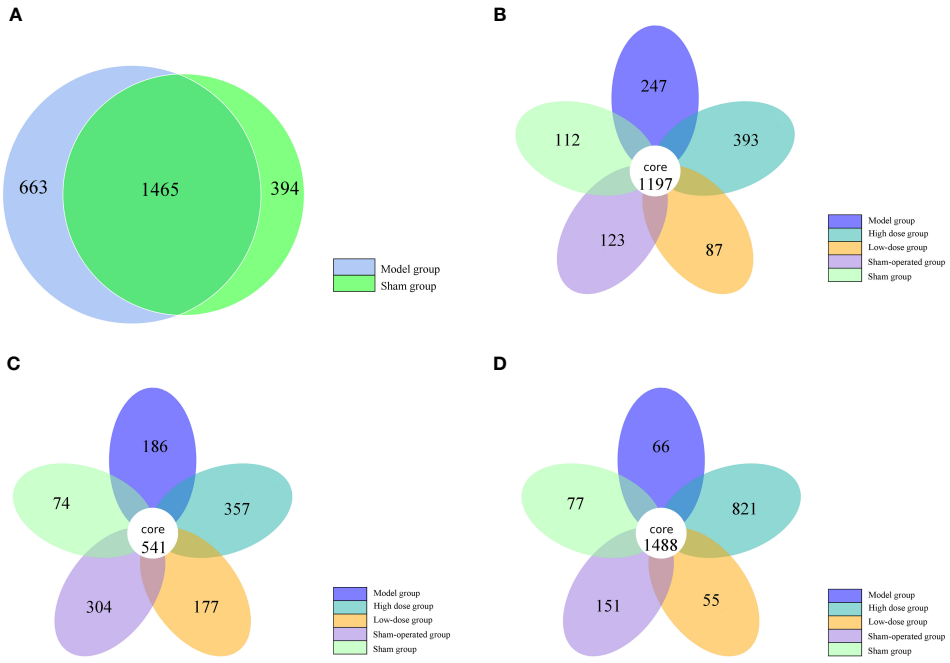

FIGURE 2
Number of OTUs of intestinal flora in five groups of rats at 0, 2, 4 and 6 weeks. **(A)** 0 weeks, **(B)** 2 weeks, **(C)** 4 weeks, **(D)** 6 weeks.

model, low-dose, and high-dose Chinese medicine groups, respectively (Table 5). In terms of genus level, Lactobacillus was the main dominant genus, and compared with the sham-operated group during the same period, the level of Lactobacillus in the model group showed a decreasing trend, at 25% at 2 weeks, 23% at 4 weeks, and 10% at 6 weeks, respectively. Compared with the model group, the low dose of Chinese medicine and high dose of Chinese medicine treatment could increase the content of Lactobacillus to different degrees (Table 6).

4.2 Using FMT as a technical platform to study the Improvement of Intestinal Flora in CRF with Fushen Granule

4.2.1 General state observation

The rats in the control donor group had significantly increased body weight, good mental condition, free movement, responsiveness, and neat and moist hair. In contrast, the rats in the model group gradually lost weight, ate less, appeared more depressed, squinted, were less active, less responsive, and had loose body hair and shaggy fur. The Fushen Granule donor group or FMT group had a better mental status, weight, activity, reaction, and coat color after treatment, but was still worse than the control group.

4.2.2 Observation of renal function indicators

Compared with the normal donor group, Cr, BUN, UA, and 24-h urine microalbumin were significantly higher in the nephrectomy + saline group at weeks 2, 4, and 6, with statistically significant differences ($P< 0.05$), indicating successful modeling of renal failure. Compared with the nephrectomy + saline group, BUN and 24-h urine microalbumin decreased significantly ($P< 0.05$) at week 2, and Cr, BUN, UA, and 24-h urine microalbumin also decreased significantly ($P< 0.05$) at weeks 4 and 6 in the nephrectomy + Fushen Granule group. In contrast, BUN, UA, and 24-h urine microalbumin also decreased significantly in the nephrectomy + normal f group at week 2 ($P< 0.05$), and Cr, BUN, UA, and 24-h urine microalbumin decreased significantly at weeks 4 and 6 ($P< 0.05$). The improvement in 24-h urinary microalbumin at weeks 2, 4, and 6 did not significantly differ between the kidney cut + Fushen Granule group and the kidney cut + normal f group ($P > 0.05$) (Table 7).

4.2.3 Observation of serum endotoxins and metabolic toxin-like indicators of enteric origin

Compared to the normal donor group, the nephrectomy + saline group showed a statistically significant increase ($P< 0.05$) in IS, PCS, D-lactic acid, and endotoxin at weeks 2, 4, and 6, indicating successful modeling of renal failure. Compared with the nephrectomy + saline group, the nephrectomy + Fushen Granule group showed a significant decrease in PCS, D-lactic acid, and endotoxin at weeks 2 and 4 ($P< 0.05$), and a significant decrease in IS at week 6 ($P< 0.05$). Similarly, compared to the nephrectomy + saline group, the nephrectomy + normal f group showed significant decreases in PCS, D-lactic acid, and endotoxin at weeks 2, 4, and 6 ($P< 0.05$), and a significant decrease in IS at weeks 4 and 6 ($P< 0.05$). The improvement in D-lactate and endotoxin in the kidney cut + Fushen Granule group at weeks 2, 4, and 6 was not significantly different from that in the kidney cut + normal f group ($P > 0.05$) (Table 8).

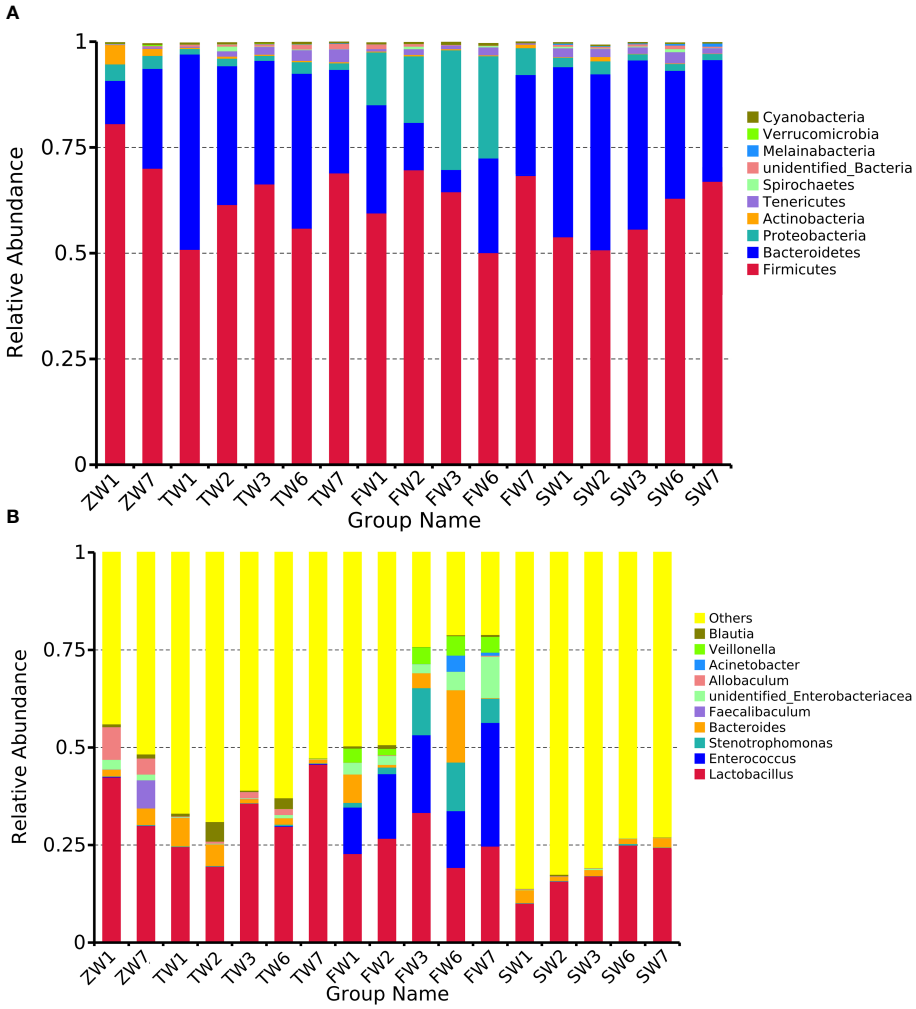

FIGURE 3
Top 10 relative abundance of intestinal flora in each group of rats **(A)** phylum level, **(B)** genus level. ZW indicates zero week, TW indicates two-week, FW indicates fourth week, SW indicates sixth week. 1 indicates model, 2 indicates fushen granule at high doses, 3 indicates fushen granule at low doses, 6 indicates sham-operated fushen granule control, 7 indicates sham-operated.

4.2.4 Analysis of intestinal bacterial diversity

4.2.4.1 Sequencing data quality and OTU analysis

In this study, the coverage of each sample library was assessed by calculating the Coverage Index, and values of the Coverage Index were obtained to be >0.99, indicating comprehensive coverage of each sample library and a high detection rate of the sample sequences (Table 9). Hierarchical abundance curves were used to simultaneously interpret the richness and evenness of the species

TABLE 4 Levels of Firmicutes and Bacteroides of rats in sham-operated and model groups at 0, 2, 4 and 6 weeks.

Group	Time Point (weeks)	Firmicutes (%)	Bacteroides (%)	Firmicutes/Bacteroidetes ratio
Sham-operated	0	70	24	2.97
	2	69	24	2.88
	4	68	22	3.1
	6	63	30	2.1
Model	0	81	10	8.1
	2	51	46	1.11
	4	60	26	2.31
	6	54	40	1.35

TABLE 5 Levels of Firmicutes and Bacteroides of rats in each group at week 2.

Group	Firmicutes (%)	Bacteroidetes (%)	Firmicutes/ Bacteroidetes ratio
Sham	69%	24%	2.88
Sham-operated	56%	37%	1.53
Model	51%	46%	1.11
Fushen Granule at low doses	66%	29%	2.27
Fushen Granule at high doses	62%	33%	1.88

TABLE 6 Levels of Lactobacillus of rats in each group at 2, 4 and 6 weeks.

Group	Lactobacillus 2 weeks	Lactobacillus 4 weeks	Lactobacillus 6 weeks
Sham	0.46	0.25	0.25
Sham-operated	0.30	0.19	0.25
Model	0.25	0.23	0.10
Fushen Granule at low doses	0.36	0.33	0.17
Fushen Granule at high doses	0.20	0.27	0.16

contained in the samples. The graph shows that the distribution of microbial species in the sequenced samples, excluding sample B2, was reasonably even, it is possible that the B2 sample was contaminated during the sampling process, resulting in a significantly different species abundance and proportion from the pre-intervention samples (Figures 4A, B). Dilution curves were used to verify that the sequencing data reflected the actual biodiversity in the samples and indirectly the species richness in the samples. The results showed that the curve levelled off as the number of sequences increased, indicating that the depth of sequencing had largely covered all species in the samples (Figures 4C, D). In addition, the results of the number of OTUs of each sample obtained by clustering using usearch software showed that the number of rat intestinal flora characteristics in groups FD, FE and FF after Fecal microbiota transplantation(FMT) showed an overall increasing trend compared to groups FA, FB and FC before FMT. In terms of the number of rat intestinal flora characteristics after FMT, the kidney cut + normal group FMT (FD) > kidney cut + Fushen Granule FMT (FF) > kidney cut + saline group FMT (FE) (Figure 4E).

4.2.4.2 Alpha diversity analysis

Alpha diversity reflects the richness and diversity of species in a single sample and is measured by various indices such as Chao, Ace, Shannon, Simpson, Coverage, and peritoneal dialysis - whole_tree. The Chao and Ace indices measure species richness, i.e., the number of species, and larger values of the Shannon and Simpson indices are used to indicate the species diversity of a sample (Grice et al., 2009). Using QIIME2 software, the Alpha Diversity Index of the samples was assessed, and the values for each sample were tallied in Table 9. In terms of flora richness, the Ace and Chao indices increased in groups FD, FE, and FF compared to groups FA, FB, and FC, indicating an increase in flora richness in rats after fecal microbiota transplantation(FMT), with statistically significant differences. In terms of bacterial diversity, the Shannon and Simpson indices were used to estimate the diversity of the flora, and the higher the value, the higher the community diversity. It was found that the Shannon and Simpson indices in groups FD, FE, and FF were higher than those in groups FA, FB, and FC. This indicates that the diversity of the rat intestinal flora was restored after FMT. In conclusion, FMT helped to restore the richness and diversity of the rat intestinal flora. In the comparison between the groups, the normal group had the best results for FMT, followed by the FMT of Fushen Granule, and finally the saline sham operation group.

4.2.4.3 Beta diversity analysis

Beta diversity analysis was conducted in this study using QIIME software to compare the extent to which different samples were similar in terms of species diversity. Principal Component Analysis (PCA), Principal Coordinate Analysis (PCoA), and Non-metric Multidimensional Scaling Analysis (NMDS) were used to examine differences between samples. PCA uses variance decomposition to reflect differences between multiple data sets on a two-dimensional coordinate plot, with the axes representing the two eigenvalues that best reflect the variance. PCoA and PCA plots showed that groups FA, FB, and FC were closer together, indicating high consistency and less variability in the samples. On the other hand, samples FD, FE, and FF after 15 days were less similar in terms of species diversity compared to groups FA, FB, and FC, suggesting that the intervention caused a change in species variability. NMDS analysis had a reliable Stress value of 0.0445 (less than 0.2), indicating its accuracy. Overall, the results suggest that the transplantation of Fushen Granule and normal flora had a moderating effect on the changes in the composition of the intestinal flora in 5/6 nephrectomized rats (Figures 5A-C).

4.2.5 Annotation and variability analysis of intestinal flora species

The primary bacteria that dominate at the phylum level include firmicutes, bacteroidetes, proteobacteria, spirochaetes, actinobacteria, patescibacteria, tenericutes, cyanobacteria, and verrucomicrobia. The relative abundance of intestinal flora at the phylum taxonomic level was analyzed in Figure 6. Compared to rats before FMT, the model + saline group, the model + Fushen Granule Donor group, and the model + normal Donor group showed a decreasing trend for Firmicutes bacteria and an increasing trend for

10.3389/fcimb.2023.1334213

TABLE 7 Indicators of renal function.

Group	Point in time	Cr	Bun	UA (μmol/L)	24-hour urine microalbumin (mg/L)
Normal Donor	Initial	44.39±0.81	20.43±0.44	102.27±1.08	20.28±2.89
	2 weeks	47.80±3.55	23.53±2.35	112.23±9.48	23.57±2.74
	4 weeks	45.89±0.98	22.89±0.95	104.83±2.04	28.32±2.53
	6 weeks	45.89±0.98	25.93±4.39	128.32±8.85	30.28±2.73
Kidney cut + saline	Initial	42.34±1.97	24.45±0.73	105.26±1.15	22.53±4.20
	2 weeks	95.78±1.96**	37.20±0.28*	145.60±1.19**	288.34±21.49***
	4 weeks	110.39±26.23**	33.33±8.98*	146.46±2.00**	482.95±32.94***
	6 weeks	110.39±26.23**	55.82±2.89*	190.33±45.55**	638.29±44.76***
Kidney cut + Fushen Decoction donor	Initial	45.12±2.49	20.81±0.64	105.87±2.73	21.15±2.46
	2 weeks	55.78±3.61###	26.06±3.51#	121.37±6.30###	75.24±7.93###
	4 weeks	38.15±1.22###	32.58±2.09	130.70±20.98###	129.27±10.89###
	6 weeks	38.15±1.22###	29.70±3.99#	128.50±5.41###	91.13±9.27###
Kidney cut + Fushen Decoction f	Initial	43.70±1.01	22.38±0.68	104.25±1.37	23.47±3.19
	2 weeks	94.04±3.57	22.56±5.68#	142.57±4.42	100.66±12.18###, Δ
	4 weeks	62.45±1.87###	23.48±1.12#	111.40±18.23###	178.82±12.34###, Δ
	6 weeks	62.45±1.87###	37.31±0.86#	93.28±3.56###	103.28±8.42###, Δ
Kidney cut + normal f	Initial	42.29±3.04	22.66±1.39	105.10±1.77	24.72±2.50
	2 weeks	98.63±0.32	24.57±1.40#	137.03±6.89###	83.47±8.82###
	4 weeks	57.04±2.81###	29.01±4.23#	63.47±1.93###	153.94±13.76###
	6 weeks	57.04±2.81###	43.92±0.51#	104.57±15.06###	98.73±7.51###

Compared with normal donor group,** P< 0.01,*** P< 0.001; compared with kidney cut + saline group, #P< 0.05, ### P< 0.001; compared with kidney cut + normal f group, Δ P > 0.05.

TABLE 8 Indicators for D-lactate, endotoxin and enteric-derived metabolic toxin categories.

Group	Point in time	Metabolic toxins of enteric origin		Serum endotoxin	
		IS (μg/mL)	PCS (μg/mL)	D-Lactic acid (μg/mL)	Endotoxin (EU/ml)
Normal Donor	Initial	0.91±0.13	0.17±0.02	7.34±0.28	0.023±0.003
	2 weeks	0.93±0.06	0.15±0.1	7.52±0.36	0.028±0.003
	4 weeks	0.85±0.21	0.13±0.02	7.88±0.42	0.032±0.002
	6 weeks	0.86±0.23	0.15±0.01	7.52±0.28	0.029±0.004
Kidney cut + saline	Initial	0.83±0.12	0.14±0.01	7.58±0.19	0.030±0.004
	2 weeks	5.69±2.87**	1.73±0.22***	18.19±0.54***	0.387±0.032***
	4 weeks	5.24±0.73***	1.8±0.21***	15.28±1.25***	0.498±0.028***
	6 weeks	6.68±2.17***	2.12±0.62***	15.28±1.25***	0.518±0.028***
Kidney Cut + Fushen Decoction Donor	Initial	0.94±0.17	0.18±0.03	7.28±0.32	0.026±0.005
	2 weeks	4.98±1.25	1.28±0.31#	12.33±0.17###	0.224±0.021###
	4 weeks	4.83±1.00	0.37±0.06###	10.25±0.93###	0.243±0.017###
	6 weeks	3.64±1.10#	0.39±0.08###	10.25±0.93###	0.217±0.014###

(Continued)

TABLE 8 Continued

Group	Point in time	Metabolic toxins of enteric origin		Serum endotoxin	
		IS (μg/mL)	PCS (μg/mL)	D-Lactic acid (μg/mL)	Endotoxin (EU/ml)
Kidney cut + Fushen Decoction f	Initial	0.89±0.12	0.16±0.02	7.69±0.33	0.028±0.002
	2 weeks	4.90±1.31	1.03±0.19$^{\#\#}$	14.28±1.23$^{\#\#\#, \Delta}$	0.258±0.028$^{\#\#\#, \Delta}$
	4 weeks	4.22±0.92	0.93±0.15$^{\#\#\#}$	12.15±1.02$^{\#\#, \Delta}$	0.305±0.020$^{\#\#\#, \Delta\Delta}$
	6 weeks	4.08±1.36$^{\#}$	0.86±0.21$^{\#\#\#}$	12.15±1.02$^{\#\#\#, \Delta}$	0.293±0.021$^{\#\#\#, \Delta}$
Kidney cut + normal f	Initial	0.86±0.09	0.15±0.01	7.21±0.21	0.027±0.003
	2 weeks	3.92±1.19	0.88±0.09$^{\#\#\#}$	13.57±0.67$^{\#\#\#}$	0.206±0.019$^{\#\#\#}$
	4 weeks	3.49±1.25$^{\#}$	0.75±0.11$^{\#\#\#}$	12.57±0.78$^{\#\#}$	0.251±0.019$^{\#\#\#}$
	6 weeks	2.78±0.64$^{\#\#}$	0.64±0.09$^{\#\#\#}$	12.57±0.78$^{\#\#\#}$	0.264±0.029$^{\#\#\#}$

Compared to the normal donor group, *** indicates P < 0.001; compared to the nephrectomy + saline group, # indicates P < 0.05, ## indicates P < 0.01, ### indicates P < 0.001; compared to the nephrectomy + normal f group, Δ indicates P > 0.05.

Bacteroidetes. Compared with the model + saline sham-operated group, the relative abundance of these two groups decreased less in the model + Fushen Granule Donor group and the model + normal Donor group, suggesting that the Fushen Granule and normal flora transplantation had a moderating effect on the relative abundance of colonic flora at the phylum level. At the genus level, the model group exhibited a decreasing trend of Lactobacillus after FMT. Compared with the Kidney-cut + saline group during the same period, the Kidney-cut + Fushen Granule Donor group and the Kidney-cut + normal Donor group had some degree of restorative effect on Lactobacillus, and the Fushen Granule FMT was superior to the other two groups.

4.2.6 LefSe analysis

In order to screen for colonies with significant differences between groups, this study employed a novel metagenomic analysis method called LefSe (Linear Discriminant Analysis Size Effect). This method is a statistical approach used in the fields of genetics and microbiology to identify high-dimensional biomarkers and reveal genomic features. LefSe analysis combines linear discriminant analysis with non-parametric tests to identify multiple biomarkers and enable comparisons between multiple groups. In this study, LDA values greater than 3.5 were used as screening criteria to examine the abundance of the flora. In an evolutionary branching tree diagram, different circles represent various taxonomic levels from inner to outer, including domain, kingdom, phylum, class, order, family, genus, and species. Different nodes in the diagram represent dominant genera, while the connections between nodes indicate their correlation. The thickness of the lines reflects the strength of the correlation; thicker lines represent stronger correlations. Additionally, the size of the nodes represents the number of associations with other microorganisms; the more associations, the larger the node. The results showed that Model Group FA had significant differences in a) uncultured_bacterium_g_Prevotella_1 and b) g_prevotella_1. Group FE exhibited significant differences in c) o_Clostridiales after FMT (Figure 7).

5 Discussion

As a progressive, irreversible disease with a complex pathogenesis, limited therapeutic modalities, and issues of tolerance and dependence, the development of effective drugs to treat or alleviate CRF has become an urgent task (Eirin and Lerman, 2014). The gut's microbial composition is a key player in renal

TABLE 9 Displays the analysis of intestinal flora diversity in each group of rats ($\bar{x} \pm s$, n = 3).

Group	Chao	Ace	Shannon	Simpson	Coverage
FA	502.8182 ± 10.0702	495.2557 ± 9.7063	5.5293 ± 0.1972	0.9363 ± 0.0128	0.9987 ± 0
FB	564.9597 ± 10.163	569.3319 ± 19.4272	6.2448 ± 0.7023	0.951 ± 0.0204	0.9983 ± 0
FC	548.2892 ± 15.9462	535.5732 ± 13.0593	5.1845 ± 0.3452	0.9081 ± 0.0152	0.9983 ± 0.0003
FD	658.0036 ± 9.4833	645.3728 ± 9.0772	6.04 ± 0.5148	0.9244 ± 0.0399	0.9989 ± 0
FE	582.801 ± 7.0036	578.1836 ± 6.6149	5.6382 ± 0.4512	0.9257 ± 0.0281	0.9985 ± 0
FF	603.0205 ± 5.3112	583.5407 ± 15.2415	5.8779 ± 0.5683	0.9368 ± 0.0241	0.9984 ± 0.0005

FA before fecal microbiota transplantation(FMT) in the model group + Donor group; FB before FMT in the model group + control Donor group; FC before model group + saline intervention; FD after FMT in the model group + control Donor group; FE after model group + saline intervention; FF after FMT in the model group + Donor group.

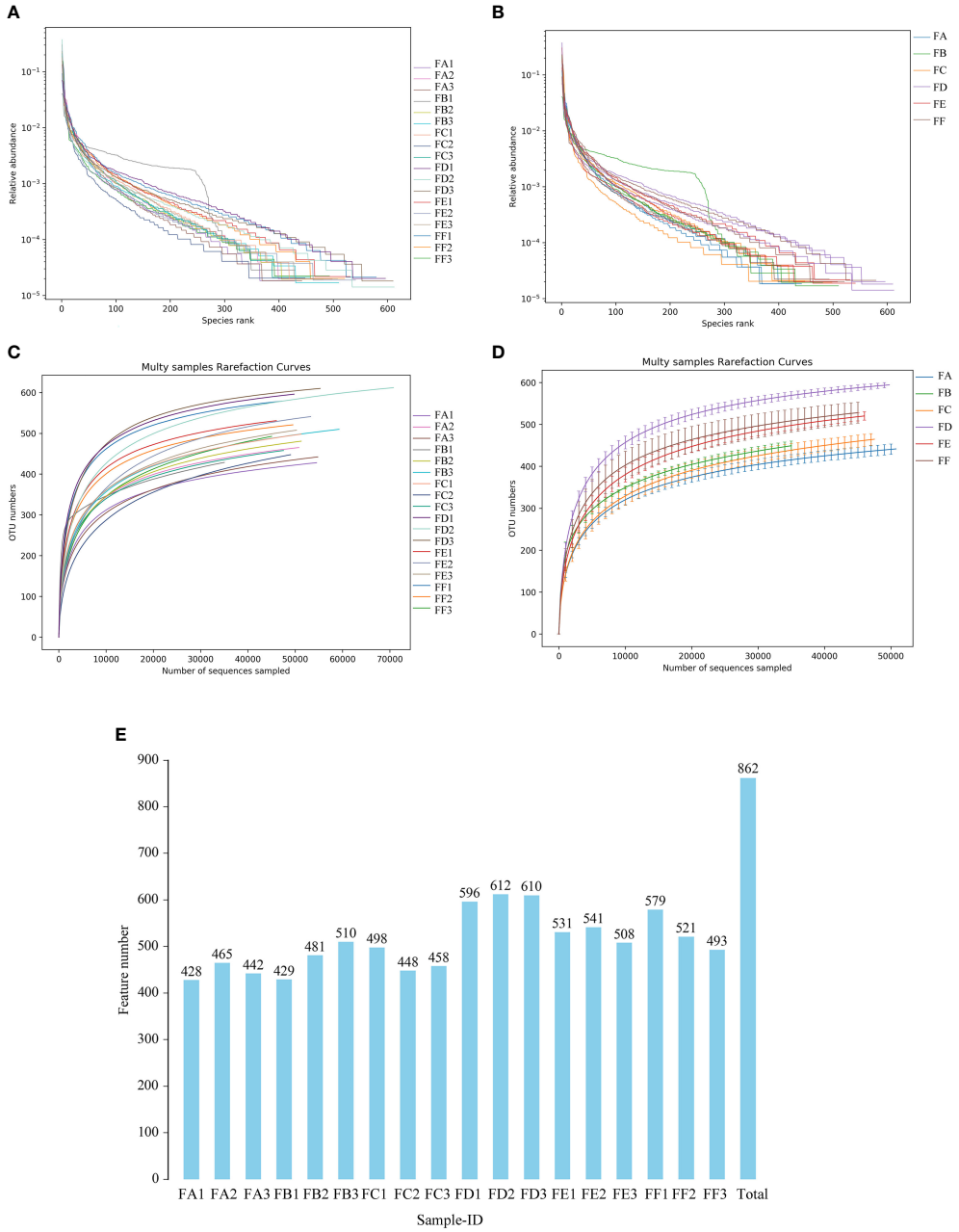

FIGURE 4
Single sample intestinal flora diversity analysis **(A, B)** Rank abundance curve The horizontal coordinate is the ordinal number sorted by the abundance of features, the vertical coordinate is the relative abundance of the corresponding features; **(C, D)** Sample dilution curve. The horizontal coordinate is the number of randomly selected sequencing strips, and the vertical coordinate is the number of features obtained based on the number of sequencing strips. Each curve represents a sample and is marked with a different color. **(E)** Plot of the number of features for each group of samples. The horizontal coordinate is the name of the sample, the vertical coordinate is the number of features, and the number above the bar is the number of OTUs for the corresponding sample.

disease and is closely related to the development of CRF (Meijers et al., 2019; Zhu et al., 2021; Krukowski et al., 2023). Based on our findings, the use of Fushen Granule can regulate the intestinal microbiota and control the progression of CRF. And we demonstrated that FMT in rats in the Fushen Granule group reversed the severe taxonomic and functional imbalance caused by CRF to a certain extent. This represents the first published study to date utilizing the combined treatment of Fushen Granules and FMT for CRF. The Fushen Granule and its compound "Fushen Granules" have been used clinically in the treatment of various kidney diseases such as peritoneal dialysis and interstitial fibrosis (Chen, 2021; Ding, 2022). Modern pharmacological studies have also shown that Astragalus, the primary component of Fushen Granule, has the ability to reduce urinary protein (Zhang et al., 2014) and protect kidney function (Zhou et al., 2017). The combination of Astragalus and Salvia miltiorrhiza can slow down

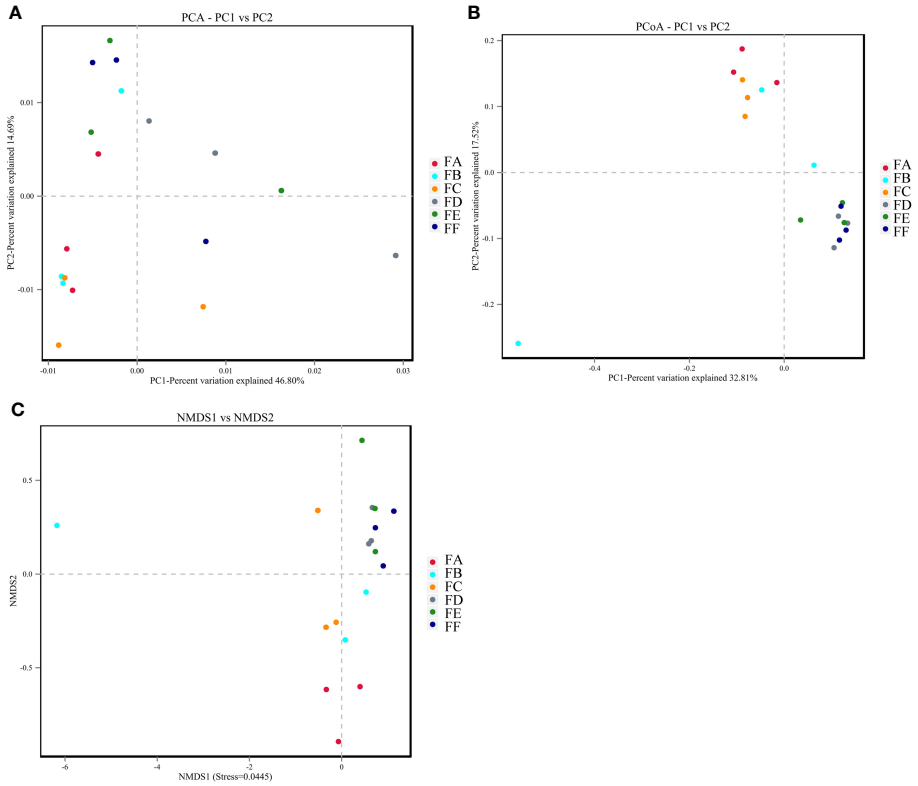

FIGURE 5
The beta diversity analysis. **(A)** PCA. The dots indicate each sample with different colors representing different groupings. The horizontal and vertical coordinates represent the two eigenvalues that cause the greatest variation between samples, with the percentage indicating the contribution of each principal component to the variation of the samples. **(B)** PCoA. Points represent each sample separately, with different colors representing different groupings. The horizontal and vertical coordinates represent the two characteristic values that cause the greatest variation between samples, and the degree of influence is represented as a percentage. The closer the samples are on the coordinate plot, the greater the similarity. **(C)** NMDS. The dots represent each sample separately, with different colors representing different groupings, and the distance between the dots indicates the degree of difference. A Stress value of less than 0.2 indicates that NMDS analysis has a certain degree of reliability, and the closer the samples are on the coordinate graph, the higher the similarity.

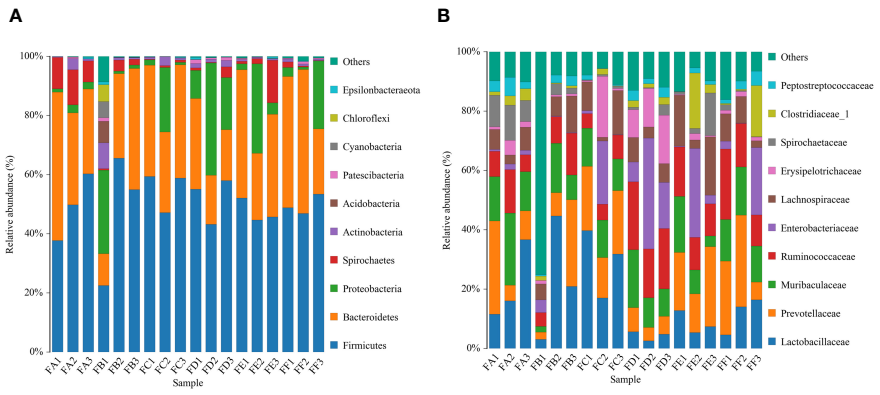

FIGURE 6
Histogram of the relative abundance of species composition of multiple samples for community composition analysis. **(A)** phylum level, **(B)** genus level. FA before FMT in the model group + Donor group; FB before FMT in the model group + control Donor group; FC before model group + saline intervention; FD after FMT in the model group + control Donor group; FE after model group + saline intervention; FF after FMT in the model group + Donor group.

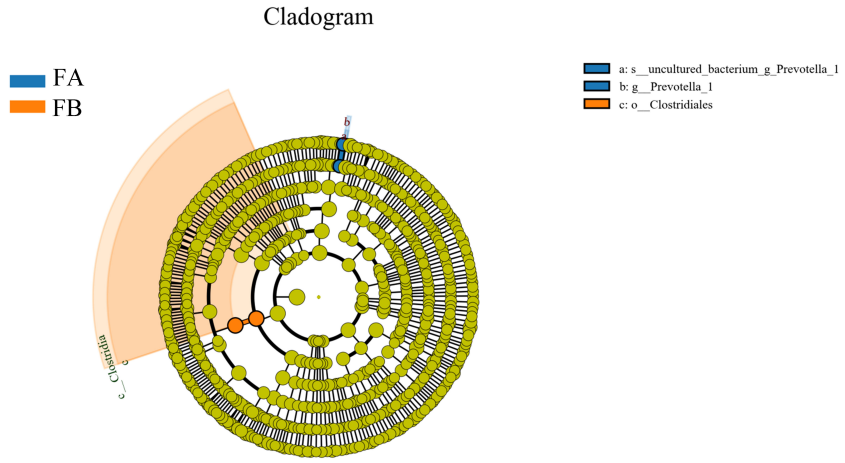

FIGURE 7
Evolutionary branching diagram for LEfSe analysis of the differences in the dominant groups. The circles radiating from the inside to the outside represent the taxonomic levels from phylum to species; each small circle at a different taxonomic level represents a taxon at that level, and the diameter of the small circles is proportional to the size of the relative abundance; the coloring principle is that species with no significant differences are colored uniformly in yellow, and other differing species are colored according to the subgroup in which the species is most abundant. Different colors indicate different subgroups, and different colored nodes indicate the microbiota that play an important role in the subgroup represented by that color.

kidney fibrosis (Han et al., 2021) and suggests a high level of drug safety. *In vitro* and clinical trials have demonstrated that Fushen Granule can, to a certain extent, correct intestinal dysfunction in peritoneal dialysis patients and delay the process of peritoneal fibrosis. Meanwhile, there is increasing evidence suggesting that traditional Chinese medicine plays a beneficial role in the treatment of chronic kidney disease by modulating dysbiosis of the intestinal microbiota (Gao et al., 2021; Ming et al., 2021). However, the effect of Fushen Granule on CRF and the specific potential mechanism remain to be elucidated. Therefore, in this experiment, the effect of Fushen Granule on CRF rats was investigated using a 5/6 nephrectomized CRF rat model. The experimental results showed that the basic conditions of CRF rats were alleviated after different doses of Fushen Granule, and the levels of the intestinal toxins indoxyl sulfate (IS) and p-cresyl sulfate (PCS), as well as D-lactic acid and endotoxin, which are indicators of intestinal barrier damage, were reduced in a dose-related manner. At the same time, the number of operational taxonomic units (OTUs), the ratio of Firmicutes to Bacteroidetes, and the number of lactic acid bacteria increased after Fushen Granule treatment, which restored to some extent the changes in the abundance and structure of the intestinal flora of the rats caused by slow renal failure.

CRF is accompanied by a progressive decrease in glomerular filtration rate and the continued accumulation of metabolic waste products that can accelerate the progression of CRF and affect its prognosis. The enteric-derived toxins indoxyl sulfate (IS) and p-cresol sulfate(PCS) are known as protein-bound toxins due to their protein-binding properties and are currently not filtered out by dialysis. In normal renal function, these two substances are secreted into the renal tubules and excreted from the body. In CRF, the intestinal tract undergoes a series of changes, including a lack of gastrointestinal motility and reduced digestive capacity of the small intestine, which increases the amount and retention time of dietary protein in the colon, which further contributes to the increase in the number of colonic proteolytic bacteria, resulting in increased production of the IS and PCS precursors indole and p-cresol, and ultimately an increase in IS and PCS generation. At the same time, renal filtration function is reduced, resulting in the accumulation of metabolic toxins such as IS and PCS in the body. The long-term retention of IS and PCS in the body can further aggravate glomerulosclerosis and renal fibrosis, leading to a vicious circle (Ito et al., 2010; Lekawanvijit et al., 2010; Niwa, 2010; Liabeuf et al., 2011; Shimizu et al., 2011; Lin et al., 2012; Liu et al., 2012). Therefore, reducing the level of IS and PCS is one of the most important problems to be solved. There is a lack of effective means of IS and PCS clearance, and most of the research on reducing IS and PCS has been conducted in the intestinal tract from the perspective of inhibiting their production, such as with AST120 (Shimoishi et al., 2007; Kikuchi et al., 2010; Asai et al., 2019). Since enteric-derived toxin precursors are primarily produced by the enzymatic processes of the intestinal flora, it is possible to reduce their production by adjusting the structure of the intestinal flora. In the present study, Fushen Granule demonstrated a notable down-regulating effect on the levels of intestine-derived metabolic toxins IS and PCS in CRF rats. It is hypothesized that the mechanism may be related to improving the intestinal tract status and promoting the excretion of toxin precursors.

Serum endotoxin is a metabolite or component of intestinal bacteria that can translocate into the circulation when the barrier is not functioning properly (Violi et al., 2023), it is used as an indicator of intestinal barrier function (Vancamelbeke and Vermeire, 2017). Fushen Granule can improve renal function indicators by repairing intestinal barrier function, reducing metabolic toxins in the serum, and enhancing renal function. D-lactate is a bacterial metabolite produced by the intestinal flora, and its level is low and relatively stable under normal conditions. Elevated levels may reveal the extent of damage to the intestinal mucosa (Guo et al., 2019). Endotoxin, a

major component of the outer membrane of Gram-negative bacteria, can translocate into the body's circulation when intestinal barrier function is compromised, transforming host immune defenses into a pro-inflammatory state (Violi et al., 2023). The endotoxin itself can further contribute to the deterioration of the mucosal barrier function (Tang et al., 2019). In this study, serum endotoxin and D-lactate levels were measured in CRF rats to assess intestinal barrier function. In the sham-operated group, serum endotoxin levels were stable, whereas in the model group, serum endotoxin levels increased with the progression of CRF. The model rats also showed a significant increase in serum D-lactate, both of which are indicative of impaired intestinal barrier function. Fushen Granule reduced the variation of endotoxin and down-regulated the serum D-lactate level, which had a protective effect on the intestinal barrier function and thus delayed the progression of CRF.

Changes in the intestinal flora play a key role in accelerating the progression of CRF, and this study found that Fushen Granule was able to modify the structure of intestinal flora in rats to slow down the progression of CRF. Previous research has reported that in patients with ESRD, the number of Firmicutes, Actinobacteria, Proteobacteria, and Lactobacillus decreased(Vaziri et al., 2013; Simões-Silva et al., 2020), while the number of Bacteroides increased (Crespo-Salgado et al., 2016). In patients with CKD, there was a lower abundance of Lactobacillus and an increased proportion of Enterobacteriaceae (Mahmoodpoor et al., 2017; Lau et al., 2018). It is evident that there is an imbalance between the intestinal flora and the host in the disease state, which may lead to the accumulation of uremic toxins while limiting the beneficial functions and products conferred by the normal flora, thereby accelerating the progression of renal disease (Vaziri et al., 2013). In contrast, the homeostatic gut microbiota serves the host through a wide range of physiological activities, including the prevention of pathogens, maintenance of the function and integrity of the intestinal epithelium, and regulation of the host immune system (Bian et al., 2022). 16S rRNA or DNA sequencing is the common method to evaluate microbial diversity and identify differential microbes in patients compared with healthy control subjects (Cao et al., 2022). The present study, combined with 16S rRNA gene sequencing experiments, aimed to investigate the mechanism of action of Fushen Granule in improving CRF from the perspective of structural changes in the intestinal flora. The results showed that the rats in the model group exhibited a decrease in the number of OTUs in the intestinal flora. At the phylum level, the relative abundance of bacteria in the Firmicutes phylum decreased in the model group after 5/6 nephrectomy compared to the sham-operated group during the same period, while the content of the Bacteroidetes phylum increased, and the ratio of the Firmicutes phylum to the Bacteroidetes phylum showed a decreasing trend. After Fushen Granule intervention, the low-dose and high-dose groups of Chinese medicine reduced this alteration to different degrees, thus restoring the normal ratio of Firmicutes and Bacteroidetes to a certain extent and repairing the alteration of the composition ratio of intestinal flora caused by slow renal failure. At the genus level, the relative abundance comparison showed that Lactobacillus was the predominant genus. This genus is a probiotic strain that can slow down the progression of kidney disease by improving the intestinal environment (Yoshifuji et al., 2016). The relative abundance of Lactobacillus in the model group showed a decreasing trend compared to the sham-operated group during the same period. In contrast, the relative abundance of Lactobacillus in the low-dose and high-dose groups of Chinese medicine showed an increasing trend after treatment. This indicates that Fushen Granule can, to a certain extent, reverse the effect of 5/6 nephrectomy on the intestinal flora of rats, correct the disorder of flora, and make it converge to the normal group, and has the effect of improving the intestinal flora of CRF rats. In conclusion, the restoration of the altered intestinal flora in the CRF state by Fushen Granule may be another mechanism of its action in delaying renal failure.

To further investigate whether Fushen Granule exerts its therapeutic effect through the regulation of intestinal flora, a FMT experiment was conducted to verify the effect of Fushen Granule. Multiple studies indicate that the transplantation of a healthy gut microbiota plays a therapeutic role in various renal diseases. A clinical case study report suggests that FMT reduces the accumulation of PBUTs in the host by modulating the intestinal microbiota's amino acid metabolism, consequently mitigating the progression of CKD (Liu et al., 2022). In investigations on IgAN, it has been reported that FMT-induced microbial transfer regulates the IgAN phenotype, thereby paving the way for new treatment modalities for IgAN patients (Lauriero et al., 2021). Furthermore, in various published studies, FMT has consistently been a valuable tool in verifying the correlation between gut microbiota dysbiosis and the progression of CRF, indicating its value in restoring the intestinal microbiota in CRF. However, there is currently limited understanding of the application of FMT in the treatment of CRF. In this study, we used a rat model to comprehensively evaluate the effects of Fushen Granule on the improvement of serum intestinal endotoxins, intestinal flora structure and diversity, and renal function in CRF with the aid of FMT technology. The results of the study showed that both the Fushen Granule Donor Group and the FMT Group could effectively improve the general status of CRF rats, enhance renal function, reduce serum levels of toxins, and improve intestinal status to promote excretion of toxin precursors, reduce D-lactate, narrow the rise of endotoxin, and protect intestinal barrier function after treatment. Alpha and beta diversity were assessed in the feces collected from each group of rats at the end of fecal microbiota transplantation(FMT). Alpha diversity was assessed mainly from the Ace, Chao, Shannon, and Simpson indices. The results showed that all the above indices exhibited different degrees of increase in the model group after FMT, suggesting that the diversity of rat intestinal flora was restored and the abundance tended to increase. The Ace, Chao, Shannon, and Simpson indices of the model + control Donor group and the model + Fushen Granule Donor group were very close to each other compared to the model + saline sham group. β diversity was demonstrated by PCA, PCoA, and NMDS, and the results showed that there was little overlap between the three groups, suggesting significant differences in the structure of the flora between the groups. Further analysis of the composition and species abundance of the intestinal flora of each group revealed that Fushen Granule and normal flora transplantation had a moderating effect on the structure and relative abundance of the intestinal flora of CRF rats.

6 Conclusion

Based on the 16SrRNA amplification and sequencing technology, this study investigated the mechanism of action of Fushen Granule in the prevention and treatment of CRF in rats with 5/6 nephrectomy as a classical renal failure animal model. The results showed that Fushen Granule was effective in the treatment of CRF rats, potentially delaying the process of CRF by repairing intestinal barrier function, reducing metabolic toxins in serum, improving renal function indicators, and adjusting the structure of intestinal flora. In addition, through FMT experiments, we found that the transplantation of feces from the Fushen Granule Group was able to replicate the intestinal flora structure of the original Fushen Granule Group to a certain extent in the subject rats, and improve the renal function and intestinal status of the CRF rats. This further demonstrates that Fushen Granule can delay the progression of CRF by regulating the "renal-intestinal axis" and improving the intestinal flora structure. This study demonstrates that the Fushen Granules are advantageous in enhancing the structure of the intestinal microbiota and play a constructive role in the prevention and treatment of CRF, thereby offering a scientific basis for its clinical application. The results also suggest that reshaping the homeostasis of the intestinal flora may be an important therapeutic target to slow down the progression of CRF.

Data availability statement

The original contributions presented in the study are included in the article/supplementary material. Further inquiries can be directed to the corresponding author.

Ethics statement

The animal study was approved by Institute of Radiology, Chinese Academy of Medical Sciences. The study was conducted in accordance with the local legislation and institutional requirements.

Author contributions

LW: Methodology, Visualization, Writing – original draft. AX: Software, Writing – original draft. JW: Software, Writing – review & editing. GF: Writing – review & editing. RL: Formal analysis, Methodology, Writing – review & editing. LJW: Data curation, Writing – review & editing. MP: Conceptualization, Funding acquisition, Writing – review & editing.

Funding

The author(s) declare financial support was received for the research, authorship, and/or publication of this article. This work is supported by the National Natural Science Foundation of China (2019YFC1709401).

Acknowledgments

The authors are thankful to Tianjin University of Traditional Chinese Medicine for the help in conducting this study.

Conflict of interest

The authors declare that the research was conducted in the absence of any commercial or financial relationships that could be construed as a potential conflict of interest.

Publisher's note

References

Ahmad, S., and Bromberg, J. S. (2016). Current status of the microbiome in renal transplantation. *Curr. Opin. Nephrol. Hypertens.* 25 (6), 570–576. doi: 10.1097/mnh.0000000000000262

Asai, M., Kumakura, S., and Kikuchi, M. (2019). Review of the efficacy of AST-120 (KREMEZIN(®)) on renal function in chronic kidney disease patients. *Ren Fail* 41 (1), 47–56. doi: 10.1080/0886022x.2018.1561376

Bian, J., Liebert, A., Bicknell, B., Chen, X. M., Huang, C., and Pollock, C. A. (2022). Faecal microbiota transplantation and chronic kidney disease. *Nutrients* 14 (12), 2. doi: 10.3390/nu14122528

Cao, C., Zhu, H., Yao, Y., and Zeng, R. (2022). Gut dysbiosis and kidney diseases. *Front. Med. (Lausanne)* 9. doi: 10.3389/fmed.2022.829349

Chen, J. (2021). A study on the intervention of TGF-β1/BMP-7/Gremlin pathway on peritoneal fibrosis based on Chinese medicine and method to explore the regulation of Fu Ren formula. Masters (Tianjin University of Chinese Medicine). doi: 10.27368/d.cnki.gtzyy.2021.000070

Chen, X. (2016). "Effect of kidney support granules on peritoneal dialysis intestinal dysfunction"," in *2016 Academic Annual Meeting of the Renal Disease Specialized Committee of the Chinese Society of Integrative Medicine*. 381.

Crespo-Salgado, J., Vehaskari, V. M., Stewart, T., Ferris, M., Zhang, Q., Wang, G., et al. (2016). Intestinal microbiota in pediatric patients with end stage renal disease: a Midwest Pediatric Nephrology Consortium study. *Microbiome* 4 (1), 50. doi: 10.1186/s40168-016-0195-9

Cui, M., Xiao, H., Luo, D., Zhang, X., Zhao, S., Zheng, Q., et al. (2016). Circadian rhythm shapes the gut microbiota affecting host radiosensitivity. *Int. J. Mol. Sci.* 17 (11), 1-2,7. doi: 10.3390/ijms17111786

Dai, P., Chang, W., Xin, Z., Cheng, H., Ouyang, W., and Luo, A. (2021). Retrospective study on the influencing factors and prediction of hospitalization expenses for chronic renal failure in China based on random forest and LASSO regression. *Front. Public Health* 9. doi: 10.3389/fpubh.2021.678276

de Almeida Duarte, J. B., de Aguilar-Nascimento, J. E., Nascimento, M., and Nochi, R. J. Jr. (2004). Bacterial translocation in experimental uremia. *Urol Res.* 32 (4), 266–270. doi: 10.1007/s00240-003-0381-7

Ding, F. (2022). Investigating the mechanism of Fu Ren Formula for the prevention and treatment of peritoneal dialysis-associated peritonitis based on TLR4/NF-κB signaling pathway. Masters (Tianjin University of Chinese Medicine). doi: 10.27368/d.cnki.gtzyy.2022.000005

Dou, Y. (2015). Effect of kidney support granules on the expression of activation factors related to peritoneal fibrosis in rats on peritoneal dialysis," in *2015 academic annual meeting of renal disease specialized committee of chinese society of integrative medicine and western medicine*. 1200–1201.

Eirin, A., and Lerman, L. O. (2014). Mesenchymal stem cell treatment for chronic renal failure. *Stem Cell Res. Ther.* 5 (4), 83. doi: 10.1186/scrt472

Fang, J., Guo, Y., Yin, W., Zhang, L., Li, G., Ma, J., et al. (2023). Neoxanthin alleviates the chronic renal failure-induced aging and fibrosis by regulating inflammatory process. *Int. Immunopharmacol.* 114, 109429. doi: 10.1016/j.intimp.2022.109429

Faria, M., and de Pinho, M. N. (2021). Challenges of reducing protein-bound uremic toxin levels in chronic kidney disease and end stage renal disease. *Transl. Res.* 229, 115–134. doi: 10.1016/j.trsl.2020.09.001

Feroze, U., Kalantar-Zadeh, K., Sterling, K. A., Molnar, M. Z., Noori, N., Benner, D., et al. (2012). Examining associations of circulating endotoxin with nutritional status, inflammation, and mortality in hemodialysis patients. *J. Ren Nutr.* 22 (3), 317–326. doi: 10.1053/j.jrn.2011.05.004

Gao, Y., Yang, R., Guo, L., Wang, Y., Liu, W. J., Ai, S., et al. (2021). Qing-re-xiao-zheng formula modulates gut microbiota and inhibits inflammation in mice with diabetic kidney disease. *Front. Med. (Lausanne)* 8. doi: 10.3389/fmed.2021.719950

Gelasco, A. K., and Raymond, J. R. (2006). Indoxyl sulfate induces complex redox alterations in mesangial cells. *Am. J. Physiol. Renal Physiol.* 290 (6), F1551–F1558. doi: 10.1152/ajprenal.00281.2004

Gonçalves, S., Pecoits-Filho, R., Perreto, S., Barberato, S. H., Stinghen, A. E., Lima, E. G., et al. (2006). Associations between renal function, volume status and endotoxaemia in chronic kidney disease patients. *Nephrol. Dial Transplant.* 21 (10), 2788–2794. doi: 10.1093/ndt/gfl273

Grice, E. A., Kong, H. H., Conlan, S., Deming, C. B., Davis, J., Young, A. C., et al. (2009). Topographical and temporal diversity of the human skin microbiome. *Science* 324 (5931), 1190–1192. doi: 10.1126/science.1171700

Guo, Y., Li, H., Liu, Z., Li, C., Chen, Y., Jiang, C., et al. (2019). Impaired intestinal barrier function in a mouse model of hyperuricemia. *Mol. Med. Rep.* 20 (4), 3292–3300. doi: 10.3892/mmr.2019.10586

Han, C., Jiang, Y. H., Li, W., and Liu, Y. (2021). Astragalus membranaceus and Salvia miltiorrhiza ameliorates cyclosporin A-induced chronic nephrotoxicity through the "gut-kidney axis". *J. Ethnopharmacol.* 269, 113768. doi: 10.1016/j.jep.2020.113768

Ito, S., Osaka, M., Higuchi, Y., Nishijima, F., Ishii, H., and Yoshida, M. (2010). Indoxyl sulfate induces leukocyte-endothelial interactions through up-regulation of E-selectin. *J. Biol. Chem.* 285 (50), 38869–38875. doi: 10.1074/jbc.M110.166686

Jiang, C., Jiao, S., and Yang, H. (2020a). Effect of kidney support granules on 1-year prognosis of patients with peritoneal dialysis-associated peritonitis. *Chin. J. Integrated Traditional West. Med.* 40 (11), 1333–1338.

Jiang, C., Lin, W., Wang, L., Lv, Y., Song, Y., Chen, X., et al. (2020b). Fushen Granule, A Traditional Chinese Medicine, ameliorates intestinal mucosal dysfunction in peritoneal dialysis rat model by regulating p38MAPK signaling pathway. *J. Ethnopharmacol.* 251, 112501. doi: 10.1016/j.jep.2019.112501

Kikuchi, K., Itoh, Y., Tateoka, R., Ezawa, A., Murakami, K., and Niwa, T. (2010). Metabolomic search for uremic toxins as indicators of the effect of an oral sorbent AST-120 by liquid chromatography/tandem mass spectrometry. *J. Chromatogr. B Anal. Technol. BioMed. Life Sci.* 878 (29), 2997–3002. doi: 10.1016/j.jchromb.2010.09.006

Krukowski, H., Valkenburg, S., Madella, A. M., Garssen, J., van Bergenhenegouwen, J., Overbeek, S. A., et al. (2023). Gut microbiome studies in CKD: opportunities, pitfalls and therapeutic potential. *Nat. Rev. Nephrol.* 19 (2), 87–101. doi: 10.1038/s41581-022-00647-z

Lau, W. L., Savoj, J., Nakata, M. B., and Vaziri, N. D. (2018). Altered microbiome in chronic kidney disease: systemic effects of gut-derived uremic toxins. *Clin. Sci. (Lond)* 132 (5), 509–522. doi: 10.1042/cs20171107

Lauriero, G., Abbad, L., Vacca, M., Celano, G., Chemouny, J. M., Calasso, M., et al. (2021). Fecal microbiota transplantation modulates renal phenotype in the humanized mouse model of igA nephropathy. *Front. Immunol.* 12. doi: 10.3389/fimmu.2021.694787

Lei, Y. (2016). "Observations on the clinical efficacy of blood purification and kidney support granules in the treatment of chronic renal failure and the impact on patients' quality of life.", in: *2016 Academic Annual Meeting of the Renal Disease Specialized Committee of the Chinese Society of Integrative Medicine)*, 1.

Lei, Y., and Yang, H. (2018). Efficacy of kidney support granules combined with colonic enema on intestinal dysfunction after peritoneal dialysis catheterization. *Chin. J. Surg. Integrated Traditional West. Med.* 24 (03), 294–298.

Lei, Y., Yang, B., Ming, P., and Yang, H. (2018a). Forty-six cases of gastrointestinal dysfunction in peritoneal dialysis patients treated by enema combined with kidney support granules. *Chin. J. Surg. Integrated Traditional West. Med.* 24 (04), 441–446.

Lei, Y., Yang, B., Pei, M., Lin, Y., and Yang, H. (2018b). Effects of Kidney Support Formula on the expression of TGF-β1, E-cadherin and α-SMA in peritoneal mesenchyme of uremic rats. *Tianjin J. Traditional Chin. Med.* 35 (07), 521–525.

Lei, Y., Yang, B., Wang, M., Qiao, Y., Zhao, Y., and Yang, H. (2018c). Discussion on the effect and mechanism of Kidney Supporting Formula on the transdifferentiation of rat peritoneal mesothelial cells. *Liaoning J. Traditional Chin. Med.* 45 (07), 1500–1503. doi: 10.13192/j.issn.1000-1719.2018.07.052

Lekawanvijit, S., Adrahtas, A., Kelly, D. J., Kompa, A. R., Wang, B. H., and Krum, H. (2010). Does indoxyl sulfate, a uraemic toxin, have direct effects on cardiac fibroblasts and myocytes? *Eur. Heart J.* 31 (14), 1771–1779. doi: 10.1093/eurheartj/ehp574

Li, J., Yang, B., and Yang, H. (2020). Overview of the mechanism of action of renal pellets in regulating decorin interference with peritoneal collagen stability. *Inner Mongolia J. Traditional Chin. Med.* 39 (02), 129–131. doi: 10.16040/j.cnki.cn15-1101.2020.02.081

Liabeuf, S., Drüeke, T. B., and Massy, Z. A. (2011). Protein-bound uremic toxins: new insight from clinical studies. *Toxins (Basel)* 3 (7), 911–919. doi: 10.3390/toxins3070911

Lin, C. J., Liu, H. L., Pan, C. F., Chuang, C. K., Jayakumar, T., Wang, T. J., et al. (2012). Indoxyl sulfate predicts cardiovascular disease and renal function deterioration in advanced chronic kidney disease. *Arch. Med. Res.* 43 (6), 451–456. doi: 10.1016/j.arcmed.2012.08.002

Liu, S., Wang, B. H., Kompa, A. R., Lekawanvijit, S., and Krum, H. (2012). Antagonists of organic anion transporters 1 and 3 ameliorate adverse cardiac remodelling induced by uremic toxin indoxyl sulfate. *Int. J. Cardiol.* 158 (3), 457–458. doi: 10.1016/j.ijcard.2012.05.022

Liu, X., Zhang, M., Wang, X., Liu, P., Wang, L., Li, Y., et al. (2022). Fecal microbiota transplantation restores normal fecal composition and delays Malignant development of mild chronic kidney disease in rats. *Front. Microbiol.* 13. doi: 10.3389/fmicb.2022.1037257

Liyanage, T., Ninomiya, T., Jha, V., Neal, B., Patrice, H. M., Okpechi, I., et al. (2015). Worldwide access to treatment for end-stage kidney disease: a systematic review. *Lancet* 385 (9981), 1975–1982. doi: 10.1016/s0140-6736(14)61601-9

Mahmoodpoor, F., Rahbar Saadat, Y., Barzegari, A., Ardalan, M., and Zununi Vahed, S. (2017). The impact of gut microbiota on kidney function and pathogenesis. *BioMed. Pharmacother.* 93, 412–419. doi: 10.1016/j.biopha.2017.06.066

Matsushita, K., Ballew, S. H., Wang, A. Y., Kalyesubula, R., Schaeffner, E., and Agarwal, R. (2022). Epidemiology and risk of cardiovascular disease in populations with chronic kidney disease. *Nat. Rev. Nephrol.* 18 (11), 696–707. doi: 10.1038/s41581-022-00616-6

Meijers, B., Evenepoel, P., and Anders, H. J. (2019). Intestinal microbiome and fitness in kidney disease. *Nat. Rev. Nephrol.* 15 (9), 531–545. doi: 10.1038/s41581-019-0172-1

Ming, Y., Cheng, S., Long, W., Wang, H. L., Xu, C., Liu, X., et al. (2021). The herbal formula granule prescription mahuang decoction ameliorated chronic kidney disease which was associated with restoration of dysbiosis of intestinal microbiota in rats. *Evid Based Complement Alternat Med.* 2021, 4602612. doi: 10.1155/2021/4602612

Miyazaki, T., Ise, M., Hirata, M., Endo, K., Ito, Y., Seo, H., et al. (1997). Indoxyl sulfate stimulates renal synthesis of transforming growth factor-beta 1 and progression of renal failure. *Kidney Int. Suppl.* 63, S211–S214.

Niwa, T. (2010). Indoxyl sulfate is a nephro-vascular toxin. *J. Ren Nutr.* 20 (5 Suppl), S2–S6. doi: 10.1053/j.jrn.2010.05.002

Pluznick, J. L. (2020). The gut microbiota in kidney disease. *Science* 369 (6510), 1426–1427. doi: 10.1126/science.abd8344

Ruiz-Ortega, M., Rayego-Mateos, S., Lamas, S., Ortiz, A., and Rodrigues-Diez, R. R. (2020). Targeting the progression of chronic kidney disease. *Nat. Rev. Nephrol.* 16 (5), 269–288. doi: 10.1038/s41581-019-0248-y

Saran, R., Robinson, B., Abbott, K. C., Agodoa, L. Y. C., Bhave, N., Bragg-Gresham, J., et al. (2018). US renal data system 2017 annual data report: epidemiology of kidney disease in the United States. *Am. J. Kidney Dis.* 71 (3 Suppl 1), A7. doi: 10.1053/j.ajkd.2018.01.002

Shimizu, H., Bolati, D., Adijiang, A., Adelibieke, Y., Muteliefu, G., Enomoto, A., et al. (2011). Indoxyl sulfate downregulates renal expression of Klotho through production of ROS and activation of nuclear factor-κB. *Am. J. Nephrol.* 33 (4), 319–324. doi: 10.1159/000324885

Shimoishi, K., Anraku, M., Kitamura, K., Tasaki, Y., Taguchi, K., Hashimoto, M., et al. (2007). An oral adsorbent, AST-120 protects against the progression of oxidative stress by reducing the accumulation of indoxyl sulfate in the systemic circulation in renal failure. *Pharm. Res.* 24 (7), 1283–1289. doi: 10.1007/s11095-007-9248-x

Simões-Silva, L., Araujo, R., Pestana, M., Soares-Silva, I., and Sampaio-Maia, B. (2020). Peritoneal microbiome in end-stage renal disease patients and the impact of peritoneal dialysis therapy. *Microorganisms* 8 (2), 4–9. doi: 10.3390/microorganisms8020173

Sun, A., and Liu, Z. (2010). Therapeutic efficacy of enema with western medicine in the treatment of chronic renal failure by Fu Ren Tang and Enema Formula. *Shaanxi J. Traditional Chin. Med.* 31 (04), 397–398.

Szeto, C. C., Kwan, B. C., Chow, K. M., Lai, K. B., Chung, K. Y., Leung, C. B., et al. (2008). Endotoxemia is related to systemic inflammation and atherosclerosis in peritoneal dialysis patients. *Clin. J. Am. Soc. Nephrol.* 3 (2), 431–436. doi: 10.2215/cjn.03600807

Tang, G., Yang, H., Lin, Y., Bu, Y., and Chen, D. (2018a). Mechanism study on the improvement of renal anemia in rats with abdominal dialysis model by supporting kidney granules. *Liaoning J. Traditional Chin. Med.* 45 (09), 1971–1973. doi: 10.13192/j.issn.1000-1719.2018.09.057

Tang, G., Yang, H., Lin, Y., Guo, S., Bu, Y., and Mei, X. (2017). Molecular mechanism of improvement of peritoneal ultrafiltration function by kidney support granules. *Chin. J. Exp. Traditional Med. Formulae* 23 (23), 103–108. doi: 10.13422/j.cnki.syfjx.2017230103

Tang, G., Yang, H., Lin, Y., Lv, Y., Wang, C., Guo, S., et al. (2018b). Study on the mechanism of inhibition of peritoneal fibrosis in peritoneal dialysis rats by regulating the production of AGEs by Fukui Kidney Granules. *China J. Traditional Chin. Med. Pharm.* 33 (07), 3052–3055.

Tang, W. H. W., Li, D. Y., and Hazen, S. L. (2019). Dietary metabolism, the gut microbiome, and heart failure. *Nat. Rev. Cardiol.* 16 (3), 137–154. doi: 10.1038/s41569-018-0108-7

Vancamelbeke, M., and Vermeire, S. (2017). The intestinal barrier: a fundamental role in health and disease. *Expert Rev. Gastroenterol. Hepatol.* 11 (9), 821–834. doi: 10.1080/17474124.2017.1343143

Vaziri, N. D., Wong, J., Pahl, M., Piceno, Y. M., Yuan, J., DeSantis, T. Z., et al. (2013). Chronic kidney disease alters intestinal microbial flora. *Kidney Int.* 83 (2), 308–315. doi: 10.1038/ki.2012.345

Violi, F., Cammisotto, V., Bartimoccia, S., Pignatelli, P., Carnevale, R., and Nocella, C. (2023). Gut-derived low-grade endotoxaemia, atherothrombosis and cardiovascular disease. *Nat. Rev. Cardiol.* 20 (1), 24–37. doi: 10.1038/s41569-022-00737-2

Wang, Z., Zhang, S., Zheng, X., and Zhang, L. (2021). Efficacy and safety of colonic dialysis combined with traditional Chinese medicine retention enema in the treatment of chronic renal failure: A protocol for systematic review and meta-analysis. *Med. (Baltimore)* 100 (50), e28082. doi: 10.1097/md.0000000000028082

Watanabe, H., Miyamoto, Y., Honda, D., Tanaka, H., Wu, Q., Endo, M., et al. (2013). p-Cresyl sulfate causes renal tubular cell damage by inducing oxidative stress by activation of NADPH oxidase. *Kidney Int.* 83 (4), 582–592. doi: 10.1038/ki.2012.448

Webster, A. C., Nagler, E. V., Morton, R. L., and Masson, P. (2017). Chronic kidney disease. *Lancet* 389 (10075), 1238–1252. doi: 10.1016/s0140-6736(16)32064-5

Wouk, N. (2021). End-stage renal disease: medical management. *Am. Fam Phys.* 104 (5), 493–499.

Wouters, O. J., O'Donoghue, D. J., Ritchie, J., Kanavos, P. G., and Narva, A. S. (2015). Early chronic kidney disease: diagnosis, management and models of care. *Nat. Rev. Nephrol.* 11 (8), 491–502. doi: 10.1038/nrneph.2015.85

Yang, H., Cao, S., Zhao, J., Lin, Y., Yang, B., Fan, S., et al. (2013). Study related to the improvement of survival quality and prevention of peritoneal fibrosis in patients with abdominal dialysis by supporting kidney granules. *Tianjin J. Traditional Chin. Med.* 30 (11), 659.

Yang, H., Lu, Y., Deng, Y., Fang, J., Liu, G., Jiang, A., et al. (2012a). A multicenter clinical study of Fukui Kidney Granules for evidence-based intervention in peritoneal dialysis patients. *Chin. J. Integrated Traditional West. Nephrol.* 13 (05), 410–412.

Yang, B., Ren, T., Li, J., Jiang, C., Xing, H., Zhang, L., et al. (2014). Clinical study on the improvement of malnutrition in peritoneal dialysis patients by supporting kidney granules. *Chin. J. Integrated Traditional West. Nephrol.* 15 (03), 234–236.

Yang, T., Richards, E. M., Pepine, C. J., and Raizada, M. K. (2018). The gut microbiota and the brain-gut-kidney axis in hypertension and chronic kidney disease. *Nat. Rev. Nephrol.* 14 (7), 442–456. doi: 10.1038/s41581-018-0018-2

Yang, B., Wang, M., Sun, L., Li, J., Qiao, Y., and Yang, H. (2021a). Effects of Kidney Support Formula on peritoneal function and VEGF, TNF-α, IL-12 and IFN-γ in uremic peritoneal dialysis rats. *Chin. J. Comp. Med.* 31 (04), 15–20.

Yang, B., Wang, M., Sun, L., Zhong, K., Li, J., and Yang, H. (2021b). Effects of Kidney Support Formula on peritoneal ultrafiltration function and VEGF-Notch signaling pathway in uremic peritoneal dialysis rats. *Tianjin Med. J.* 49 (07), 699–705.

Yang, B., and Yang, H. (2015). "The effect of kidney support granules on the nutritional status of elderly patients with chronic kidney disease stage 4," in *2015 Academic Annual Meeting of Renal Disease Specialized Committee of Chinese Society of Integrative Medicine and Western Medicine*. 1194–1195.

Yang, H., Zhang, J., Zhao, J., and Yang, B. (2012b). Experimental study on the effect of kidney support granules on peritoneal dialysis-associated peritoneal fibrosis and its mechanism of action. *Chin. J. Integrated Traditional West. Nephrol.* 13 (06), 482–486.

Yoshifuji, A., Wakino, S., Irie, J., Tajima, T., Hasegawa, K., Kanda, T., et al. (2016). Gut Lactobacillus protects against the progression of renal damage by modulating the gut environment in rats. *Nephrol. Dial Transplant.* 31 (3), 401–412. doi: 10.1093/ndt/gfv353

Zhang, H. W., Lin, Z. X., Xu, C., Leung, C., and Chan, L. S. (2014). Astragalus (a traditional Chinese medicine) for treating chronic kidney disease. *Cochrane Database Syst. Rev.* 10), Cd008369. doi: 10.1002/14651858.CD008369.pub2

Zhang, L., Wang, F., Wang, L., Wang, W., Liu, B., Liu, J., et al. (2012). Prevalence of chronic kidney disease in China: a cross-sectional survey. *Lancet* 379 (9818), 815–822. doi: 10.1016/s0140-6736(12)60033-6

Zhang, L., and Yang, H. (2016). "Clinical study on the integrated treatment of chronic kidney disease stage 4 with traditional Chinese medicine," in *2016 Academic Annual Meeting of the Renal Disease Specialized Committee of the Chinese Society of Integrative Medicine*. 347.

Zhang, L., and Yang, H. (2018a). Experimental study on the modulation of microinflammatory state by fusiform renal fluid in rats with chronic renal failure. *Liaoning J. Traditional Chin. Med.* 45 (08), 1740–1743. doi: 10.13192/j.issn.1000-1719.2018.08.059

Zhang, L., and Yang, H. (2018b). "Study on the inhibition of microinflammatory state in rats with chronic renal insufficiency model by Compound Kidney Supporting Liquid," in *2018 Academic Annual Meeting of Renal Disease Specialized Committee of Chinese Society of Integrative Medicine and Western Medicine*. 428.

Zhao, X., Zhang, X., Li, M., and Wang, Y. (2022). Effects of Kidney Supporting Formula on renal pathology and expression of CTGF, FN and Vimentin in UUO rats. *Tianjin J. Traditional Chin. Med.* 39 (02), 232–237.

Zhou, X., Sun, X., Gong, X., Yang, Y., Chen, C., Shan, G., et al. (2017). Astragaloside IV from Astragalus membranaceus ameliorates renal interstitial fibrosis by inhibiting inflammation via TLR4/NF-κB in *vivo* and in *vitro*. *Int. Immunopharmacol.* 42, 18–24. doi: 10.1016/j.intimp.2016.11.006

Zhu, H., Cao, C., Wu, Z., Zhang, H., Sun, Z., Wang, M., et al. (2021). The probiotic L. casei Zhang slows the progression of acute and chronic kidney disease. *Cell Metab.* 33 (10), 1926–1942.e1928. doi: 10.1016/j.cmet.2021.06.014

frontiers | Frontiers in Cellular and Infection Microbiology

TYPE Original Research
PUBLISHED 11 January 2024
DOI 10.3389/fcimb.2023.1305375

OPEN ACCESS

EDITED BY
Gang Ye,
Sichuan Agricultural University, China

REVIEWED BY
Li-Da Wu,
Nanjing Medical University, China
Hanbin Cui,
Ningbo First Hospital, China

*CORRESPONDENCE
Hongyan Cai
hyflykm@sina.com
Yong Duan
daunyong7@139.com

RECEIVED 19 October 2023
ACCEPTED 26 December 2023
PUBLISHED 11 January 2024

CITATION
Wang J, Hu Z, Xu Q, Shi Y, Cao X, Ma Y, Wang M, Zhang C, Luo X, Lin F, Li X, Duan Y and Cai H (2024) Gut microbiome-based noninvasive diagnostic model to predict acute coronary syndromes.
Front. Cell. Infect. Microbiol. 13:1305375.
doi: 10.3389/fcimb.2023.1305375

Gut microbiome-based noninvasive diagnostic model to predict acute coronary syndromes

Jincheng Wang[1], Zhao Hu[2], Qiuyue Xu[3], Yunke Shi[1], Xingyu Cao[1], Yiming Ma[1], Mingqiang Wang[1], Chaoyue Zhang[1], Xiang Luo[1], Fanru Lin[1], Xianbin Li[1], Yong Duan[3]* and Hongyan Cai[1]*

[1]Department of Cardiology, the First Affiliated Hospital of Kunming Medical University, Kunming, China, [2]Department of Geriatric Cardiology, the First Affiliated Hospital of Kunming Medical University, Kunming, China, [3]Department of Clinical Laboratory, The First Affiliated Hospital of Kunming Medical University, Yunnan Key Laboratory of Laboratory Medicine, Yunnan Province Clinical Research Center for Laboratory Medicine, Kunming, China

Background: Previous studies have shown that alterations in the gut microbiota are closely associated with Acute Coronary Syndrome (ACS) development. However, the value of gut microbiota for early diagnosis of ACS remains understudied.

Methods: We recruited 66 volunteers, including 29 patients with a first diagnosis of ACS and 37 healthy volunteers during the same period, collected their fecal samples, and sequenced the V4 region of the 16S rRNA gene. Functional prediction of the microbiota was performed using PICRUSt2. Subsequently, we constructed a nomogram and corresponding webpage based on microbial markers to assist in the diagnosis of ACS. The diagnostic performance and usefulness of the model were analyzed using boostrap internal validation, calibration curves, and decision curve analysis (DCA).

Results: Compared to that of healthy controls, the diversity and composition of microbial community of patients with ACS was markedly abnormal. Potentially pathogenic genera such as *Streptococcus* and *Acinetobacter* were significantly increased in the ACS group, whereas certain SCFA-producing genera such as *Blautia* and *Agathobacter* were depleted. In addition, in the correlation analysis with clinical indicators, the microbiota was observed to be associated with the level of inflammation and severity of coronary atherosclerosis. Finally, a diagnostic model for ACS based on gut microbiota and clinical variables was developed with an area under the receiver operating characteristic (ROC) curve (AUC) of 0.963 (95% CI: 0.925–1) and an AUC value of 0.948 (95% CI: 0.549–0.641) for bootstrap internal validation. The calibration curves of the model show good consistency between the actual and predicted probabilities. The DCA showed that the model had a high net clinical benefit for clinical applications.

Conclusion: Our study is the first to characterize the composition and function of the gut microbiota in patients with ACS and healthy populations in Southwest China and demonstrates the potential effect of the microbiota as a non-invasive marker for the early diagnosis of ACS.

KEYWORDS

acute coronary syndrome, gut microbiome, diagnostic model, nomogram, 16SrRNA

Introduction

Acute coronary syndromes (ACS), including ST-segment elevation myocardial infarction (STEMI), non-ST-segment elevation myocardial infarction (NSTEMI), and unstable angina (UA), are leading causes of morbidity and mortality worldwide (Bergmark et al., 2022). Its major pathological mechanism is the rupture or erosion of unstable atherosclerotic plaques, leading to myocardial ischaemia and thrombosis, which is characterized by sudden onset and rapid progression, and may lead to malignant and life-threatening lesions at any time if left untreated(Bhatt et al., 2022). Currently, ACS diagnosis relies on clinical symptoms, electrocardiographic dynamics, and alterations in myocardial necrosis markers such as myoglobin, creatine kinase isoenzyme MB (CK-MB), cardiac troponin T (cTnT), and cardiac troponin I (cTnI) (Byrne et al., 2023). However, one of the main problems in the clinical diagnosis ACS is the late onset of disease symptoms or only atypical symptoms, which may lead to a delay in consultation and miss the optimal time to save the patient's life(Brieger et al., 2004). In addition, myocardial necrosis markers are not released from the myocardium until after myocardial ischaemia and necrosis, and are not elevated in unstable angina or in the early stages of acute myocardial infarction, making it impossible to diagnose early ischaemia(Mair, 1997; Braunwald, 2012). Therefore, the identification of novel biomarkers for the early diagnosis of ACS is an emerging priority, as it may facilitate the timely receipt of appropriate treatment and reduce the mortality and disability of patients(Katus et al., 2017).

Recently, a growing body of evidence has shown that gut microbiota is closely related to the pathogenesis of cardiovascular diseases, particularly coronary artery disease(Koeth et al., 2013; Jie et al., 2017; Zhu et al., 2018; Liu et al., 2019), hypertension(Yang et al., 2015), and heart failure(Pasini et al., 2016). This interaction between the gut and the heart is known as the "gut-heart axis"(Du et al., 2020; Troseid et al., 2020). On the one hand, Dysbiosis of the gut microbiota contributes to the progression of cardiovascular diseases by manipulating the host immune response and exacerbating the inflammatory response(Chistiakov et al., 2015; van den Munckhof et al., 2018). On the other hand, the microbial community in the gut can produce various metabolites, including trimethylamine oxides, bile acids, and short-chain fatty acids, which enter the systemic circulation and affect the host's lipid metabolism, bile acid metabolism, and energy metabolism(Zhu et al., 2016; Fatkhullina et al., 2018; Haghikia et al., 2022; Tousoulis et al., 2022). Numerous studies have demonstrated the presence of gut microbiota dysbiosis in patients with coronary artery disease, accompanied by changes in the structure, composition and function of the microbiota(Jie et al., 2017; Zhu et al., 2018). Furthermore, a diagnostic model based on gut microbiota and clinical features was developed to improve the diagnostic performance of CAD(Zheng et al., 2020). Recently, the composition and function of the gut microbiota were shown to vary in patients with different subtypes of coronary artery disease. In particular, the microbiota profile of patients with ACS is significantly different from that of patients with stable coronary artery disease(Liu et al., 2019; Khan et al., 2022; Dong et al., 2023). However, no study has established a gut microbiome-based diagnostic model for ACS.

To address these questions, we investigated the characteristics and differences in gut microbiota composition between patients with ACS and healthy populations by 16S rRNA gene sequencing and explored the effectiveness of gut microbiota as a tool for early diagnosis of ACS.

Materials and method

Study population

This was a single-center cross-sectional study. We consecutively recruited 29 patients with newly diagnosed ACS, including those with ST-segment elevation myocardial infarction (STEMI), non-ST-segment elevation myocardial infarction (NSTEMI), and unstable angina (UA), January 2022–June 2022 at the First Affiliated Hospital of Kunming Medical University. The diagnosis of ACS was based on a combination of clinical symptoms, electrocardiograms, myocardial enzymes, and coronary angiography and the detailed diagnostic criteria were based on the ESC guidelines(Byrne et al., 2023). The control group comprised 37 asymptomatic healthy volunteers who underwent routine physical examination at the First Affiliated Hospital of Kunming Medical University during the same period. All participants were

long-term local residents, aged between 18 and 80 years, and volunteered to provide a complete medical history, clinical examination parameters, and stool samples. We excluded patients with previous coronary artery disease, heart failure, structural heart disease, gastrointestinal disease (including peptic ulcer, acute gastroenteritis, inflammatory bowel disease, etc.), severe liver or kidney disease, autoimmune disease, malignant tumours, antibiotic or probiotic use in the past three months, and those with a history of prolonged diarrhoea or constipation. The study protocol was approved by the Ethics Committee of the First Affiliated Hospital of Kunming Medical University and all patients provided written informed consent to participate in the study. All procedures were performed in accordance with the ethical standards of the Declaration of Helsinki and its subsequent revisions.

Clinical data and sample collection

Clinical data were collected from all participants, including demographic characteristics such as age, sex, height, weight, smoking and drinking habits, and medical history. All patients underwent coronary angiography, the results of which were independently confirmed by two professional cardiologists, and the severity of coronary atherosclerosis was assessed using the Gensini score (Gensini, 1983). Five milliliters of fasting peripheral venous blood were collected from each participant on the morning of the day following admission, and routine blood tests, liver function, renal function, and lipid analyses were performed. All participants were asked to collect stool samples within the next day of admission and were trained in sample collection. Each subject was provided with a sterile disposable tray and sterile stool sampler with a spoon for stool sample collection by researchers beforehand. All participants were asked to empty their urine, wash their hands, and wear disposable gloves prior to stool collection. The subjects' stools were collected in sterile disposable trays and the middle portion of the stool was collected using a sterile stool sampler with a spoon. Each subject's stool sample was then divided equally into five portions of 200 mg each and transported immediately to the laboratory for freezing at -80°C.

DNA extraction and 16S rRNA gene V4 region sequencing

The fecal bacterial DNA was extracted using cetyltrimethylammonium bromide (CTAB) method. The DNA concentration and purity were monitored on a 1% agarose gel. According to the concentration, DNA was diluted to 1ng/μL using sterile water. The V4 region of the 16S rRNA gene was amplified by polymerase chain reaction (PCR) using the extracted DNA as template. The sequence of the forwarding primers used was 515F (5'-GTGCCAGCMGCCGCGGTAA-3') and the reverse primer used sequence was 806R (5'-GGACTACHVGGGTWTCTAAT-3'). Sequencing libraries were generated using the TruSeq® DNA PCR-Free Sample Preparation Kit (Illumina, USA) and index codes were added according to the manufacturer's recommendations. Library quality was assessed using a Qubit@ 2.0 Fluorometer (Thermo Scientific) and an Agilent Bioanalyzer 2100 system. Finally, the validated libraries were sequenced using an Illumina NovaSeq 6000 (NovoGene, Beijing, China), generating 250 bp paired-end reads according to the manufacturer's instructions.

Gut microbiome analyses

The data for each sample was split from the downstream data based on the barcode and PCR amplification primer sequences and after truncating the barcode and primer sequences, the reads for each sample were spliced using FLASH (V1.2.7, http://ccb.jhu.edu/software/FLASH/) to obtain the raw tags. Quality filtering of raw tags was performed under specific filtering conditions to obtain high-quality clean tags according to the QIIME (V1.9.1, http://qiime.org/scripts/split_libraries_fastq.html) quality-controlled process. Then the tags were then compared with a reference database (Silva database, https://www.arb-silva.de/) using the UCHIME algorithm (http://www.drive5.com/usearch/manual/uchime_algo.html) to remove chimeric sequences and obtain effective tags. Operational taxonomic units (OTUs) were analyzed for clustering and species classification based on effective data using UPARSE software(Edgar, 2013). Sequences with ≥ 97% similarity were grouped into the same OTU and representative sequences from each OTU were annotated with taxonomic information based on the Mothur algorithm using the Silva database. The community composition of each sample was assessed at different taxonomic levels (phylum, order, order, family, and genus) and compared among groups of taxonomic levels. Alpha and beta diversity analyses were performed using the QIIME software (V1.9.1) and R software (V4.3.1). The alpha diversity of the samples was described using the observed species and Chao1 and ACE indices and *p*-values were calculated using Wilcoxon's test. Beta diversity was assessed using an unweighted UniFrac distance matrix and visualized using principal coordinate analysis (PCoA) and non-metric multidimensional scaling (NMDS) plots; while differences in microbial community composition between the two groups were compared using ANOSIM analysis. We used a hierarchical clustering method, the Unweighted Pair-group Method with Arithmetic Means (UPGMA), which interprets distance matrices using average linkage via the QIIME software (version 1.9.1), for comparing the similarity of the gut microbiota in each group of samples. Linear discriminant analysis effect size (LEfSe) was used to identify key microbial taxa that differed significantly between the two groups(Segata et al., 2011) with an LDA threshold greater than 3.0 (NovoMagic Cloud Platform, https://magic.novogene.com/). To reveal potential differences in metabolism, a phylogenetic investigation of communities by reconstruction of unobserved state analysis (PICRUSt2) based on the MetaCyc database was used to predict the functional pathways in the microbiota(Douglas et al., 2020). The relative predicted abundance of the MetaCyc pathways was calculated by dividing the abundance of each pathway by the sum of the abundance of all pathways per sample.

Construction and validation of diagnostic models

For clinical modeling, univariate logistic regression analysis combined with ROC curve analysis was used to screen out

clinical variables with significant predictive value ($p < 0.05$, AUC ≥ 0.7). These variables were then included in the multivariate logistic regression analysis and those with $p < 0.05$ were further screened as independent risk factors for ACS and included in the final model. The "Forestplot" package in R was used to generate a forest map to show the Odds Ratio (OR), lower/upper 95% CI, and *p*-value. For microbiome modelling, we built a 10-fold cross-validated random forest model via "randomForest" R package to identify the microbiota biomarkers. Further, three diagnostic models were developed: clinical, microbiome and combined models. The accuracy of each model was assessed using the AUC value for the area under the ROC curve. The internal validation of the models was carried out using a bootstrap resampling method with a total of 1,000 resamples and was implemented using the "caret" R package and the ROC curves were plotted using the "pROC" R package. Based on the selected clinical variables and gut microbiome, a nomogram was constructed using the R package "rms" and a visualised dynamic nomogram web page with an interactive interface was developed using the R package "DynNom" to facilitate clinical application. The calibration of the model was assessed by Hosmer-Lemeshow test and calibration curves using the "rms" and "ResourceSelection" R packages. Decision curve analysis (DCA) was also performed using the "rmda" R package to assess the clinical utility of the diagnostic model.

Statistical analysis

The continuous variables were expressed as mean ± standard deviation or median and interquartile range (IQR), and categorical variables were expressed as frequencies (percentages). Analysis of differences between groups that conformed to normal distribution was performed using the independent samples t-test and non-normally distributed differences were compared using the Mann–Whitney test. Categorical variables between the two groups were analyzed using the chi-squared test. Correlations between microbiota and clinical parameters as well as metabolic pathways were analyzed using Spearman's correlation coefficients and presented visually by the R package "pheatmap". All data analyses were performed using SPSS software (version 26.0), GraphPad Prism 9.0, and R 4.3.1 software. $P < 0.05$ was considered statistically significant.

Results

Baseline characteristics of the participants

After rigorous screening and exclusion criteria, 66 individuals, including 29 patients with ACS and 37 healthy controls, were included in the study. As shown in Table 1, patients with ACS had significantly higher levels of white blood cells (WBC), neutrophils (NEU), aspartate aminotransferase (AST), alanine aminotransferase (ALT), creatinine (Cr), and uric acid (UA), as well as higher rates of smoking history and hypertension, and significantly lower levels of beats per minute (BPM) and left ventricular ejection fraction (LVEF) compared to healthy controls. No significant differences were observed in demographic data, including age, body mass index (BMI), history of drinking, diabetes mellitus, hyperlipidemia, systolic blood pressure (SBP), total bilirubin (TBIL), blood urea nitrogen (BUN), fasting blood glucose (FBG), and serum lipid levels between the two groups.

Data quality assessment and gut microbiota diversity

Gut microbiota analyses were performed using 16S rRNA sequencing of fecal samples from the included study population. To determine whether the sample size was sufficient to estimate the abundance of the microbial community, the species accumulation boxplot showed a gradual increase in species diversity with increasing sample size, with the curve flattening out at 66 samples (Figure 1A). This suggests that the current sequencing sample size was sufficient to detect most species in each sample. The abundance rank curves indicated high species richness and evenness in each sample group (Figure 1B). Through 16S rRNA gene sequencing, the sequenced samples were clustered into OTUs at a 97% similarity level, and 2614 OTUs were obtained. The Venn diagram (Figure 1C) displays the identified OTUs and shows a decreasing trend in the number of OTUs in patients with acute myocardial infarction (AMI) and unstable angina pectoris (UA) compared to the control group. In addition, the number of OTUs was significantly higher in the AMI group than in the UA group. Alpha-diversity analyses consistently showed similar results. Although no significant difference was observed in α-diversity between the ACS and control groups (Figures 1D–F), further subgroup analyses showed that the bacterial community richness and diversity were significantly increased in the AMI group compared to those in UA group (Figures 1G–I). To assess the overall structure of the gut microbiota, a principal coordinate analysis (PCoA) score plot was constructed based on the unweighted UniFrac distance. The results showed that the ACS group and healthy control group were separated, and the distribution between the two groups was approximately symmetrical (Figure 2A, $P < 0.001$). Analysis of non-parametric similarity (ANOSIM) further showed that the distribution and composition of the gut microbiota were significantly different between the two groups ($R = 0.229$, $p = 0.001$, Figure 2B). In addition, subgroup analyses using principal coordinate analysis (PCoA) score plots and non-metric multidimensional scaling (NMDS) analyses showed a clear separation between the AMI and control groups, with significant differences in the distribution of bacterial communities (Figures 2C, D).

Composition and comparison of the gut microbiota in patients with ACS and healthy controls

Based on the species annotation results, the top ten species of phyla and genera with the highest relative abundance were selected,

10.3389/fcimb.2023.1305375

TABLE 1 Baseline characteristics of the participants.

Variables	ACS(n=29)	Control(n=37)	*P*-values
Age, years	57.17 ± 9.86	57.78 ± 12.9	0.833
Male, n (%)	26(89.66)	22(59.46)	0.006
BMI, kg/m^2	24.97 ± 3.60	23.91 ± 3.24	0.213
Smoking, n (%)	14(48.28)	6(16.22)	0.005
Drinking, n (%)	4(13.79)	3(8.11)	0.157
Hypertension, n (%)	20(68.97)	10(27.03)	0.001
Hyperlipidemia, n (%)	4(13.79)	5(13.51)	0.974
DM, n (%)	3(10.34)	3(8.11)	0.754
Type of ACS			
STEMI, n (%)	7(24.14)	NA	NA
NSTEMI, n (%)	12(41.38)	NA	NA
UA, n (%)	10(34.48)	NA	NA
No. of stenosed vessels			
1, n (%)	11(37.93)	NA	NA
2, n (%)	9(31.03)	NA	NA
3, n (%)	9(31.03)	NA	NA
Gensini score	68.55 ± 32.07	NA	NA
SBP, mmHg	126.59 ± 17.57	121 ± 17.48	0.203
BPM	78.66 ± 11.47	87.78 ± 11.58	0.002
LVEF(%)	66.59 ± 7.06	71.41 ± 5.21	0.002
Laboratory results			
WBC, ×10^9/L	7.99(6.04,10.72)	5.54(4.73,6.42)	<0.001
NEU, ×10^9/L	5.64(3.42,8.35)	2.77(2.47,4.00)	<0.001
LYM, ×10^9/L	1.61(1.14,2.25)	1.79(1.30,2.12)	0.752
Hb, g/L	151.28 ± 16.22	144.30 ± 17.41	0.101
PLT, ×10^9/L	226.34 ± 56.98	234.46 ± 53.88	0.556
ALB, g/L	42.17 ± 6.58	41.26 ± 3.66	0.482
AST, U/L	36(18.15,67.55)	18.2(15.1,23.55)	<0.001
ALT, U/L	28.5(18.15,42.5)	18.6(13.75,25.55)	0.010
TBIL, umol/L	12.09 ± 3.85	10.75 ± 4.28	0.194
BUN, mmol/L	5.42 ± 1.81	5.78 ± 1.52	0.378
Cr, umol/L	86.46 ± 19.62	74.4 ± 13.66	0.005
UA, umol/L	411.98 ± 108.36	358.98 ± 93.68	0.037
FBG, mmol/L	6.34 ± 2.63	5.24 ± 1.87	0.063
TC, mmol/L	4.63 ± 1.11	4.64 ± 0.85	0.949
TG, mmol/L	1.88 ± 1.27	1.53 ± 0.83	0.182
LDL-C, mmol/L	2.77 ± 0.89	2.79 ± 0.72	0.928
HDL-C, mmol/L	1.09 ± 0.27	1.22 ± 0.30	0.073

Continuous variables are presented as mean ± SD or median (interquartile range). Categorical variables are expressed as n (%). BMI, body mass index; DM, diabetes mellitus; STEMI, ST-segment elevation myocardial infarction; NSTEMI, non-ST-segment elevation myocardial infarction; UA, unstable angina; LVEF, left ventricular ejection fraction; SBP, systolic blood pressure; DBP, diastolic blood pressure; BPM, beat per minute; WBC, white blood cells; NEU, neutrophil; LYM, lymphocyte; Hb, hemoglobin; PLT, platelets; ALB, albumin; AST, aspartate aminotransferase; ALT, alanine aminotransferase; TBIL, total bilirubin; BUN, blood urea nitrogen; Cr, creatinine; UA, uric acid; FBG, fasting blood glucose; TC, total cholesterol; TG, triglyceride; LDL-C, low-density lipoprotein cholesterol; HDL-C, high-density lipoprotein cholesterol.

and relative abundance histograms were generated. At the phylum level, *Firmicutes* (AMI: 54.1%, UA: 53.3%, control: 58.7%) and *Bacteroidota* (AMI: 21.9%, UA: 35.9%, control: 20.5%) were the dominant phyla in all three groups (Figure 3A). The ratio of *Firmicutes* to *Bacteroidota* (F/B ratio) has been reported to be associated with metabolic disease (Magne et al., 2020). In our study, no significant differences were observed among the three groups in terms of the *Firmicutes* phylum (Figure 3C). The abundance of *Bacteroidota* was significantly higher, and the F/B ratio was significantly lower in the UA group than in the control and AMI groups (Figures 3D, E), which is consistent with the results of a previous multicenter study(Zheng et al., 2020). At the genus level, *Bacteroides* (AMI: 16.6%, UA: 29.2%, control: 16.3%) and *Faecalibacterium* (AMI: 6.6%, UA: 8.3%, control: 10.2%) were the most abundant genera in the three groups (Figure 3B). Further, we compared the differences in expression abundance among the three groups at the genus level and found that five genera were significantly different (Figures 4A, B). Overall, the genera *Bacteroides*, *Streptococcus* and *Allobaculum* were significantly more abundant in the case group than in the control group, whereas *Megamonas* and *Prevotella_9* were significantly less abundant. In addition, we observed subtle differences in the characteristics between the AMI and UA groups. In the UA group, a significant increase was observed in the genera *Bacteroides*, whereas the AMI group was characterized by a significant increase in *Streptococcus* spp. and *Allobaculum* spp abundance. To investigate the similarities between different samples, we constructed a cluster tree of the samples by UPGMA (Unweighted Pair-group Method with Arithmetic Mean) cluster analysis (Figure 5). The results showed that the clustering of the samples in the ACS and healthy control groups was clearly separated, whereas the AMI and UA samples in the ACS group were very close to each other, suggesting that the overall structure of the gut microbiota within the ACS group was similar. Therefore, we took acute coronary syndrome as a whole and further analysed the differences in gut microbiota between the ACS and control group, using linear discriminant analysis effect size (LEfSe) to identify specific differential genera between the two groups. The cladogram shows the phylogenetic distribution of the gut microbiota in

10.3389/fcimb.2023.1305375

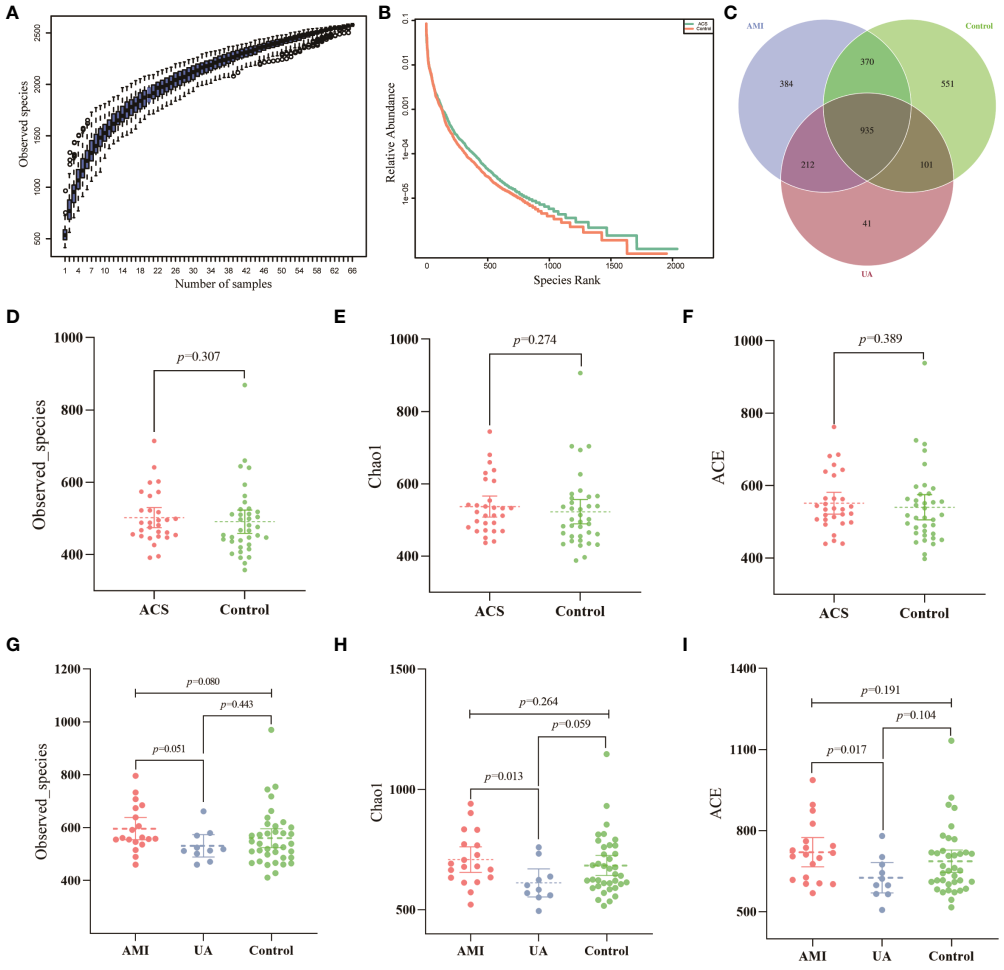

FIGURE 1
Data quality and alpha diversity of microbial sequences. **(A)** The species accumulation curve showed a flattening of the curve as the sample size increased, suggesting that the sample size was sufficient to show the richness of the community. **(B)** The rank abundance curve indicated high species diversity and good species evenness in the sample. **(C)** Venn diagram showing the number of unique OTUs and their shared OTUs in the AMI, UA and control groups. **(D)** Observed species index for ACS and control groups. **(E)** Chao1 index for ACS and control groups. **(F)** ACE index for ACS and control groups. **(G)** Observed species index for the three groups. **(H)** Chao1 index for the three groups. **(I)** ACE index for the three groups.

patients with ACS and healthy controls (Figure 6A), and the LDA score plot showed that 22 genera were significantly different between the two groups (Figure 6B). Specifically, 10 genera such as *Streptococcus, Acinetobacter, Allobaculum and Dubosiella* were significantly enriched in ACS group; whereas 12 genera of *Blautia, Agathobacter, Clostridium_sensu_stricto_1, Ruminococcus* and *Megamonas* were more abundant in healthy controls (all *p*s < 0.05, LDA > 3).

Correlations between the gut microbiome and clinical characteristics

Subsequently, we analyzed the correlation between these different genera and key clinical indicators to identify the key bacteria that are closely associated with the occurrence of ACS (Figure 6C). The results showed that the microbiota was significantly more strongly correlated with smoking, hypertension history, inflammation levels, and Genisi scores; whereas it was weakly correlated with lipid levels and a history of diabetes and hyperlipidemia. Specifically, we found that the microbiota was significantly associated with cardiovascular risk factors including smoking, hypertension, and levels of inflammation assessed by WBC count and NLR, with *Acinetobacter* showing the strongest positive correlations with WBC count (r = 0.419, $p < 0.05$) and NLR (r = 0.401, $p < 0.05$). In addition, the microbiota were strongly associated with cardiovascular protective factors, including HDL-C and LVEF, with *Anaerostipes* showing the highest positive correlation with HDL-C (r = 0.356, $p < 0.05$) and LVEF (r= 0.393, $p < 0.05$). Finally, we also observed that among these 22 genera, 21 genera had significant correlations with the severity of coronary atherosclerosis assessed by the Genisi score (10 positive and 11 negative), with *Acinetobacter* showing the highest positive correlation with the Genisi score (r= 0.799, $p < 0.05$) and *Dorea* showing the highest negative correlation with Genisi score (r= -0.511, $p< 0.05$). These results suggest that alterations in microbial communities, particularly those of *Acinetobacter*, *Dorea*, and *Anaerostipes*, may indicate changes in inflammation,

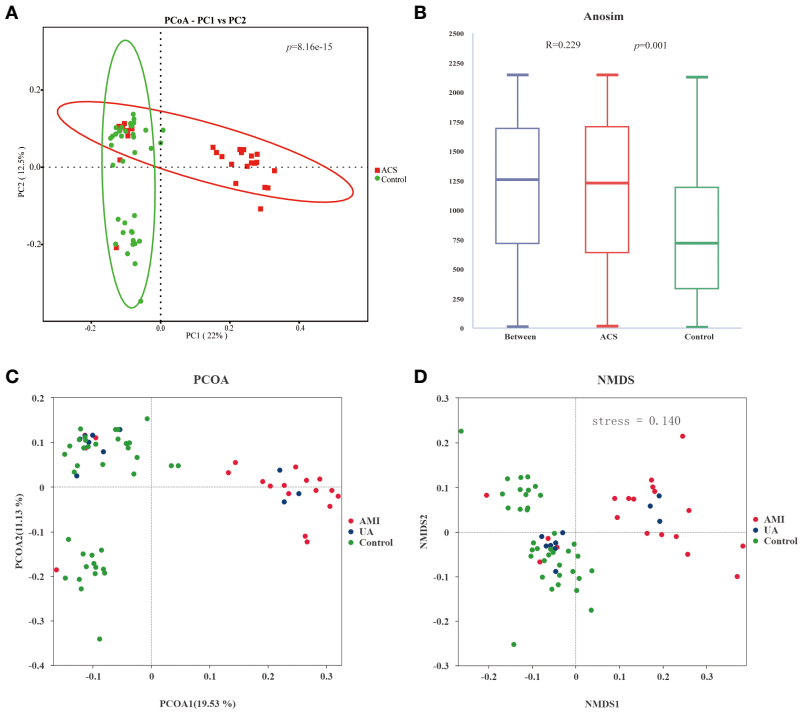

FIGURE 2
Analysis of the beta diversity of the gut microbiota. **(A)** PCoA score plot showing that samples from the ACS group (red) and the control group (green) were significantly separated (p<0.001). **(B)** ANOSIM showed a significant difference between the two groups (R = 0.229, p = 0.001). **(C)** PCoA score plot for AMI, UA and control groups. **(D)** NMDS analysis of AMI, UA and control groups(stress=0.14 (< 0.2)).

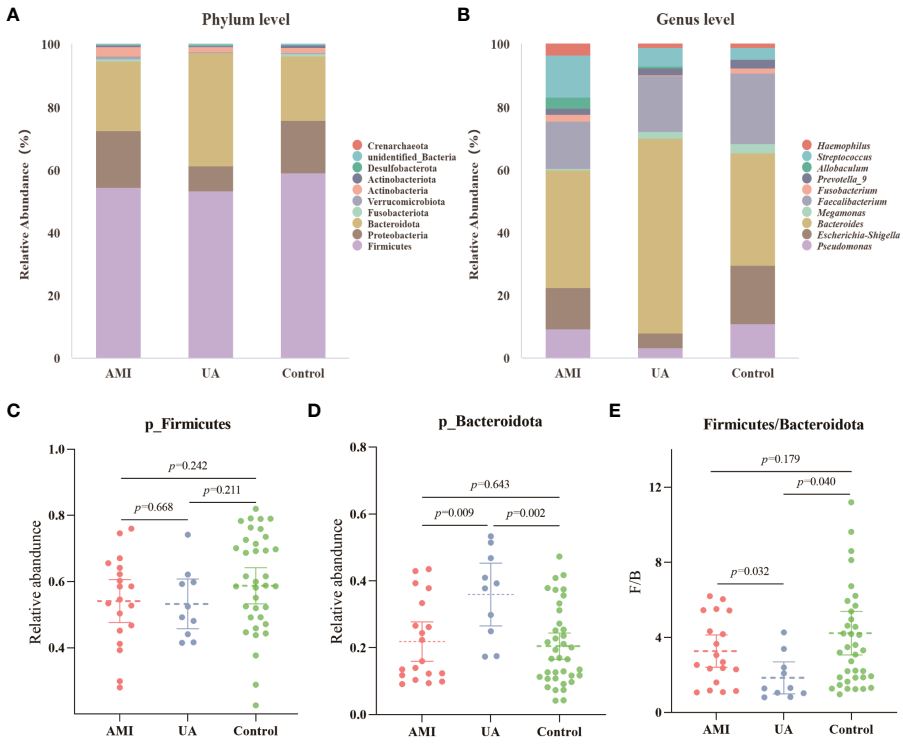

FIGURE 3
Analysis of microbial composition. **(A)** Composition of gut microbiota at the phylum level. **(B)** Composition of gut microbiota at the genus level. **(C)** Differences in abundance of *Firmicutes* phyla between the three groups. **(D)** Differences in abundance of *Bacteroidota* phyla between the three groups. **(E)** Differences in the ratio of *Firmicutes* to *Bacteroidota* (F/B) between the three groups.

10.3389/fcimb.2023.1305375

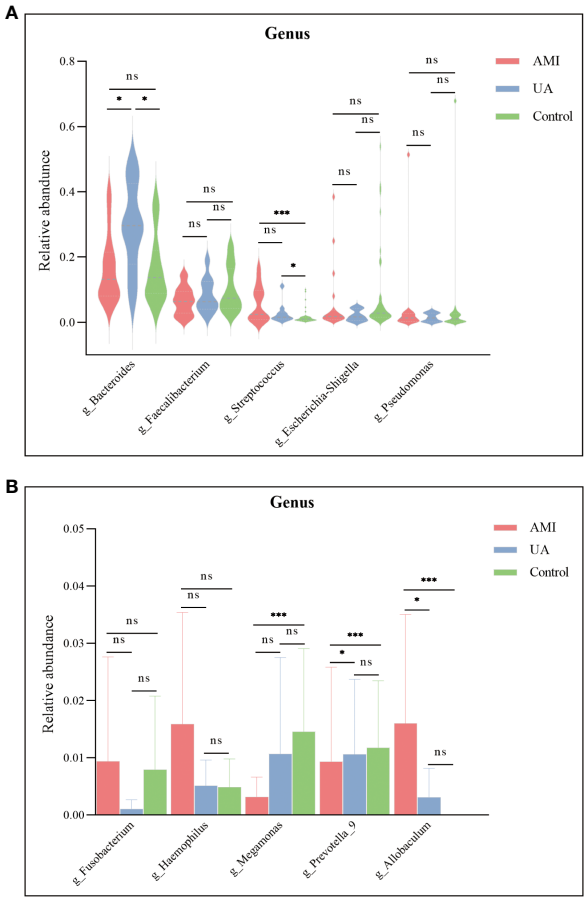

FIGURE 4
Differences in the relative abundance of major genera among the three groups. **(A)** Significant differences were observed in the genera *Bacteroides* and *Streptococcus*. **(B)** *Megamonas*, *Prevotella_9*, and *Allobaculum* were significantly different between the three groups. ns, no significance; *$p < 0.05$; **$p < 0.01$; ***$p < 0.001$.

metabolism, and severity of coronary atherosclerosis in patients with ACS.

Microbial function prediction analysis

To investigate functional alterations in the microbial community of patients with ACS, we identified the functional potential of the gut microbiota using the PICRUSt2 tool based on the MetaCyc database. A total of 94 metabolic pathways were significantly different ($p < 0.05$, FDR < 0.2; Figure 7A, Table S1) (56 pathways enriched and 38 pathways depleted in the ACS group). The results showed that the pathways of glycolysis, homolactic fermentation, pyrimidine deoxyribonucleotides *de novo* biosynthesis, purine nucleotides *de novo* biosynthesis were enriched in the ACS group, whereas adenosylcobalamin biosynthesis, glycogen degradation, L-glutamate and L-glutamine biosynthesis, L-lysine biosynthesis and thiamin salvage were enriched in the control group. Notably, glycolytic metabolic pathways were highly enriched in the ACS microbiome, whereas adenosylcobalamin biosynthesis was significantly reduced, which may be related to the disease state. Furthermore, these metabolic pathways were closely associated with important differential microbiota (Figure 7B). The glycolytic pathway was positively associated with the ACS-enriched genera, particularly *Acinetobacter* and *Allobaculum*, whereas the adenosine synthesis pathway was positively associated with the ACS-negative genera.

ACS diagnostic models based on gut microbiome and clinical features

Subsequently, to identify important microbial biomarkers for the construction of diagnostic models, we constructed a random forest model with a 10-fold cross-validation among the different genera screened. As shown in Figure 8A, random forest analysis filtered the top 10 genera that were most important for distinguishing patients with ACS from healthy controls based on the mean decrease accuracy index. Among the top five genera in terms of variable importance were selected as gut microbiome markers, including *Acinetobacter*, *Dubosiella*, *Exiguobacterium*, *Coriobacteriaceae_UCG.002*, and *Allobaculum*. Based on the five selected gut microbial markers, we calculated the Probability of Disease (POD) index, which reflects the diagnostic value of microbial markers in the ACS group and healthy

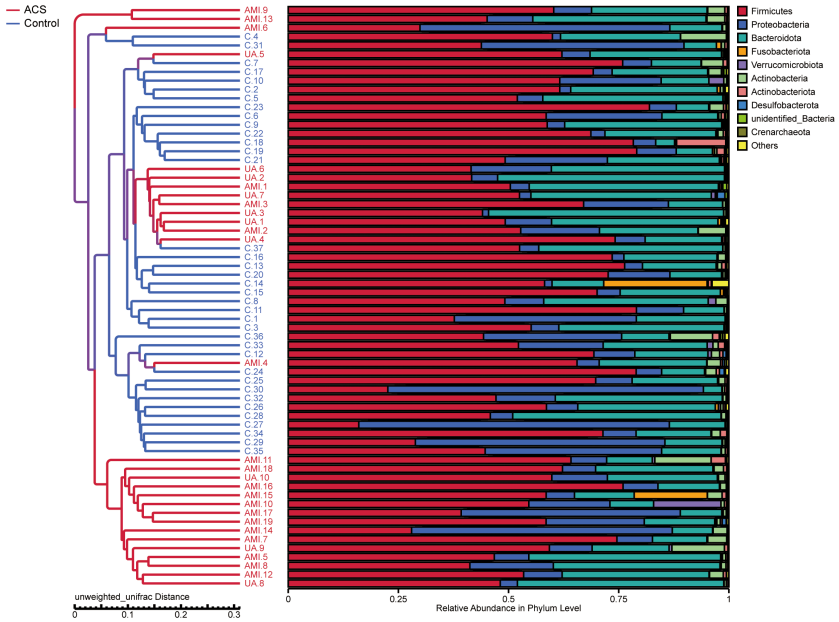

FIGURE 5
UPGMA (unweighted pair-group method with arithmetic mean) sample clustering tree showing the distribution of samples in the ACS and control groups.

controls(Zheng et al., 2020). As shown in Figure 8B, the POD index was significantly higher in ACS samples than in control samples ($p < 0.001$). The POD index was then used to construct the microbiome model and ROC curves were plotted, reaching an AUC value of 0.947 with a 95% CI of 0.899–0.995 (Figure 8D). These results indicated that the diagnostic model based on microbial markers had good diagnostic efficacy. Although the gut microbiome has performed well in diagnosing ACS, it alone may not be sufficient owing to the complexity of the disease. Therefore, we screened clinical indicators for inclusion in the diagnostic model to optimize their performance in disease prediction. To screen for candidate clinical variables, univariate regression and ROC curves (with AUC) were first utilized to screen for clinical indicators with $p < 0.05$ and AUC ≥ 0.7, and four predictive clinical factors were identified (Table 2). Multivariate logistic regression was then performed on these four factors, and the results showed that a history of hypertension ($p = 0.004$), elevated WBC count ($p = 0.047$), and elevated AST ($p = 0.027$) were independent risk factors for ACS (Figure 8C). Finally, these three independent risk factors were included in the logistic regression analysis to construct a clinical model with an AUC value of 0.906 (95% Cl: 0.829–0.982) (Figure 8E). This indicated that the diagnostic efficacy of the microbiome model was superior to that of the clinical model.

Combined model and nomogram for predicting ACS

To optimize diagnostic efficiency, we constructed a combined diagnostic model by combining the gut microbiome POD index with screened clinical indicators and developed a nomogram to visualize the risk of ACS (Figure 9A). Simultaneously, a web-based dynamic nomogram was developed to predict the risk of ACS and to its facilitate clinical application (https://wjcww.shinyapps.io/dynnomapp/). For example, patients were randomly selected from a population. The patient was diagnosed with hypertension, with a WBC of 8 x10^9/L, and an AST level of 49 U/L. Microbiological tests were performed on the stool samples, and the POD index was calculated as 0.6. Entering the above information into this diagnostic model, the probability of ACS in this patient is 97.8%, and the results are shown in Figure 9B. The results showed a higher predictive power of the combined model than that of the clinical model (AUC: 0.963 vs. AUC: 0.906) or microbiome model (AUC: 0.963 vs. AUC: 0.947) alone(Figure 10A). In addition, the consistency index (C-index) of 0.951 was used to assess the diagnostic performance of the combined mode. For internal validation, we used the bootstrap method to internally validate the model with 1,000 bootstrap resamples, resulting in an AUC value of 0.948, sensitivity of 0.89, and specificity of 0.83 (Figure 10B). The model showed good diagnostic efficacy during resampling, indicating that it was stable. Regarding the assessment of the model calibration, a Hosmer-Lemeshow goodness-of-fit test was performed, which resulted in $p = 0.729$ (>0.05), and the calibration curves also showed no significant deviation between the observed and predicted probabilities (Figure 10C). To assess the utility of the model in decision-making, a decision curve analysis was performed. As shown in Figure 10D, the model curve deviated from the two extreme curves (none and all), indicating that the diagnostic model yielded a high net clinical benefit in patients with ACS. These results suggest that a diagnostic model based on the gut microbiome and clinical variables has favorable diagnostic efficacy and utility.

10.3389/fcimb.2023.1305375

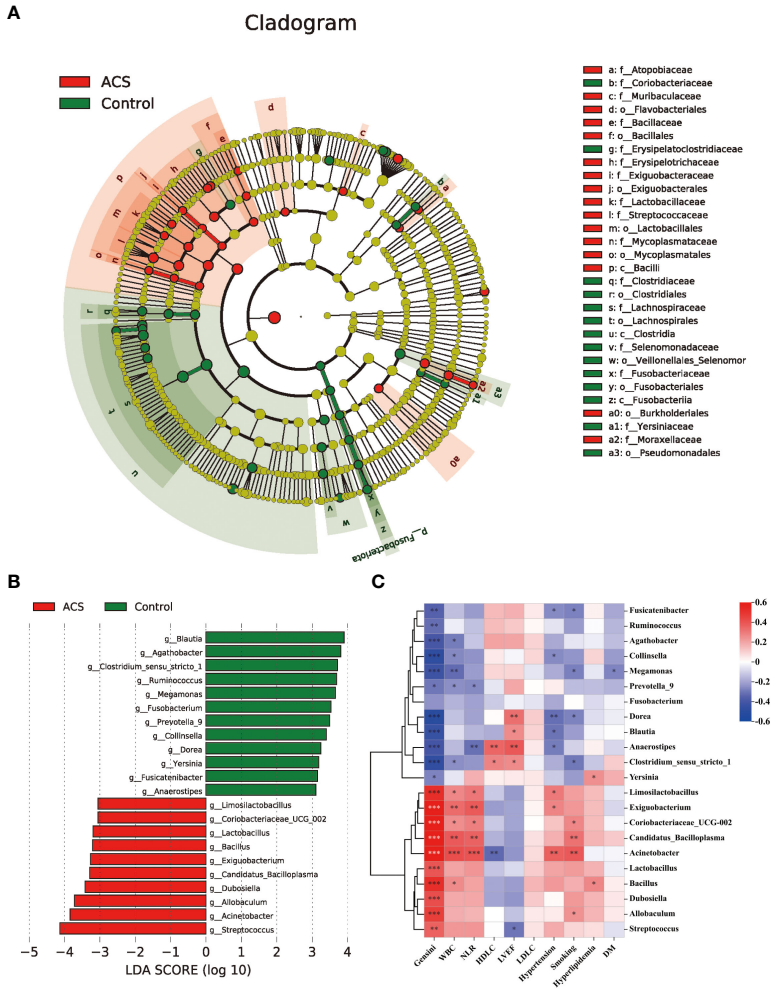

FIGURE 6
Analysis of specific differential microbiota in the ACS and control groups. **(A)** Cladogram generated by the LEfSe method showed the phylogenetic distribution of the gut microbiota associated with patients with ACS and healthy controls. **(B)** Histogram of LDA scores of the gut microbiota showing significant differences at the genus level between the ACS (red) and the control group (green). The default criteria LDA > 3 and $p < 0.05$ indicate that species are different, with one group being more abundant than the other. **(C)** Heat map of Spearman's correlation between the differential genera and clinical characteristics. Colours represent positive (red) or negative (blue) correlations and p values are denoted as follows: $^{*}p < 0.05$, $^{**}p < 0.01$, $^{***}p < 0.001$. LVEF, left ventricular ejection fraction; WBC, white blood cell; NLR, neutrophils/lymphocytes.

Discussion

Recent studies have found that the gut microbiota can be used as noninvasive biomarkers for the early diagnosis and prognostic assessment of disease; however, differences in the gut microbiota and the efficiency of the models are affected by regional variations (He et al., 2018). Therefore, investigating the characteristics of the gut microbiota in patients from different regions is crucial for elucidating possible pathogenic mechanisms and establishing diagnostic models. In this study, we first characterized the differences in gut microbiota between patients with ACS and healthy people in Southwest China and constructed a diagnostic model based on the microbiome, which significantly improved the diagnostic accuracy in patients with ACS and had a high clinical utility value.

A balanced intestinal microecology is important for maintaining normal physiological functions in the human body (Xu et al., 2020). Our study showed that the diversity and composition of the gut microbiota were significantly disturbed in patients with ACS compared to those in healthy controls. LEfSe analysis revealed that certain potentially pathogenic bacteria were significantly enriched in the ACS group, such as *Streptococcus* spp. and *Acinetobacter* spp. This is not the first time that the relationship between *Streptococcus* spp. and coronary artery disease has been reported. More than a decade ago, Koren et al.(Koren et al., 2011) detected *Streptococcus* spp. in the gut and oral cavity of patients with atherosclerosis and the same DNA was detected in atherosclerotic plaque samples. Recent studies have shown that the abundance of *Streptococcus* spp. is significantly increased in patients with subclinical atherosclerosis(Sayols-Baixeras et al.,

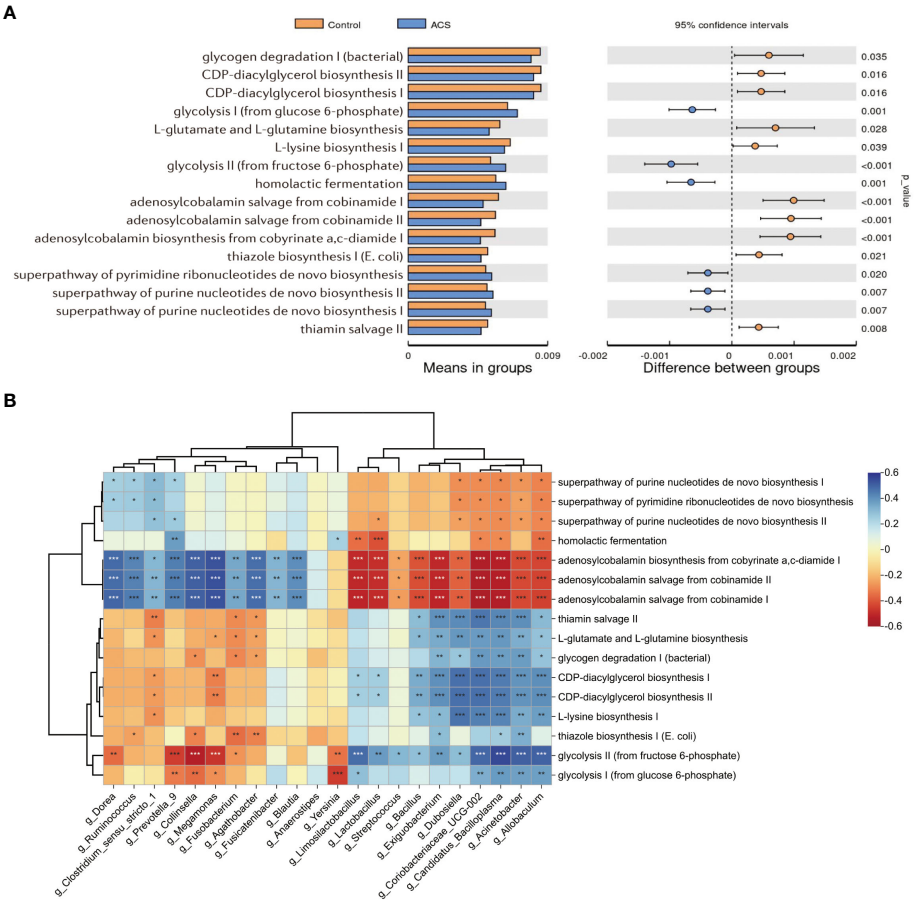

FIGURE 7
Microbial function prediction analysis. **(A)** PICRUSt2 analysis was used to predict alterations in metabolic pathways and showed that a total of 94 MetaCyc pathways were significantly different between the two groups, with a mean proportion of pathways greater than 0.005 being displayed. **(B)** The correlation heatmap demonstrated the association between major metabolic pathways and important differential genera. *$p < 0.05$, **$p < 0.01$, ***$p < 0.001$.

2023), stable coronary artery disease(Jie et al., 2017), and acute myocardial infarction(Dong et al., 2023), and has a high predictive value for disease. Our study found that the abundance of *Streptococcus* spp. was significantly elevated in both the AMI and UA groups compared to the control group, however, this elevation was more pronounced in the AMI group (Figure 4A, $p<0.001$). This indicates that changes in *Streptococcus* spp. abundance may be associated with the formation of atherosclerotic plaques or thrombi and may be a valuable marker for detecting the progression of ACS. Furthermore, we found that the number of OTUs and the diversity of the gut microbiota were also significantly higher in the AMI group than in the UA group, which is different from the results of other studies(Gao et al., 2020a; Qian et al., 2022). This may be due to the unique pathophysiological processes of acute myocardial infarction, such as acute thrombosis, myocardial necrosis, inflammation, and activation of the neuroendocrine system, which may cause changes in the characteristics of the gut microbiota in patients with AMI. Ventricular dysfunction after acute myocardial infarction may lead to hemodynamic disturbances, such as inadequate intestinal perfusion and congestion, which can lead to increased intestinal permeability and intestinal dysfunction, allowing the intestinal microbiota to divert into circulation and cause endotoxemia, which may exacerbate the onset and progression of AMI(Zhou et al., 2018). Therefore, further study of the mechanisms of gut microbiota translocation may contribute to improving the diagnosis and treatment of myocardial infarction.

Notably, we found that abnormal enrichment of *Acinetobacter* spp. seemed to have a significant impact on the diagnosis of ACS. A small cohort study found that *Acinetobacter* was the most commonly detected genus in the coronary balloons of patients with obstructive coronary atherosclerosis(Serra e Silva Filho et al., 2014). In addition, a recent prospective cohort study found that *Acinetobacter* was also detected in cerebral thrombus samples from

10.3389/fcimb.2023.1305375

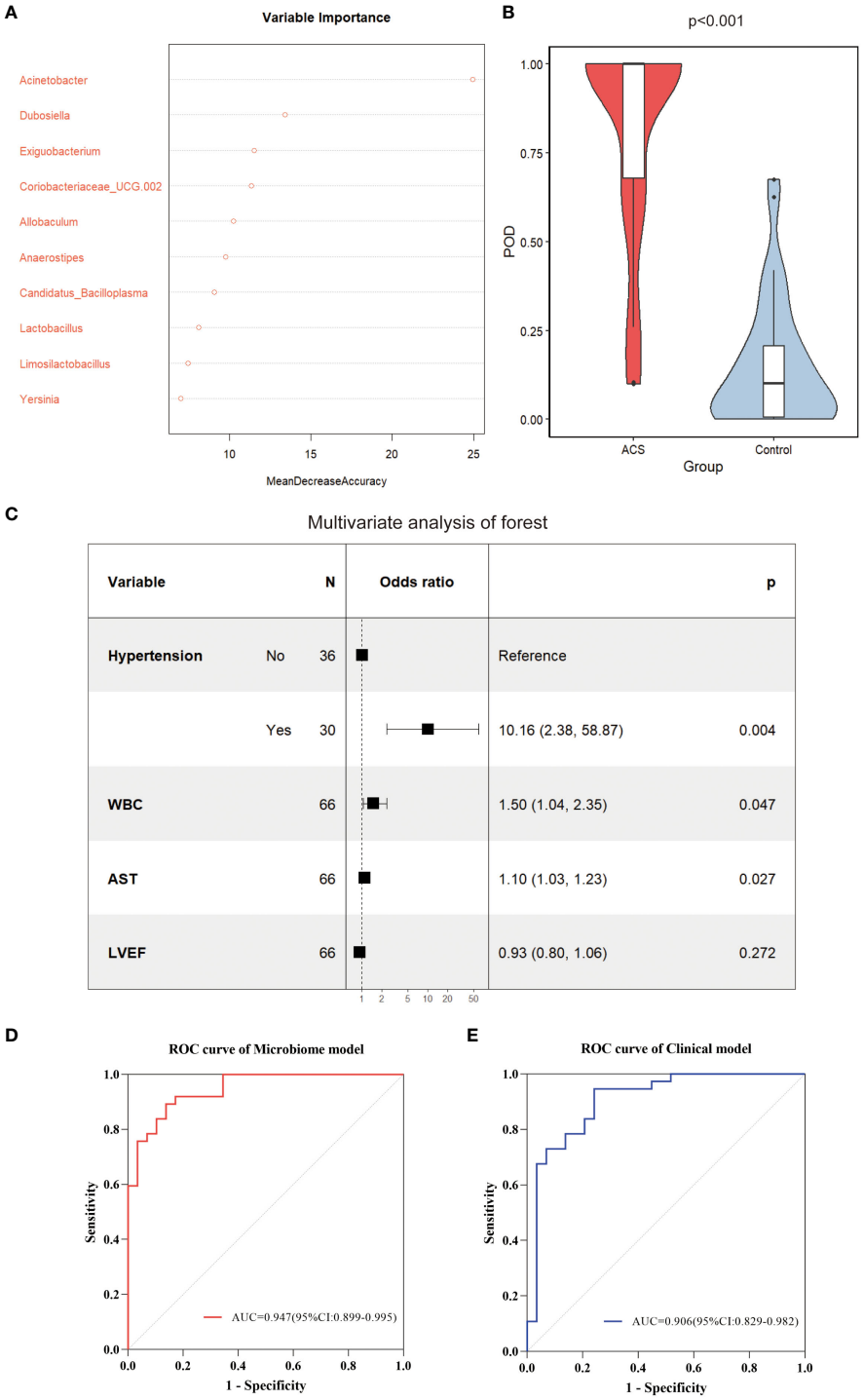

FIGURE 8
Identification of important microbial markers and clinical variables. **(A)** The top 10 genera most important for distinguishing ACS from healthy controls were screened by Random Forest (RF). Each genus was ranked according to mean decrease accuracy. **(B)** Comparison of gut microbiome POD index between ACS and control groups ($p < 0.001$). **(C)** Candidate variables for clinical model development were presented as forest plots. **(D)** ROC curves with AUC for diagnostic performance of the microbiome model. **(E)** ROC curves with AUC for diagnostic performance of the clinical model. POD, probability of disease; AUC, area under the curve.

patients with large-vessel occlusive stroke, and that the abundance of *Acinetobacter* was positively associated with the risk of perioperative adverse events and death within three months(Liao et al., 2022). Therefore, we hypothesized that *Acinetobacter* in the intestine may be transferred to coronary atherosclerotic plaques or thrombi via blood circulation, thereby exacerbating the formation of inflammation and the progression of atherosclerotic plaques. However, this requires further study. However, we did not perform

TABLE 2 Candidate variables for clinical model development.

Variables	AUC	*P*-values	95%CI
Male	0.651	0.011	0.043-0.662
BMI	0.562	0.214	0.947-1.276
Smoking	0.660	0.007	0.066-0.647
Hypertension	0.710	0.001	0.057-0.486
WBC	0.771	0.001	1.233-2.147
AST	0.778	0.003	1.030-1.151
ALT	0.687	0.331	0.990-1.029
BUN	0.417	0.374	0.642-1.181
Cr	0.686	0.010	1.011-1.085
UA	0.646	0.042	1.000-1.011
FBG	0.676	0.076	0.975-1.661
TC	0.506	0.948	0.591-1.636
TG	0.582	0.191	0.848-2.280
HDL-C	0.635	0.078	0.032-1.203
LDL-C	0.497	0.926	0.523-1.803
LVEF	0.709	0.005	0.798-0.961

16S rRNA gene sequencing of coronary plaque or thrombus samples, which is a limitation of our study. Although the relationship between *Acinetobacter* and ACS remains unclear, we observed that the abundance of *Acinetobacter* in the gut was significantly and positively correlated with the level of inflammation and the severity of coronary atherosclerosis. In addition, microbial function prediction analyses have shown a significant positive correlation between *Acinetobacter* and the glycolytic pathway, which is the most critical pathway for glucose metabolism in humans(Chen et al., 2023). Studies have found that during myocardial ischemia-reperfusion, myocardial metabolism shifts from oxidative phosphorylation to aerobic glycolysis, leading to an abnormal accumulation of glycolytic intermediates. This drives mitochondrial dysfunction and increases the formation of reactive oxygen species (ROS), further leading to the apoptosis of cardiomyocytes(Ait-Aissa et al., 2019; Dambrova et al., 2021). Therefore, further investigation of the link and mechanism between *Acinetobacter*, glycolytic metabolic pathways, and ACS is of great interest, and will provide potential opportunities for microbial metabolic pathways as targets for therapeutic intervention in cardiovascular disease.

Contrarily, the genera *Blautia, Agathobacter, Ruminococcus, Dorea*, and *Anaerostipes* were depleted in patients with ACS and significantly enriched in healthy controls. These genera have been reported to ferment carbohydrates to produce short-chain fatty acids, which are essential for maintaining the integrity of intestinal epithelial cells and preventing bacterial translocation into the bloodstream and subsequent endotoxaemia(Makki et al., 2018; Wan et al., 2019). In our study, the genus *Blautia* had the highest LDA values among the healthy controls and was negatively correlated with the severity of coronary atherosclerosis. Gao et al. (Gao et al., 2020b) showed that *Blautia* may play an important role in α-linolenic acid-mediated improvement in intestinal barrier integrity and anti-inflammatory effects, and that exacerbation of inflammation is critical in the pathophysiology of ACS (Dziedzic et al., 2022). In addition, a Mendelian randomization relating gut microbiota to ischaemic heart disease and its risk factors showed nominal associations of *Acidaminococcus*, *Aggregatibacter*, *Anaerostipes*, *Blautia*, *Desulfovibrio*, *Dorea*, and *Faecalibacterium* with a modestly lower risk of T2DM, lower adiposity, more beneficial lipid profiles, and higher HOMA-IR(Yang et al., 2018).

Several studies have shown that the gut microbiota and metabolic profiles can be altered through dietary interventions, which may have a significant impact on cardiovascular risk factors (So et al., 2018; Wan et al., 2019). For example, dietary intervention with high-fiber rye foods resulted in changes in the composition of the gut microbiota and increased the abundance of butyric acid-producing *Agrobacterium*, which may be associated with intervention-induced weight loss and improvement in metabolic risk indicators(Iversen et al., 2022). In addition, statins have been reported to modulate the gut microbiota of patients with ACS, increasing beneficial flora (such as *Bifidobacterium longum subsp. longum, Anaerostipes hadrus* and *Ruminococcus obeum*) to a healthier state, thus reducing the metabolic risk of patients(Hu et al., 2021). These results suggest that targeted modulation of gut microbiota through probiotic supplementation may be a novel approach for the prevention and treatment of cardiovascular diseases. However, there are few reports on the mechanisms by which probiotics improve cardiovascular disease, which should be a direction for future research.

In our study, we found that hypertension, WBC count, and AST levels were independent risk factors for ACS, consistent with the results of previous studies(Kaminska et al., 2018; Li et al., 2021). However, studies have found that up to 20% of patients with ACS do not have traditional clinical risk factors (Figtree and Vernon, 2021), limiting the clinical application of predictive models that include only clinical indicators. Therefore, we combined clinical variables with the gut microbiome to construct a combined diagnostic model with an AUC value of 0.963. The predictive power of the combined model was significantly better than that of the other two models. More importantly, even after bootstrap internal validation, the model showed good performance (AUC = 0.948), indicating that our model was stable.

The gut microbiota has been used to predict coronary artery disease in several recent studies and has shown high a predictive value(Zhang et al., 2022; Dong et al., 2023), suggesting the potential of the gut microbiota to predict ACS. However, these studies only constructed predictive models and did not validate the calibration

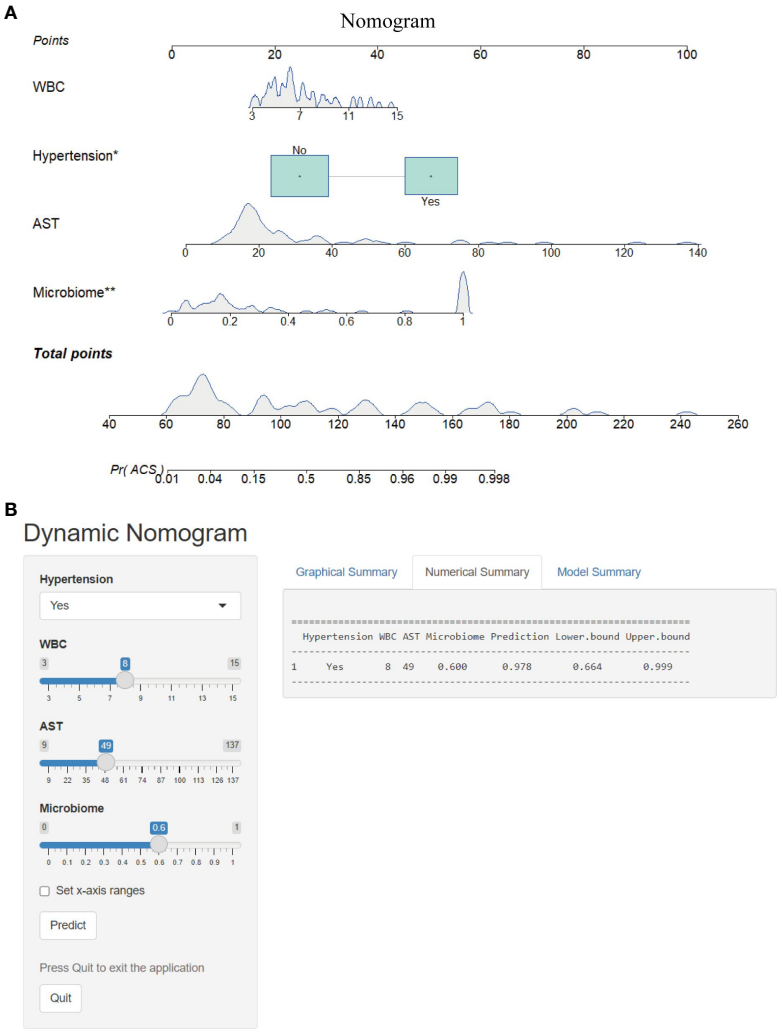

FIGURE 9
Nomogram and its webpage development. **(A)** The nomogram was constructed based on hypertension, WBC, AST and microbiome to predict the probability of developing ACS. To use the nomogram, a vertical line is drawn from the risk factor to the "Points" axis to determine the score for each risk factor in the nomogram. The scores for all risk factors are summed and a vertical line is drawn from the "Total Score" axis to the "Probability of ACS" axis, the corresponding value of which is the probability of developing ACS. **(B)** Web-based risk calculator (Dynamic Nomogram (https://wjcww.shinyapps.io/dynnomapp/) to predict incidence rate of ACS. *p < 0.05, **p < 0.01.

and utility of the models, making it difficult to generalize the models for clinical use because of the lack of clinical application tools. Considering the importance of the early diagnosis of ACS, we developed a nomogram and a corresponding online webpage based on the gut microbiome and clinical indicators to visualize the model and assist in the clinical diagnosis and risk assessment of ACS. A previous study constructed a disease classifier based on a combination of 24 bacterial co-abundance groups (CAGs) and 72 serum metabolites, which accurately differentiated between stable coronary artery disease and acute coronary syndromes, with an AUC value of 0.897(Liu et al., 2019). However, this model requires the incorporation of many microbial indicators as well as invasive blood sampling to detect metabolites and is relatively complex and expensive to implement, which may limit its use in clinical settings. Conversely, our model was characterized by its simplicity, non-invasiveness, and accuracy, which was achieved by incorporating only a few microbiota and common clinical indicators. In our study, all participants were from the same region, and their lifestyles and diets were similar, which reduced the potential confounding effects of geographic and dietary differences on the microbiota. In addition, our study population included newly diagnosed and untreated patients with ACS who were at a relatively early stage of the

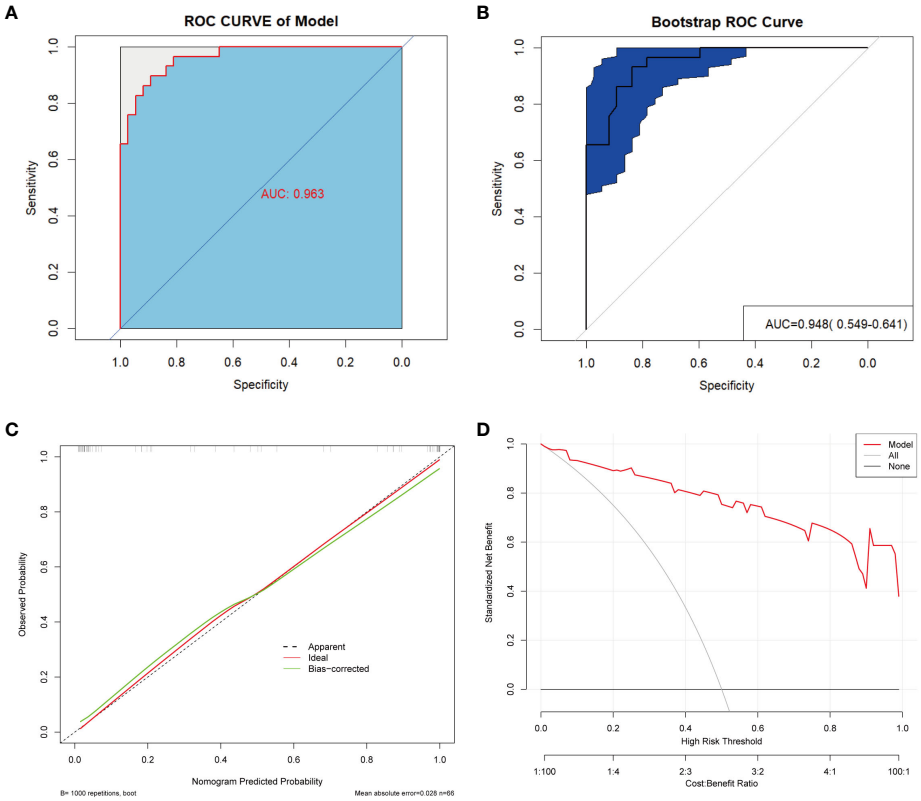

FIGURE 10
Validation and assessment of the model. **(A)** ROC curve with AUC for the diagnostic performance of the Nomogram. **(B)** The AUC for Nomogram bootstrap internal validation. **(C)** Calibration curve of the nomogram, with the x-axis representing the probability predicted by the nomogram and the y-axis representing the actual observed probability. **(D)** Decision curve analysis (DCA) of the nomogram showed the net benefit of using the model to diagnose ACS compared to the "treat all" or "treat none" strategy at different decision thresholds.

disease, which reduced the impact of confounding factors, such as medication and disease progression, on the microbiome analysis. Therefore, the developed model is more informative for the early diagnosis of ACS.

Our study has several limitations. First, we only sequenced the 16S rRNA gene in fecal samples; we did not assess the metabolites of the microbiota, and the mechanisms are understudied. Second, although we established an accurate diagnostic model based on the gut microbiota, the specific functions of these microbiota remains unclear. Finally, this was a single-center study with a limited sample size, which did not allow for external validation in different regions. Bootstrap resampling was performed to ensure internal validity.

In conclusion, the current study showed that the diversity and composition of the intestinal mycobiota of patients with ACS was significantly disturbed and was characterized by significant enrichment of certain potentially pathogenic genera and a significant reduction in certain SCFA-producing genera. Our study provides novel insights into the association between the gut microbiota and ACS and more targeted studies of these critical microbiota will be valuable in the future. In addition, we constructed a noninvasive diagnostic model based on the gut microbiome and common clinical indicators, providing a novel approach to assist in the early diagnosis and risk warning of ACS.

Data availability statement

The datasets presented in this study can be found in online repositories. The names of the repository/repositories and accession number(s) can be found below: https://www.ncbi.nlm.nih.gov/sra/PRJNA1020457.

Ethics statement

The studies involving humans were approved by the Ethics Committee of the First Affiliated Hospital of Kunming Medical University. The studies were conducted in accordance with the local legislation and institutional requirements. The participants provided their written informed consent to participate in this study. Written informed consent was obtained from the individual(s) for the publication of any potentially identifiable images or data included in this article.

Author contributions

JW: Visualization, Writing – original draft, Conceptualization, Data curation, Formal Analysis, Investigation, Methodology, Software. ZH: Conceptualization, Funding acquisition, Resources, Writing – review & editing, Supervision, Validation. QX: Conceptualization, Investigation, Methodology, Supervision, Writing – original draft. YS: Formal Analysis, Funding acquisition, Methodology, Resources, Software, Writing – original draft. XC: Resources, Data curation, Methodology, Writing – original draft. YM: Data curation, Investigation, Methodology, Writing – original draft. MW: Data curation, Investigation, Writing – original draft. CZ: Conceptualization, Investigation, Methodology, Writing – original draft. XL: Data curation, Methodology, Software, Writing – original draft. FL: Data curation, Investigation, Methodology, Writing – original draft. XBL: Data curation, Investigation, Methodology, Writing – original draft. YD: Conceptualization, Funding acquisition, Investigation, Project administration, Resources, Supervision, Validation, Writing – review & editing. HC: Conceptualization, Funding acquisition, Investigation, Project administration, Resources, Supervision, Writing – review & editing, Formal Analysis, Methodology, Validation, Visualization.

Funding

The author(s) declare financial support was received for the research, authorship, and/or publication of this article. This study was supported by the National Natural Science Foundation of China (82260087), the Yunnan Province High-level Health Technical Talents (leading talents) (No. L-2019025), the Yunnan Province High-level Health Technical Talents (reserve talents) (No. H-2019052) and the Special Foundation Projects of Joint Applied Basic Research of Yunnan Provincial Department of Science and Technology with Kunming Medical University (No. 202301AY070001-119).

Acknowledgments

We are grateful to the staff of the Department of Cardiology and the Department of Laboratory Medicine at the First Affiliated Hospital of Kunming Medical University for their support during the sample collection process, and especially thank all participants for providing valuable samples for this study.

Conflict of interest

The authors declare that the research was conducted in the absence of any commercial or financial relationships that could be construed as a potential conflict of interest.

Publisher's note

Supplementary material

The Supplementary Material for this article can be found online at: https://www.frontiersin.org/articles/10.3389/fcimb.2023.1305375/full#supplementary-material

References

Ait-Aissa, K., Blaszak, S. C., Beutner, G., Tsaih, S. W., Morgan, G., Santos, J. H., et al. (2019). Mitochondrial oxidative phosphorylation defect in the heart of subjects with coronary artery disease. *Sci. Rep.* 9 (1), 7623. doi: 10.1038/s41598-019-43761-y

Bergmark, B. A., Mathenge, N., Merlini, P. A., Lawrence-Wright, M. B., and Giugliano, R. P. (2022). Acute coronary syndromes. *Lancet* 399 (10332), 1347–1358. doi: 10.1016/S0140-6736(21)02391-6

Bhatt, D. L., Lopes, R. D., and Harrington, R. A. (2022). Diagnosis and treatment of acute coronary syndromes: A review. *JAMA* 327 (7), 662–675. doi: 10.1001/jama.2022.0358

Braunwald, E. (2012). Unstable angina and non-ST elevation myocardial infarction. *Am. J. Respir. Crit. Care Med.* 185 (9), 924–932. doi: 10.1164/rccm.201109-1745CI

Brieger, D., Eagle, K. A., Goodman, S. G., Steg, P. G., Budaj, A., White, K., et al. (2004). Acute coronary syndromes without chest pain, an underdiagnosed and undertreated high-risk group: insights from the Global Registry of Acute Coronary Events. *Chest* 126 (2), 461–469. doi: 10.1378/chest.126.2.461

Byrne, R. A., Rossello, X., Coughlan, J. J., Barbato, E., Berry, C., Chieffo, A., et al. (2023). 2023 ESC Guidelines for the management of acute coronary syndromes. *Eur. Heart J* 44 (38), 3720-3826. doi: 10.1093/eurheartj/ehad191

Chen, S., Zou, Y., Song, C., Cao, K., Cai, K., Wu, Y., et al. (2023). The role of glycolytic metabolic pathways in cardiovascular disease and potential therapeutic approaches. *Basic Res. Cardiol.* 118 (1), 48. doi: 10.1007/s00395-023-01018-w

Chistiakov, D. A., Bobryshev, Y. V., Kozarov, E., SoBenin, I. A., and Orekhov, A. N. (2015). Role of gut microbiota in the modulation of atherosclerosis-associated immune response. *Front. Microbiol.* 6. doi: 10.3389/fmicb.2015.00671

Dambrova, M., Zuurbier, C. J., Borutaite, V., Liepinsh, E., and Makrecka-Kuka, M. (2021). Energy substrate metabolism and mitochondrial oxidative stress in cardiac ischemia/reperfusion injury. *Free Radic. Biol. Med.* 165, 24–37. doi: 10.1016/j.freeradbiomed.2021.01.036

Dong, C., Yang, Y., Wang, Y., Hu, X., Wang, Q., Gao, F., et al. (2023). Gut microbiota combined with metabolites reveals unique features of acute myocardial infarction patients different from stable coronary artery disease. *J. Adv. Res.* 46, 101–112. doi: 10.1016/j.jare.2022.06.008

Douglas, G. M., Maffei, V. J., Zaneveld, J. R., Yurgel, S. N., Brown, J. R., Taylor, C. M., et al. (2020). PICRUSt2 for prediction of metagenome functions. *Nat. Biotechnol.* 38 (6), 685–688. doi: 10.1038/s41587-020-0548-6

Du, Z., Wang, J., Lu, Y., Ma, X., Wen, R., Lin, J., et al. (2020). The cardiac protection of Baoyuan decoction via gut-heart axis metabolic pathway. *Phytomedicine* 79, 153322. doi: 10.1016/j.phymed.2020.153322

Dziedzic, E. A., Gasior, J. S., Tuzimek, A., Paleczny, J., Junka, A., Dabrowski, M., et al. (2022). Investigation of the associations of novel inflammatory biomarkers-systemic inflammatory index (SII) and systemic inflammatory response index (SIRI)-with the severity of coronary artery disease and acute coronary syndrome occurrence. *Int. J. Mol. Sci.* 23 (17), 9553. doi: 10.3390/ijms23179553

Edgar, R. C. (2013). UPARSE: highly accurate OTU sequences from microbial amplicon reads. *Nat. Methods* 10 (10), 996–998. doi: 10.1038/nmeth.2604

Fatkhullina, A. R., Peshkova, I. O., Dzutsev, A., Aghayev, T., McCulloch, J. A., Thovarai, V., et al. (2018). An interleukin-23-interleukin-22 axis regulates intestinal microbial homeostasis to protect from diet-induced atherosclerosis. *Immunity* 49 (5), 943–957.e949. doi: 10.1016/j.immuni.2018.09.011

Figtree, G. A., and Vernon, S. T. (2021). Coronary artery disease patients without standard modifiable risk factors (SMuRFs)- a forgotten group calling out for new discoveries. *Cardiovasc. Res.* 117 (6), e76–e78. doi: 10.1093/cvr/cvab145

Gao, J., Yan, K. T., Wang, J. X., Dou, J., Wang, J., Ren, M., et al. (2020a). Gut microbial taxa as potential predictive biomarkers for acute coronary syndrome and post-STEMI cardiovascular events. *Sci. Rep.* 10 (1), 2639. doi: 10.1038/s41598-020-59235-5

Gao, X., Chang, S., Liu, S., Peng, L., Xie, J., Dong, W., et al. (2020b). Correlations between alpha-linolenic acid-improved multitissue homeostasis and gut microbiota in mice fed a high-fat diet. *mSystems* 5 (6), e00391-20. doi: 10.1128/mSystems.00391-20

Gensini, G. G. (1983). A more meaningful scoring system for determining the severity of coronary heart disease. *Am. J. Cardiol.* 51 (3), 606. doi: 10.1016/s0002-9149(83)80105-2

Haghikia, A., Zimmermann, F., Schumann, P., Jasina, A., Roessler, J., Schmidt, D., et al. (2022). Propionate attenuates atherosclerosis by immune-dependent regulation of intestinal cholesterol metabolism. *Eur. Heart J.* 43 (6), 518–533. doi: 10.1093/eurheartj/ehab644

He, Y., Wu, W., Zheng, H. M., Li, P., McDonald, D., Sheng, H. F., et al. (2018). Author Correction: Regional variation limits applications of healthy gut microbiome reference ranges and disease models. *Nat. Med.* 24 (12), 1940. doi: 10.1038/s41591-018-0219-z

Hu, X., Li, H., Zhao, X., Zhou, R., Liu, H., Sun, Y., et al. (2021). Multi-omics study reveals that statin therapy is associated with restoration of gut microbiota homeostasis and improvement in outcomes in patients with acute coronary syndrome. *Theranostics* 11 (12), 5778–5793. doi: 10.7150/thno.55946

Iversen, K. N., Dicksved, J., Zoki, C., Fristedt, R., Pelve, E. A., Langton, M., et al. (2022). The effects of high fiber rye, compared to refined wheat, on gut microbiota composition, plasma short chain fatty acids, and implications for weight loss and metabolic risk factors (the ryeWeight study). *Nutrients* 14 (8), 1669. doi: 10.3390/nu14081669

Jie, Z., Xia, H., Zhong, S. L., Feng, Q., Li, S., Liang, S., et al. (2017). The gut microbiome in atherosclerotic cardiovascular disease. *Nat. Commun.* 8 (1), 845. doi: 10.1038/s41467-017-00900-1

Kaminska, J., Koper, O. M., Siedlecka-Czykier, E., Matowicka-Karna, J., Bychowski, J., and Kemona, H. (2018). The utility of inflammation and platelet biomarkers in patients with acute coronary syndromes. *Saudi J. Biol. Sci.* 25 (7), 1263–1271. doi: 10.1016/j.sjbs.2016.10.015

Katus, H., Ziegler, A., Ekinci, O., Giannitsis, E., Stough, W. G., Achenbach, S., et al. (2017). Early diagnosis of acute coronary syndrome. *Eur. Heart J.* 38 (41), 3049–3055. doi: 10.1093/eurheartj/ehx492

Khan, I., Khan, I., Usman, M., Jianye, Z., Wei, Z. X., Ping, X., et al. (2022). Analysis of the blood bacterial composition of patients with acute coronary syndrome and chronic coronary syndrome. *Front. Cell Infect. Microbiol.* 12. doi: 10.3389/fcimb.2022.943808

Koeth, R. A., Wang, Z., Levison, B. S., Buffa, J. A., Org, E., Sheehy, B. T., et al. (2013). Intestinal microbiota metabolism of L-carnitine, a nutrient in red meat, promotes atherosclerosis. *Nat. Med.* 19 (5), 576–585. doi: 10.1038/nm.3145

Koren, O., Spor, A., Felin, J., Fak, F., Stombaugh, J., Tremaroli, V., et al. (2011). Human oral, gut, and plaque microbiota in patients with atherosclerosis. *Proc. Natl. Acad. Sci. U S A.* 108 Suppl 1 (Suppl 1), 4592–4598. doi: 10.1073/pnas.1011383107

Li, J., Zhao, Z., Jiang, H., Jiang, M., Yu, G., and Li, X. (2021). Predictive value of elevated alanine aminotransferase for in-hospital mortality in patients with acute myocardial infarction. *BMC Cardiovasc. Disord.* 21 (1), 82. doi: 10.1186/s12872-021-01903-z

Liao, Y., Zeng, X., Xie, X., Liang, D., Qiao, H., Wang, W., et al. (2022). Bacterial signatures of cerebral thrombi in large vessel occlusion stroke. *mBio* 13 (4), e0108522. doi: 10.1128/mbio.01085-22

Liu, H., Chen, X., Hu, X., Niu, H., Tian, R., Wang, H., et al. (2019). Alterations in the gut microbiome and metabolism with coronary artery disease severity. *Microbiome* 7 (1), 68. doi: 10.1186/s40168-019-0683-9

Magne, F., Gotteland, M., Gauthier, L., Zazueta, A., Pesoa, S., Navarrete, P., et al. (2020). The firmicutes/bacteroidetes ratio: A relevant marker of gut dysbiosis in obese patients? *Nutrients* 12 (5), 1474. doi: 10.3390/nu12051474

Mair, J. (1997). Progress in myocardial damage detection: new biochemical markers for clinicians. *Crit. Rev. Clin. Lab. Sci.* 34 (1), 1–66. doi: 10.3109/10408369709038215

Makki, K., Deehan, E. C., Walter, J., and Backhed, F. (2018). The impact of dietary fiber on gut microbiota in host health and disease. *Cell Host Microbe* 23 (6), 705–715. doi: 10.1016/j.chom.2018.05.012

Pasini, E., Aquilani, R., Testa, C., Baiardi, P., Angioletti, S., Boschi, F., et al. (2016). Pathogenic gut flora in patients with chronic heart failure. *JACC Heart Fail.* 4 (3), 220–227. doi: 10.1016/j.jchf.2015.10.009

Qian, X., Liu, A., Liang, C., He, L., Xu, Z., and Tang, S. (2022). Analysis of gut microbiota in patients with acute myocardial infarction by 16S rRNA sequencing. *Ann. Transl. Med.* 10 (24), 1340. doi: 10.21037/atm-22-5671

Sayols-Baixeras, S., Dekkers, K. F., Baldanzi, G., Jonsson, D., Hammar, U., Lin, Y. T., et al. (2023). Streptococcus species abundance in the gut is linked to subclinical coronary atherosclerosis in 8973 participants from the SCAPIS cohort. *Circulation* 148 (6), 459–472. doi: 10.1161/CIRCULATIONAHA.123.063914

Segata, N., Izard, J., Waldron, L., Gevers, D., Miropolsky, L., Garrett, W. S., et al. (2011). Metagenomic biomarker discovery and explanation. *Genome Biol.* 12 (6), R60. doi: 10.1186/gb-2011-12-6-r60

Serra e Silva Filho, W., Casarin, R. C., Nicolela, E. L. Jr., Passos, H. M., Sallum, A. W., and Goncalves, R. B. (2014). Microbial diversity similarities in periodontal pockets and atheromatous plaques of cardiovascular disease patients. *PloS One* 9 (10), e109761. doi: 10.1371/journal.pone.0109761

So, D., Whelan, K., Rossi, M., Morrison, M., Holtmann, G., Kelly, J. T., et al. (2018). Dietary fiber intervention on gut microbiota composition in healthy adults: a systematic review and meta-analysis. *Am. J. Clin. Nutr.* 107 (6), 965–983. doi: 10.1093/ajcn/nqy041

Tousoulis, D., Guzik, T., Padro, T., Duncker, D. J., De Luca, G., Eringa, E., et al. (2022). Mechanisms, therapeutic implications, and methodological challenges of gut microbiota and cardiovascular diseases: a position paper by the ESC Working Group on Coronary Pathophysiology and Microcirculation. *Cardiovasc. Res.* 118 (16), 3171–3182. doi: 10.1093/cvr/cvac057

Troseid, M., Andersen, G. O., Broch, K., and Hov, J. R. (2020). The gut microbiome in coronary artery disease and heart failure: Current knowledge and future directions. *EBioMedicine* 52, 102649. doi: 10.1016/j.ebiom.2020.102649

van den Munckhof, I. C. L., Kurilshikov, A., Ter Horst, R., Riksen, N. P., Joosten, L. A. B., Zhernakova, A., et al. (2018). Role of gut microbiota in chronic low-grade inflammation as potential driver for atherosclerotic cardiovascular disease: a systematic review of human studies. *Obes. Rev.* 19 (12), 1719–1734. doi: 10.1111/obr.12750

Wan, Y., Wang, F., Yuan, J., Li, J., Jiang, D., Zhang, J., et al. (2019). Effects of dietary fat on gut microbiota and faecal metabolites, and their relationship with cardiometabolic risk factors: a 6-month randomised controlled-feeding trial. *Gut* 68 (8), 1417–1429. doi: 10.1136/gutjnl-2018-317609

Xu, H., Wang, X., Feng, W., Liu, Q., Zhou, S., Liu, Q., et al. (2020). The gut microbiota and its interactions with cardiovascular disease. *Microb. Biotechnol.* 13 (3), 637–656. doi: 10.1111/1751-7915.13524

Yang, Q., Lin, S. L., Kwok, M. K., Leung, G. M., and Schooling, C. M. (2018). The roles of 27 genera of human gut microbiota in ischemic heart disease, type 2 diabetes mellitus, and their risk factors: A mendelian randomization study. *Am. J. Epidemiol.* 187 (9), 1916–1922. doi: 10.1093/aje/kwy096

Yang, T., Santisteban, M. M., Rodriguez, V., Li, E., Ahmari, N., Carvajal, J. M., et al. (2015). Gut dysbiosis is linked to hypertension. *Hypertension* 65 (6), 1331–1340. doi: 10.1161/HYPERTENSIONAHA.115.05315

Zhang, T., Ren, H., Du, Z., Zou, T., Guang, X., Zhang, Y., et al. (2022). Diversified shifts in the cross talk between members of the gut microbiota and development of coronary artery diseases. *Microbiol. Spectr.* 10 (6), e0280422. doi: 10.1128/spectrum.02804-22

Zheng, Y. Y., Wu, T. T., Liu, Z. Q., Li, A., Guo, Q. Q., Ma, Y. Y., et al. (2020). Gut microbiome-based diagnostic model to predict coronary artery disease. *J. Agric. Food Chem.* 68 (11), 3548–3557. doi: 10.1021/acs.jafc.0c00225

Zhou, X., Li, J., Guo, J., Geng, B., Ji, W., Zhao, Q., et al. (2018). Gut-dependent microbial translocation induces inflammation and cardiovascular events after ST-elevation myocardial infarction. *Microbiome* 6 (1), 66. doi: 10.1186/s40168-018-0441-4

Zhu, Q., Gao, R., Zhang, Y., Pan, D., Zhu, Y., Zhang, X., et al. (2018). Dysbiosis signatures of gut microbiota in coronary artery disease. *Physiol. Genomics* 50 (10), 893–903. doi: 10.1152/physiolgenomics.00070.2018

Zhu, W., Gregory, J. C., Org, E., Buffa, J. A., Gupta, N., Wang, Z., et al. (2016). Gut microbial metabolite TMAO enhances platelet hyperreactivity and thrombosis risk. *Cell* 165 (1), 111–124. doi: 10.1016/j.cell.2016.02.011

frontiers | Frontiers in Cellular and Infection Microbiology

TYPE Original Research
PUBLISHED 08 March 2024
DOI 10.3389/fcimb.2024.1371371

OPEN ACCESS

EDITED BY
Wenle Li,
Xiamen University, China

REVIEWED BY
Jinxiang Wang,
Sun Yat-sen University, China
Penghao Xu,
Georgia Institute of Technology, United States
Yanlong Shi,
Nanjing Medical University, China

*CORRESPONDENCE
Xing-Hua Gao
hurryman1999@sina.com
Meng-Pan Li
mengpanli163@163.com

†These authors have contributed equally to this work

RECEIVED 16 January 2024
ACCEPTED 26 February 2024
PUBLISHED 08 March 2024

CITATION
Tu J-B, Liao W-J, Long S-P, Li M-P and Gao X-H (2024) Construction and validation of a machine learning model for the diagnosis of juvenile idiopathic arthritis based on fecal microbiota.
Front. Cell. Infect. Microbiol. 14:1371371.
doi: 10.3389/fcimb.2024.1371371

Construction and validation of a machine learning model for the diagnosis of juvenile idiopathic arthritis based on fecal microbiota

Jun-Bo Tu[1†], Wei-Jie Liao[2†], Si-Ping Long[3], Meng-Pan Li[3,4*] and Xing-Hua Gao[5*]

[1]Department of Orthopaedics, Xinfeng County People's Hospital, Xinfeng, Jiangxi, China, [2]Department of ICU, GanZhou People's Hospital, GanZhou, Jiangxi, China, [3]The First Clinical Medical College of Nanchang University, Nanchang, China, [4]Department of Orthopedics, Shanghai General Hospital, Shanghai Jiao Tong University School of Medicine, Shanghai, China, [5]Department of Orthopaedics, Guangzhou First People's Hospital, South China University of Technology, Guangzhou, China

Purpose: Human gut microbiota has been shown to be significantly associated with various inflammatory diseases. Therefore, this study aimed to develop an excellent auxiliary tool for the diagnosis of juvenile idiopathic arthritis (JIA) based on fecal microbial biomarkers.

Method: The fecal metagenomic sequencing data associated with JIA were extracted from NCBI, and the sequencing data were transformed into the relative abundance of microorganisms by professional data cleaning (KneadData, Trimmomatic and Bowtie2) and comparison software (Kraken2 and Bracken). After that, the fecal microbes with high abundance were extracted for subsequent analysis. The extracted fecal microbes were further screened by least absolute shrinkage and selection operator (LASSO) regression, and the selected fecal microbe biomarkers were used for model training. In this study, we constructed six different machine learning (ML) models, and then selected the best model for constructing a JIA diagnostic tool by comparing the performance of the models based on a combined consideration of area under receiver operating characteristic curve (AUC), accuracy, specificity, F1 score, calibration curves and clinical decision curves. In addition, to further explain the model, Permutation Importance analysis and Shapley Additive Explanations (SHAP) were performed to understand the contribution of each biomarker in the prediction process.

Result: A total of 231 individuals were included in this study, including 203 JIA patients and Non-JIA individuals. In the analysis of diversity at the genus level, the alpha diversity represented by Shannon value was not significantly different between the two groups, while the belt diversity was slightly different. After selection by LASSO regression, 10 fecal microbe biomarkers were selected for model training. By comparing six different models, the XGB model showed the best performance, which average AUC, accuracy and F1 score were 0.976, 0.914 and 0.952, respectively, thus being used to construct the final JIA diagnosis model.

Conclusion: A JIA diagnosis model based on XGB algorithm was constructed with excellent performance, which may assist physicians in early detection of JIA patients and improve the prognosis of JIA patients.

KEYWORDS

juvenile idiopathic arthritis, fecal microbes, machine learning, diagnosis, XGB algorithm

Introduction

The gut microbiota plays a crucial role in immune system development and regulation. Autoimmune diseases, marked by the immune system's attack on healthy cells, lead to inflammation and tissue damage. Dysbiosis in the gut microbiome, such as abnormal enrichment of certain symbionts, diversity loss, or pathogen invasion, has been shown to cause various human diseases. For example, Zaky et al. have identified the role of the gut microbiome in diabetes and obesity-related kidney diseases (Zaky et al., 2021). And several studies have found that gut microbiota disorder is linked to the activity of rheumatic diseases (Yu et al., 2021; Bao et al., 2020).

Juvenile Idiopathic Arthritis (JIA), the most common chronic rheumatic disease in children, is marked by its mysterious origins and sustained arthritis for over six weeks in individuals under 16 years old. The disease exhibits a varied incidence rate, estimated between 1.6 and 23 cases, and a prevalence ranging from 3.8 to 400 per 100,000 children (Gibiino et al., 2018; Weiss, 2022). It often severely impacts the physical and mental health of children, restricting growth and causing joint deformities, thus diminishing the quality of life and social participation (Haverman et al., 2012). Early diagnosis and treatment are critical to improving outcomes and preventing deformities. Clinical symptoms and imaging findings are helpful in the diagnosis of JIA. However, the etiology of JIA remains elusive and inflammatory findings are not always evident as early symptoms, which may delay the diagnosis of JIA and further aggravate the progression of the disease. By identifying particular signs of chronic inflammation, imaging studies are essential to the early diagnosis of JIA. They are also beneficial in tracking the illness and assessing the efficacy of treatment. Nevertheless, this approach is still in its infancy (Stevens and Rudd, 2013; Tsujioka et al., 2023). Previous research indicated that the diagnosis of JIA often necessitates referrals to three different physicians, with an average median time of three months for a definitive diagnosis, indicating that the diagnosis of JIA is currently difficult (Aoust et al., 2017). Therefore, it is of great significance to develop a tool that can accurately diagnose JIA.

With the emergence of digital health and gene sequencing, artificial intelligence (AI) has shown a broad prospect in medical field (Kim et al., 2021). At present, the emergence of electronic medical records (EMR) and the expansion of databases present significant opportunities for ML application in the medical field. Additionally, ML algorithms are frequently employed for prediction of clinical outcomes, tailored treatment, and early illness diagnosis (Goecks et al., 2020; Huang et al., 2018). For instance, Liu et al. had developed efficient machine learning (ML) models for predicting metastatic bone tumors (Liu WC. et al., 2021). Similarly, Li et al. had designed a ML model to predict the incidence of pulmonary infections following spinal cord injuries (Li et al., 2023). With the advent of software for quality control and precise alignment of metagenomic sequencing data (such as kneaddata, bracken, Kracken, etc.) (Wood et al., 2019; Lu et al., 2022), our understanding of gut microbiota has become more accurate and in-depth, and it is also possible for gut microbiota to be used as predictors for the construction of machine learning prediction models. For example, Su et al. used species based on fecal microbial species level to construct a machine learning predictive model for the prediction of multiple diseases (Su et al., 2022).

In previous studies, the relationship between fecal microbiome and JIA had been explored (Tejesvi et al., 2016). Many studies have pointed out that the pathophysiology of JIA is linked to the gut microbiome (De Filippo et al., 2019; van Dijkhuizen et al., 2019; Qian et al., 2020). A study by Tejesvi et al. (2016) found that the fecal microbiota in JIA presents a high level of Bacteroidetes and a low level of Firmicutes, and changes in the gut microbial ecology may put genetically predisposed individuals' mucosal immune systems at risk, which could lead to local proinflammatory cascades and the development of JIA. However, fecal microbiome-based ML diagnostic models for JIA are rare. Therefore, in this study, we aimed to integrate phylum and genus-level gut biomarkers to construct and validate a high-performance ML model for assisting JIA diagnosis.

Methods

Metagenomic datasets

The metagenomic data utilized in this study were derived from the NCBI project PRJNA379123. We downloaded the FASTQ files of 16S rRNA gene sequences extracted from the fecal samples. Metagenomic data from the experimental group were exclusively

derived from fecal samples collected from juvenile idiopathic arthritis (JIA) patients at the initial treatment phase. Figure 1 illustrated the research flow of this study.

Sequencing data processing and microbiome profiling

Firstly, we used the KneadData tool to clean and control the raw FASTQ file. The quality of all reads was managed with Trimmomatic (version 0.39), with parameters set to SLIDINGWINDOW:4:20 MINLEN:50 LEADING:3 TRAILING:3 (Bolger et al., 2014). Reads containing human sequences were filtered out using Bowtie2 (version 2.4.5), applying the human reference database (hg37_and_human_contamination) recommended by KneadData, with parameters configured to –very-sensitive –dovetail (Langmead and Salzberg, 2012).

Subsequently, the cleansed FASTQ data were compared against sequences from known microbes with the goal of translating metagenomic 16S rRNA sequencing data into species abundance information. The metagenomic data were classified using Kraken software version 2.2.1.3, with reference to the official Kraken2/Bracken 16S RNA indexes (Silva 138) (Wood et al., 2019; Lu et al., 2022). For precise quantification of microbial abundance as determined by Kraken2, Bracken version 2.9 was employed (Lu et al., 2017). The read counts were converted into relative abundances of gut microbiota at both the phylum and genus levels through Bracken software for subsequent analysis.

Microbiome analysis and screening

Microbiome analysis and screening and statistical analysis were performed using Python 3.8 and R version 4.3.2. Descriptive statistics were assessed using chi-square tests or Fisher's exact tests as appropriate. Continuous variables were compared using Student's t-tests or rank-sum tests. P-value of less than 0.05 considered statistically significant.

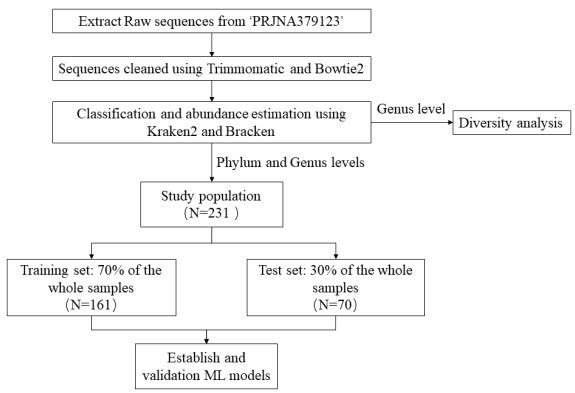

FIGURE 1
The flow chart of the study.

To understand the distribution of gut microbiota in the study population, we performed diversity analysis at the genus level, including α-diversity and β-diversity, based on the data after kraken2 classification and bracken abundance estimation. Alpha diversity is often used to measure the number of species in a single sample or environment (richness) and how evenly these species are distributed (evenness). We calculated the Shannon's α-diversity index (Sh) for each sample using the alpha_diversity.py script from KrakenTools. However, beta diversity is often used to measure the differences in species composition across environments or regions. In this study, β-diversity was examined using Principal Coordinates Analysis (PCoA) based on the Bray–Curtis distance matrix, which was computed using the relative abundances of microbial genus. This facilitated the visualization of sample clustering according to their genus-level compositional profiles. Differences in microbiome composition among various phenotypes were determined using permutational multivariate analysis of variance (PERMANOVA) with distance matrices (adonis) via the adonis function of the vegan R package v.2.6-4.

To reduce the risk of overfitting the prediction model, we need to screen suitable variables before training the model. Initially, we selected the top three phyla and the top twenty genera ranked by average abundance to reduce the influence of technical error on the results. Subsequently, to refine the variables used to train the ML model, these 23 variables were further filtered by least absolute shrinkage and selection operator (Lasso) regression. Features with nonzero regression coefficients in the LASSO model were chosen to train the subsequent ML predictive models.

Model establishment and evaluation

In this study, all data were randomly divided into training and test sets in a 7:3 ratio. The Synthetic Minority Over-sampling Technique (SMOTE) method was used to oversampling the training set to mitigate the potential impact of imbalanced data on model training (Solihah et al., 2020; Wu et al., 2019). The secret to this approach is to oversample the small class data samples in order to increase the number of small class data samples and boost the model's accuracy. To identify the most effective ML model for diagnosing juvenile idiopathic arthritis, we trained six commonly used ML models, including three ensemble algorithms and three simple classification algorithms: Random Forest (RF), eXtreme Gradient Boosting (XGB) and Gradient Boosting Machine (GBM) are ensemble algorithms. Naive Bayes Classifiers (NBC), Decision Tree (DT) and Logistic Regression (LR) are three simple classification algorithms. In model construction, each model underwent internal ten-fold cross-validation and tuned hyperparameters. Subsequently, ROC curves and calibration curves for each model were plotted in both the training and test sets to comprehensively assess model performance, aiming to select the model with optimal efficacy for the diagnosis of juvenile idiopathic arthritis. Additionally, to visually demonstrate the net benefit of each model at varying clinical decision thresholds, clinical decision curves were plotted for the models in both training and test sets. Ultimately, the best-performing model for disease diagnosis

was selected based on a combined consideration of AUC value, accuracy, specificity, F1 score, calibration curves, and clinical decision curves.

Feature importance analysis and model demonstration

Shapley Additive Explanations (SHAP) and Permutation Importance analysis are frequently utilized for elucidating ML models (Altmann et al., 2010; Li et al., 2022). The presentation of feature importance not only aids in interpreting the predictive process of ML models but also substantially contributes to our understanding of the roles various microbiota play in the onset and progression of diseases. Through a randomization of the feature test data values and measuring the average error they introducing into the model, permutation importance determines which features are more accurate for a trained model. Different from permutation importance, the SHAP computes each feature's contribution to the predicted value in order to identify the feature's significance (Goings and Hammes-Schiffer, 2020; Liu LP. et al., 2021). Therefore, both methods were used to explain the prediction models in this study. In addition, for a more transparent demonstration, we conducted SHAP value visualization by randomly selecting samples from both the experimental and control groups. This approach distinctly illustrates the contribution of different features to the final prediction value when the model predicts outcomes for individual samples.

Results

Basic characteristics of the dataset

The present investigation sourced its dataset from the NCBI project PRJNA379123, submitted by the Bambino Gesù Children's Hospital, IRCCS, Rome, Italy, incorporating a cohort of 231 European individuals. This dataset spans across four distinct phenotypes: three stages of JIA—baseline, inactive, and persistent activity—and a cohort of healthy controls. Our analysis consolidates all JIA conditions into a unified experimental group to delineate the association between the gut microbiota and JIA. Consequently, the study designates 203 individuals as the experimental group and 28 as the control group, with the intent to construct ML models for JIA diagnosis.

Microbiome analysis and biomarkers screening

Following metagenomic data processing, including cleaning, taxonomic classification, and abundance estimation, our study performed a diversity analysis of gut microbiota at the genus level. As shown in Figure 2A, alpha diversity was evaluated by Shannon index, and there was no significant difference between the JIA group and the healthy group (mean values were 2.47 and 2.52, respectively, P=0.568). However, Principal Component Analysis (PCA) in Figure 2B indicated subtle distinctions in beta diversity between JIA patients and healthy individuals (P=0.001).

To train a high-performance diagnostic model, we initially selected biomarkers based on the top three phyla and top twenty genera by average abundance, with their distribution across the experimental and control groups presented in Table 1. At the phylum level, Firmicutes dominate the gut microbial distribution in this population, with a higher relative abundance in healthy individuals than in JIA patients. Bacteroidota and Proteobacteria followed, with higher prevalence in the JIA group. In addition, at the genus level, only Faecalibacterium, with a mean relative abundance exceeding 0.1, showed no significant difference between the groups. To prevent overfitting due to an excess of biomarkers, a LASSO regression was applied to the 23 preselected biomarkers, culminating in the identification of 10 variables for the subsequent model construction and validation, including 3 phylum-level biomarkers (Firmicutes, Bacteroidota and Proteobacteria) and 7 genus-level biomarkers (Faecalibacterium, Alloprevotella, UCG-002, Dialister, Lachnoclostridium, Monoglobus and Veillonella) (Figure 3).

Model selection and performance evaluation

After screening the variables, we trained six ML models based the ten biomarkers. In internal ten-fold cross-validation, the

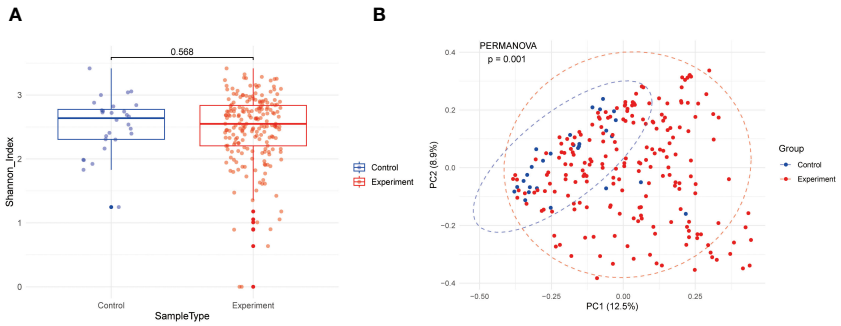

FIGURE 2
Genus-level diversity of fecal microorganisms. **(A)** alpha diversity; **(B)** belt diversity.

TABLE 1 Summary descriptives table by groups of `juvenile idiopathic arthritis'.

Gut microflora	Control	Experiment	*P*-value
	N=28	*N=203*	
Phylum level			
Firmicutes_1672	0.91 (0.11)	0.66 (0.26)	<0.001
Bacteroidota_43868	0.05 (0.09)	0.17 (0.18)	<0.001
Proteobacteria_2375	0.01 (0.01)	0.12 (0.19)	<0.001
Genus level			
Faecalibacterium_45544	0.22 (0.19)	0.13 (0.14)	0.023
Bacteroides_43874	0.02 (0.06)	0.07 (0.11)	0.001
Subdoligranulum_45553	0.07 (0.06)	0.06 (0.10)	0.477
Escherichia.Shigella_46463	0.00 (0.01)	0.04 (0.09)	<0.001
Alloprevotella_43941	0.01 (0.01)	0.04 (0.08)	<0.001
Ruminococcus_45552	0.05 (0.08)	0.03 (0.08)	0.144
Blautia_45422	0.04 (0.05)	0.03 (0.05)	0.414
Streptococcus_1853	0.02 (0.03)	0.03 (0.07)	0.188
UCG.002_45530	0.07 (0.08)	0.02 (0.07)	0.009
Dialister_45783	0.06 (0.13)	0.02 (0.06)	0.131
Bacillus_1688	0.03 (0.05)	0.02 (0.06)	0.430
Christensenellaceae.R.7.group_45329	0.03 (0.04)	0.02 (0.07)	0.296
Lachnoclostridium_45446	0.00 (0.00)	0.02 (0.09)	0.001
Pseudomonas_3723	0.00 (0.00)	0.02 (0.08)	0.001
uncultured_43978	0.01 (0.03)	0.02 (0.06)	0.113
Alistipes_43965	0.01 (0.01)	0.02 (0.05)	0.005
Flavobacterium_44221	0.01 (0.02)	0.01 (0.05)	0.152
Monoglobus_45507	0.03 (0.06)	0.01 (0.03)	0.177
Akkermansia_46831	0.01 (0.01)	0.01 (0.05)	0.048
Veillonella_45786	0.00 (0.01)	0.01 (0.04)	<0.001

XGBoost (XGB) model emerged as the most effective, achieving an average AUC of 0.976 (Figure 4A). The ROC curves for both training and test sets underscored the XGB model's exceptional performance (Figure 4B). Calibration curves for each model further substantiated the XGB model's accuracy and interpretability, showcasing a closer alignment with perfect calibration in both datasets (Figure 4C). Other performance metrics such as accuracy, AUC, Recall, precision, and F1 index of the six models in the test set are detailed in Table 2, where the RF, GBC, and XGB models demonstrated remarkable effectiveness. Clinical decision curve analysis confirmed the XGB model's superior net benefit across nearly all risk thresholds, especially in the test dataset (Figure 4D). Considering the overall performance, the XGB model was selected as the diagnostic tool for JIA. Figure 5 presented the confusion matrix of the final diagnostic model in the training and test sets.

Feature importance analysis and prediction process presentation

To explain the role of different biomarkers in the predictive mechanism, we performed a feature importance analysis. Initially, a permutation feature importance assessment across all six models highlighted that Proteobacteria and genus UCG-002 provided the most substantial contribution within the top-performing models—RF, GBC, and XGB (Figure 6). The subsequent SHAP analysis of the XGB model also yielded the same result that the contributions of these two biomarkers were significantly higher than those of other biomarkers, followed by Bacteroidota, among others (Figure 7).

In addition, Figure 8 presented the diagnostic model's analytic process through SHAP value visualization. Figure 8A specifically demonstrates the model's predictive sequence for a JIA sample, with an outcome of f(x) = 0.99, suggesting a high likelihood of JIA as

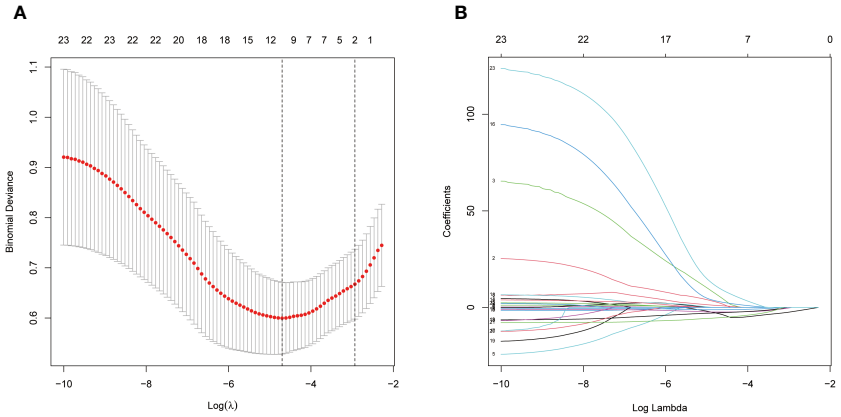

FIGURE 3
Through LASSO binary logistic regression analysis, ten fecal microbe biomarkers were selected, 3 phylum-level biomarkers (Firmicutes, Bacteroidota and Proteobacteria) and 7 genus-level biomarkers (Faecalibacterium, Alloprevotella, UCG-002, Dialister, Lachnoclostridium, Monoglobus and Veillonella). **(A)** Penalty maps of the Lasso model for 23 biomarkers; **(B)** LASSO coefficient mapping of 23 biomarkers.

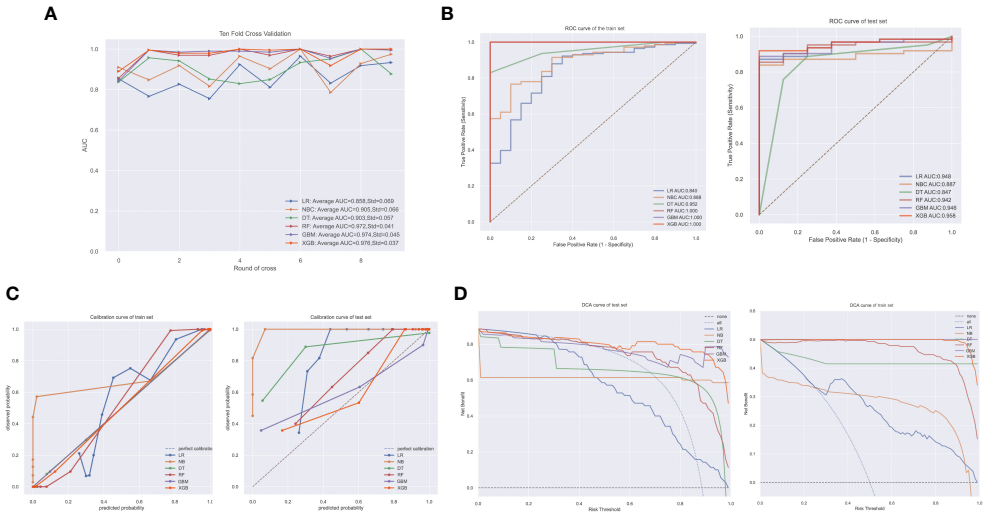

FIGURE 4
Demonstration of model performance. **(A)** ten-fold cross-validation results of different machine learning (ML) models in training dataset; **(B)** ROC curves of different ML models in training set and test set; **(C)** calibration curves of different ML models in training set and test set; **(D)** decision curve analysis (DCA) of different ML models in training set and test set.

TABLE 2 Performance metrics of different models.

Models	Accuracy	AUC	Recall	Precision	F1
LR	0.700	0.948	0.661	1.000	0.796
NB	0.671	0.887	0.629	1.000	0.772
DT	0.771	0.847	0.758	0.979	0.855
RF	0.900	0.942	0.903	0.983	0.941
GBM	0.886	0.946	0.919	0.950	0.934
XGB	0.914	0.958	0.952	0.952	0.952

RF, Random Forest; XGB, eXtreme Gradient Boosting; GBM, Gradient Boosting Machine; NBC, Naive Bayes Classifiers; DT, Decision Tree; LR, Logistic Regression.

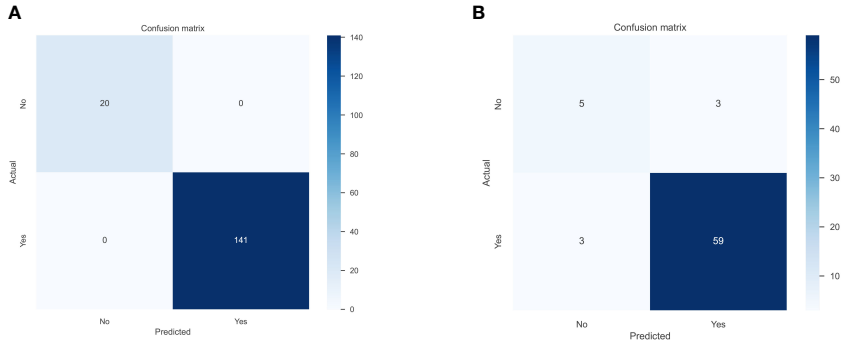

FIGURE 5
Confusion matrix of the diagnostic model constructed by the XGB algorithm. **(A)** training set; **(B)** test set.

FIGURE 6
Permutation importance analysis of different models.

assessed by the diagnostic model. The numbers following the biomarkers detailed their individual contributions to the prediction. Figure 8B showed the prediction process of the model for a healthy sample.

Discussion

Juvenile Idiopathic Arthritis (JIA) is a relatively uncommon disease that not only affects joints but can also involve other organs. The limited understanding of JIA among pediatricians and general practitioners, coupled with the absence of characteristic symptoms, leads to a high incidence of misdiagnosis, missed diagnosis, and delayed diagnosis. A retrospective study from France, analyzing the diagnostic journey of 67 JIA patients, highlighted these challenges (Aoust et al., 2017). The study revealed that prior to a confirmed diagnosis of JIA, patients had consulted with an average of three physicians, and the median time to diagnosis was 3 months, underscoring the significant difficulties encountered in accurately diagnosing JIA. The most common initial misdiagnoses were Reactive Arthritis (34%) and Septic Arthritis (24%) (Aoust et al., 2017). The treatment approaches for these conditions differ markedly from JIA, and misdiagnosis resulting in prolonged antibiotic use not only hinders recovery but may also promote the development of JIA by disrupting the balance of the human microbiome (Horton et al., 2015). Therefore, the development of a simple and effective tool for diagnosing JIA is of great significance.

Artificial intelligence (AI) is a broad field that enables computers to mimic human intelligence to perform tasks, including understanding language, recognizing images, solving scientific problems, and learning (Laskaris, 2015). Machine Learning (ML), a subset of AI, focuses on developing algorithms and techniques that allow computers to learn from data and make decisions or predictions (Alhusain et al., 2013). ML algorithms achieve learning by analyzing and identifying patterns in data (Alhusain et al., 2013). Considering the abundance of data

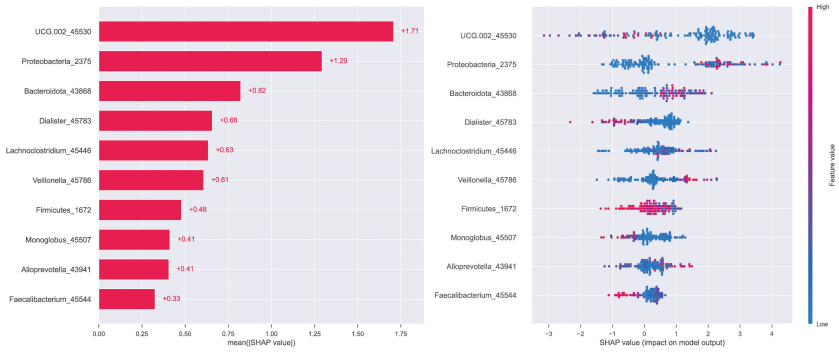

FIGURE 7
SHAP features analysis of the XGB model.

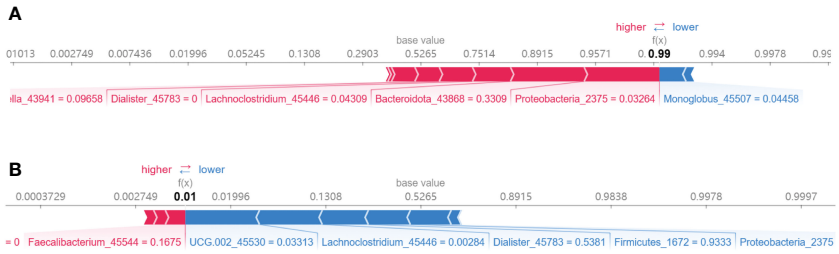

FIGURE 8
Demonstration of the prediction process of the XGB model. **(A)** A JIA sample; **(B)** A health sample.

accessible online and the emergence of electronic medical records (EMR), more clinical data sets, including clinical diagnoses and laboratory data, could be obtained conveniently, thus making ML bring a bright future in medical filed (Deo, 2015; Handelman et al., 2018; Toh et al., 2019; Bhavsar et al., 2021).

In this study, we innovatively constructed six different ML classification models based on fecal microbiomics, including the conventional logistic regression model and ensemble ML models commonly used in the medical field, such as RF, GBM and XGB. Ultimately, XGB model was chosen to construct the diagnostic tool for JIA. Previously, the RF model was commonly employed for processing fecal microbiomics data, and it was generally considered more suitable for handling such data. For instance, Huang et al. developed an RF model based on fecal microbiomics data to predict tumor patients' responses to PD-L1 antibodies (Huang et al., 2023), and Su et al. also constructed an RF model for multi-disease classification using fecal microbiome data (Su et al., 2022). In our study, an RF model was also developed in the pre-construction phase of the models, which demonstrated excellent performance across various evaluation metrics. However, compared to the XGB model, the RF model was slightly inferior in all aspects, particularly in the calibration curve and clinical decision curve in the test set. This indicates that the XGB model may has stronger generalizability and can bring greater benefits to clinical diagnosis. The XGB algorithm is a scalable, adaptable and effective ML algorithm classifier that has been applied extensively in the medical field, such chronic kidney disease, COVID-19, and bone metastasis (BM) in non-small cell lung cancer (Ogunleye and Wang, 2020; Guan et al., 2021; Li et al., 2022). Li et al. compared six commonly machine learning algorithms and found the XGB algorithm performed best, thus building a web predictor of BM from non-small cell lung cancer (Li et al., 2022). The XGB algorithm included a regular term in the objective function in order to prevent overfitting and manage model complexity. Additionally, it supported column sampling to improve model stability. This could be contributing to the fact that it performed the best in this study (Ester et al., 2022).

In this study, the diversity assessments were conducted at the genus level, which might introduce some deviations compared to the species level. This limitation was due to sequencing quality issues, which prevented accurate extraction of relative abundance of species at the species level (Caporaso et al., 2011; Kuczynski et al., 2011). In addition, the abundance of gut microbiota at phylum level and genus level were extracted to further analyze the influence of gut microbiota on JIA. At the phylum level, a significant reduction in Firmicutes was observed in JIA patients compared to healthy individuals. Firmicutes play a crucial role in immune regulation, as elucidated in the literature. Clarke et al. had explored the relationship between Firmicutes and the immune system, revealing that the gut can process and release glycoconjugates from Firmicutes, promoting cytokine IL-34 release (Jordan et al., 2023). This cytokine stimulates macrophage proliferation,

enhancing the body's defense mechanisms. Additionally, IL-34-mediated Mtorc1 activation in sentinel cells can remove glycoconjugates in peripheral tissues, maintaining immune homeostasis. Our findings indicated a significantly lower proportion of Firmicutes in JIA patients, potentially linked to decreased immune regulation functions.

In evaluating model feature importance and SHAP analysis, we focused on two significant biomarkers: Bacteroidetes and UCG-002. We observed a notably higher relative abundance of Bacteroidetes in the JIA group compared to healthy individuals, with SHAP analysis indicating a positive impact of this biomarker on predicting JIA. As the largest phylum of Gram-negative bacteria found in our guts, Bacteroidetes are regarded as crucial participants in maintaining the complex and healthy homeostasis. It has been proved that several Bacteroidetes genera are linked to the emergence of immunological dysregulation, neurological problems, and systemic diseases including metabolic syndrome (Gibiino et al., 2018). The abundance of the proteobacteria phylum is significantly increased in patients with moderate-to-severe COPD, especially in those with exacerbation of the disease (Pragman et al., 2012). In inflammatory bowel disease, this group of bacteria was also significantly increased (Sartor, 2008). This suggests that the Proteobacteria are important for inflammation promotion, but the underlying mechanisms remain unclear (Rizzatti et al., 2017). UCG-002, belonging to the Ruminococcaceae family, is a key indicator in gut microbiome studies. Lee et al. showed that the high relative abundance of Ruminococcaceae UCG-002 is associated with IgE-mediated food allergy in children (Lee et al., 2021), and Rhee et al. also suggested that Ruminococcaceae UCG-002 genus is a potential factor for psychiatric disorders such as bipolar disorder and major depression (Rhee et al., 2020). Our research found that UCG-002 contributed significantly to JIA, but the underlying mechanisms remain unclear.

Although this study constructed a ML model for JIA diagnosis based on feces with excellent performance, there were still some limitations. First, only sequencing data from a single center were used in this study. In future studies, multi-center data including different ethnic groups are needed for further training of the model to increase the generalization ability of the model. Second, because the data came from a public database, some common confounding factors such as age and gender that may affect the onset of JIA could not be excluded. Third, since species-level relative abundance could not be extracted, only species at the genus and phylum levels were analyzed in this study, and more subdivided species may be more beneficial to construct prediction models with excellent performance in future studies.

Conclusion

In this study, based on the relative abundance of 10 fecal biomarkers, we used XGB algorithm to construct a JIA diagnosis model with excellent performance, which can assist physicians in early detection of JIA patients and improve the prognosis of JIA patients.

Data availability statement

The datasets presented in this study can be found in online repositories. The names of the repository/repositories and accession number(s) can be found in the article/supplementary material.

Ethics statement

This study was approved by the Ethics Committee of Guangzhou First People's Hospital.

Author contributions

J-BT: Conceptualization, Investigation, Project administration, Writing – original draft, Writing – review & editing. W-JL: Conceptualization, Data curation, Investigation, Writing – review & editing. S-PL: Conceptualization, Formal analysis, Supervision, Writing – review & editing. M-PL: Conceptualization, Data curation, Formal analysis, Funding acquisition, Investigation, Methodology, Project administration, Resources, Software, Supervision, Validation, Visualization, Writing – original draft, Writing – review & editing. X-HG: Data curation, Funding acquisition, Investigation, Resources, Validation, Writing – original draft, Writing – review & editing.

Funding

The author(s) declare that no financial support was received for the research, authorship, and/or publication of this article.

Acknowledgments

We thank the researchers from Bambino Gesù Children's Hospitals for their contributions on the fecal microbial data.

Conflict of interest

The authors declare that the research was conducted in the absence of any commercial or financial relationships that could be construed as a potential conflict of interest.

Publisher's note

References

Alhusain, S., Coupland, S., John, R., Kavanagh, M.Ieee (2013). "Towards machine learning based design pattern recognition," in *13th UK Workshop on Computational Intelligence (UKCI)*, (New York, NY: IEEE).

Altmann, A., Toloşi, L., Sander, O., and Lengauer, T. (2010). Permutation importance: a corrected feature importance measure. *Bioinf. (Oxford England).* 26, 1340–1347. doi: 10.1093/bioinformatics/btq134

Aoust, L., Rossi-Semerano, L., Koné-Paut, I., and Dusser, P. (2017). Time to diagnosis in juvenile idiopathic arthritis: a french perspective. *Orphanet J. rare diseases.* 12, 43. doi: 10.1186/s13023-017-0586-4

Bao, Y., Dong, C., Ji, J., and Gu, Z. (2020). Dysregulation of gut microbiome is linked to disease activity of rheumatic diseases. *Clin. Rheumatol.* 39, 2523–2528. doi: 10.1007/s10067-020-05170-9

Bhavsar, K. A., Abugabah, A., Singla, J., AlZubi, A. A., Bashir, A. K., and Nikita, (2021). A comprehensive review on medical diagnosis using machine learning. *Cmc-Computers Materials Continua.* 67, 1997–2014. doi: 10.32604/cmc.2021.014943

Bolger, A. M., Lohse, M., and Usadel, B. (2014). Trimmomatic: a flexible trimmer for Illumina sequence data. *Bioinf. (Oxford England).* 30, 2114–2120. doi: 10.1093/bioinformatics/btu170

Caporaso, J. G., Lauber, C. L., Walters, W. A., Berg-Lyons, D., Lozupone, C. A., Turnbaugh, P. J., et al. (2011). Global patterns of 16S rRNA diversity at a depth of millions of sequences per sample. *Proc. Natl. Acad. Sci. United States America.* 108 Suppl 1, 4516–4522. doi: 10.1073/pnas.1000080107

De Filippo, C., Di Paola, M., Giani, T., Tirelli, F., and Cimaz, R. (2019). Gut microbiota in children and altered profiles in juvenile idiopathic arthritis. *J. autoimmunity.* 98, 1–12. doi: 10.1016/j.jaut.2019.01.001

Deo, R. C. (2015). Machine learning in medicine. *Circulation.* 132, 1920–1930. doi: 10.1161/CIRCULATIONAHA.115.001593

Ester, M., Kriegel, H. P., and Xu, X. (2022). "XGBoost: A scalable tree boosting system," in *Proceedings of the 22Nd ACM SIGKDD International Conference on Knowledge Discovery and Data Mining.* (Hoboken, NJ: Wiley), Vol. 785. 2016.

Gibiino, G., Lopetuso, L. R., Scaldaferri, F., Rizzatti, G., Binda, C., and Gasbarrini, A. (2018). Exploring Bacteroidetes: Metabolic key points and immunological tricks of our gut commensals. *Digestive liver Dis. Off. J. Ital. Soc. Gastroenterol. Ital. Assoc. Study Liver.* 50, 635–639. doi: 10.1016/j.dld.2018.03.016

Goecks, J., Jalili, V., Heiser, L. M., and Gray, J. W. (2020). How machine learning will transform biomedicine. *Cell.* 181, 92–101. doi: 10.1016/j.cell.2020.03.022

Goings, J. J., and Hammes-Schiffer, S. (2020). Nonequilibrium dynamics of proton-coupled electron transfer in proton wires: concerted but asynchronous mechanisms. *ACS Cent. science.* 6, 1594–1601. doi: 10.1021/acscentsci.0c00756

Guan, X., Zhang, B., Fu, M., Li, M., Yuan, X., Zhu, Y., et al. (2021). Clinical and inflammatory features based machine learning model for fatal risk prediction of hospitalized COVID-19 patients: results from a retrospective cohort study. *Ann. Med.* 53, 257–266. doi: 10.1080/07853890.2020.1868564

Handelman, G. S., Kok, H. K., Chandra, R. V., Razavi, A. H., Lee, M. J., and Asadi, H. (2018). eDoctor: machine learning and the future of medicine. *J. Internal Med.* 284, 603–619. doi: 10.1111/joim.12822

Haverman, L., Grootenhuis, M. A., van den Berg, J. M., van Veenendaal, M., Dolman, K. M., Swart, J. F., et al. (2012). Predictors of health-related quality of life in children and adolescents with juvenile idiopathic arthritis: results from a Web-based survey. *Arthritis Care Res.* 64, 694–703. doi: 10.1002/acr.21609

Horton, D. B., Scott, F. I., Haynes, K., Putt, M. E., Rose, C. D., Lewis, J. D., et al. (2015). Antibiotic exposure and juvenile idiopathic arthritis: A case-control study. *Pediatrics.* 136, e333–e343. doi: 10.1542/peds.2015-0036

Huang, X., Hu, M., Sun, T., Li, J., Zhou, Y., Yan, Y., et al. (2023). Multi-kingdom gut microbiota analyses define bacterial-fungal interplay and microbial markers of pan-cancer immunotherapy across cohorts. *Cell Host Microbe* 31, 1930–43.e4. doi: 10.1016/j.chom.2023.10.005

Huang, Z., Dong, W., Duan, H., and Liu, J. (2018). A regularized deep learning approach for clinical risk prediction of acute coronary syndrome using electronic health records. *IEEE Trans. Bio-med. Eng.* 65, 956–968. doi: 10.1109/tbme.2017.2731158

Jordan, C. K. I., Brown, R. L., Larkinson, M. L. Y., Sequeira, R. P., Edwards, A. M., and Clarke, T. B. (2023). Symbiotic Firmicutes establish mutualism with the host via innate tolerance and resistance to control systemic immunity. *Cell Host Microbe* 31, 1433–49.e9. doi: 10.1016/j.chom.2023.07.008

Kim, H. S., Kwon, I. H., and Cha, W. C. (2021). Future and development direction of digital healthcare. *Healthcare Inf. Res.* 27, 95–101. doi: 10.4258/hir.2021.27.2.95

Kuczynski, J., Lauber, C. L., Walters, W. A., Parfrey, L. W., Clemente, J. C., Gevers, D., et al. (2011). Experimental and analytical tools for studying the human microbiome. *Nat. Rev. Genet.* 13, 47–58. doi: 10.1038/nrg3129

Langmead, B., and Salzberg, S. L. (2012). Fast gapped-read alignment with Bowtie 2. *Nat. Methods* 9, 357–359. doi: 10.1038/nmeth.1923

Laskaris, R. (2015). Artificial intelligence: A modern approach, 3rd edition. *Library J.* 140, 45.

Lee, K. H., Guo, J., Song, Y., Ariff, A., O'Sullivan, M., Hales, B., et al. (2021). Dysfunctional gut microbiome networks in childhood igE-mediated food allergy. *Int. J. Mol. Sci.* 22. doi: 10.3390/ijms22042079

Li, M. P., Liu, W. C., Sun, B. L., Zhong, N. S., Liu, Z. L., Huang, S. H., et al. (2022). Prediction of bone metastasis in non-small cell lung cancer based on machine learning. *Front. Oncol.* 12, 1054300. doi: 10.3389/fonc.2022.1054300

Li, M. P., Liu, W. C., Wu, J. B., Luo, K., Liu, Y., Zhang, Y., et al. (2023). Machine learning for the prediction of postoperative nosocomial pulmonary infection in patients with spinal cord injury. *Eur. Spine J. Off. Publ. Eur. Spine Society Eur. Spinal Deformity Society Eur. Section Cervical Spine Res. Society.* 32, 3825–3835. doi: 10.1007/s00586-023-07772-8

Liu, L. P., Zhao, Q. Y., Wu, J., Luo, Y. W., Dong, H., Chen, Z. W., et al. (2021). Machine learning for the prediction of red blood cell transfusion in patients during or after liver transplantation surgery. *Front. Med.* 8, 632210. doi: 10.3389/fmed.2021.632210

Liu, W. C., Li, Z. Q., Luo, Z. W., Liao, W. J., Liu, Z. L., and Liu, J. M. (2021). Machine learning for the prediction of bone metastasis in patients with newly diagnosed thyroid cancer. *Cancer Med.* 10, 2802–2811. doi: 10.1002/cam4.3776

Lu, J., Breitwieser, F. P., Thielen, P., and Salzberg, S. L. (2017). Bracken: estimating species abundance in metagenomics data. *Peerj Comput. Sci.* doi: 10.7717/peerj-cs.104

Lu, J., Rincon, N., Wood, D. E., Breitwieser, F. P., Pockrandt, C., Langmead, B., et al. (2022). Metagenome analysis using the Kraken software suite. *Nat. Protoc.* 17, 2815–2839. doi: 10.1038/s41596-022-00738-y

Ogunleye, A., and Wang, Q. G. (2020). XGBoost model for chronic kidney disease diagnosis. *IEEE/ACM Trans. Comput. Biol. Bioinf.* 17, 2131–2140. doi: 10.1109/tcbb.2019.2911071

Pragman, A. A., Kim, H. B., Reilly, C. S., Wendt, C., and Isaacson, R. E. (2012). The lung microbiome in moderate and severe chronic obstructive pulmonary disease. *PloS One* 7, e47305. doi: 10.1371/journal.pone.0047305

Qian, X., Liu, Y. X., Ye, X., Zheng, W., Lv, S., Mo, M., et al. (2020). Gut microbiota in children with juvenile idiopathic arthritis: characteristics, biomarker identification, and usefulness in clinical prediction. *BMC Genomics* 21, 286. doi: 10.1186/s12864-020-6703-0

Rhee, S. J., Kim, H., Lee, Y., Lee, H. J., Park, C. H. K., Yang, J., et al. (2020). Comparison of serum microbiome composition in bipolar and major depressive disorders. *J. Psychiatr. Res.* 123, 31–38. doi: 10.1016/j.jpsychires.2020.01.004

Rizzatti, G., Lopetuso, L. R., Gibiino, G., Binda, C., and Gasbarrini, A. (2017). Proteobacteria: A common factor in human diseases. *BioMed. Res. Int.* 2017, 9351507. doi: 10.1155/2017/9351507

Sartor, R. B. (2008). Microbial influences in inflammatory bowel diseases. *Gastroenterology.* 134, 577–594. doi: 10.1053/j.gastro.2007.11.059

Solihah, B., Azhari, A., and Musdholifah, A. (2020). Enhancement of conformational B-cell epitope prediction using CluSMOTE. *PeerJ Comput. science.* 6, e275. doi: 10.7717/peerj-cs.275

Stevens, J. A., and Rudd, R. A. (2013). The impact of decreasing U.S. hip fracture rates on future hip fracture estimates. *Osteoporos Int.* 24, 2725–2728. doi: 10.1007/s00198-013-2375-9

Su, Q., Liu, Q., Lau, R. I., Zhang, J., Xu, Z., Yeoh, Y. K., et al. (2022). Faecal microbiome-based machine learning for multi-class disease diagnosis. *Nat. Commun.* 13, 6818. doi: 10.1038/s41467-022-34405-3

Tejesvi, M. V., Arvonen, M., Kangas, S. M., Keskitalo, P. L., Pirttilä, A. M., Karttunen, T. J., et al. (2016). Faecal microbiome in new-onset juvenile idiopathic arthritis. *Eur. J. Clin. Microbiol. Infect. Dis. Off. Publ. Eur. Soc. Clin. Microbiol.* 35, 363–370. doi: 10.1007/s10096-015-2548-x

Toh, T. S., Dondelinger, F., and Wang, D. (2019). Looking beyond the hype: Applied AI and machine learning in translational medicine. *EBioMedicine.* 47, 607–615. doi: 10.1016/j.ebiom.2019.08.027

Tsujioka, Y., Nishimura, G., Sugimoto, H., Nozaki, T., Kono, T., and Jinzaki, M. (2023). Imaging findings of juvenile idiopathic arthritis and autoinflammatory diseases in children. *Japanese J. radiology.* 41, 1186–1207. doi: 10.1007/s11604-023-01447-6

van Dijkhuizen, E. H. P., Del Chierico, F., Malattia, C., Russo, A., Pires Marafon, D., Ter Haar, N. M., et al. (2019). Microbiome analytics of the gut microbiota in patients with juvenile idiopathic arthritis: A longitudinal observational cohort study. *Arthritis Rheumatol. (Hoboken NJ).* 71, 1000–1010. doi: 10.1002/art.40827

Weiss, J. E. (2022). Prediction model for juvenile idiopathic arthritis: challenges and opportunities. *J. pediatrics.* 251, 46–49. doi: 10.1016/j.jpeds.2022.07.045

Wood, D. E., Lu, J., and Langmead, B. (2019). Improved metagenomic analysis with Kraken 2. *Genome Biol.* 20, 257. doi: 10.1186/s13059-019-1891-0

Wu, Y., Byrne, E. M., Zheng, Z., Kemper, K. E., Yengo, L., Mallett, A. J., et al. (2019). Genome-wide association study of medication-use and associated disease in the UK Biobank. *Nat. Commun.* 10, 1891. doi: 10.1038/s41467-019-09572-5

Yu, D., Du, J., Pu, X., Zheng, L., Chen, S., Wang, N., et al. (2021). The gut microbiome and metabolites are altered and interrelated in patients with rheumatoid arthritis. *Front. Cell. infection Microbiol.* 11, 763507. doi: 10.3389/fcimb.2021.763507

Zaky, A., Glastras, S. J., Wong, M. Y. W., Pollock, C. A., and Saad, S. (2021). The role of the gut microbiome in diabetes and obesity-related kidney disease. *Int. J. Mol. Sci.* 22. doi: 10.3390/ijms22179641

frontiers | Frontiers in Cellular and Infection Microbiology

TYPE Original Research
PUBLISHED 08 March 2024
DOI 10.3389/fcimb.2024.1369661

OPEN ACCESS

EDITED BY
Gang Ye,
Sichuan Agricultural University, China

REVIEWED BY
Marek Petráš,
Charles University, Czechia
Toho Qiyo,
Hebei Medical University, China
Ye Song,
Harbin Medical University, China
Yudong Cao,
Central South University, China

*CORRESPONDENCE
Shi Chen
Krystalchen1999@163.com
Chengcheng Wei
chengchengwei@hust.edu.cn

†These authors share first authorship

RECEIVED 12 January 2024
ACCEPTED 19 February 2024
PUBLISHED 08 March 2024

CITATION
Yang Q, Li B, Luan T, Wang X, Duan B, Wei C and Chen S (2024) Exploring blood lipids-immunity associations following HBV vaccination: evidence from a large cross-sectional study. *Front. Cell. Infect. Microbiol.* 14:1369661. doi: 10.3389/fcimb.2024.1369661

Exploring blood lipids-immunity associations following HBV vaccination: evidence from a large cross-sectional study

Qian Yang[1,2†], Benhua Li[1,2†], Tiankuo Luan[2], Xiaoyu Wang[2], Bixia Duan[2], Chengcheng Wei[3*] and Shi Chen[1*]

[1]Clinical Molecular Medicine Testing Center, The First Affiliated Hospital of Chongqing Medical University, Chongqing, China, [2]Chongqing Key Laboratory of Molecular Oncology and Epigenetics, The First Affiliated Hospital of Chongqing Medical University, Chongqing, China, [3]Department of Urology, Union Hospital, Tongji Medical College, Huazhong University of Science and Technology, Wuhan, China

Introduction: Serological responses following hepatitis B vaccination are crucial for preventing hepatitis B (HBV). However, the potential relationship between serum lipid levels and immunity from HBV vaccination remains poorly understood.

Methods: In this study, we conducted an analysis of the National Health and Nutrition Examination Survey (NHANES) data spanning from 2003 to 2016. Multivariable weighted logistic regression models, generalized linear analysis, stratified models, smooth curve fitting, segmentation effect analysis and sensitivity analysis were utilized to assess the relationships.

Results: After adjusting for relevant covariates, we observed that low levels of high-density lipoprotein cholesterol (HDL) were independently linked to a significantly lower seroprotective rate. Compared to HDL levels of ≥ 60 mg/dL, the odds ratios (ORs) for individuals with borderline levels (40-59 mg/dL for men, 50-59 mg/dL for women) and low levels (< 40 mg/dL for men, < 50 mg/dL for women) were 0.83 (95% CI 0.69-0.99) and 0.65 (95% CI 0.56-0.78), respectively. This association was particularly pronounced in individuals aged 40 or older. Conversely, higher levels of the triglyceride to HDL (TG/HDL) ratio (OR, 0.90; 95% CI, 0.84-0.98), total cholesterol to HDL (Chol/HDL) ratio (OR, 0.77; 95% CI, 0.64-0.92), and low-density lipoprotein to HDL (LDL/HDL) ratio (OR, 0.85; 95% CI, 0.76-0.96) were associated with a decreased likelihood of seroprotection.

Conclusion: This study suggests that lipid levels may play a role in modulating the immune response following HBV vaccination.

KEYWORDS

lipid, hepatitis B vaccination, immunity, HDL, HBV - hepatitis B virus

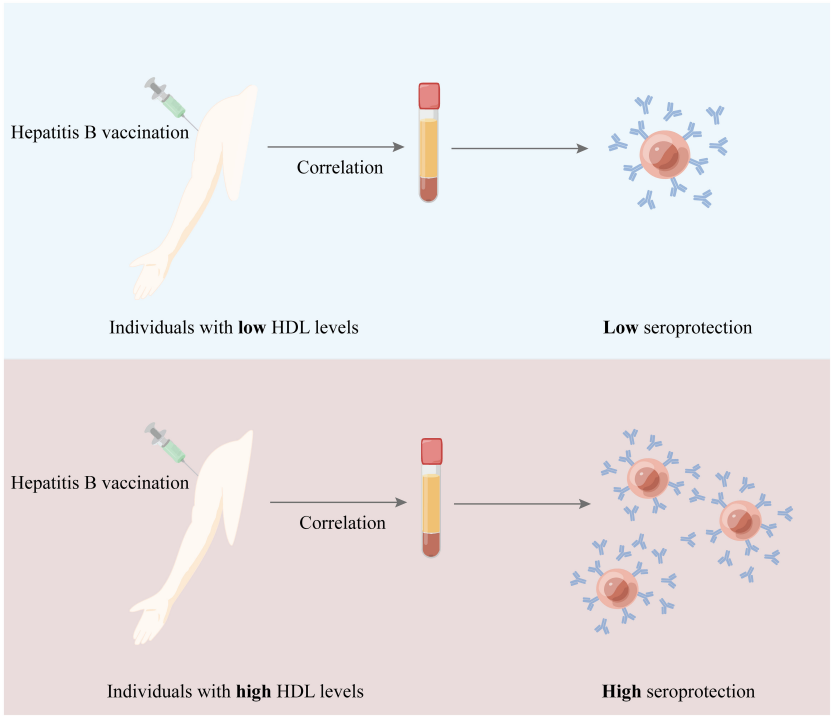

GRAPHICAL ABSTRACT

1 Introduction

HBV infection can advance to chronic hepatitis B and, in more severe cases, lead to cirrhosis and hepatocellular carcinoma (Global, regional, and national burden of hepatitis B, 1990-2019: a systematic analysis for the Global Burden of Disease Study 2019, 2022). As per a survey by the World Health Organization, an estimated 296 million people globally (3.8%) are chronically infected with HBV, resulting in approximately 820,000 deaths annually (Cui et al., 2023; Jeng et al., 2023). In response to this significant health burden, hepatitis B vaccination, including the administration of a birth dose, has been implemented as a key component of the Immunization Agenda 2030 (IA2030), which is endorsed by the World Health Assembly. Serological protection from vaccination is considered achieved when anti-HBs titers are ≥ 10 mIU/mL. However, despite the demonstrated effectiveness of the hepatitis B vaccine, a subset of individuals fails to attain seroprotection (Muhoza et al., 2021; Chang et al., 2022; El-Sayed and Feld, 2022; Wong et al., 2022). Identifying the factors that influence seroprotection is crucial for enhancing vaccination strategies and reducing the impact of HBV-related diseases. While factors such as age, sex, obesity, smoking, and HIV infection have been reported to affect the immune response to hepatitis B vaccination, additional determinants of seroprotection warrant further investigation (Alavian et al., 2008; Deng et al., 2022; Di Lello et al., 2022; Fonzo et al., 2022; Lian and Morrish, 2022).

Abnormal levels of lipids, including Chol, TG, HDL, and LDL, are associated with various health conditions. Elevated LDL levels are implicated in the development of cardiovascular diseases, while hypertriglyceridemia is linked to nonalcoholic fatty liver disease and acute pancreatitis. The TG/HDL ratio is recognized as a marker for metabolic syndrome (Ryan et al., 2018; Sulaiman, 2020; Pirillo et al., 2021). Lipid metabolism also plays a significant role in modulating immune responses, with implications for T cells, macrophages, dendritic cells, and other immune cell types in diseases such as nonalcoholic fatty liver disease, pancreatic fibrosis, and cancer progression (Yan and Horng, 2020; Liu et al., 2021; Yu et al., 2021; Lim et al., 2022; Zhao et al., 2022). Additionally, lipid-based nanoparticles have been shown to be effective vaccine adjuvants, enhancing antibody responses in vaccines targeting pathogens like SARS-CoV-2, HIV, and HBV (Di Paolo et al., 2010; Bartlett et al., 2020; Lou et al., 2020; Park et al., 2021; Bevers et al., 2022). Despite these findings, the impact of serum lipid levels on immunity following vaccination remains underexplored.

This study aims to investigate the association between serum lipid levels and seroprotection following hepatitis B vaccination, using a large sample of individuals who have received three doses of the vaccine from the National Health and Nutrition Examination Survey (NHANES).

2 Materials and methods

2.1 Research population

NHANES database is a comprehensive program designed to assess the health and nutritional status of adults and children in the

United States. It employs a biennial sampling strategy to select a nationally representative sample of approximately 10,000 individuals through a meticulous sampling process. Participants are randomly chosen to partake in interviews that cover demographic, socioeconomic, dietary, and health-related topics, in addition to undergoing medical, dental, and physiological measurements and laboratory tests.

For this cross-sectional study, we analyzed data from seven NHANES cycles spanning from 2003 to 2016 (Figure 1). Out of the total 71,058 subjects (35,122 men and 35,936 women), 33,665 had completed three doses of the hepatitis B vaccine, and 25,524 had available anti-HBs data. We excluded individuals who tested positive for HBsAg, anti-HBc, or HIV antibodies, indicative of potential immunosuppression. The final study subjects comprised 6,530 unique participants with available data on serum lipids and covariates. This population was further divided into two groups: those with seroprotection against HBV vaccination (n=3,276) and those susceptible to hepatitis B (n=3,254).

2.2 Hepatitis B serology assessment

HBV serological markers, including hepatitis B surface antigen (HBsAg), hepatitis B surface antibody (anti-HBs), and hepatitis B core antibody (anti-HBc), were evaluated using the VITROS ECi/ECiQ Immunodiagnostic Systems and VITROS 3600 immunodiagnostic system (Ortho Clinical Diagnostics). The combined assessment of these markers enabled the evaluation of immunity against HBV infection. Individuals with anti-HBs levels equal to or exceeding 10 mIU/mL were considered to have acquired immunity either from vaccination or from the resolution of a previous HBV infection. The presence of HBsAg indicated acute or chronic HBV infection, while anti-HBc positivity suggested previous or ongoing HBV infection. In our study, only participants negative for HBsAg and anti-HBc and positive for anti-HBs were considered to have immunity from vaccination (seroprotection), while those negative for all these markers were classified as nonresponsive after vaccination.

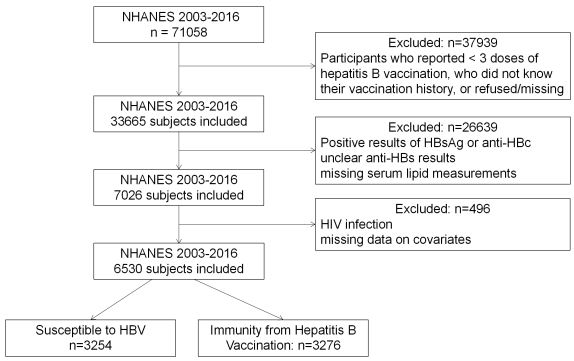

FIGURE 1
Flow chart of the population included in the final analysis of our study.

2.3 Serum lipid level assessment

In this study, cholesterol (Chol), LDL, HDL, and triglycerides (TG) were measured using the UniCel® DxC 800 Synchron & UniCel® DxC 660i Synchron Access Clinical Systems (Beckman Coulter Diagnostics) or Cobas 6000 Chemistry Analyzer (Roche Diagnostics). Chol and HDL assessments were conducted for participants aged 6 and above, while TG and LDL measurements were taken for those aged 12 and older during the morning session. These measurements were categorized according to clinical guidelines (Christensen et al., 2015). Hyperlipidemia was defined as total cholesterol ≥ 200 mg/dL, triglycerides ≥ 150 mg/dL, LDL ≥ 130 mg/dL, or HDL ≤ 40 mg/dL in men and ≤ 50 mg/dL in women, following the National Cholesterol Education Program (NCEP) guidelines for adults (Executive summary of the third report of the national cholesterol education program (NCEP) expert panel on detection, evaluation, and treatment of high blood cholesterol in adults (Adult treatment panel III), 2001). Additionally, we calculated the Chol/HDL (Conraads et al., 2003), TG/HDL (Oliveri et al., 2024), and LDL/HDL (Di Taranto et al., 2019) ratios to evaluate their relevance to seroprotection from the hepatitis B vaccine.

2.4 Covariates

Based on factors known to potentially impact the immune response to the hepatitis B vaccine and serum lipid levels, as outlined in the CDC's Red Book and previous studies (Christensen et al., 2015; Penina Haber and Schillie, 2023), we selected several covariates, including age, sex, body mass index (BMI), race/ethnicity, family poverty-to-income ratio (PIR), country of birth, and smoking status. BMI was used to categorize participants into normal weight (< 25 kg/m^2), overweight (25-29.9 kg/m^2), and obese (≥ 30 kg/m^2) according to CDC cutoffs for adults (CDC, 2023). Participants were classified as exposed to environmental smoke or active smokers (≥ 10 ng/mL) and nonsmokers (< 10 ng/mL) based on their serum cotinine levels (Andrews et al., 2021).

2.5 Statistical analysis

Given the complex multistage probability sampling and oversampling of specific subgroups within the NHANES dataset, we applied data weighting using a "survey design" approach to enhance the accuracy of statistics and ensure they more accurately reflect the true distribution of the U.S. population. We employed the 2-Year Mobile Examination Center Weight for Fasting Subsample (WTSAF2YR) in our weighted analysis, as triglyceride measurements were collected in the fasting subsample. For the final analysis, the sample weight was determined as the average of the "WTSAF2YR" values from seven NHANES survey cycles.

Continuous variables, such as Chol, TG, HDL, and LDL, were categorized based on previous literature (Executive summary of the third report of the national cholesterol education program (NCEP) expert panel on detection, evaluation, and treatment of high blood

cholesterol in adults (Adult treatment panel III), 2001). Summary statistics, including survey-weighted means and 95% confidence intervals for continuous variables, as well as unweighted sample sizes and survey-weighted percentages for categorical variables, described the baseline characteristics of the study participants. In the analysis of continuous variables, we utilized the Kruskal-Wallis rank sum test, and for situations involving fewer than ten theoretical count variables, the Fisher's exact probability test was applied. Categorical data were subjected to *p*-value determination through weighted chi-square analysis (refer to Table 1).

Furthermore, we conducted four statistical tests, namely, the Anderson-Darling normality test, the Cramer-von Mises normality test, the Lilliefors (Kolmogorov-Smirnov) normality test, and the Pearson chi-square normality test (refer to Supplementary Table S2). We employed the "ggplot2" R package to create visual representations of the data distribution, as illustrated in Figure 2. And we applied a log2 transformation during regression analysis to account for non-normality. To assess the independent impact of lipid concentrations on the response to the HBV vaccine, we utilized multivariable weighted linear regression models. These models included Model I, which was unadjusted for covariates; Model II, adjusted for age, PIR, and sex; and Model III, adjusted for age, race, sex, PIR, serum cotinine, place of birth, and BMI. Covariate selection adhered to internationally recognized practices, introducing or removing variables based on their effect on the regression coefficient of X exceeding 10%.

To evaluate potential nonlinear relationships, we performed smooth curve fitting and segmentation effect analysis. Subsequently, we conducted a subgroup analysis employing stratified multivariate logistic regression and interaction testing to explore stratified relationships between serum lipid levels and HBV vaccine-induced immunity, as well as the interactive effects of covariates on this relationship.

For sensitivity analysis, we categorized HDL, TG, and other lipid-related indexes into quartiles (Q1-Q4), as shown in Supplementary Table S4. All statistical analyses were performed using R software (Version 4.2.3), the R package, and EmpowerStats (www.empowerstats.com), with a significance level set at $P < 0.05$. FigDraw was utilized for graphical illustrations.

3 Results

3.1 Baseline characteristics

The analysis included a total of 6,530 individuals, comprising 3,276 participants with immunity following hepatitis B vaccination and 3,254 individuals susceptible to HBV. Table 1 outlines the baseline characteristics, highlighting significant differences between those with post-vaccination immunity and those susceptible to HBV concerning age, gender, race, PIR, BMI, smoking status, as well as levels of HDL, TG, TG/HDL ratio, Chol/HDL ratio, LDL/HDL ratio, and the presence of hyperlipidemia.

The seroprotection group was characterized by a higher proportion of females (59.0%), a younger age demographic (age < 40), non-smokers (82.1%), non-Hispanic whites (67.6%), individuals with a PIR ≥ 3.5, higher HDL levels (55.9 mg/dL, 95% CI 55.2-56.7), lower TG levels (100.0 mg/dL, 95% CI 97.0-103.1), a lower TG/HDL ratio (2.0, 95% CI 1.9-2.1), a lower Chol/HDL ratio (3.4, 95% CI 3.3-3.4), a lower LDL/HDL ratio (2.0, 95% CI 1.9-2.0), and a lower prevalence of hyperlipidemia (97.5%).

When examining lipid levels as categorical variables, the seroprotection group demonstrated a higher percentage of individuals with 'desirable' levels of HDL and TG compared to the susceptible group. Nevertheless, no significant differences were observed in Chol and LDL levels between these two groups.

3.2 The connection between serum lipid levels and immunity from hepatitis B vaccination

To investigate the association between serum lipid levels and HBV vaccination-induced immunity, we developed three weighted logistic regression models, as presented in Table 2. In Model 1, where no variables were taken into account, we observed significant association between HDL, TG, LDL/HDL, TG/HDL, and TC/HDL ratios and post-vaccination immunity. Remarkably, even after comprehensive adjustments for all variables, these associations persisted.

Specifically, a reduction in HBV vaccination-induced immunity was associated with lower HDL levels, but higher TG, TG/HDL, Chol/HDL, and LDL/HDL ratios. Using HDL levels of ≥ 60 mg/dL as a reference, the ORs for the borderline group (40/50-59 mg/dL) and the low group (<40 mg/dL for men, <50 mg/dL for women) were 0.83 (95% CI 0.69-0.99) and 0.65 (95% CI 0.56-0.78), respectively, indicating a 17% and 35% reduction in serological protection following vaccination. Additionally, for each 1-unit increment in log2-TG/HDL, log2-Chol/HDL, and log2-LDL/HDL ratios, vaccine-induced immunity decreased by 10%, 23%, and 15%, respectively.

3.3 Stratified analysis

In the fully adjusted model, we delved deeper into the association between serum lipid concentrations and seroprotection following vaccination within specific subgroups categorized by sex, BMI, and age, as depicted in Figure 3. Furthermore, we conducted interaction analyses on the three regression models, considering variables such as age, gender, BMI, smoking, PIR, and race, as detailed in Supplementary Table S3.

We observed that these variables did not exhibit significant interactions concerning the association between LDL/HDL, Chol/HDL, and post-HBV vaccination immunity. However, an interaction emerged with smoking and TG/HDL, where individuals in the smoking group experienced a 16% reduction in the likelihood of post-HBV vaccination immunity for each unit increase in TG/HDL.

Additionally, age demonstrated an interaction effect with HDL, underscoring a more pronounced association between HDL and post-HBV vaccination immunity among individuals aged 40 and older.

10.3389/fcimb.2024.1369661

TABLE 1 Characteristics of 6530 participants in NHANES data, 2003-2016.

Characteristics	Susceptible to HBV N=3254	Immunity from Hepatitis B Vaccination N=3276	*P* value
	Mean (95% CI) or n(%)	Mean (95% CI) or n(%)	
Age(years)	32.6 (31.8,33.4)	29.4 (28.5,30.4)	<0.01
Age(years)			<0.01
6-19	1437 (31.5)	1821 (33.5)	
20-39	933 (35.2)	934 (41.0)	
40-59	568 (24.7)	377 (20.3)	
≥ 60	316 (8.6)	144 (5.3)	
Sex			<0.01
Male	1603 (48.0)	1418 (41.0)	
Female	1651 (52.0)	1858 (59.0)	
Race/Ethnicity			<0.01
Mexican American	681 (10.7)	670 (7.7)	
Other Hispanic	283 (6.2)	223 (4.7)	
Non-Hispanic White	1159 (63.5)	1207 (67.6)	
Non-Hispanic Black	876 (14.8)	868 (12.0)	
Other Race - Including Multi-Racial	255 (5.8)	308 (8.1)	
Country of Birth			0.41
U.S.- born	2699 (87.9)	2755 (87.9)	
non-U.S.-born	553 (12.0)	520 (12.0)	
Refused	2 (0.1)	1 (0.0)	
Family poverty/ income ratio			<0.01
< 1.5	1455 (31.6)	1327 (25.4)	
1.5-3.5	1039 (34.7)	987 (29.7)	
≥ 3.5	760 (33.7)	962 (44.9)	
Serum Cotinine (ng/mL)			<0.01
non-smoker (< 10)	2614 (77.6)	2778 (82.1)	
Smoker (≥ 10)	640 (22.4)	498 (17.9)	
Body Mass Index (kg/m^2)			<0.01
Normal weight (< 25)	1460 (41.0)	1854 (51.2)	
Overweight (25-29.9)	802 (25.9)	754 (26.0)	
Obese (≥ 30)	992 (33.1)	668 (22.8)	
HDL (mg/dL)	52.1 (51.5,52.8)	55.9 (55.2,56.7)	<0.01
HDL (mg/dL)			<0.01
Desirable(≥ 60)	896 (26.0)	1109 (35.0)	
Borderline (40/50-59)	1446 (43.7)	1400 (42.4)	
Low (< 40 for man, < 50 for women)	912 (30.3)	767 (22.6)	
TG (mg/dL)	109.0 (105.9,112.1)	100.0 (97.0,103.1)	<0.01
TG (mg/dL)			<0.01
Desirable (< 150)	2640 (79.5)	2848 (84.9)	
Borderline (150–199)	333 (10.8)	243 (8.5)	
High (200–499)	281 (9.7)	185 (6.5)	
LDL (mg/dL)	105.6 (103.7,107.6)	103.3 (101.7,104.9)	0.07
LDL (mg/dL)			0.23
Desirable for high risk (< 70)	500 (12.5)	575 (14.0)	
Desirable (70–99)	1226 (35.4)	1308 (36.2)	
Near optimal (100–129)	899 (29.4)	906 (29.8)	
Borderline (130–159)	434 (15.5)	354 (14.6)	
High (160–189)	151 (5.6)	94 (3.9)	
Very high (≥ 190)	44 (1.6)	39 (1.6)	
Chol (mg/dL)	179.5 (177.4,181.6)	179.2 (177.2,181.3)	0.84
Chol (mg/dL)			0.39
Desirable(< 200)	2472 (71.8)	2600 (73.3)	
Borderline (200–239)	782 (20.1)	675 (19.8)	
High (≥ 240)	0 (8.1)	1 (6.9)	
TG/HDL	2.4 (2.3,2.5)	2.0 (1.9,2.1)	<0.01
Chol/HDL	3.7 (3.6,3.7)	3.4 (3.3,3.4)	<0.01
LDL/HDL	2.2 (2.1,2.2)	2.0 (1.9,2.0)	<0.01
Hyperlipidemia			<0.01
No	3150 (95.9)	3211 (97.5)	
Yes	104 (4.1)	65 (2.5)	

(Continued)

TABLE 1 Continued

Chol, total cholesterol; LDL, LDL cholesterol; HDL, HDL cholesterol; TG, triglycerides.
For continuous variables, the data were presented as survey-weighted mean (95% CI). For categorical variables, the data were presented as unweighted sample sizes and survey-weighted percentage.

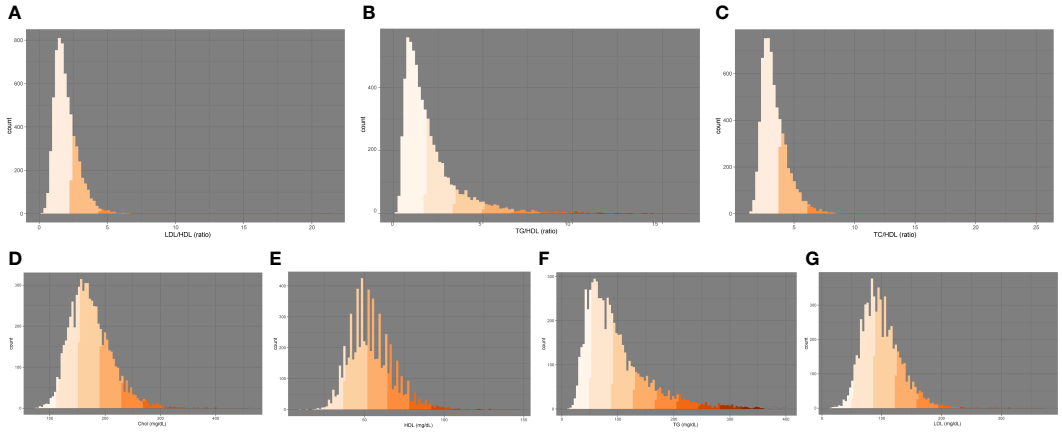

FIGURE 2
Distribution of serum lipid markers: **(A)** LDL/HDL, **(B)** TG/HDL, **(C)** TC/HDL, **(D)** Chol, **(E)** HDL, **(F)** TG, **(G)** LDL. Chol, total cholesterol; HDL, high-density lipoprotein cholesterol, TG, triglycerides, LDL, low-density lipoprotein cholesterol.

TABLE 2 Associations between lipid levels and immunity from Hepatitis B vaccination in NHANES, 2003-2016.

Exposure	Model 1 cOR (95% CI)	Model 2 aOR (95% CI)	Model 3 aOR (95% CI)
HDL (mg/dL)			
Desirable (≥ 60)	Reference	Reference	Reference
Borderline (40/50-59)	0.72*** (0.61-0.85)	0.80* (0.67-0.96)	0.83* (0.69-0.99)
Low (< 40 for man, < 50 for women)	0.55**** (0.47-0.66)	0.60**** (0.50-0.71)	0.65**** (0.56-0.78)
TG (mg/dL)			
Desirable (< 150)	Reference	Reference	Reference
Borderline (150–199)	0.74** (0.61-0.90)	0.86 (0.70-1.06)	0.91 (0.74-1.13)
High (200–499)	0.63*** (0.49-0.82)	0.74* (0.57-0.97)	0.79 (0.60-1.05)
Log2-TG/HDL	0.80**** (0.75-0.86)	0.87*** (0.81-0.94)	0.90* (0.84-0.98)
Log2-Chol/HDL	0.57**** (0.49-0.67)	0.70*** (0.59-0.83)	0.77** (0.64-0.92)
Log2-LDL/HDL	0.70**** (0.63-0.78)	0.80*** (0.71-0.90)	0.85** (0.76-0.96)

The reference group for the outcome variable is the population that did not acquire immunity after hepatitis B vaccination.
95% CI, 95% Confidence Interval; OR, Odds Ratio.
model I, unadjusted for covariates; model II, adjusted for age, sex, and PIR; model III, adjusted for age, sex, PIR, serum cotinine, place of birth, race, and BMI.
*P-value < 0.05; ** P-value < 0.01; ***P-value < 0.001; ****P-value < 0.0001.

3.4 Nonlinear or linear association between lipid levels and serological protection

In the final phase of our analysis, we implemented smooth curve fitting to examine potential partitioning of the independent variable into multiple intervals, as visualized in Figure 4. Additionally, we explored the segmentation effect, employing the saturation threshold effect, which is outlined in Table 3.

Notably, our findings unveiled a relationship between HDL concentration and an increase in seroprotection. Conversely, TG/HDL and Chol/HDL displayed a linear association with a decrease in seroprotection. Furthermore, we identified negative segmental linear effects in the case of LDL/HDL. Even after adjusting for variables such as sex, age, race, PIR, BMI, and place of birth, LDL/HDL levels ≥ 2.54 exhibited a significant association with a decrease in seroprotection, with an OR of 0.82 (95% CI 0.72-0.95).

3.5 Sensitivity analysis

In our sensitivity analysis, serum lipid concentrations were discretized from continuous variables into categorical variables (Q1-Q4). The outcomes of this sensitivity analysis were consistent with the results obtained from the weighted linear regression models. Notably, we observed that as HDL levels increased, the impact on seroprotection following HBV vaccination became progressively more significant. These sensitivity analysis findings revealed that the segment of the American population with higher serum lipid concentrations exhibited a stronger association with post-HBV vaccination immunity compared to the segment with lower serum lipid concentrations. Additional details regarding the sensitivity analysis can be found in Supplementary Table S4.

4 Discussion

This study delved into the potential association between serum lipid levels and immunity following HBV vaccination, utilizing data from the NHANES database spanning from 2003 to 2016, representative of the US population. Our analysis of 6,530 participants revealed distinct patterns: individuals with seroprotection from vaccination were more likely to be female, younger, and nonsmokers, aligning with previous research (Alavian

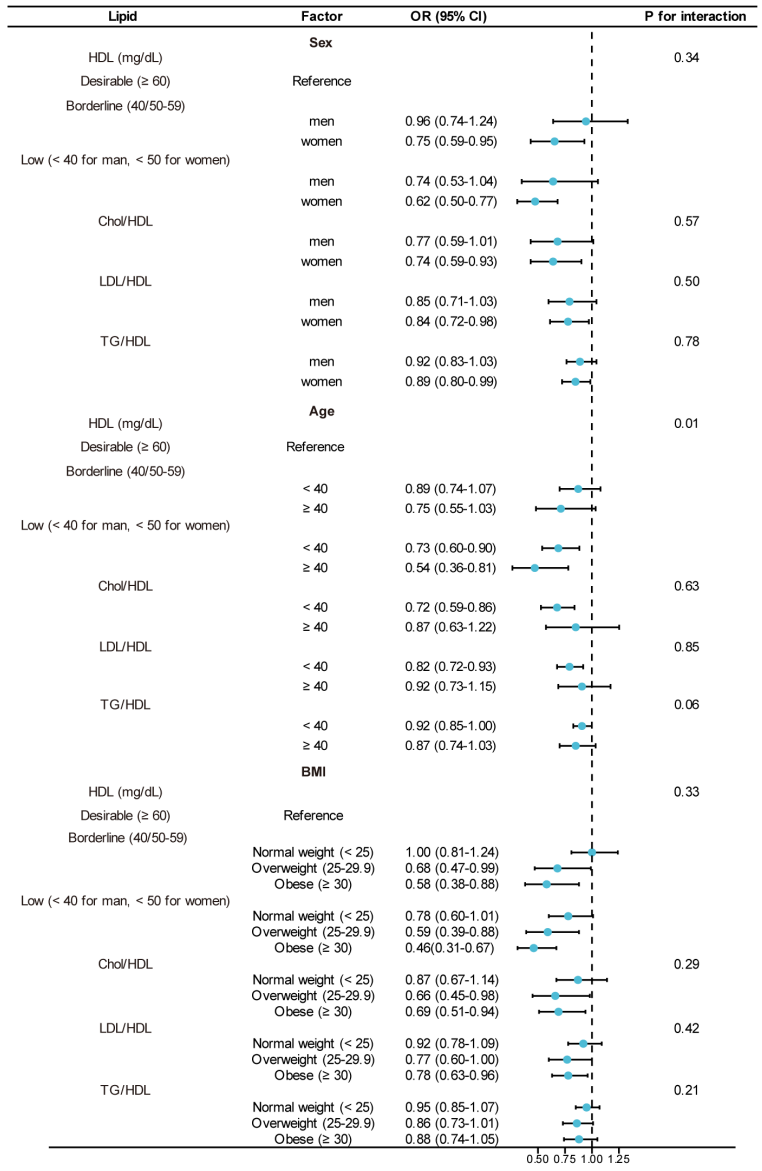

FIGURE 3
Subgroup analysis for the association between lipid levels and immunity from Hepatitis B vaccination: 95% CI, 95% Confidence Interval; OR, Odds Ratio. Adjusted for age, sex, PIR, serum cotinine, place of birth, race, and BMI. The model was not adjusted for the stratification variable itself.

et al., 2008; Deng et al., 2022; Di Lello et al., 2022; Fonzo et al., 2022; Lian and Morrish, 2022). Notably, our study was the first to establish a significant association between elevated HDL levels and reduced TG, TG/HDL, Chol/HDL, and LDL/HDL levels with seroprotection from HBV vaccination. Even after adjusting for pertinent covariates, these lipid levels remained independent risk factors for HBV vaccination immunity. Additionally, among participants aged 40 and older, heightened HDL levels were associated with a significant enhancement in seroprotection. Furthermore, our research unveiled that when LDL/HDL exceeded 2.54, the likelihood of HBV vaccination-induced immunity significantly declined.

Recent years have seen clinical database analysis significantly advancing disease diagnosis and prognosis, providing fresh insights into disease diagnosis and treatment (Zhang J. et al., 2023; Ren et al., 2023; Chi et al., 2023; Zhang P. et al., 2023; Zhang S. et al., 2023; Zhang et al., 2024; Zhang D. et al., 2023). Among these, several studies have examined the relationship between inflammatory markers and lipid levels. For instance, Xiao et al. reported a linear negative association between the systemic immune inflammation (SII) index and TG (Xiao et al., 2023). In contrast, Mahemuti et al. found a notable positive correlation between SII and hyperlipidemia (Mahemuti et al., 2023). In a separate study involving uterine leiomyoma patients, the neutrophil-lymphocyte ratio and SII exhibited a significant positive correlation with TG, while the monocyte-lymphocyte ratio demonstrated a notable negative correlation with TG (Duan et al., 2023). Discrepancies in these study outcomes may arise from variations in the studied populations and the utilization of different indicators. Moreover, Li et al. identified an inverse

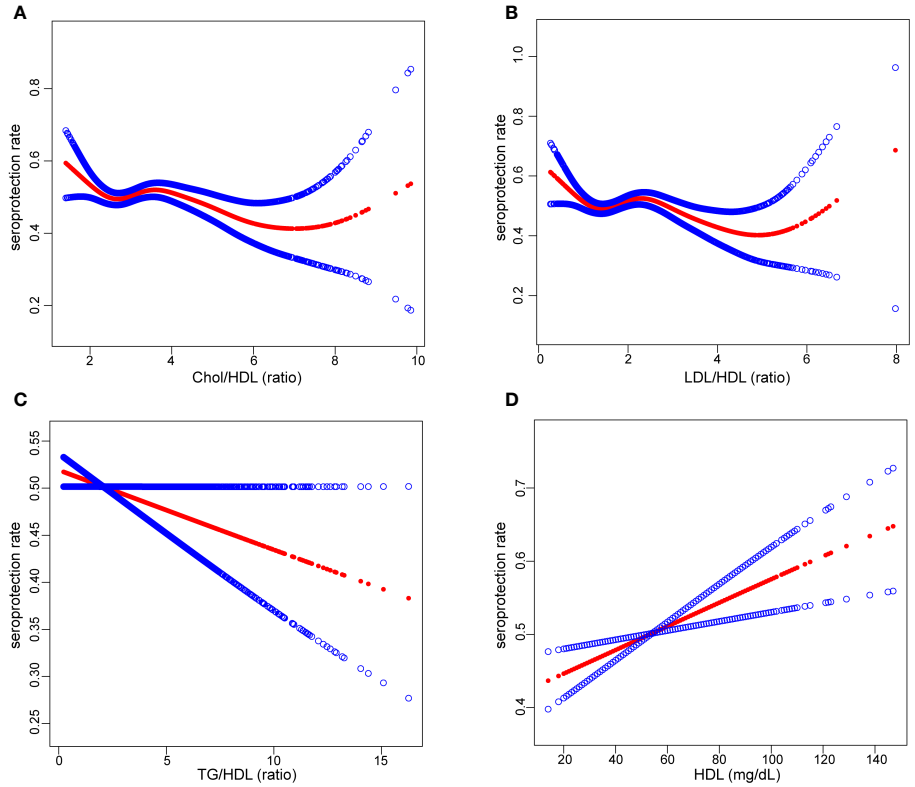

FIGURE 4
The relationship between serum lipid levels and seroprotection rate: Liner and non-liner association between Chol/HDl **(A)**, LDL/HDL **(B)**, TG/HDL **(C)**, HDl **(D)** and seroprotection rate. The solid red line represents the smooth curve fit between variables. Blue bands represent the 95% confidence interval from the fit. Chol, total cholesterol; HDL, high-density lipoprotein cholesterol, TG, triglycerides, LDL, low-density lipoprotein cholesterol.

TABLE 3 Treshold effect analysis of Lipid-related Index on Immunity from Hepatitis B Vaccination using Segmented regression models.

	Crude OR (95% CI)	*P*		Adjusted OR (95% CI)	*P*
LDL/HDL		0.19	**LDL/HDL**		0.04
LDL/HDL < 2.50	0.82*** (0.74, 0.91)		LDL/HDL < 2.54	1.02 (0.92, 1.14)	
LDL/HDL ≥ 2.50	0.72*** (0.63, 0.82)		LDL/HDL ≥ 2.54	0.82** (0.72, 0.95)	
Chol/HDL		0.54	**Chol/HDL**		0.07
Chol/HDL < 3.90	0.82*** (0.75, 0.90)		Chol/HDL < 2.29	0.55* (0.30, 0.99)	
Chol/HDL ≥ 3.90	0.78*** (0.71, 0.86)		Chol/HDL ≥ 2.29	0.96 (0.90, 1.01)	
TG/HDL		0.04	**TG/HDL**		0.08
TG/HDL < 2.50	0.82*** (0.75, 0.88)		TG/HDL < 1.14	1.25 (0.94, 1.65)	
TG/HDL ≥ 2.50	0.92*** (0.88, 0.96)		TG/HDL ≥ 1.14	0.95* (0.92, 0.99)	

The reference group for the outcome variable is the population that did not acquire immunity after hepatitis B vaccination.
Crude OR: unadjusted for covariates.
Adjusted OR: adjusted for age, sex, PIR, serum cotinine, place of birth, race, and BMI.
95% CI, 95% Confidence Interval; OR, Odds Ratio.
*P-value < 0.05; **P-value < 0.01; ***P-value < 0.001.

relationship between thyroglobulin antibody positivity and HDL levels, as well as a direct association with LDL levels in the general population with normal thyrotropin levels. This relationship was also influenced by gender (Li et al., 2021). These prior findings offer potential support for the observations presented in this study. However, it is important to note that the association between lipid levels and immunity remains a topic of ongoing debate.

The underlying mechanisms governing the association between lipid levels and immunity remain elusive. For instance, Kochumon et al. have demonstrated the pivotal role of IL-23 in the pathogenesis of inflammation induced by elevated low-

density lipoprotein cholesterol (Kochumon et al., 2022). Furthermore, lipoxins and metabolites of omega-3 fatty acids have been linked to inflammation resolution (Bäck et al., 2015). In a review by Nancy R. Webb, it was proposed that high-density lipoprotein may contribute to the *in vivo* regulation of serum amyloid A, thereby influencing the inflammatory response (Webb, 2021). Additionally, lipid mediators like leukotrienes and prostaglandins have been shown to modulate mast cell (MC) functions (Hagemann et al., 2019). Abnormal accumulation of endogenous lipids or their oxidation products can activate NLRP3, subsequently triggering inflammatory responses (Liang et al., 2021). Short-chain fatty acids have been reported to impact immune function through the stimulation of GPR43 or GPR41, leading to increased regulatory T cell numbers and enhanced function, while also reducing inflammatory cytokines (Tan et al., 2023). Schümann et al. reviewed ApoE (and potentially other apolipoproteins)-mediated lipid antigen transport, revealing its critical role in tumor immune surveillance and offering new perspectives for immunotherapy and vaccines (Schümann and De Libero, 2006). In summary, the interplay between lipid levels and immunity involves intricate mechanisms that warrant further investigation.

The present study unveils a novel association between serum lipid levels and immunity from HBV vaccination. Specifically, HDL cholesterol levels exhibit an association with an increase in seroprotection, while TG/HDL, Chol/HDL, and LDL/HDL levels display associations with a decrease in seroprotection. Our study boasts several merits. Firstly, the extensive dataset sourced from NHANES bolsters the reliability and applicability of our findings. Secondly, we meticulously employed appropriate methodologies to mitigate the influence of confounding variables. Furthermore, our results underwent weighting to reduce the potential bias stemming from population selection and augment overall representativeness.

However, it is crucial to acknowledge several limitations. Firstly, while the NHANES sample is extensive and representative of the US population, it may not comprehensively reflect other demographics or geographic regions. Secondly, despite our efforts to control for pertinent covariates, we cannot entirely dismiss the impact of unmeasured confounding factors on the observed associations. Thirdly, due to the natural exposure and time-dependent waning of serological protection following vaccine administration, there exists a potential for inherent bias in the outcomes of this study (31, Van Damme et al., 2017; Kushner et al., 2020). Lastly, this study, based on real-world data from a large population sample, sheds light on the potential association between serum lipid levels and the serological protection conferred by hepatitis B vaccination. However, further prospective research or animal-level verification is still needed to confirm the causal relationship between serum lipid levels and serological protection following hepatitis B vaccination.

Notwithstanding these constraints, our findings provide valuable insights into the prospective role of lipid metabolism in HBV vaccine response, potentially leading to enhanced vaccination strategies and more robust protection against HBV-related diseases.

5 Conclusion

Through the utilization of weighted logistic regression models and saturation threshold effect analysis, we highlight a distinctive relationship between lipid levels and immunity post HBV vaccination. Our findings underscore the positive association of HDL with seroprotection, while indicating negative associations of TG/HDL, LDL/HDL, and Chol/HDL with seroprotection. To substantiate potential causal links within our results, comprehensive prospective studies are imperative.

Data availability statement

The datasets presented in this study can be found in online repositories. The names of the repository/repositories and accession number(s) can be found in the article/Supplementary Material.

Author contributions

SC: Conceptualization, Writing – review & editing. QY: Writing – original draft, Writing – review & editing. BL: Methodology, Visualization, Writing – review & editing. TL: Methodology, Visualization, Writing – review & editing. XW: Data curation, Software, Writing – review & editing. BD: Data curation, Software, Writing – review & editing. CW: Resources, Supervision, Writing – review & editing.

Funding

The author(s) declare that no financial support was received for the research, authorship, and/or publication of this article.

Conflict of interest

The authors declare that the research was conducted in the absence of any commercial or financial relationships that could be construed as a potential conflict of interest.

Publisher's note

All claims expressed in this article are solely those of the authors and do not necessarily represent those of their affiliated organizations, or those of the publisher, the editors and the reviewers. Any product that may be evaluated in this article, or claim that may be made by its manufacturer, is not guaranteed or endorsed by the publisher.

Supplementary material

The Supplementary Material for this article can be found online at: https://www.frontiersin.org/articles/10.3389/fcimb.2024.1369661/full#supplementary-material

References

Alavian, S.-M., Mansouri, S., Abouzari, M., Assari, S., Bonab, M. S., and Miri, S.-M. (2008). Long-term efficacy of hepatitis B vaccination in healthcare workers of Oil Company Hospital, Tehran, Iran (1989-2005). *Eur. J. Gastroenterol. Hepatol.* 20, 131–134. doi: 10.1097/MEG.0b013e3282f1cc28

Andrews, F. V., Smit, E., Welch, B. M., Ahmed, S. M., and Kile, M. L. (2021). Urinary polycyclic aromatic hydrocarbons concentrations and hepatitis B antibody serology in the United States (NHANES, 2003-2014). *Environ. Res.* 195, 110801. doi: 10.1016/j.envres.2021.110801

(2022). Global, regional, and national burden of hepatitis B, 1990-2019: a systematic analysis for the Global Burden of Disease Study 2019. *Lancet Gastroenterol. Hepatol.* 7, 796–829. doi: 10.1016/S2468-1253(22)00124-8

(2001). Executive summary of the third report of the national cholesterol education program (NCEP) expert panel on detection, evaluation, and treatment of high blood cholesterol in adults (Adult treatment panel III). *JAMA* 285, 2486–2497. doi: 10.1001/jama.285.19.2486

Bäck, M., Weber, C., and Lutgens, E. (2015). Regulation of atherosclerotic plaque inflammation. *J. Intern. Med.* 278, 462–482. doi: 10.1111/joim.12367

Bartlett, S., Skwarczynski, M., and Toth, I. (2020). Lipids as activators of innate immunity in peptide vaccine delivery. *Curr. Med. Chem.* 27, 2887–2901. doi: 10.2174/0929867325666181026100849

Bevers, S., Kooijmans, S. A. A., Van de Velde, E., Evers, M. J. W., Seghers, S., Gitz-Francois, J. J. J. M., et al. (2022). mRNA-LNP vaccines tuned for systemic immunization induce strong antitumor immunity by engaging splenic immune cells. *Mol. Ther.* 30 (9), 3078–3094. doi: 10.1016/j.ymthe.2022.07.007

CDC. (2023). *About Adult BMI*. Available online at: https://www.cdc.gov/healthyweight/assessing/bmi/adult_bmi/index.html (Accessed 7 July, 2023).

Chang, K.-C., Chang, M.-H., Chen, H.-L., Wu, J. F., Chang, C. H., Hsu, H. Y., et al. (2022). Universal infant hepatitis B virus (HBV) vaccination for 35 years: moving toward the eradication of HBV. *J. Infect. Dis.* 225 (3), 431–435. doi: 10.1093/infdis/jiab401

Chi, H., Gao, X., Xia, Z., Yu, W., Yin, X., Pan, Y., et al. (2023). FAM family gene prediction model reveals heterogeneity, stemness and immune microenvironment of UCEC. *Front. Mol. Biosci.* 10:1200335. doi: 10.3389/fmolb.2023.1200335

Christensen, K., Werner, M., and Malecki, K. (2015). Serum selenium and lipid levels: Associations observed in the National Health and Nutrition Examination Survey (NHANES) 2011-2012. *Environ. Res.* 140, 76–84. doi: 10.1016/j.envres.2015.03.020

Conraads, V. M., Bosmans, J. M., Schuerwegh, A. J., De Clerck, L. S., Bridts, C. H., Wuyts, F. L., et al. (2003). Association of lipoproteins with cytokines and cytokine receptors in heart failure patients. Differences between ischaemic versus idiopathic cardiomyopathy. *Eur. Heart J.* 24 (24), 2221–2226. doi: 10.1016/j.ehj.2003.09.023

Cui, F., Blach, S., Manzengo Mingiedi, C., Gonzalez, M. A., Sabry Alaama, A., Mozalevskis, A., et al. (2023). Global reporting of progress towards elimination of hepatitis B and hepatitis C. *Lancet Gastroenterol. Hepatol.* 8(4), 332–342. doi: 10.1016/S2468-1253(22)00386-7

Deng, H., Feng, Q., Wu, Y., Lin, H., Cao, X., Xiang, F., et al. (2022). Immune response to hepatitis B vaccination in human immunodeficiency virus-positive patients in China: A 2-year retrospective study. *J. Med. Virol.* 94(6), 2684–2693. doi: 10.1002/jmv.27523

Di Lello, F. A., Martínez, A. P., and Flichman, D. M. (2022). Insights into induction of the immune response by the hepatitis B vaccine. *World J. Gastroenterol.* 28, 4249–4262. doi: 10.3748/wjg.v28.i31.4249

Di Paolo, D., Lenci, I., Cerocchi, C., Tariciotti, L., Monaco, A., Brega, A., et al. (2010). One-year vaccination against hepatitis B virus with a MPL-vaccine in liver transplant patients for HBV-related cirrhosis. *Transpl. Int.* 23 (11), 1105–1112. doi: 10.1111/j.1432-2277.2010.01104.x

Di Taranto, M. D., de Falco, R., Guardamagna, O., Massini, G., Giacobbe, C., Auricchio, R., et al. (2019). Lipid profile and genetic status in a familial hypercholesterolemia pediatric population: exploring the LDL/HDL ratio. *Clin. Chem. Lab. Med.* 57 (7), 1102–1110. doi: 10.1515/cclm-2018-1037

Duan, Y., Guo, L., Peng, Y., Shi, X., Zhao, Y., Liu, K., et al. (2023). Correlation between inflammatory marker and lipid metabolism in patients with uterine leiomyomas. *Front. Med. (Lausanne)* 10:1124697. doi: 10.3389/fmed.2023.1124697

El-Sayed, M. H., and Feld, J. J. (2022). Vaccination at the forefront of the fight against hepatitis B and C. *Nat. Rev. Gastroenterol. Hepatol.* 19, 87–88. doi: 10.1038/s41575-021-00570-x

Fonzo, M., Nicolli, A., Maso, S., Carrer, L., Trevisan, A., and Bertoncello, C. (2022). Body mass index and antibody persistence after measles, mumps, rubella and hepatitis B vaccinations. *Vaccines (Basel)* 10 (7), 1152. doi: 10.3390/vaccines10071152

Hagemann, P. M., Nsiah-Dosu, S., Hundt, J. E., Hartmann, K., and Orinska, Z. (2019). Modulation of mast cell reactivity by lipids: the neglected side of allergic diseases. *Front. Immunol.* 10. doi: 10.3389/fimmu.2019.01174

Jeng, W.-J., Papatheodoridis, G. V., and Lok, A. S. F. (2023). Hepatitis B. *Lancet* 401, 1039–1052. doi: 10.1016/S0140-6736(22)01468-4

Kochumon, S., Hasan, A., Al-Rashed, F., Sindhu, S., Thomas, R., Jacob, T., et al. (2022). Increased adipose tissue expression of IL-23 associates with inflammatory markers in people with high LDL cholesterol. *Cells* 11 (19), 3072. doi: 10.3390/cells11193072

Kushner, T., Chen, Z., Tressler, S., Kaufman, H., Feinberg, J., and Terrault, N. A. (2020). Trends in hepatitis B infection and immunity among women of childbearing age in the United States. *Clin. Infect. Dis.* 71, 586–592. doi: 10.1093/cid/ciz841

Li, J., Wang, Z., Liu, H., Fu, J., Qin, F., Guan, H., et al. (2021). Serum lipids are novel predictors for thyroid autoimmunity in the general population with normal TSH levels from a cross-sectional study. *Endocrine* 73 (2), 331–338. doi: 10.1007/s12020-021-02731-z

Lian, P. C. S., and Morrish, B. (2022). Antibody response to an accelerated course of Hepatitis B vaccination. *Occup. Med. (Lond)* 72, 446–451. doi: 10.1093/occmed/kqac054

Liang, J. J., Fraser, I. D. C., and Bryant, C. E. (2021). Lipid regulation of NLRP3 inflammasome activity through organelle stress. *Trends Immunol.* 42, 807–823. doi: 10.1016/j.it.2021.07.005

Lim, S. A., Su, W., Chapman, N. M., and Chi, H. (2022). Lipid metabolism in T cell signaling and function. *Nat. Chem. Biol.* 18, 470–481. doi: 10.1038/s41589-022-01017-3

Liu, X., Hartman, C. L., Li, L., Albert, C. J., Si, F., Gao, A., et al. (2021). Reprogramming lipid metabolism prevents effector T cell senescence and enhances tumor immunotherapy. *Sci. Transl. Med.* 13(587):eaaz6314. doi: 10.1126/scitranslmed.aaz6314

Lou, G., Anderluzzi, G., Schmidt, S. T., Woods, S., Gallorini, S., Brazzoli, M., et al. (2020). Delivery of self-amplifying mRNA vaccines by cationic lipid nanoparticles: The impact of cationic lipid selection. *J. Control Release* 325, 370–379. doi: 10.1016/j.jconrel.2020.06.027

Mahemuti, N., Jing, X., Zhang, N., Liu, C., Li, C., Cui, Z., et al. (2023). Association between systemic immunity-inflammation index and hyperlipidemia: A population-based study from the NHANES (2015-2020). *Nutrients* 15(5):1177. doi: 10.3390/nu15051177

Muhoza, P., Danovaro-Holliday, M. C., Diallo, M. S., Murphy, P., Sodha, S. V., Requejo, J. H., et al. (2021). Routine vaccination coverage - worldwide, 2020. *MMWR Morb. Mortal Wkly. Rep.* 70 (43), 1495–1500. doi: 10.15585/mmwr.mm7043a1

Oliveri, A., Rebernick, R. J., Kuppa, A., Pant, A., Chen, Y., Du, X., et al. (2024). Comprehensive genetic study of the insulin resistance marker TG : HDL-C in the UK Biobank. *Nat. Genet.* 56 (2), 212–221. doi: 10.1038/s41588-023-01625-2

Park, K. S., Bazzill, J. D., Son, S., Nam, J., Shin, S. W., Ochyl, L. J., et al. (2021). Lipid-based vaccine nanoparticles for induction of humoral immune responses against HIV-1 and SARS-CoV-2. *J. Control Release* 330, 529–539. doi: 10.1016/j.jconrel.2020.12.031

Penina Haber, M., and Schillie, S. (2023). *Hepatitis B*. Available online at: https://www.cdc.gov/vaccines/pubs/pinkbook/hepb.html (Accessed 7 July, 2023).

Pirillo, A., Casula, M., Olmastroni, E., Norata, G. D., and Catapano, A. L. (2021). Global epidemiology of dyslipidaemias. *Nat. Rev. Cardiol.* 18, 689–700. doi: 10.1038/s41569-021-00541-4

Ren, Q., Zhang, P., Lin, H., Feng, Y., Chi, H., Zhang, X., et al. (2023). A novel signature predicts prognosis and immunotherapy in lung adenocarcinoma based on cancer-associated fibroblasts. *Front. Immunol.* 14, 1201573. doi: 10.3389/fimmu.2023.1201573

Ryan, A., Heath, S., and Cook, P. (2018). Managing dyslipidaemia for the primary prevention of cardiovascular disease. *BMJ* 360, k946. doi: 10.1136/bmj.k946

Schümann, J., and De Libero, G. (2006). Serum lipoproteins: Trojan horses of the immune response? *Trends Immunol.* 27 (2), 57–59. doi: 10.1016/j.it.2005.12.005

Sulaiman, R. A. (2020). Inherited metabolic disorders and dyslipidaemia. *J. Clin. Pathol.* 73, 384–390. doi: 10.1136/jclinpath-2019-205910

Tan, J. K., Macia, L., and Mackay, C. R. (2023). Dietary fiber and SCFAs in the regulation of mucosal immunity. *J. Allergy Clin. Immunol.* 151, 361–370. doi: 10.1016/j.jaci.2022.11.007

Van Damme, P., Leroux-Roels, G., Suryakiran, P., Folschweiller, N., and van der Meeren, O. (2017). Persistence of antibodies 20 y after vaccination with a combined hepatitis A and B vaccine. *Hum. Vaccin. Immunother.* 13, 972–980. doi: 10.1080/21645515.2016.1274473

Webb, N. R. (2021). High-density lipoproteins and serum amyloid A (SAA). *Curr. Atheroscler. Rep.* 23, 7. doi: 10.1007/s11883-020-00901-4

Wong, G. L.-H., Hui, V. W.-K., Yip, T. C.-F., Liang, L. Y., Zhang, X., Tse, Y. K., et al. (2022). Universal HBV vaccination dramatically reduces the prevalence of HBV infection and incidence of hepatocellular carcinoma. *Aliment Pharmacol. Ther.* 56 (5), 869–877. doi: 10.1111/apt.17120

Xiao, S., Wang, X., Zhang, G., Tong, M., Chen, J., Zhou, Y., et al. (2023). Association of systemic immune inflammation index with estimated pulse wave velocity, atherogenic index of plasma, triglyceride-glucose index, and cardiovascular disease: A large cross-sectional study. *Mediators Inflamm.* 2023, 1966680. doi: 10.1155/2023/1966680

Yan, J., and Horng, T. (2020). Lipid metabolism in regulation of macrophage functions. *Trends Cell Biol.* 30, 979–989. doi: 10.1016/j.tcb.2020.09.006

Yu, W., Lei, Q., Yang, L., Qin, G., Liu, S., Wang, D., et al. (2021). Contradictory roles of lipid metabolism in immune response within the tumor microenvironment. *J. Hematol. Oncol.* 14 (1), 187. doi: 10.1186/s13045-021-01200-4

Zhang, S., Jiang, C., Jiang, L., Chen, H., Huang, J., Gao, X., et al. (2023). Construction of a diagnostic model for hepatitis B-related hepatocellular carcinoma using machine learning and artificial neural networks and revealing the correlation by immunoassay. *Tumour Virus Res.* 16, 200271. doi: 10.1016/j.tvr.2023.200271

Zhang, P., Pei, S., Wu, L., Xia, Z., Wang, Q., Huang, X., et al. (2023). Integrating multiple machine learning methods to construct glutamine metabolism-related signatures in lung adenocarcinoma. *Front. Endocrinol. (Lausanne)* 14:1196372. doi: 10.3389/fendo.2023.1196372

Zhang, J., Peng, G., Chi, H., Yang, J., Xie, X., Song, G., et al. (2023). CD8 + T-cell marker genes reveal different immune subtypes of oral lichen planus by integrating single-cell RNA-seq and bulk RNA-sequencing. *BMC Oral. Health* 23 (1), 464. doi: 10.1186/s12903-023-03138-0

Zhang, D., Zhao, F., Li, J., Qin, X., Li, S., and Niu, R. (2023). A novel and robust pyroptosis-related prognostic signature predicts prognosis and response to immunotherapy in esophageal squamous cell carcinoma. *Aging (Albany NY)* 15, 7811–7830. doi: 10.18632/aging.204946

Zhang, D., Zhao, F., Liu, H., Guo, P., Li, Z., and Li, S. (2024). FABP6 serves as a new therapeutic target in esophageal tumor. *Aging (Albany NY)* 16, 1640–1662. doi: 10.18632/aging.205448

Zhao, H., Yu, Y., Wang, Y., Zhao, L., Yang, A., Hu, Y., et al. (2022). Cholesterol accumulation on dendritic cells reverses chronic hepatitis B virus infection-induced dysfunction. *Cell Mol. Immunol.* 19 (12), 1347–1360. doi: 10.1038/s41423-022-00939-1

frontiers | Frontiers in Cellular and Infection Microbiology

TYPE Mini Review
PUBLISHED 03 April 2024
DOI 10.3389/fcimb.2024.1380136

OPEN ACCESS

EDITED BY
Wenle Li,
Xiamen University, China

REVIEWED BY
Jindong Xie,
Sun Yat-sen University Cancer Center (SYSUCC), China
Dongsheng Di,
Huazhong University of Science and Technology, China

*CORRESPONDENCE
Shenqi Zhang
19154571592@163.com

RECEIVED 01 February 2024
ACCEPTED 19 March 2024
PUBLISHED 03 April 2024

CITATION
Shao Z, Gao H, Wang B and Zhang S (2024) Exploring the impact of pathogenic microbiome in orthopedic diseases: machine learning and deep learning approaches. *Front. Cell. Infect. Microbiol.* 14:1380136. doi: 10.3389/fcimb.2024.1380136

Exploring the impact of pathogenic microbiome in orthopedic diseases: machine learning and deep learning approaches

Zhuce Shao, Huanshen Gao, Benlong Wang and Shenqi Zhang*

Department of Joint and Sports Medicine, Zaozhuang Municipal Hospital, Affiliated to Jining Medical University, Zaozhuang, China

Osteoporosis, arthritis, and fractures are examples of orthopedic illnesses that not only significantly impair patients' quality of life but also complicate and raise the expense of therapy. It has been discovered in recent years that the pathophysiology of orthopedic disorders is significantly influenced by the microbiota. By employing machine learning and deep learning techniques to conduct a thorough analysis of the disease-causing microbiome, we can enhance our comprehension of the pathophysiology of many illnesses and expedite the creation of novel treatment approaches. Today's science is undergoing a revolution because to the introduction of machine learning and deep learning technologies, and the field of biomedical research is no exception. The genesis, course, and management of orthopedic disorders are significantly influenced by pathogenic microbes. Orthopedic infection diagnosis and treatment are made more difficult by the lengthy and imprecise nature of traditional microbial detection and characterization techniques. These cutting-edge analytical techniques are offering previously unheard-of insights into the intricate relationships between orthopedic health and pathogenic microbes, opening up previously unimaginable possibilities for illness diagnosis, treatment, and prevention. The goal of biomedical research has always been to improve diagnostic and treatment methods while also gaining a deeper knowledge of the processes behind the onset and development of disease. Although traditional biomedical research methodologies have demonstrated certain limits throughout time, they nevertheless rely heavily on experimental data and expertise. This is the area in which deep learning and machine learning approaches excel. The advancements in machine learning (ML) and deep learning (DL) methodologies have enabled us to examine vast quantities of data and unveil intricate connections between microorganisms and orthopedic disorders. The importance of ML and DL in detecting, categorizing, and forecasting harmful microorganisms in orthopedic infectious illnesses is reviewed in this work.

KEYWORDS

pathogenic microbiome, orthopedic, machine learning, deep learning, applications, individuation, osteoporosis, arthritis

Introduction

Orthopedic problems, such as osteoporosis, arthritis, and fractures, are becoming a more significant public health concern as the world's population ages, these illnesses not only significantly lower patients' quality of life on a daily basis, but they also significantly increase the financial strain on the healthcare system (Safiri et al., 2020; Steinmetz et al., 2023). The involvement of pathogenic microorganisms in the onset and progression of orthopedic illnesses has come to the attention of scientists in recent years. Research has indicated that some bacteria and viruses have the ability to directly impact bone health and accelerate the course of illness. However, classic biological techniques struggle to disclose the complex and diverse processes underlying pathogen-host interactions.

Researchers are focusing more and more on the role that pathogenic microorganisms play in orthopedic diseases because they can even directly infect orthopedic patients, such those who have fractures. Improvements in microbial detection technology have also led to an increase in the number of organisms at the site of Periprosthetic Joint Infections (PJIs) (Anagnostakos and Fink, 2021).

Machine learning and deep learning are novel methods that have gradually emerging in recent years. Many researchers have described the concepts, applications or application fields of machine learning and deep learning (Goodfellow et al., 2016; Shinde and Shah, 2018; Campesato, 2020; Janiesch et al., 2021).

In this regard, new research instruments have been made available by the emergence of machine learning and deep learning methodologies. By analyzing vast quantities of intricate biological data, spotting possible biomarkers, and forecasting illness patterns, these technologies can shed light on the connection between infections and orthopedic disorders. For instance, machine learning algorithms can predict the relationship between particular bacteria and osteoporosis by examining the genetic information and microbiological makeup of a patient. Convolutional neural networks and other deep learning techniques have been used to automatically identify lesions in imaging pictures to aid in the diagnosis of orthopedic diseases, including fractures.

Even while deep learning and machine learning have made some initial strides in this area, they still face several obstacles. There are still issues to be resolved about the interpretability of models, the quantity and quality of data restrictions, and the efficient integration of these technologies into clinical practice. Furthermore, the effective use of these technologies depends on multidisciplinary cooperation that brings together the knowledge of biologists, computer scientists, and medical professionals.

The objective of this study is to incorporate the most recent findings about the involvement of pathogenic microorganisms in orthopedic disorders, with a specific focus on the use of machine learning and deep learning techniques to enhance disease prevention, diagnosis, and therapy. We intend to give patients hope by evaluating the most recent study findings and offering recommendations for future research initiatives.

Techniques based on data, such as machine learning and deep learning, can manage vast amounts of biomedical data, including genetic, protein, and clinical data. The advent of these sophisticated methods has given scholars access to useful resources (Jordan and Mitchell, 2015; LeCun et al., 2015). To improve our comprehension of biological processes and our ability to employ data mining techniques for clinical prediction, image analysis, drug development, and other purposes, patterns and relationships in the data can be found (Rajkomar et al., 2019). Furthermore, machine learning algorithms may uncover genetic variations linked to certain diseases by examining genomic data, which aids researchers in identifying possible treatment targets.

Standing on the shoulders of the "giants" of machine learning and deep learning for future deeper analysis of the impact of microbes on osteoporosis

Osteoporosis is a diagnosable and treatable disease, a systemic bone disease due to a decrease in bone density and bone mass and destruction of the bone microstructure due to a variety of causes, resulting in increased bone brittleness and thus susceptibility to fracture, and the concept of osteoporosis has been addressed in many studies (Schapira and Schapira, 1992; Raisz, 2005; Marcus and Bouxsein, 2008; Akkawi and Zmerly, 2018).

An international public health concern, osteoporosis is becoming more common as the world's population ages. Patients' quality of life is significantly impacted by the condition, which makes bones brittle and increases the chance of fractures. In spite of the fact that a variety of variables, including heredity, poor diet, and inactivity, are linked to the development of osteoporosis (Riggs and Melton Iii, 1995; Clynes et al., 2020; Salari et al., 2021), new studies have indicated that pathogenic microbes may also be a significant contributing factor (Hao et al., 2019; De Martinis et al., 2020; Cronin et al., 2022).

Pathogenic microorganisms, especially bacteria and viruses, may accelerate the process of bone loss and structural damage. Due to the complexity of pathogen host interactions and the limitations of traditional biological research methods in managing large-scale biomedical data, the exact relationship and mechanism of action between infection and osteoporosis are still unclear. This is the benefits and significance of machine learning and deep learning. With the advancement of these technologies, new tools have emerged to solve these problems, extracting patterns and features from a large amount of complex data, providing new insights into the relationship between osteoporosis and pathogenic microorganisms. For example, by using machine learning algorithms to analyze a large amount of data on the host genome, microbiome, and proteome, future research may focus on identifying microbial biomarkers associated with high risk of osteoporosis. The composition and function of the gut microbiome have a significant impact on bone metabolism, providing new ideas for the prevention and treatment of osteoporosis. Machine learning and deep learning provide more future possibilities for research in this field.

Pathogenic microorganisms have a high correlation with several established modifiable variables, which in turn function as mediators to further impact bone accrual, maintenance, and decline in the geriatric population. Preliminary research on the connection between microbes and bone health has shown that microbes can affect how interactions between bone metabolism occur, and that the gut microbiome plays a role in the regulation of bone metabolism, osteoporosis pathogenesis, prevention, and treatment (Hernandez, 2017; Ding et al., 2020; Seely et al., 2021; Guan et al., 2022).

With the rapid development of machine learning and deep learning in recent years, new perspectives have been provided to study the relationship between pathogenic microorganisms and osteoporosis. Several studies have been conducted in related fields, for example, many studies have utilized machine learning or deep learning on osteoporosis fracture rates or bioinformatics involving osteoporosis (Engels et al., 2020; Ulivieri et al., 2021; Liu et al., 2022). Most of these studies do not incorporate microbial information, which has been a limitation of previous researchers, and as more and more studies demonstrate the significant effects of certain microbes on osteoporosis, there is a need to incorporate microbial data into subsequent studies in order to obtain more rigorous and scientific results.

In order to detect osteoporosis signals in imaging data, deep learning techniques like Convolutional Neural Networks (CNNs) have made great strides in the field of medical image processing. This information may then be utilized to forecast the course of the illness and evaluate the effectiveness of treatment. Furthermore, deep learning may be utilized to combine data from other biological data sources, such microbiome data and clinical characteristics, to increase the precision of osteoporosis progression prediction.

Figure 1 shows how pathogenic microorganisms, especially intestinal flora, can indirectly affect bone metabolism and bone mineral density through inflammatory responses or by affecting calcium and phosphorus absorption, or through the gut-bone axis, which has been found to affect the immune system, the metabolites produced (e.g., short-chain fatty acids), and by affecting the absorption of nutrients. In the future, in the study of microbial influence on osteoporosis, the addition of already mature clinical data information and bioinformatic data, and then through the powerful medium of machine learning and deep learning, will certainly bring new life and opportunities for research in related fields.

Visualization of keywords in the field of pathogenic microorganisms using machine learning or deep learning, and a brief overview of related orthopedic diseases affected by microorganisms

In order to have a better analysis of the use of machine learning and deep learning methods to study the impact of pathogenic microorganisms in orthopedic diseases, we have attempted to provide an intuitive visualization of how researchers have used machine learning and deep learning methods to study pathogenic microorganisms in recent years, and we have utilized visualization tools to demonstrate this with the aim of getting a better grasp of the direction of development of studies exploring the impact of pathogenic microbiomes in orthopedic diseases using the premise of machine learning and deep learning methods, or an outlook on the frontiers of the future.

Table 1 shows the top 10 keywords in terms of frequency of occurrence of machine learning and deep learning methods for

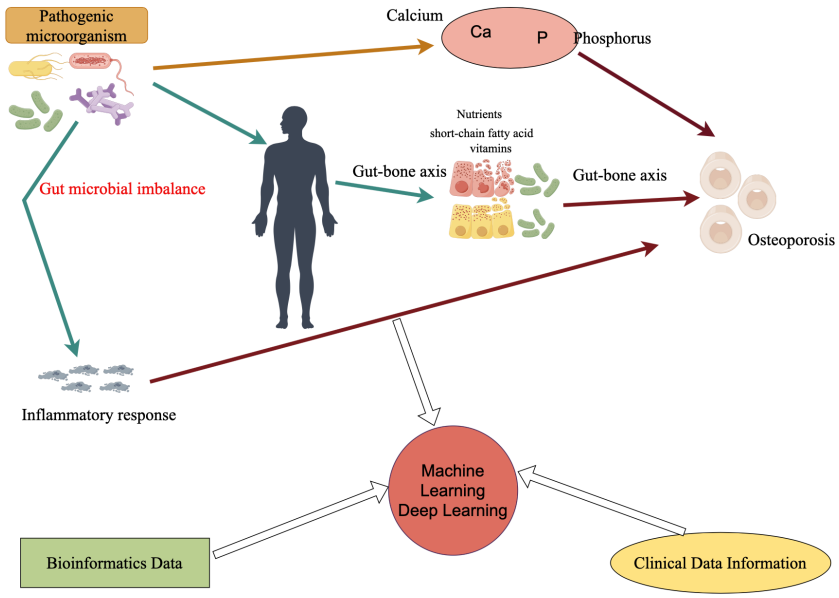

FIGURE 1
Microbes affect osteoporosis and how deep learning or machine learning can be utilized in the future. Ca refers to calcium, P refers to phosphorus, and microorganisms directly or indirectly (such as inflammatory reactions) affect the occurrence of osteoporosis.

10.3389/fcimb.2024.1380136

TABLE 1 Top 10 keywords with the highest frequency of occurrence in studies analyzing pathogenic microorganisms using machine learning and deep learning methods.

ID	Keyword	Occurrences	Total link strength
1	Machine learning	104	101
2	Identification	28	53
3	Deep learning	26	33
4	Microbiology	24	42
5	Artificial intelligence	23	51
6	Classification	23	37
7	Prediction	23	53
8	Bacteria	17	22
9	Antimicrobial resistance	15	24
10	Clinical microbiology	13	18

research on pathogenic microorganisms, and it can be clearly found that "Artificial intelligence", "Prediction", "Antimicrobial resistance" are the key focus of research in this field, and also the possible future research of orthopedic microorganisms with the support of machine learning or deep learning methods.

We selected the WoS database on January 10, 2024 for an intuitive visual analysis of keywords for research in this area. Figure 2A is a collaborative linkage diagram of keywords that appear more frequently in the research of pathogenic microorganisms analyzed using machine learning and deep learning methods from 2000 to 2024, which can well show the relationship between keywords in this research field, the larger the circle indicates that this keyword plays a greater role in the research of this field, the higher the frequency of appearance, and the more the linkage between keywords indicates that the more the keyword is used in the research of this field, the more the linkage between keywords indicates that the keyword is used in the research of this field. the closer the connection between them. Figure 2B shows which orthopedic related diseases can be affected by microorganisms.

Visualization analysis of keywords related to research in the field of machine learning or deep learning and pathogenic microorganisms can help us identify the current focus of attention among researchers in this field and explore potential future research hotspots in this field. For example, we can see that this field seems to be closely related to " therapy", "expression", "diagnosis", etc., which may also indicate the direction of future development.

Pathogenic microorganisms associated with orthopedic diseases

The most prevalent pathogens in orthopedic disorders are bacteria. The most frequent cause of infections, both hospital- and community-acquired, is Staphylococcus aureus. Furthermore, gram-negative bacteria like Escherichia coli and streptococci are frequently the cause of an event. Staphylococcus aureus-caused osteomyelitis is a dangerous bone infection that can result in bone death. Surgery and/or long-term antibiotic therapy are typically needed to treat this illness.

Although they are less prevalent in orthopedic diseases, fungal infections can nevertheless pose a major risk to individuals with weakened immune systems. Aspergillus and Candida are common fungi that cause problems. Patients with weakened immune systems, such those receiving organ transplants or HIV, are more likely to get fungal infections. Antifungal drugs are typically needed to treat these infections.

Even though measles and rubella viruses are not common, they can still impact bone health. This is the case with viral bone disease. The goal of treating viral bone disease is to improve the immune system's capacity to combat the virus while also managing its symptoms.

Machine learning and deep learning techniques have become valuable tools in orthopedic disease research and therapy, particularly in the understanding and management of infections caused by pathogenic microorganisms. Large volumes of biological data may be processed and analyzed using these sophisticated computational techniques to provide information on pathogen

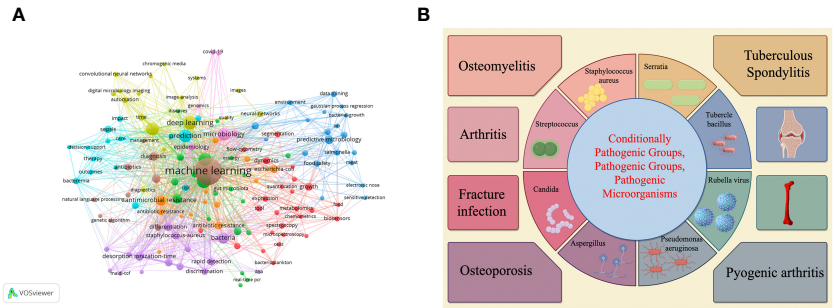

FIGURE 2
(A, B) Respectively demonstrate the use of machine learning or deep learning to visualize keywords in the field of pathogenic microorganisms and provide a brief overview of the types of orthopedic diseases affected by microorganisms.

features, infection patterns, illness development, and patient response to therapy.

Identification and categorization of pathogens

Researchers can precisely detect and categorize microorganisms that cause orthopedic illnesses from clinical samples by utilizing deep learning algorithms (Bernard et al., 2022; Hu et al., 2023). This includes common bacteria like Staphylococcus aureus and other Gram-negative bacteria like Streptococcus and Escherichia coli. Physicians are able to promptly adopt focused treatment measures, such choosing the appropriate medications to fight certain bacterial illnesses, by precisely and swiftly detecting these organisms. Some studies have used machine learning or deep learning to analyze infections that cause orthopedic diseases, and some of these infections also include factors associated with pathogenic microorganisms (Martínez-Pastor et al., 2009; Goswami et al., 2022).

Forecasting patterns of infection

Additionally, particular pathogen infection patterns, including hospital and community transmission, may be predicted using machine learning algorithms. By examining past infection data and patient characteristics, these models forecast infection outbreaks, assisting hospital management and public health officials in taking proactive steps to stop the spread of diseases (Genevès et al., 2018; Sharma et al., 2018; Teeple et al., 2020).

Analysis of drug susceptibility

The most effective medications for Staphylococcus aureus-caused severe osteomyelitis can be identified with the use of machine learning techniques. Individualized treatment plans can be created to increase treatment effectiveness while lowering the emergence of antibiotic resistance by evaluating the pathogen's susceptibility to various antibiotics.

Figure 2B shows the impact of different microorganisms on different orthopedic diseases and the utilization of deep learning or machine learning.

Pathogenic microorganisms and arthritis

Arthritis is a group of diseases that affect millions of people worldwide and are characterized by joint inflammation, pain and dysfunction. Although the exact causes of arthritis are varied and include genetics, immune system dysregulation and environmental factors, there is growing evidence that pathogenic microorganisms, such bacteria and viruses, also play an important role in the development and progression of arthritis (Li et al., 2013; Bo et al., 2020; Berthelot et al., 2021). Arthritis is a common inflammatory joint disease involving one or more joints. Its main symptoms include joint pain, swelling, stiffness and limited movement. Depending on the cause and presentation, arthritis can be categorized into a number of types, the two most common of which are osteoarthritis (OA) and rheumatoid arthritis (RA), which puts a huge financial strain on the world's arthritis sufferers (March and Bachmeier, 1997; Leifer et al., 2022). While the causes of arthritis are diverse, there is growing evidence that pathogenic microorganisms play a key role in many types of arthritis. It is difficult to determine the precise microbe that causes arthritis, though, as it requires removing and evaluating a lot of data from intricate biological samples. Recent years have seen a considerable advancement in the field of biomedical research, particularly in the areas of pathogen identification, genomes analysis, and illness prediction, thanks to the fast adoption of machine learning and deep learning techniques. These technological advancements provide novel approaches to the diagnosis and treatment of arthritis by processing and analyzing vast amounts of biological data, recognizing disease patterns, and forecasting the relationship between infections and illnesses. In the future, patients can receive individualized diagnoses and treatment plans by merging machine learning models with patient-specific data. These cutting-edge techniques, such deep learning and machine learning, will pave the way for customized therapy. This approach may also be used to promote collaboration between biologists, computer scientists, and doctors in order to create more efficient methods of arthritis diagnosis and treatment.

In the future, to promote research on the relationship between pathogenic microorganisms and arthritis, researchers will need to generate larger and more complete public datasets in order to better use machine learning and deep learning methodologies.

Robust methods for comprehending the intricate connection between pathogenic microorganisms and arthritis are offered by machine learning and deep learning methodologies. The advancement of these technologies offers fresh hope for the identification and management of arthritis, notwithstanding the difficulties. In the future, we anticipate seeing more creative ideas that will result in improved therapies for arthritis patients as multidisciplinary collaboration grows and technology progresses.

Recognizing and categorizing infections

Researchers can reliably identify the bacteria that cause infectious arthritis from joint fluids and other clinical samples by using deep learning algorithms (Lo and Lai, 2023). These algorithms can differentiate between various bacteria and viruses by examining their gene sequences and patterns of protein expression, which serves as a foundation for creating specialized treatment plans (Choi et al., 2021). In clinical practice and medical research, precise pathogen identification and categorization is essential for infectious arthritis. Numerous bacteria and viruses can cause infectious arthritis, a dangerous condition for which a

prompt and precise diagnosis is essential to the development of a successful treatment strategy. From joint fluids and other clinical samples, researchers can now reliably identify the bacteria and viruses that cause infectious arthritis thanks to the growing use of deep learning algorithms in bioinformatics and clinical diagnostics.

The novel applications of deep learning, a cutting-edge machine learning approach, include pathogen identification and classification, protein expression pattern recognition, and gene sequence analysis. Researchers can collect and analyze complicated biological data to pinpoint the precise species of germs that cause diseases by training deep neural networks. These algorithms are an effective diagnostic tool for infectious arthritis because they are particularly good at identifying patterns and characteristics from large volumes of data.

In the future, deep learning will be used in pathogen identification research in novel ways, with a focus on integrating additional kinds of biological data, optimizing algorithm performance, and increasing model interpretability. Additionally, as personalized medicine gains traction, deep learning methods will be used to customize treatment regimens based on the unique genetic make-up and clinical presentation of each patient (Zhang et al., 2018; Agarwal et al., 2020; Wason et al., 2020). Furthermore, improved management and treatment results for infectious arthritis will come from a closer integration of machine learning models with clinical decision support systems.

Forecasting the course of an illness

A patient's genetic makeup, way of life, and past infection history may all be analyzed by machine learning algorithms to determine their likelihood of having a particular kind of arthritis. These models reveal patterns and trends linked to the course of disease, which aids doctors in early diagnosis and intervention (Norgeot et al., 2019; Kedra et al., 2021).

Discussion

The biomedical area has witnessed a tremendous advancement in machine learning and deep learning technologies, which has made them very promising for investigating the intricate connections between pathogenic microorganisms and orthopedic illnesses. Several studies have also shown how machine learning and deep learning can be used to predict the course of diseases, find links between particular pathogenic microorganisms and the emergence of orthopedic disorders, and develop novel approaches to illness prevention, diagnosis, and treatment.

It is our belief that the relationship between pathogenic microbes and orthopedic illnesses may be successfully shown by integrating cutting-edge techniques like machine learning and deep learning to assess microbiome data and clinical factors. Future risk and development of orthopedic disorders, including osteoarthritis, fracture infections, and spinal ailments, can be effectively predicted with the use of these technologies. Additionally, researchers have started to progressively uncover how these harmful bacteria impact the onset and progression of illnesses by examining the makeup of microorganisms and the interactions among hosts (Jansma and El Aidy, 2021; Zhou et al., 2022).

Future research should concentrate on the following areas to overcome these issues and progress the field: first, creating bigger, better-quality datasets that are more complete; second, enhancing data standards and sharing to make model training and validation easier. Second, the creation of fresh models and algorithms to enhance model interpretability and prediction accuracy, particularly when simulating intricate relationships between pathogenic microbes and their hosts. Furthermore, multidisciplinary cooperation—which calls for tight coordination between biologists, doctors, data scientists, and computer scientists—is essential to comprehending these intricate systems.

In addition to advancing our knowledge of pathogenic microbes and orthopedic disorders, the use of machine learning and deep learning technologies in these fields has the potential to completely transform clinical diagnoses and therapeutic approaches. For instance, doctors may monitor treatment outcomes, apply individualized therapies, and detect high-risk patients sooner thanks to the knowledge these technologies give. These technologies can also aid in the development of novel therapeutic approaches, such the targeting of certain pathogenic microorganisms or the modification of host-microbe interactions in the prevention or treatment of orthopedic illnesses.

In conclusion, there is a lot of promise and difficulty in the rapidly developing field of applying machine learning and deep learning to the study of pathogenic microorganisms and orthopedic illnesses. Through the removal of current obstacles and ongoing advancements in this field of study, we seek to provide new opportunities for the diagnosis, treatment, and prevention of orthopedic disorders as well as offer patients better access to healthcare.

In the study of pathogenic microorganisms in orthopedic diseases, machine learning and deep learning technologies offer new research directions and trends. These are primarily reflected in the areas of microbial community analysis, personalized healthcare, pathogen resistance prediction, fast and accurate pathogen identification and classification, and monitoring and outbreak prediction. Individual susceptibility to specific pathogenic microbial infections can be predicted by combining machine learning and deep learning techniques to analyze genetic data, lifestyle, and environmental factors of patients. This data can then be used to support personalized prevention and treatment plans. In the study of pathogenic microorganisms in orthopedic illnesses, machine learning and deep learning technologies have demonstrated considerable promise. They aid in quick diagnosis, accurate treatment, and efficient prevention, all of which enhance patient outcomes and quality of life. These technologies will have more comprehensive and long-lasting uses in this industry as long as they continue to grow and improve.

Conclusions

Specifically, deep learning and machine learning techniques are employed to comprehend and forecast the complex relationships

between these microorganisms and orthopedic disorders. The role of pathogenic microorganisms in orthopedic illnesses is examined in this research. Through a review of the present literature, we can see that although deep learning and machine learning offer strong instruments for locating, categorizing, and forecasting the role of pathogenic microorganisms in orthopedic disorders, there are some challenges to be addressed. High-quality, standardized, and annotated biological data are currently hard to come by, which limits their application in model training and validation. Although machine learning and deep learning models are quite good at identifying patterns and predicting outcomes, interpretability is still a big problem. This is particularly true in the medical domain, where it is necessary for researchers and doctors to be able to comprehend the results made by models with ease. It can occasionally be challenging for a single machine learning or deep learning model to collect all the pertinent biological signals due to the complexities of pathogen-host interactions. Further study must look at more complex models and algorithms to accurately depict these complex biological processes.

Author contributions

ZS: Conceptualization, Data curation, Formal analysis, Funding acquisition, Investigation, Methodology, Project administration, Resources, Software, Supervision, Validation, Visualization, Writing – original draft, Writing – review & editing. HG: Conceptualization, Data curation, Investigation, Software, Supervision, Writing – original draft. BW: Conceptualization, Investigation, Software, Visualization, Writing – original draft. SZ: Conceptualization, Data curation, Formal analysis, Investigation, Methodology, Project administration, Software, Supervision, Validation, Writing – original draft.

Funding

The author(s) declare that no financial support was received for the research, authorship, and/or publication of this article.

Conflict of interest

The authors declare that the research was conducted in the absence of any commercial or financial relationships that could be construed as a potential conflict of interest.

Publisher's note

References

Agarwal, P., Hassan, S. I., Mustafa, S. K., and Ahmad, J. (2020). "An effective diagnostic model for personalized healthcare using deep learning techniques," in *Applications of Deep Learning and Big Iot on Personalized Healthcare Services* (IGI Global), 70–88.

Akkawi, I., and Zmerly, H. (2018). Osteoporosis: current concepts. *Joints* 6, 122–127. doi: 10.1055/s-0038-1660790

Anagnostakos, K., and Fink, B. (2021). Antibiotics in orthopedic infections. *Antibiotics (Basel)* 10. doi: 10.3390/antibiotics10111297

Bernard, E., Peyret, T., Plinet, M., Contie, Y., Cazaudarré, T., Rouquet, Y., et al. (2022). The dendrischip® Technology as a new, rapid and reliable molecular method for the diagnosis of Osteoarticular infections. *Diagnostics* 12, 1353. doi: 10.3390/diagnostics12061353

Berthelot, J.-M., Bandiaky, O. N., Le Goff, B., Amador, G., Chaux, A.-G., Soueidan, A., et al. (2021). Another look at the contribution of oral microbiota to the pathogenesis of rheumatoid arthritis: A narrative review. *Microorganisms* 10, 59. doi: 10.3390/microorganisms10010059

Bo, M., Jasemi, S., Uras, G., Erre, G. L., Passiu, G., and Sechi, L. A. (2020). Role of infections in the pathogenesis of rheumatoid arthritis: focus on mycobacteria. *Microorganisms* 8, 1459. doi: 10.3390/microorganisms8101459

Campesato, O. (2020). *Artificial Intelligence, Machine Learning, and Deep Learning* (Mercury Learning and Information). doi: 10.1515/9781683924654

Choi, E. S., Sim, J. A., Na, Y. G., Seon, J. K., and Shin, H. D. (2021). Machine-learning algorithm that can improve the diagnostic accuracy of septic arthritis of the knee. *Knee Surgery Sports Traumatology Arthroscopy* 29, 3142–3148. doi: 10.1007/s00167-020-06418-2

Clynes, M. A., Harvey, N. C., Curtis, E. M., Fuggle, N. R., Dennison, E. M., and Cooper, C. (2020). The epidemiology of osteoporosis. *Br. Med. Bull.* 133, 105–117. doi: 10.1093/bmb/ldaa005

Cronin, O., Lanham-New, S. A., Corfe, B. M., Gregson, C. L., Darling, A. L., Ahmadi, K. R., et al. (2022). Role of the microbiome in regulating bone metabolism and susceptibility to osteoporosis. *Calcif Tissue Int.* 110, 273–284. doi: 10.1007/s00223-021-00924-2

De Martinis, M., Ginaldi, L., Allegra, A., Sirufo, M. M., Pioggia, G., Tonacci, A., et al. (2020). The osteoporosis/microbiota linkage: the role of Mirna. *Int. J. Mol. Sci.* 21, 8887. doi: 10.3390/ijms21238887

Ding, K., Hua, F., and Ding, W. (2020). Gut microbiome and osteoporosis. *Aging Dis.* 11, 438. doi: 10.14336/AD.2019.0523

Engels, A., Reber, K. C., Lindlbauer, I., Rapp, K., Büchele, G., Klenk, J., et al. (2020). Osteoporotic hip fracture prediction from risk factors available in administrative claims data–a machine learning approach. *PLoS One* 15, e0232969. doi: 10.1371/journal.pone.0232969

Genevès, P., Calmant, T., Layaïda, N., Lepelley, M., Artemova, S., and Bosson, J.-L. (2018). Scalable machine learning for predicting at-risk profiles upon hospital admission. *Big Data Res.* 12, 23–34. doi: 10.1016/j.bdr.2018.02.004

Goodfellow, I., Bengio, Y., and Courville, A. (2016). *Deep Learning* (MIT press).

Goswami, K., Clarkson, S., Phillips, C. D., Dennis, D. A., Klatt, B. A., O'Malley, M. J., et al. (2022). An enhanced understanding of culture-negative periprosthetic joint infection with next-generation sequencing: A multicenter study. *JBJS* 104, 1523–1529. doi: 10.2106/JBJS.21.01061

Guan, Z., Luo, L., Liu, S., Guan, Z., Zhang, Q., Li, X., et al. (2022). The role of depletion of gut microbiota in osteoporosis and osteoarthritis: A narrative review. *Front. Endocrinol.* 13, 847401. doi: 10.3389/fendo.2022.847401

Hao, M.-l., Wang, G.-y., Zuo, X.-q., Qu, C.-j., Yao, B.-c., and Wang, D.-l. (2019). Gut microbiota: an overlooked factor that plays a significant role in osteoporosis. *J. Int. Med. Res.* 47, 4095–4103. doi: 10.1177/0300060519860027

Hernandez, C. J. (2017). The microbiome and bone and joint disease. *Curr. Rheumatol. Rep.* 19, 1–6. doi: 10.1007/s11926-017-0705-1

Hu, X., Chen, J., Zheng, X., Li, J., and Zhou, M. (2023). Establishment and application of Tsdpso-Svm model combined with multi-dimensional feature fusion method in the identification of fracture-related infection. *Sci. Rep.* 13, 19632. doi: 10.1038/s41598-023-46526-w

Janiesch, C., Zschech, P., and Heinrich, K. (2021). Machine learning and deep learning. *Electronic Markets* 31, 685–695. doi: 10.1007/s12525-021-00475-2

Jansma, J., and El Aidy, S. (2021). Understanding the host-microbe interactions using metabolic modeling. *Microbiome* 9, 1–14. doi: 10.1186/s40168-020-00955-1

Jordan, M. I., and Mitchell, T. M. (2015). Machine learning: trends, perspectives, and prospects. *Science* 349, 255–260. doi: 10.1126/science.aaa8415

Kedra, J., Davergne, T., Braithwaite, B., Servy, H., and Gossec, L. (2021). Machine learning approaches to improve disease management of patients with rheumatoid arthritis: review and future directions. *Expert Rev. Clin. Immunol.* 17, 1311–1321. doi: 10.1080/1744666X.2022.2017773

LeCun, Y., Bengio, Y., and Hinton, G. (2015). Deep learning. *nature* 521, 436–444. doi: 10.1038/nature14539

Leifer, V., Katz, J., and Losina, E. (2022). The burden of oa-health services and economics. *Osteoarthritis cartilage* 30, 10–16. doi: 10.1016/j.joca.2021.05.007

Li, S., Yu, Y., Yue, Y., Zhang, Z., and Su, K. (2013). Microbial infection and rheumatoid arthritis. *J. Clin. Cell. Immunol.* 4 (6), 174. doi: 10.4172/2155-9899.1000174

Liu, J., Zhang, D., Cao, Y., Zhang, H., Li, J., Xu, J., et al. (2022). Screening of crosstalk and pyroptosis-related genes linking periodontitis and osteoporosis based on bioinformatics and machine learning. *Front. Immunol.* 13, 955441. doi: 10.3389/fimmu.2022.955441

Lo, C.-M., and Lai, K.-L. (2023). Deep learning-based assessment of knee septic arthritis using transformer features in sonographic modalities. *Comput. Methods Programs Biomedicine* 237, 107575. doi: 10.1016/j.cmpb.2023.107575

March, L. M., and Bachmeier, C. J. (1997). 10 economics of osteoarthritis: A global perspective. *Bailliere's Clin. Rheumatol.* 11, 817–834. doi: 10.1016/S0950-3579(97)80011-8

Marcus, R., and Bouxsein, M. (2008). The nature of osteoporosis. *Osteoporosis* 1, 27–36. doi: 10.1016/B978-012370544-0.50004-5

Martínez-Pastor, J. C., Munoz-Mahamud, E., Vilchez, F., García-Ramiro, S., Bori, G., Sierra, J., et al. (2009). Outcome of acute prosthetic joint infections due to gram-negative bacilli treated with open debridement and retention of the prosthesis. *Antimicrobial Agents chemotherapy* 53, 4772–4777. doi: 10.1128/AAC.00188-09

Norgeot, B., Glicksberg, B. S., Trupin, L., Lituiev, D., GianFrancesco, M., Oskotsky, B., et al. (2019). Assessment of a deep learning model based on electronic health record data to forecast clinical outcomes in patients with rheumatoid arthritis. *JAMA network Open* 2, e190606–e. doi: 10.1001/jamanetworkopen.2019.0606

Raisz, L. G. (2005). Pathogenesis of osteoporosis: concepts, conflicts, and prospects. *J. Clin. Invest.* 115, 3318–3325. doi: 10.1172/JCI27071

Rajkomar, A., Dean, J., and Kohane, I. (2019). Machine learning in medicine. *New Engl. J. Med.* 380, 1347–1358. doi: 10.1056/NEJMra1814259

Riggs, B. L., and Melton Iii, L. (1995). The worldwide problem of osteoporosis: insights afforded by epidemiology. *Bone* 17, S505–SS11. doi: 10.1016/8756-3282(95)00258-4

Safiri, S., Kolahi, A.-A., Smith, E., Hill, C., Bettampadi, D., Mansournia, M. A., et al. (2020). Global, regional and national burden of osteoarthritis 1990-2017: A systematic analysis of the global burden of disease study 2017. *Ann. rheumatic Dis.* 79, 819–828. doi: 10.1136/annrheumdis-2019-216515

Salari, N., Ghasemi, H., Mohammadi, L., Behzadi, M. H., Rabieenia, E., Shohaimi, S., et al. (2021). The global prevalence of osteoporosis in the world: A comprehensive systematic review and meta-analysis. *J. orthopaedic Surg. Res.* 16, 1–20. doi: 10.1186/s13018-021-02772-0

Schapira, D., and Schapira, C. (1992). Osteoporosis: the evolution of a scientific term. *Osteoporosis Int.* 2, 164–167. doi: 10.1007/BF01623921

Seely, K. D., Kotelko, C. A., Douglas, H., Bealer, B., and Brooks, A. E. (2021). The human gut microbiota: A key mediator of osteoporosis and osteogenesis. *Int. J. Mol. Sci.* 22, 9452. doi: 10.3390/ijms22179452

Sharma, S., Datta, P. K., and Bansal, G. (2018). "Machine learning based hospital-acquired infection control system," in *Machine Learning and Iot* (Britain, Taylor: CRC Press), 193–215.

Shinde, P. P., and Shah, S. (Eds.). (2018). "A review of machine learning and deep learning applications," in *2018 Fourth international conference on computing communication control and automation (ICCUBEA)* (United States: IEEE). doi: 10.1109/ICCUBEA.2018.8697857

Steinmetz, J. D., Culbreth, G. T., Haile, L. M., Rafferty, Q., Lo, J., Fukutaki, K. G., et al. (2023). Global, regional, and national burden of osteoarthritis, 1990–2020 and projections to 2050: A systematic analysis for the global burden of disease study 2021. *Lancet Rheumatol.* 5, e508–ee22. doi: 10.1016/S2665-9913(23)00163-7

Teeple, E., Hartvigsen, T., Sen, C., Claypool, K. T., and Rundensteiner, E. A. (Eds.). (2020). *Clinical Performance Evaluation of a Machine Learning System for Predicting Hospital-Acquired Clostridium Difficile Infection* (HEALTHINF). doi: 10.5220/0009157406560663

Ulivieri, F. M., Rinaudo, L., Piodi, L. P., Messina, C., Sconfienza, L. M., Sardanelli, F., et al. (2021). Bone strain index as a predictor of further vertebral fracture in osteoporotic women: an artificial intelligence-based analysis. *PloS One* 16, e0245967. doi: 10.1371/journal.pone.0245967

Wason, R., Goyal, D., Jain, V., Balamurugan, S., and Baliyan, A. (2020). *Applications of Deep Learning and Big Iot on Personalized Healthcare Services* (IGI Global).

Zhang, S., Bamakan, S. M. H., Qu, Q., and Li, S. (2018). Learning for personalized medicine: A comprehensive review from a deep learning perspective. *IEEE Rev. Biomed. Eng.* 12, 194–208. doi: 10.1109/RBME.2018.2864254

Zhou, H., Beltrán, J. F., and Brito, I. L. (2022). Host-microbiome protein-protein interactions capture disease-relevant pathways. *Genome Biol.* 23, 72. doi: 10.1186/s13059-022-02643-9

frontiers | Frontiers in Cellular and Infection Microbiology

TYPE Original Research
PUBLISHED 15 April 2024
DOI 10.3389/fcimb.2024.1373737

OPEN ACCESS

EDITED BY
Wenle Li,
Xiamen University, China

REVIEWED BY
Ruiping Hu,
Fudan University, China
Yu Yan,
Capital Medical University, China

*CORRESPONDENCE
Hongmei Wen
wenhongm@mail.sysu.edu.cn
Chao Li
lichao25@mail2.sysu.edu.cn

†These authors have contributed equally to this work and share first authorship

‡These authors have contributed equally to this work

RECEIVED 20 January 2024
ACCEPTED 25 March 2024
PUBLISHED 15 April 2024

CITATION
Zhao F, Chen J, Shan Y, Hong J, Ye Q, Dai Y, Hu J, Zhang J, Li C and Wen H (2024) Comprehensive assessment of HF-rTMS treatment mechanism for post-stroke dysphagia in rats by integration of fecal metabolomics and 16S rRNA sequencing. *Front. Cell. Infect. Microbiol.* 14:1373737. doi: 10.3389/fcimb.2024.1373737

Comprehensive assessment of HF-rTMS treatment mechanism for post-stroke dysphagia in rats by integration of fecal metabolomics and 16S rRNA sequencing

Fei Zhao[1†], Jiemei Chen[1†], Yilong Shan[1†], Jiena Hong[1], Qiuping Ye[1,2], Yong Dai[2], Jiahui Hu[2], Jiantao Zhang[1], Chao Li[1*‡] and Hongmei Wen[1*‡]

[1]The Third Affiliated Hospital of Sun Yat-sen University, Department of Rehabilitation Medicine, Guangzhou, Guangdong, China, [2]Guangzhou University of Chinese Medicine, Clinical Medical College of Acupuncture Moxibustion and Rehabilitation, Guangzhou, Guangdong, China

Background: The mechanism by which high-frequency repetitive transcranial magnetic stimulation (HF-rTMS) improves swallowing function by regulating intestinal flora remains unexplored. We aimed to evaluate this using fecal metabolomics and 16S rRNA sequencing.

Methods: A Post-stroke dysphagia (PSD) rat model was established by middle cerebral artery occlusion. The magnetic stimulation group received HF-rTMS from the 7th day post-operation up to 14th day post-surgery. Swallowing function was assessed using a videofluoroscopic swallowing study (VFSS). Hematoxylin-eosin (H&E) staining was used to assess histopathological changes in the intestinal tissue. Intestinal flora levels were evaluated by sequencing the 16S rRNA V3-V4 region. Metabolite changes within the intestinal flora were evaluated by fecal metabolomics using liquid chromatography-tandem mass spectrometry.

Results: VFSS showed that the bolus area and pharyngeal bolus speed were significantly decreased in PSD rats, while the bolus area increased and pharyngeal transit time decreased after HF-rTMS administration ($p < 0.05$). In the PSD groups, H&E staining revealed damaged surface epithelial cells and disrupted cryptal glands, whereas HF-rTMS reinforced the integrity of the intestinal epithelial cells. 16S rRNA sequencing indicated that PSD can disturb the intestinal flora and its associated metabolites, whereas HF-rTMS can significantly regulate the composition of the intestinal microflora. Firmicutes and Lactobacillus abundances were lower in the PSD group than in the baseline group at the phylum and genus levels, respectively; however, both increased after HF-rTMS administration. Levels of ceramides (Cer), free fatty acids (FA), phosphatidylethanolamine (PE), triacylglycerol (TAG), and sulfoquinovosyl diacylglycerol were increased in the PSD group. The Cer, FA, and DG levels decreased after HF-rTMS treatment, whereas the TAG levels increased. Peptococcaceae was negatively correlated with Cer, Streptococcus was

negatively correlated with DG, and Acutalibacter was positively correlated with FA and Cer. However, these changes were effectively restored by HF-rTMS, resulting in recovery from dysphagia.

Conclusion: These findings suggest a synergistic role for the gut microbiota and fecal metabolites in the development of PSD and the therapeutic mechanisms underlying HF-rTMS.

KEYWORDS

stroke, middle cerebral artery, rats, dysphagia, gut microbiota, metabolite profiles, HF-rTMS

Introduction

Post-stroke dysphagia (PSD) has emerged as a prevalent and consequential complication subsequent to an episode of stroke, with a prevalence of more than 50% (Bonilha et al., 2014; Zhang et al., 2021). Moreover, more than 10% of patients have persistent symptoms of dysphagia until six months after onset (Dawson et al., 2016). PSD is associated with a risk of aspiration pneumonia, malnutrition, dehydration, and death (Shigematsu and Fujishima, 2015). Therefore, there is an urgent need to develop effective therapeutic methods for reducing these risks. Routine therapies such as postural substitution and adjustment of food texture do not have satisfactory effectiveness (Reyes-Torres et al., 2019; Lin et al., 2021). However, recent studies have reported that noninvasive brain stimulation such as transcranial magnetic stimulation (TMS) is effective in improving swallow function (Chiang et al., 2019; Du et al., 2022; Hammad et al., 2022).

A meta-analysis unveiled a heightened effect size in dysphagia rehabilitation within the high-frequency rTMS (HF-rTMS) subgroup, surpassing that observed in the low-frequency rTMS (LF-rTMS) subgroup (Liao et al., 2017). In line with this, Khedr et al. (Khedr and Abo-Elfetoh, 2009) administered HF-rTMS (3 Hz) treatment to dysphagia patients, observing superior clinical outcomes in the treatment group compared to the sham group. Regarding to the stimulation site of HF-rTMS, Park et al. (Park et al., 2013) found that when 5Hz HF-rTMS applied to the contralateral cerebral hemisphere of patients with PSD, the swallowing function of the treatment group was significantly better than that of the sham stimulation group. Cheng et al. (Cheng et al., 2015) also proved that HF-rTMS applied over the tongue region of the motor cortex of the unaffected hemisphere improves the swallowing performance in stroke patients with chronic dysphagia. These studies focus on the mechanism of HF-rTMS at the central level. It is noteworthy that a previous study has suggested a potential impact of ischemic stroke on the gut microbiota, resulting in increased intestinal permeability and activation of the intestinal immune system. This, in turn, exacerbates ischemia-reperfusion injury through the brain-gut axis. Conversely, fecal microbiota transplantation is neuroprotective after stroke (Singh et al., 2016). Furthermore, gut microbiota metabolites can affect the physiological status of the host, both within the gut and after entering the bloodstream, by acting as a bridge between the microbiome and host. For example, short-chain fatty acids (SCFAs) may affect post-stroke outcomes via local and systemic inflammation and other pathways (Benakis et al., 2020). A recent study suggested that stimulation of the dorsolateral prefrontal cortex by HF-rTMS modifies brain-gut interactions in humans, for example, by modifying fine contractions of the gastrointestinal tract (Aizawa et al., 2021). Similarly, in rat model of depression, HF-rTMS (10 Hz) primarily contributes to the increased abundance of Firmicutes (Seewoo et al., 2022). These studies suggest that HF-rTMS can affect intestinal flora, but studies on its role in PSD have not been reported. In this study, we hypothesized that PSD could influence the composition of gut microbial communities and metabolites, which may be modified by HF-rTMS, resulting in improved swallowing function. To verify this, we investigated these mechanisms by integrating fecal metabolomics and 16S rRNA sequencing at the rat level.

Materials and methods

Animals

Thirty-six male Sprague-Dawley (SD) rats (aged 6-8 weeks) were purchased from the Guangdong Medical Laboratory Animal Center (Guangzhou, China). The rats were housed under a 12 h light-dark cycle (lights on 07:00) with controlled temperature (20-26°C), relative humidity (40-70%), and had free access to food and water. The rats were randomly assigned to experimental

groups. Rats were allowed to acclimate for five days before the experiments were started. All animal experiments were approved by the Animal Care Committee of the South China Agricultural University (Guangzhou, China. Approval number NO.2020d030) and were performed in accordance with the ARRIVE Guidelines.

PSD models and experimental grouping

The rat PSD model was established using transient middle cerebral artery occlusion (tMCAO). Thirty SD rats were randomly selected for left transient middle cerebral artery occlusion. After administering intraperitoneal anesthesia with 0.4% pentobarbital (40 mg/kg), the rats were fixed on a flat plate, the hair on the neck region was removed and disinfected with iodine. An incision (10 mm long) was made on the left side of the neck to expose the common carotid artery (CCA) and external carotid artery (ECA). The proximal ends of the left CCA and the ECA were ligated. A monofilament nylon line (50 mm in length; 0.26 mm in diameter) coated with 5-mm silica gel in the distal segment was used. Monofilament lines were inserted into the internal carotid artery (ICA) through a left CCA incision. The line was then inserted at a depth of 18-20 mm (beginning at the carotid bifurcation) to block the left middle cerebral artery. Finally, the skin was sutured and the rats were placed on a thermal insulation blanket. After 90 min of ischemia, the monofilament lines were carefully extracted from the ICA to induce reperfusion. Seventeen rats survived beyond 7 days postoperatively without mortality. Based on Videofluoroscopy swallowing study (VFSS) assessments, 12 of the 17 surviving rats that displayed dysphagia were randomly divided into two groups: the PSD group (n = 6) and the PSD+HF-rTMS group (n = 6). During the VFSS enrollment assessment of the 12 model rats, stroke severity was evaluated using the Longa scale. The scores obtained ranged from 1 to 2 points, indicating uniformity in neurological function severity among the rats (Zhong et al., 2022). Additionally, the sham operation group (n = 6) of SD rats was subjected to the same protocol without monofilament insertion. The detailed experimental schedule is shown in Figure 1A.

HF-rTMS treatment

HF-rTMS was administered using a customized stimulator (YRDCCI, Wuhan, China). On the 7th day post-operation, the magnetic stimulation group received rTMS treatment, which was continued until the 14th day post-surgery. A round prototype coil (23mm diameter with 3.5T peak magnetic welds) was positioned perpendicular to the cortical surface projection area of the right primary motor cortex (M1). TMS-induced electric field modeled in the animal's brain is 140 V/m. The treatment protocol was as follows: stimulation for 5 s and then, rest for 60 s (repeated 10 times); stimulation intensity, 33% of the maximum stimulator output; stimulation frequency, 10Hz. The animal special coil mechanism diagram and pictures of rTMS administered in animal models in Figures 2A-C.

Videofluoroscopy swallowing study (VFSS) assessments

The rats underwent VFSS on the day before surgery (baseline) and 2 weeks after surgery (day 14). The rats were fasted for 12 h before the VFSS assessments. A mixture of experimental rat breeding feed and iohexol (1:1) was placed on a platform in a transparent plastic box. During ad libitum feeding of the feed mixture, videos were obtained at 30 fps using swallowing radiography equipment (digital fluoroscopic X-ray machine PLD8100C, Zhuhai, China). Only swallows with clear sagittal views were analyzed. The mean fluoroscopic results for each rat were calculated using 8-10 swallows.

ImageJ software (National Institutes of Health, Bethesda, MD) was used to assess swallowing function, including 1) bolus area (mm^2): bolus size measured after swallow initiation and before the head of the bolus passed through the second cervical vertebra (C2); 2) Pharyngeal Transit Time (PTT, s): initiated on bolus passing through the posterior oropharynx and ended on it completely passing through C2, while the position was near the upper esophageal sphincter; 3) pharyngeal bolus speed (mm/s): the maximum speed at which the head of the bolus traveled from the initiation point to C2; and 4) inter-swallow interval (s): time interval between two successive swallows during uninterrupted eating (Russell et al., 2013; Welby et al., 2021).

Hematoxylin–eosin (H&E) staining of intestinal tissue

All rats were sacrificed on the 14th days after surgery. The Intestinal tissues (3 samples of each group) were placed in 4% paraformaldehyde for 24 h, mounted with gelatin, and then, embedded in paraffin. The tissues were cut into 10 μm slices; after which the sections were deparaffinized and stained with histopathological and eosin (Servicebio, G1076).

Fecal collection

We collected feces early in the morning after lights were turned on at the housing facility. The rats were temporarily placed individually in empty autoclaved cages and allowed to defecate. Approximately two fecal pellets were collected aseptically from each rat and placed in a sterile 2-mL tube. Fecal samples from four rats were collected from each group and stored at -80.0°C refrigerator. The time point for fecal sample collection coincided with that of the VFSS assessments.

DNA extraction and 16S rRNA gene sequencing of fecal samples

The stool samples of each group were removed from the -80°C refrigerator. Total genomic DNA from stool samples was extracted using the CTAB/SDS method, and its concentration and purity were monitored using 1% agarose gels according to the concentration. The DNA was diluted to 1 ng/μL using sterile water. Primers were designed

to amplify the variable V3-V4 regions of the 16S rRNA gene. PCRs was performed with 15 mL of Phusion® High-Fidelity PCR Master Mix (New England Biolabs, USA), 0.2 mM forward and reverse primers, and approximately 10 ng of template DNA. The initial denaturation temperature was set at 98°C for 1 min, followed by denaturation at 98°C for 10 s (30 cycles), annealing at 50°C for 30 s, extension at 72°C for 1 min, and final elongation at 72°C for 8 min and storage at 10°C. PCR products were electrophoresed on a 2% agarose gel and purified using the Qiagen Gel Extraction Kit (Qiagen, Germany). The TruSeq DNA PCR-Free Sample Preparation Kit (Illumina, USA) was used to construct the library, which was assessed using an Agilent Bioanalyzer 2100 system. After the library was qualified, the Illumina NovaSeq was used for 16S rRNA V3-V4 sequencing. We spliced and filtered the original data to remove contaminated data and to obtain accurate and reliable data.

Evaluation of microbiome composition based on 16S rRNA sequences and informatics analysis

Uparse software was used to cluster clean reads from all samples, and sequence clustering was converted into OTUs) by default with 97% identity. Species annotation analysis was performed using the Silva Database based on the Mothur algorithm to evaluate the differences and community composition of the dominant species in different samples. Raw data were analyzed using BioTree Biotechnology Co., Ltd. (Shanghai, China). Alpha and beta diversities were calculated using the breakaway method implemented in Quantitative Insights into Microbial Ecology, version 2.0. Finally, linear discriminant analysis effect size and linear discriminant analysis were used to identify the dominant bacterial taxa in the different groups of rats.

Liquid chromatography–mass spectrometry (LC-MS/MS) based metabolomics

A total of 25 mg of fecal sample was weighed and placed in an EP tube. Then, 200 µL of water and 480 µL of extract solution (MTBE: MeOH = 5:1) were added sequentially. After vortexing for 30 s, the samples were homogenized for 4 min at 35 Hz and sonicated for 5 min in an ice-water bath. Homogenization and sonication cycles were repeated three times. Next, the samples were

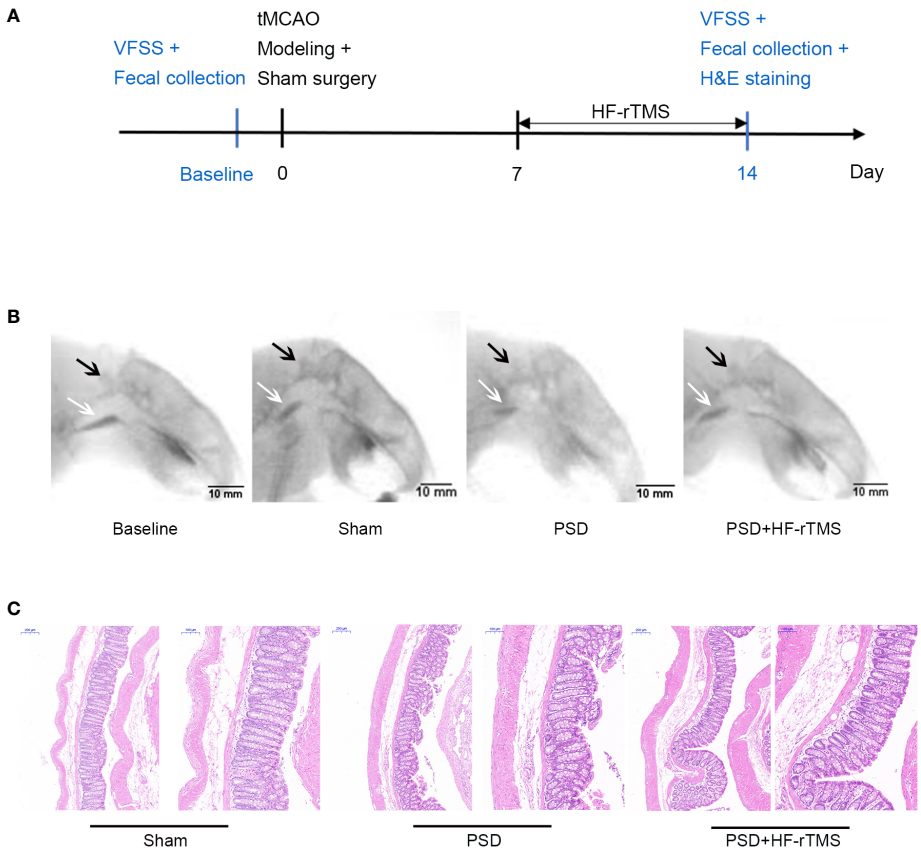

FIGURE 1
Schematics of experimental design **(A)**, representative radiographic image from rats undergoing videofluorography **(B)**, and Hematoxylin-eosin (H&E) Staining of the colon tissue **(C)**. (scale bar = 200 and 100 µm). VFSS, Videofluoroscopy swallowing study; C2, the second cervical vertebra; black arrow, C2; white arrow, bolus.

incubated at -40°C for 1 h and centrifuged at 3000 rpm for 15 min at 4°C. The supernatant (300 µL) was transferred to a fresh tube and dried under vacuum at 37°C. Then, The dried samples were reconstituted in 200 µL of 50% methanol in dichloromethane by sonication for 10 min in ice water bath. The mixture was then centrifuged at 13000 rpm for 15 min at 4°C, and 150 µL of the supernatant was collected and stored in a refrigerator at -20°C until LC-MS/MS analysis was performed.

LC-MS/MS analysis was performed using a UHPLC system (Vanquish, Thermo Fisher Scientific) with a UPLC HSS T3 column (2.1 mm × 100 mm; 1.8 µm) coupled with a Q Exactive HFX mass spectrometer (Orbitrap MS, Thermo). The Mobile phase A consisted of 40% water, 60% acetonitrile, and 10 mM ammonium formate. The Mobile phase B consisted of 10% acetonitrile and 90% isopropanol, which was added with 50 mL of 10 mmol/L ammonium formate for every 1000 mL mixed solvent. Analysis was performed using an elution gradient. The column temperature was 55°C. The autosampler temperature was maintained at 4°C. A Triple TOF 5600 + mass spectrometer (AB SCIEX, USA) was used for the electrospray ionization (ESI) positive and negative ion mass spectrometry analyses. ESI conditions: ion source gas 1:60, ion source gas 2:60, temperature 600°C, voltage ± 5500 V in positive and negative modes, mass scanning range m/z:60-1000 Da, first-level scanning range 25-1000 Da, scanning time 0.2 s, and high-sensitivity mode was used. For the second mass spectrometry, the delustering voltages of the positive and negative modes were ± 60 V and the high collision energy was (35 ± 15) eV.

Screening and identification of main differential metabolites

The raw data files were converted to files in the mzXML format using the 'msconvert' program from ProteoWizard. The CentWave algorithm in XCMS was used for peak detection, extraction, alignment, and integration; the minfrac for annotation was set at 0.5, and the cutoff for annotation was set at 0.3. Supervised orthogonal projections to latent structure discriminant analysis (OPLS-DA) was used to screen for the differential metabolites. Variable importance in projection (VIP) ≥ 1.0 and absolute fold change ≥ 3.0, were used as criteria for differential metabolite selection.

Statistical analyses

Data are presented as mean ± standard error of the mean (SEM). One-way ANOVA variance was performed to compare the continuous variables across multiple groups. All statistical analyses and correlation graphs were generated using GraphPad Prism 8 (GraphPad Software, San Diego, CA, United States).

Three different parameters (observed operational taxonomic units (OTUs) and Shannon and Simpson indices) were used to assess the alpha diversity. Beta diversity between samples was assessed using principal coordinate analysis (PCoA) and permutational multivariate analysis of variance (PERMANOVA). Phylogenetic Investigation of Communities by Reconstruction of

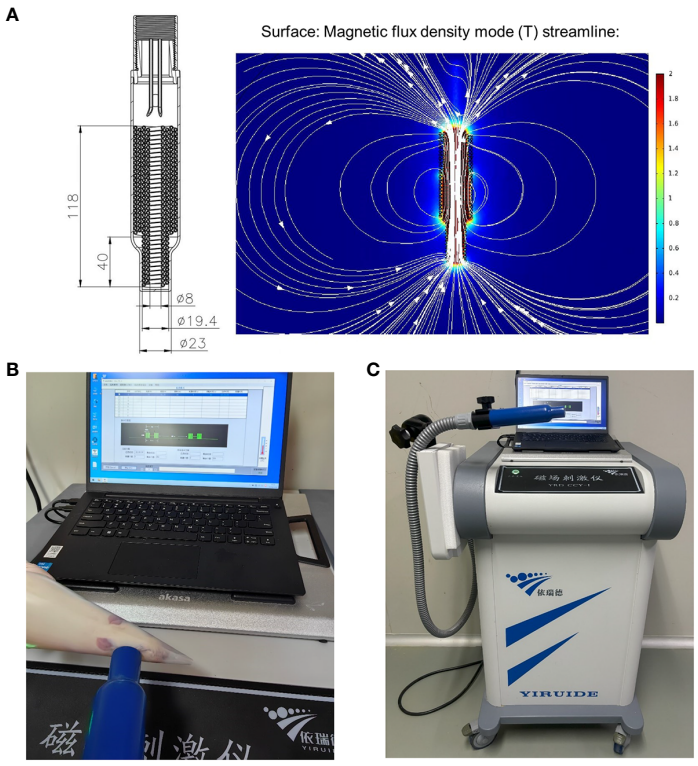

FIGURE 2
The animal special coil mechanism diagram **(A)** and pictures of rTMS administered in animal model **(B, C)**.

Unobserved States (PICRUSt) was utilized to explore differences in the Kyoto Encyclopedia of Genes and Genomes (KEGG) pathways in bacterial taxa between groups. MetaboAnalyst 5.0 (Xia Lab, McGill University, Canada) was used to analyze metabolomics data, including a pathway analysis overview. The association between the main differential metabolites and gut butyrate-producing bacteria was assessed using Spearman's rank correlation and correlation heat maps were drawn using R Studio (version 3.6.1, Boston, Massachusetts, USA). p-value < 0.05.

Results

VFSS analysis

A total of 24 recorded swallowing videos (six rats at baseline and six rats each from the PSD, PSD+HF-rTMS, and Sham groups on the 14th postoperative day) were manually analyzed. As shown in Table 1, compared with the baseline group, the bolus area and pharyngeal bolus speed were significantly decreased in the PSD group, and there were significant increases in the bolus area and decreases in PTT following HF-rTMS intervention (p < 0.05). Representative radiographic images of the rats undergoing videofluorography are shown in Figure 1B. According to these results, middle cerebral artery occlusion can result in dysphagia, which can be mitigated by HF-rTMS intervention.

Histopathological changes of intestinal tissue

H&E staining revealed that the colon epithelial cells of rats in the sham group had intact structures and were tightly arranged. In contrast, the rats in the PSD group exhibited damaged surface epithelial cells and disrupted cryptal glands. However, in the PSD+HF-rTMS group, there was a reduction in damage, thickening of the intestinal mucous layer, and recovery of the appearance of the surface epithelium (Figure 1C). These findings suggest that HF-rTMS intervention may have a positive restorative effect on intestinal tissues in rats with PSD, thereby further reinforcing intestinal epithelial cell integrity.

Gut microbial profiles

The rarefaction, Shannon-Wiener, and rank-abundance curves in the three groups tended to be flat or plateaued, thus demonstrating satisfactory sequencing depth (Supplementary Figure 1).

Alpha diversity analysis revealed no significant differences in the observed OTUs and Chao1 and Shannon indices among the baseline, PSD, and HF-rTMS groups (Figures 3A-C). The PCoA and PERMANOVA analysis of variance for beta diversity revealed a significant difference in the composition and abundance of the gut microbiota between the baseline and PSD groups. (Bray-Curtis p < 0.05; R^2 = 0.287) (Figure 3D). The PCoA and PERMANOVA analyses did not show significant differences in the composition and abundance of the gut microbiota between the PSD+HF-rTMS group and PSD group (Bray-Curtis p > 0.05, R^2 = 0.173) (Figure 3E).

Effect of PSD and HF-rTMS on gut microbiota

Taxon-dependent analysis revealed the top 10 phyla in the Baseline, PSD, and PSD+HF-rTMS groups, with *Firmicutes*, *Bacteroidetes*, *Verrucomicrobia*, *Tenericutes*, and *Proteobacteria* being the most dominant phyla (Figures 4A, E). Although no significant differences in the gut microbiota composition at the phylum level were observed among the three groups, the abundance of the phylum *Firmicutes* was significantly lower in the PSD group than in the baseline group (p < 0.05) (Figure 4C), and the abundance of *Verrucomicrobia* showed an increasing trend without statistical significance (p > 0.05). Notably, the abundance of *Firmicutes* increased after HF-rTMS treatment in the PSD+HF-rTMS group (p < 0.05) (Figure 4G).

The most relative abundant genera (> 1.0%) in the three groups are shown in Figures 4B, F. At the genus level, the proportion of *Lactobacillus*, *Anaerotruncus*, *Romboutsia*, *Turicibacter*, *Ruminococcaceae_NK4A214_group*, *Allobaculum*, *Dubosiella*, and *Faecalibaculum* (p < 0.05) decreased, whereas those of *Ruminococcaceae_UCG-014* and *Odoribacter* increased in the PSD group (p < 0.05) (Figure 4D). In the PSD+HF-rTMS group, the relative abundance of *Lactobacillus* and *uncultured_bacterium_f_Prevotellaceae* showed an increasing trend; however, the difference

TABLE 1 Results of VFSS swallowing assessment.

	Baseline group (n=6)	Sham group (n=6)	PSD group (n=6)	PSD+ HF-rTMS group (n=6)
Bolus Area (mm^2)	20.73 ± 1.04	18.27 ± 1.24	8.45 ± 0.61*	18.65 ± 0.77†
Pharyngeal Transit Time (PTT, s)	1.37 ± 0.17	1.17 ± 0.14	1.67 ± 0.28	1.03 ± 0.17†
Pharyngeal Bolus Speed (mm/s)	375.68 ± 35.81	366.06 ± 14.35	297.05 ± 21.20*	344.09 ± 11.30
Inter-Swallow Interval (ISI, s)	1.59 ± 0.13	1.69 ± 0.28	2.7 ± 0.30	2.45 ± 0.65

Data were presented as the mean ± SEM. VFSS, Videofluoroscopy swallowing study.
*: Compared with Baseline group, p < 0.05.
†: Compared with PSD group, p < 0.05.

was not statistically significant. Although the relative abundance was < 1.0%, the proportion of *uncultured_bacterium_Peptococcaceae* and *Marvinbryantia* increased, whereas the abundance of *[Eubacterium]_xylanophilum_group* decreased ($p < 0.05$) (Figure 4H).

Identification of group gut microbiota biomarkers

Linear discriminant analysis effect size (LEfSe) was used to identify potential microbiota biomarkers among different groups. *Firmicutes* exhibited a relatively higher abundance at the phylum level in the baseline group than in the PSD group. At the genus level, *Quinella* and *Lactobacillus* were the most abundant at baseline, whereas *Ruminococcaceae_UCG_014*, *Enterococcus*, and *Phascolarctobacterium* were enriched in the PSD group (linear discriminant analysis (LDA) > 3, $p < 0.05$) (Figures 5A, C). These microbes might be considered as biomarkers for the Baseline and PSD groups.

At the phylum level, *Firmicutes* was remarkably enriched in the PSD+HF-rTMS group compared to that in the PSD group. At the genus level, the abundance of *uncultured_bacterium_Peptococcaceae* was relatively high in the PSD+HF-rTMS group. The abundance of *Streptococcus*, *Acutalibacter*, and *Ruminiclostridium_9* were relatively high in the PSD group (LDA > 3, $p < 0.05$) (Figures 5B, D).

Pathway analysis of microbiotas

Several KEGG pathways, such as cell growth, cancer-specific types, and immune diseases, were significantly different between the Baseline and PSD group ($p < 0.05$) (Supplementary Figure 2A). The pathways in the PSD group and PSD+HF-rTMS group differed in cardiovascular and infectious diseases (viral) ($p < 0.05$) (Supplementary Figure 2B).

Identification of group differential metabolites

LC-MS/MS was used to determine the metabolic characteristics of rats in the three groups. OPLS-DA models showed that the metabolic profile of the PSD group was significantly different from that of the baseline group in both the negative and positive ion modes (Figures 6A, D). Similarly, the PSD+HF-rTMS group was significantly different from the PSD group (Figures 7A, D).

Differential metabolites were identified using VIP > 1 and $p < 0.05$. A total of 699 differential metabolites [357 upregulated and 342 downregulated]) were screened and identified in the PSD group compared with those in the baseline group in the negative mode (Figure 6B). In Figure 6C, the heatmap displays a subset of 17 named metabolites (15 upregulated and two downregulated) out of

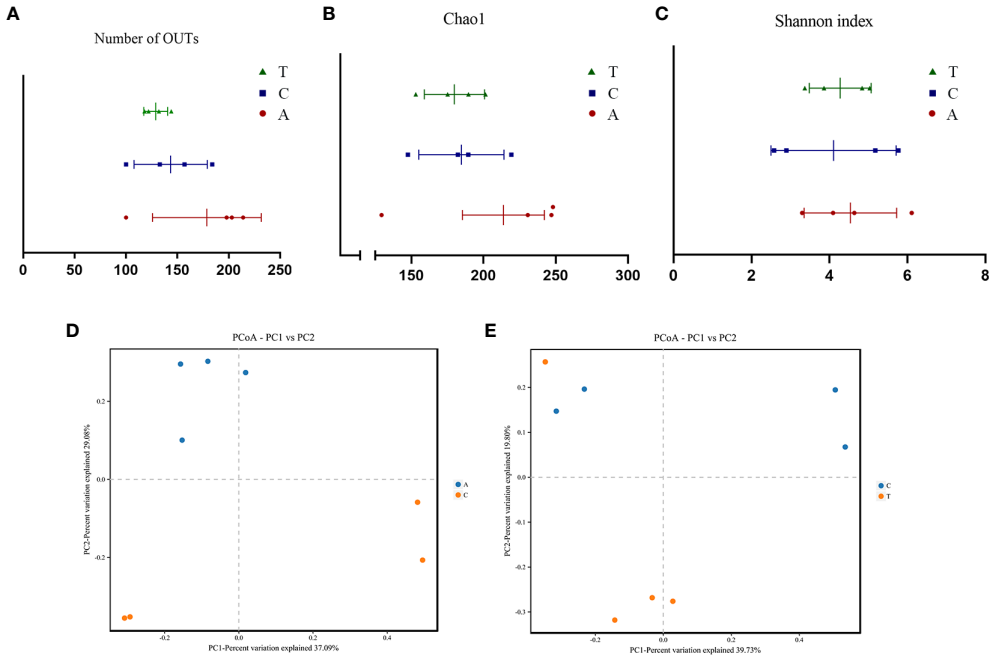

FIGURE 3
The α-diversity and PCoA analysis of fecal samples based on 16S rRNA gene sequences. Community Richness was quantified based on the number of observed species **(A)** and Chao1 index **(B)**, and community diversity was characterized using the Simpson index **(C)**. Neither richness or diversity differed significantly among the three groups. PCoA analysis between Baseline and PSD group **(D)** and PSD and PSD+HF-rTMS group **(E)**, based on Bray-Curtis distances at the OTU level. OTU, operational taxonomic unit; PCoA, principal coordinates analysis; A, Baseline group; C, PSD group; T, PSD+HF-rTMS group.

10.3389/fcimb.2024.1373737

the 699 differential metabolites analyzed. Additionally, in positive-mode analysis (Figure 6E), 403 metabolites (234 upregulated and 169 downregulated) were identified and compared. Furthermore, among the 403 differentially expressed metabolites, three upregulated metabolites were visualized with their names in the form of a heat map, as presented in Figure 6F. Briefly, the expression levels of differential metabolites in lipid classes, such as ceramides (Cer), free fatty acids (FA), phosphatidylethanolamine (PE), triacylglycerol (TAG), and sulfoquinovosyl diacylglycerol, were increased in PSD.

In the negative mode, a comprehensive analysis of the PSD+HF-rTMS group compared to the PSD group identified 1470 differential metabolites (963 upregulated and 507 downregulated) (Figure 7B). Among these 1470 metabolites, 26 specifically named metabolites (11 upregulated and 14 downregulated) were selected for visualization in the form of a

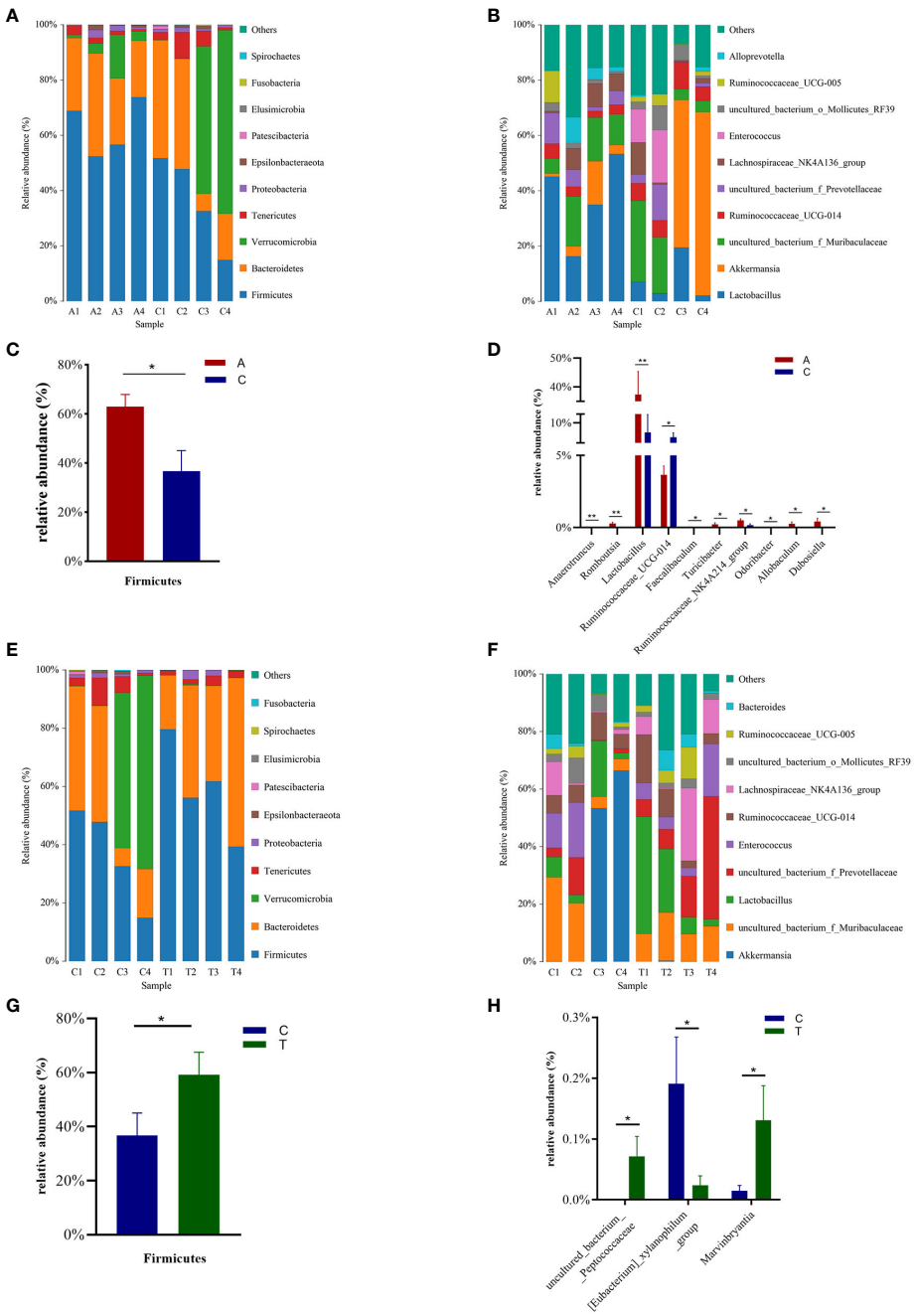

FIGURE 4
The distributions of the predominant bacteria among the Baseline, tMCAO, and PSD+HF-rTMS group rats. Significantly differential microbes are shown as mean ± SEM. Results at the phylum level **(A, C, E, G)**. Results at the genus level **(B, D, F, H)**. A, Baseline group; C, PSD group; T, PSD+HF-rTMS group; SEM, Standard error of mean; * $p < 0.05$, ** $p < 0.01$ (one-way ANOVA).

heat map (Figure 7C). Additionally, in the positive-mode analysis, 919 metabolites (260 upregulated and 659 downregulated) were identified (Figure 7E). Figure 7F presents a heatmap that displays 20 named metabolites (11 upregulated and 15 downregulated) from the total pool of 919 differential metabolites analyzed. Briefly, the levels of the differential lipids Cer, FA, and DG decreased after HF-rTMS treatment, whereas TAG levels increased.

Analysis of metabolic pathways

The MetaboAnalyst 5.0 was used for MetaboAnalyst pathway analysis of group differential metabolites, with $p < 0.05$. As shown in Figure 8A, metabolic pathways, such as glycerolipid, sphingolipid, glycerophospholipid, and urine metabolism, were altered in rats with PSD. HF-rTMS induced changes in sphingolipid, cysteine, methionine, glycerophospholipid, and pyrimidine metabolism in the PSD+HF-rTMS group (Figure 8B).

Correlations between the gut microbiome biomarkers and differential metabolites

Spearman correlation analysis was performed to explore the association between gut microbiota biomarkers and the aforementioned group of differential metabolites (including negative and positive modes). At the genus level, a relationship between the four genera and 21 metabolites was observed between the PSD and Baseline groups (Figure 6G). Specifically, Enterococcus was positively correlated with Cer, FA, and PE in the PSD rats. Similarly, a relationship between the four genera and 45 metabolites was observed between the PSD+HF-rTMS and PSD groups.

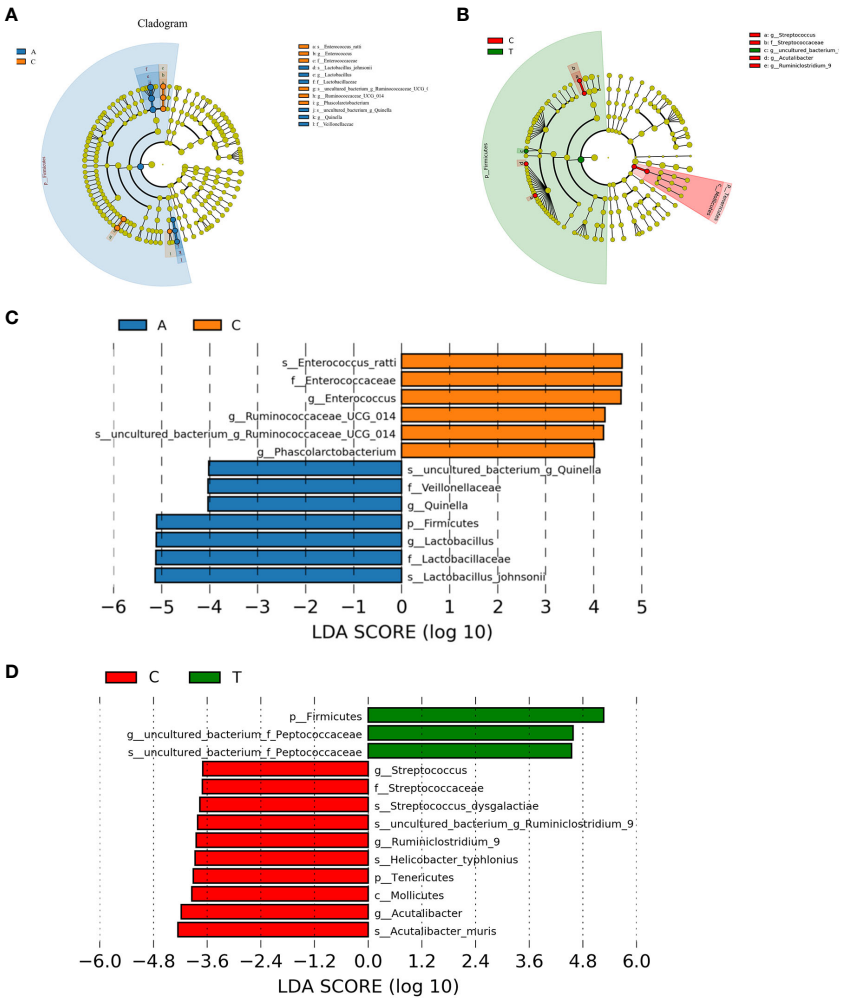

FIGURE 5
The potential biomarkers were defined based on effect size (LEfSe) combined with linear discriminant analysis (LDA). Cladogram for taxonomic representation of significant differences between Baseline and tMCAO group **(A)** and PSD and PSD+HF-rTMS groups **(B)**. The colored nodes from the inner to the outer circles represent taxa from the phylum to species level. Histogram of the LDA scores for differentially abundant features among groups **(C, D)**. The threshold on the logarithmic LDA score for discriminative features was set to 3.0. A, Baseline group; C, PSD group; T, PSD+HF-rTMS group.

Peptococcaceae was negatively correlated with Cer, Streptococcus was negatively correlated with DG, and Acutalibacter was positively correlated with FA and Cer (Figure 7G).

Discussion

Using VFSS, we found that performing HF-rTMS on the M1 cortex of the unaffected hemisphere for one week can improve swallowing function in PSD rats. This is especially true for bolus area and pharyngeal bolus speed. We observed that PSD rats exhibited damaged surface epithelial cells, disrupted cryptal glands in the colon, and altered intestinal microbiota and associated metabolites, which were ameliorated by the HF-rTMS intervention. These findings highlight the effects of HF-rTMS on the gut microbiota and its metabolites, which are associated with its therapeutic effects.

Numerous studies have demonstrated the efficacy of rTMS in enhancing swallowing function. Both HF-rTMS and LF-rTMS interventions have shown positive outcomes in various studies targeting the ipsilateral or contralateral cerebral cortex of lesion (Cheng et al., 2015; Lee et al., 2015; Park et al., 2017; Du et al., 2022; Hammad et al., 2022). Park et al. (Park et al., 2013) proved that HF-rTMS (5 Hz) over the pharyngeal motor cortex of the unaffected hemisphere significantly improved swallowing function, which is consistent with our findings. This mechanism may involve enhanced stimulation of bulbar motor neurons projecting to the pharynx and further increase corticobulbar excitability (Park et al., 2013). A recent study (Aizawa et al., 2021) suggested that stimulation of the dorsolateral prefrontal cortex by rTMS modifies brain-gut interactions in humans. A comprehensive study has indicated that stroke has the potential to elevate intestinal permeability and activate the intestinal immune system, thus exacerbating ischemia-reperfusion injury through the brain-gut axis. However, some metabolites produced by the intestinal flora attenuate ischemia-reperfusion injury by suppressing the post-stroke inflammatory response and promoting the repair of neurological function through the axis (Hu et al., 2022). Using

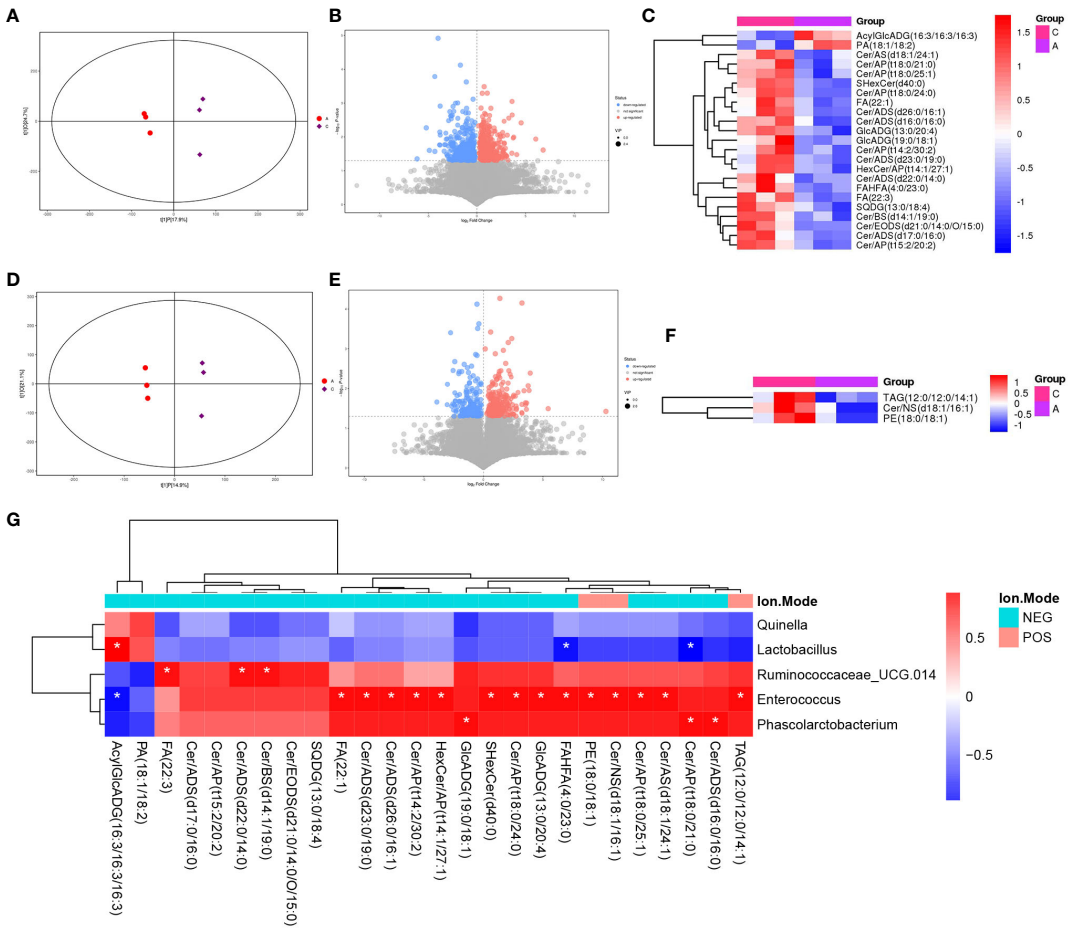

FIGURE 6
PLS-DA score plots **(A)**, volcano map **(B)**, and heatmap **(C)** of differential metabolites between Baseline and PSD group in the negative ion patterns. PLS-DA score plots **(D)**, volcano map **(E)**, and heatmap **(F)** of differential metabolites in the positive ion patterns. Heatmap of correlation **(G)** between the differential gut microbes and differential metabolites between Baseline and PSD group. NES, Negative Ion Mode; POS, Positive Ion Mode; A, Baseline group; C, PSD group; T, PSD+HF-rTMS group. * $p < 0.05$.

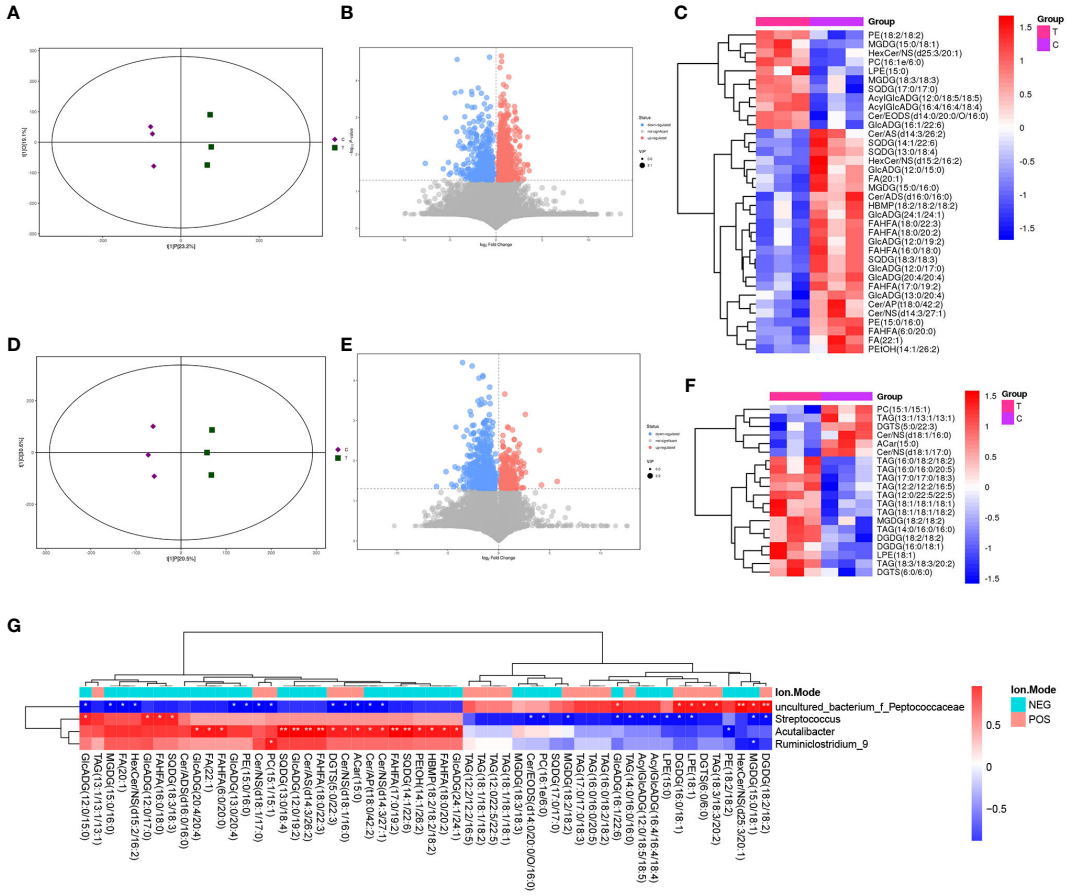

FIGURE 7
PLS-DA score plots **(A)**, volcano map **(B)**, and heatmap **(C)** of differential metabolites between the PSD+HF-rTMS and PSD group in the negative ion patterns. PLS-DA score plots **(D)**, volcano map **(E)**, and heatmap **(F)** of differential metabolites in the positive ion patterns. Heatmap of correlation **(G)** between the differential gut microbes and differential metabolites between PSD+HF-rTMS and PSD group. NES, Negative Ion Mode; POS, Positive Ion Mode; A, Baseline group; C, PSD group; T, PSD+HF-rTMS group. * $p < 0.05$, ** $p < 0.01$.

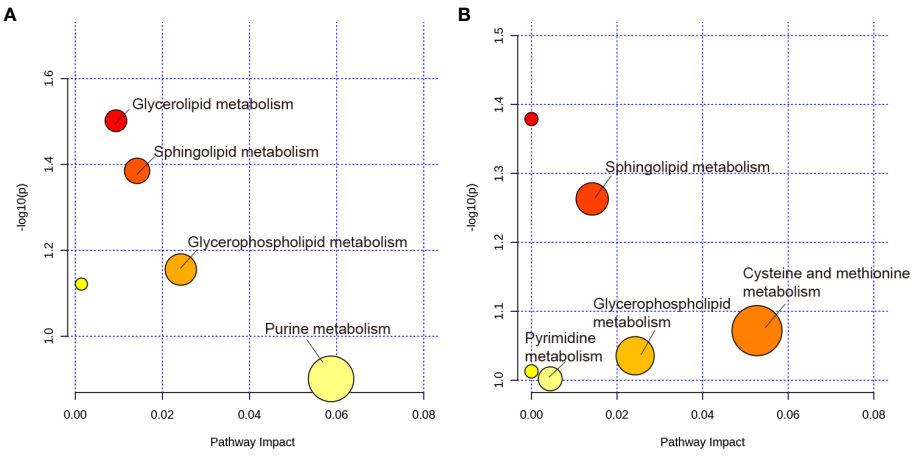

FIGURE 8
KEGG pathway analysis of group differential metabolites. **(A)** KEGG pathway enrichment analysis of group differential metabolites between the Baseline and PSD group. **(B)** Analysis of group differential metabolites between the PSD+HF-rTMS and PSD group. The metabolic pathways are displayed as distinctly colored circles depending on their enrichment analysis scores (vertical axis, shade of red) and topology (pathway impact, horizontal axis, circle diameter) using MetaboAnalyst 5.0.

16S sequencing, we found that HF-rTMS promoted the restoration of intestinal flora balance. Therefore, after indirect excitatory stimulation, the vagus nerve in the medulla may play an active role via brain-gut interactions.

Using 16S rRNA gene sequencing, we observed that although no significant differences in gut microbiota composition at the phylum level were observed among the three groups, the abundance of the phylum *Firmicutes* was significantly decreased in the PSD group compared with that at baseline. This finding was consistent with the results of previous studies, both in a rat model and in patients (Li et al., 2020; Haak et al., 2021; Wu et al., 2021). *Firmicutes* are the predominant phylum in the intestinal microbiota and contribute to the maintenance of the normal gastrointestinal tract (Ley et al., 2006). The results showed that HF-rTMS increased the abundance of *Firmicutes* to help restore gut microbiota balance. Similarly, Seewoo et al. (Seewoo et al., 2022) found that rTMS (10HZ) is primarily responsible for maintaining a high abundance of *Firmicutes* in a rat model of depression. The abundance of the genus Lactobacillus (phylum Firmicutes), an important type of host probiotic bacterium, was considerably affected in the PSD group. Chen et al. (Chen et al., 2019b) found that the level of *Lactobacillus* decreased in monkeys after MCAO, which was consistent with our findings. *Lactobacillus* can produce SCFAs such as butyrate and acetate, which can improve wound healing, reinforce intestinal epithelial cell integrity in mice with stroke, and inhibit bacterial migration (Cushing et al., 2015; Zou et al., 2022). After HF-rTMS treatment, the relative abundance of *Lactobacillus* showed an upward trend, but did not reach statistical significance, which may be related to the treatment time; prolonging the treatment time may be a better choice. Moreover, H&E staining results further substantiated the effectiveness of HF-rTMS in reinforcing intestinal epithelial cell integrity, which may be correlated with SCFAs. The LEfSe analysis indicated that *Ruminococcaceae_UCG_014*, *Enterococcus*, and *Phascolarctobacterium* were enriched in the PSD group. *Ruminococcaceae_UCG_014* and *Phascolarctobacterium* can produce SCFAs including acetate and propionate (Wu et al., 2017; Tian et al., 2021). Their enrichment in the PSD group may be related to a compensatory response secondary to the massive reduction in the level of SCFA-producing bacteria, especially butyrate-producing bacteria such as *Lactobacillus*. *Enterococcus* is an opportunistic pathogen that can cause pneumonia and bacteremia in patients with stroke, resulting in unfavorable outcomes even 3 month post-stoke (Stanley et al., 2016; Sun et al., 2021). Furthermore, LEfSe analysis showed that the abundance of *uncultured_bacterium_Peptococcaceae* was relatively high after HF-rTMS treatment, whereas *Streptococcus*, *Acutalibacter*, and *Ruminiclostridium_9* were enriched in the PSD group. *Peptococcaceae* and *Ruminiclostridium_9* are also groups of bacteria characterized by the production of SCFA after the degradation of indigestible plant-derived polysaccharides (Bernad-Roche et al., 2021). *Streptococcus* and *Acutalibacter* are proinflammatory bacteria. PSD increased the levels of opportunistic pathogens and decreased the levels of SCFA-producing bacteria, particularly *Lactobacillus*, whereas HF-rTMS increased SCFA-producing bacteria and decreased pro-inflammatory bacteria levels. Chen et al. demonstrated that interfering with the gut microbiota by transplanting SCFA-rich fecal bacteria is an effective treatment for cerebral ischemic stroke (Chen et al., 2019a). Thus, HF-rTMS may enhances brain-gut interactions via SCFA to effectively improve PSD swallowing function, and the effect was similar to that of transplanting feces.

Combined with untargeted metabolomic analysis, we found that PSD was associated with disturbances in fecal metabolomics. Pathway analysis showed that these metabolites are primarily involved in glycerolipid, sphingolipid, glycerophospholipid, and urine metabolism. A previous study has shown that stroke is related to urine and sphingolipid metabolism (Ding et al., 2022). Furthermore, the results indicated that sphingolipid metabolism, cysteine and methionine metabolism, glycerophospholipid metabolism, and pyrimidine metabolism are potential target metabolic pathways of HF-rTMS. Moreover, we investigated the association between gut microbiota and fecal metabolites. This analysis showed that *Enterococcus* was positively correlated with Cer, FA, and PE levels in the PSD rats. As these levels were all significantly increased in the PSD group, they may be risk factors for PSD. After administration of HF-rTMS, *Peptococcaceae* was negatively correlated with Cer, *Streptococcus* was negatively correlated with DG, *Acutalibacter* was positively correlated with FA and Cer. These untargeted metabolomics findings suggest that HF-rTMS has the potential to induce modifications in the composition of the gut microbiota, thus influencing the levels of fecal metabolites. These alterations in metabolites are expected to affect specific metabolic pathways, ultimately resulting in therapeutic effects in PSD.

In summary, our research findings validate that HF-rTMS can effectively ameliorate intestinal flora imbalance and reinstate the integrity of the intestinal wall. This restoration may potentially mitigate intestinal inflammation and diminish the influx of toxins into the bloodstream, thus alleviating cerebral ischemia injury. Additionally, HF-rTMS augments the population of SCFAs-producing bacteria, leading to the production of metabolites such as SCFAs. These metabolites exhibit a protective role against cerebral ischemic injury and facilitate the functional recovery of PSD by curbing inflammation, restraining bacterial migration, among other mechanisms (Cushing et al., 2015; Zou et al., 2022). Presently, a multitude of animal models predominantly utilize fecal microbiota transplantation (FMT) to rectify intestinal flora imbalances. This approach proves to be financially burdensome in clinical settings and is not readily available in general hospital settings. Furthermore, FMT encounters formidable hurdles stemming from the potential transmission of diseases between donors and recipients, patient reluctance, adverse repercussions, and the ambiguity surrounding its impact on the recipient's immune system, encompassing conditions such as peripheral neuropathy and idiopathic thrombocytopenic purpura (Wang et al., 2019; Porcari et al., 2023). rTMS therapy, a non-invasive treatment that does not require the special cooperation of the patient, which can be used as an alternative therapy to bacterial transplantation, improves intestinal flora disorders through the brain-gut axis and in turn promotes stroke rehabilitation.

This study had some limitations. Although we propose a potential contribution of HF-rTMS to the gut microbiome and fecal metabolites, the mechanisms underlying the gut-brain

interactions remain unclear and require further elucidation. Therefore, extensive evaluation of additional metabolites, including neurotransmitters and SCFAs, is crucial for establishing the comprehensive efficacy of HF-rTMS. Prior investigations (Aizawa et al., 2021; Seewoo et al., 2022) have highlighted the impact of HF-rTMS on the gastrointestinal system. Notably, in our study, we observed a significant increase in rat defecation rates following HF-rTMS stimulation. We hypothesize that the application of high-frequency transcranial magnetic stimulation to the M1 region in rat models could activate the dorsal vagal nucleus situated within the medulla oblongata. This activation, in turn, may enhance gastrointestinal motility via the vagus nerve, potentially mitigating dysbiosis. So subsequent studies will focus on assessing the role of the dorsal vagal complex and vagus nerve in the therapeutic mechanism of HF-rTMS. Understanding the involvement of the dorsal vagal complex-vagus nerve-gut axis holds a tempting prospect for advancing our knowledge in this field. Finally, further clinical research is warranted to validate our findings.

Conclusion

In conclusion, we employed a combination of intestinal pathology, 16S rRNA gene sequencing, and LC-MS analysis to compare the colonic structure, composition, and abundance of gut microbiota and fecal metabolites among three groups: Baseline, PSD, and PSD with HF-rTMS treatment. We observed that PSD rats exhibited damaged surface epithelial cells and disrupted cryptal glands in the colon, which were ameliorated by HF-rTMS. Our investigation of the gut microbiota revealed a significant decrease in the presence of SCFA-producing bacteria in rats with PSD, with notable augmentation following the HF-rTMS intervention. Moreover, using fecal metabolomic analysis, we identified distinct metabolites that exhibited variation across groups. Finally, our integrated analysis demonstrated a correlation between the gut microbiota and dysregulated metabolites. These findings suggest a synergistic role for the gut microbiota and fecal metabolites in the development of PSD and the therapeutic mechanisms underlying HF-rTMS. This mechanism may be related to changes in the brain-gut axis and warrants further investigation to fully understand and use HF-rTMS for treating PSD.

Data availability statement

The data presented in the study are deposited in the National Center for Biotechnology Information (NCBI) repository, accession number PRJNA1086134.

Ethics statement

All animal experiments were approved by the Animal Care Committee of the South China Agricultural University (Guangzhou, China) and were performed in accordance with the Guidelines for the Care and Use of Laboratory Animals issued by the Chinese Council on Animal Research. The study was conducted in accordance with the local legislation and institutional requirements.

Author contributions

FZ: Conceptualization, Data curation, Formal analysis, Writing – original draft, Writing – review & editing. JC: Conceptualization, Data curation, Methodology, Writing – original draft. YS: Conceptualization, Methodology, Data curation, Writing – original draft. JNH: Methodology, Writing – original draft. QY: Methodology, Writing – original draft. YD: Methodology, Software, Writing – original draft. JHH: Methodology, Software, Writing – original draft. JZ: Methodology, Writing – original draft. CL: Funding acquisition, Project administration, Writing – original draft. HW: Funding acquisition, Supervision, Conceptualization, Writing – review & editing.

Funding

The author(s) declare financial support was received for the research, authorship, and/or publication of this article. This study was supported by the National Natural Science Foundation of China (grant number 82372569 to HW, grant number 82102668 to CL, grant number 82002383 to YS), Guangdong Basic and Applied Basic Research Foundation (grant number 2023A1515011138 to HW), Guangzhou Science and Technology Plan (grant number 2023A03J0214 to HW).

Conflict of interest

The authors declare that the research was conducted in the absence of any commercial or financial relationships that could be construed as a potential conflict of interest.

Publisher's note

Supplementary material

The Supplementary Material for this article can be found online at: https://www.frontiersin.org/articles/10.3389/fcimb.2024.1373737/full#supplementary-material

References

Aizawa, Y., Morishita, J., Kano, M., Kanazawa, M., and Fukudo, S. (2021). Modification of rectal function and emotion by repetitive transcranial magnetic stimulation in humans. *Neurosci. Res.* 168, 54–63. doi: 10.1016/j.neures.2021.05.013

Benakis, C., Martin-Gallausiaux, C., Trezzi, J., Melton, P., Liesz, A., and Wilmes, P. (2020). The microbiome-gut-brain axis in acute and chronic brain diseases. *J. Mol. Neurosci.* 61, 1–9. doi: 10.1016/j.conb.2019.11.009

Bernad-Roche, M., Bellés, A., Grasa, L., Casanova-Higes, A., and Mainar-Jaime, R. (2021). Effects of dietary supplementation with protected sodium butyrate on gut microbiota in growing-finishing pigs. *Anim. (Basel).* 11(7):2137. doi: 10.3390/ani11072137

Bonilha, H., Simpson, A., Ellis, C., Mauldin, P., Martin-Harris, B., and Simpson, K. (2014). The one-year attributable cost of post-stroke dysphagia. *Dysphagia* 29, 545–552. doi: 10.1007/s00455-014-9543-8

Chen, Y., Liang, J., Ouyang, F., Chen, X., Lu, T., Jiang, Z., et al. (2019b). Persistence of gut microbiota dysbiosis and chronic systemic inflammation after cerebral infarction in cynomolgus monkeys. *Front. Neurol.* 10. doi: 10.3389/fneur.2019.00661

Chen, R., Xu, Y., Wu, P., Zhou, H., Lasanajak, Y., Fang, Y., et al. (2019a). Transplantation of fecal microbiota rich in short chain fatty acids and butyric acid treat cerebral ischemic stroke by regulating gut microbiota. *Pharmacol. Res.* 148, 104403. doi: 10.1016/j.phrs.2019.104403

Cheng, I., Chan, K., Wong, C., and Cheung, R. (2015). Preliminary evidence of the effects of high-frequency repetitive transcranial magnetic stimulation (rTMS) on swallowing functions in post-stroke individuals with chronic dysphagia. *Int. J. Lang Commun. Disord.* 50, 389–396. doi: 10.1111/1460-6984.12144

Chiang, C., Lin, M., Hsiao, M., Yeh, Y., Liang, Y., and Wang, T. (2019). Comparative efficacy of noninvasive neurostimulation therapies for acute and subacute poststroke dysphagia: A systematic review and network meta-analysis. *Arch. Phys. Med. Rehabil.* 100, 739–750.e734. doi: 10.1016/j.apmr.2018.09.117

Cushing, K., Alvarado, D., and Ciorba, M. (2015). Butyrate and mucosal inflammation: new scientific evidence supports clinical observation. *Clin. Transl. Gastroenterol.* 6, e108. doi: 10.1038/ctg.2015.34

Dawson, J., Pierce, D., Dixit, A., Kimberley, T., Robertson, M., Tarver, B., et al. (2016). Safety, feasibility, and efficacy of vagus nerve stimulation paired with upper-limb rehabilitation after ischemic stroke. *Stroke* 47, 143–150. doi: 10.1161/STROKEAHA.115.010477

Ding, X., Liu, Z., Liu, Y., Xu, B., Chen, J., Pu, J., et al. (2022). Comprehensive evaluation of the mechanism of Blume in ameliorating cerebral ischemia-reperfusion injury based on integrating fecal metabonomics and 16S rDNA sequencing. *Front. Cell Infect. Microbiol.* 12. doi: 10.3389/fcimb.2022.1026627

Du, Y., Wei, L., Lu, Y., and Gao, H. (2022). The effects of different frequencies of repetitive transcranial magnetic stimulation (rTMS) on patients with swallowing disorders after cerebral infarction. *NeuroRehabilitation* 50, 115–122. doi: 10.3233/NRE-210176

Haak, B., Westendorp, W., van Engelen, T., Brands, X., Brouwer, M., Vermeij, J., et al. (2021). Disruptions of anaerobic gut bacteria are associated with stroke and post-stroke infection: a prospective case-control study. *Transl. Stroke Res.* 12, 581–592. doi: 10.1007/s12975-020-00863-4

Hammad, A., Elhamrawy, E., Abdel-Tawab, H., Shafik, M., Sallam, Y., Elzomor, H., et al. (2022). Transcranial magnetic stimulation versus transcutaneous neuromuscular electrical stimulation in post stroke dysphagia: A clinical randomized controlled trial. *J. Stroke Cerebrovasc. Dis.* 31, 106554. doi: 10.1016/j.jstrokecerebrovasdis.2022.106554

Hu, W., Kong, X., Wang, H., Li, Y., and Luo, Y. (2022). Ischemic stroke and intestinal flora: an insight into brain-gut axis. *Eur. J. Med. Res.* 27, 73. doi: 10.1186/s40001-022-00691-2

Khedr, E. M., and Abo-Elfetoh, N. (2009). Treatment of post-stroke dysphagia with repetitive transcranial magnetic stimulation. *Acta Neurol. Scand.* 119, 155–161. doi: 10.1111/ane.2009.119.issue-3

Lee, J., Kim, S., Lee, K., Lee, S., and Lee, J. (2015). Effect of repetitive transcranial magnetic stimulation according to the stimulation site in stroke patients with dysphagia. *Ann. Rehabil. Med.* 39, 432–439. doi: 10.5535/arm.2015.39.3.432

Ley, R., Peterson, D., and Gordon, J. (2006). Ecological and evolutionary forces shaping microbial diversity in the human intestine. *Cell* 124, 837–848. doi: 10.1016/j.cell.2006.02.017

Li, H., Zhang, X., Pan, D., Liu, Y., Yan, X., Tang, Y., et al. (2020). Dysbiosis characteristics of gut microbiota in cerebral infarction patients. *Transl. Neurosci.* 11, 124–133. doi: 10.1515/tnsci-2020-0117

Liao, X., Xing, G., Guo, Z., Jin, Y., Tang, Q., He, B., et al. (2017). Repetitive transcranial magnetic stimulation as an alternative therapy for dysphagia after stroke: a systematic review and meta-analysis. *Clin. Rehabil.* 31, 289–298. doi: 10.1177/0269215516644771

Lin, C., Chung, S., Lin, C., and Hwu, Y. (2021). Effect of tongue-to-palate resistance training on tongue strength in healthy adults. *Auris Nasus Larynx.* 48, 116–123. doi: 10.1016/j.anl.2020.07.014

Park, E., Kim, M., Chang, W., Oh, S., Kim, Y., Lee, A., et al. (2017). Effects of bilateral repetitive transcranial magnetic stimulation on post-stroke dysphagia. *rain Stimul.* 10, 75–82. doi: 10.1016/j.brs.2016.08.005

Park, J., Oh, J., Lee, J., Yeo, J., and Ryu, K. (2013). The effect of 5Hz high-frequency rTMS over contralesional pharyngeal motor cortex in post-stroke oropharyngeal dysphagia: a randomized controlled study. *Neurogastroenterol Motil.* 25, 324–e250. doi: 10.1111/nmo.12063

Porcari, S., Benech, N., Valles-Colomer, M., Segata, N., Gasbarrini, A., Cammarota, G., et al. (2023). Key determinants of success in fecal microbiota transplantation: From microbiome to clinic. *Cell Host Microbe* 31, 712–733. doi: 10.1016/j.chom.2023.03.020

Reyes-Torres, C., Castillo-Martínez, L., Reyes-Guerrero, R., Ramos-Vázquez, A., Zavala-Solares, M., Cassis-Nosthas, L., et al. (2019). Design and implementation of modified-texture diet in older adults with oropharyngeal dysphagia: a randomized controlled trial. *Eur. J. Clin. Nutr.* 73, 989–996. doi: 10.1038/s41430-019-0389-x

Russell, J., Ciucci, M., Hammer, M., and Connor, N. (2013). Videofluorographic assessment of deglutitive behaviors in a rat model of aging and Parkinson disease. *Dysphagia* 28, 95–104. doi: 10.1007/s00455-012-9417-x

Seewoo, B., Chua, E., Arena-Foster, Y., Hennessy, L., Gorecki, A., Anderton, R., et al. (2022). Changes in the rodent gut microbiome following chronic restraint stress and low-intensity rTMS. *Neurobiol. Stress* 17, 100430. doi: 10.1016/j.ynstr.2022.100430

Shigematsu, T., and Fujishima, I. (2015). Dysphagia and swallowing rehabilitation. *Brain Nerve.* 67, 169–182. doi: 10.11477/mf.1416200109

Singh, V., Roth, S., Llovera, G., Sadler, R., Garzetti, D., Stecher, B., et al. (2016). Microbiota dysbiosis controls the neuroinflammatory response after stroke. *J. Neurosci.* 36, 7428–7440. doi: 10.1523/JNEUROSCI.1114-16.2016

Stanley, D., Mason, L., Mackin, K., Srikhanta, Y., Lyras, D., Prakash, M., et al. (2016). Translocation and dissemination of commensal bacteria in post-stroke infection. *Nat. Med.* 22, 1277–1284. doi: 10.1038/nm.4194

Sun, H., Gu, M., Li, Z., Chen, X., and Zhou, J. (2021). Gut microbiota dysbiosis in acute ischemic stroke associated with 3-month unfavorable outcome. *Front. Neurol.* 12. doi: 10.3389/fneur.2021.799222

Tian, B., Zhao, J., Zhang, M., Chen, Z., Ma, Q., Liu, H., et al. (2021). Lycium ruthenicum anthocyanins attenuate high-fat diet-induced colonic barrier dysfunction and inflammation in mice by modulating the gut microbiota. *Mol. Nutr. Food Res.* 65, e2000745. doi: 10.1002/mnfr.202000745

Wang, J.-W., Kuo, C.-H., Kuo, F.-C., Wang, Y.-K., Hsu, W.-H., Yu, F.-J., et al. (2019). Fecal microbiota transplantation: Review and update. *J. Formos Med. Assoc.* 118 (1), S23–S31. doi: 10.1016/j.jfma.2018.08.011

Welby, L., Ukatu, C., Thombs, L., and Lever, T. (2021). A mouse model of dysphagia after facial nerve injury. *Laryngoscope* 131, 17–24. doi: 10.1002/lary.28560

Wu, F., Guo, X., Zhang, J., Zhang, M., Ou, Z., and Peng, Y. (2017). Phascolarctobacterium faecium abundant colonization in human gastrointestinal tract. *Exp. Ther. Med.* 14, 3122–3126. doi: 10.3892/etm.2017.4878

Wu, W., Sun, Y., Luo, N., Cheng, C., Jiang, C., Yu, Q., et al. (2021). Integrated 16S rRNA gene sequencing and LC-MS analysis revealed the interplay between gut microbiota and plasma metabolites in rats with ischemic stroke. *J. Mol. Neurosci.* 71, 2095–2106. doi: 10.1007/s12031-021-01828-4

Zhang, M., Li, C., Zhang, F., Han, X., Yang, Q., Lin, T., et al. (2021). Prevalence of dysphagia in China: an epidemiological survey of 5943 participants. *Dysphagia* 36, 339–350. doi: 10.1007/s00455-020-10138-7

Zhong, Y., Gu, L., Ye, Y., Zhu, H., Pu, B., Wang, J., et al. (2022). JAK2/STAT3 axis intermediates microglia/macrophage polarization during cerebral ischemia/reperfusion injury. *Neuroscience* 496, 119–128. doi: 10.1016/j.neuroscience.2022.05.016

Zou, X., Wang, L., Xiao, L., Wang, S., and Zhang, L. (2022). Gut microbes in cerebrovascular diseases: Gut flora imbalance, potential impact mechanisms and promising treatment strategies. *Front. Immunol.* 13. doi: 10.3389/fimmu.2022.975921

10.3389/fcimb.2024.1373737

Glossary

Acar	Acylcarnitine
AcylGlcADG	Acylglucuronosyldiacylglycerol
Cer/ADS	Ceramide alpha-hydroxy fatty aciddihydrosphingosine
Cer/AP	Ceramide alpha-hydroxy fatty acidphytospingosine
Cer/AS	Ceramide alpha-hydroxy fatty acid-sphingosine
Cer/ BS	Ceramide beta-hydroxy fatty acid-sphingosine
Cer/EODS	Ceramide Esterified omega-hydroxy fatty acid-dihydrosphingosine
Cer/NS	Ceramide non-hydroxyfatty acid-sphingosine
DGDG	Digalactosyldiacylglycerol
DGTS	Diacylglyceryl trimethylhomoserine
FA	Free fatty acid
FAHFA	Fatty acid ester of hydroxyl fatty acid
GlcADG	glucuronosyldiacylglycerol
HBMP	Hemibismonoacylglycerophosphate
HexCer/AP	Hexosylceramide alphahydroxy fatty acid-phytospingosine
HexCer/NS	Hexosylceramide nonhydroxyfatty acid-sphingosine
HF-TMS	High frequency repetitive transcranial magnetic stimulation
ISI	inter-swallow interval
LEfSe	Linear discriminant analysis Effect Size
LF-rTMS	Low frequency repetitive transcranial magnetic stimulation
LPE	Lysophosphatidylethanolamine
M1	Primary motor cortex
MGDG	Monogalactosyldiacylglycerol
NSS	neurological severity scores
OPLSDA	Orthogonal Projections to Latent Structures Discriminant Analysis
OTUs	operational taxonomic units
PA	Phosphatidic acid
PC	Phosphatidylcholine
PCA	Principal component analysis
PCoA	principal coordinate analysis
PE	Phosphatidylethanolamine
PEtOH	Phosphatidylethanol
PSD	post-stroke dysphagia
PTT	pharyngeal transit time
SCFAs	short-chain fatty acids
SHexCer	SulfurHexosylceramide hydroxyfatty acid
SQDG	Sulfoquinovosyl diacylglycerol
TAG	triacylglycerol
tMCAO	transient middle cerebral artery occlusion
VFSS	Videofluoroscopy swallowing study

frontiers | Frontiers in Cellular and Infection Microbiology

TYPE Original Research
PUBLISHED 23 April 2024
DOI 10.3389/fcimb.2024.1395716

OPEN ACCESS

EDITED BY
Gang Ye,
Sichuan Agricultural University, China

REVIEWED BY
Ge Zhang,
The First Affiliated Hospital of Zhengzhou University, China
Zhongjia Yu,
Foshan University, China

*CORRESPONDENCE
Guojing Liu
lgj@hospital.cqmu.edu.cn

†These authors have contributed equally to this work

RECEIVED 04 March 2024
ACCEPTED 01 April 2024
PUBLISHED 23 April 2024

CITATION
Ke Y, Yue J, He J and Liu G (2024) Integrating machine learning algorithms and single-cell analysis to identify gut microbiota-related macrophage biomarkers in atherosclerotic plaques. *Front. Cell. Infect. Microbiol.* 14:1395716. doi: 10.3389/fcimb.2024.1395716

Integrating machine learning algorithms and single-cell analysis to identify gut microbiota-related macrophage biomarkers in atherosclerotic plaques

Yin Ke[1,2†], Jian Yue[3†], Jiaming He[4] and Guojing Liu[1*]

[1]Department of Neurosurgery, The University-Town Hospital of Chongqing Medical University, Chongqing, China, [2]Department of Nursing, The Maternal and Child Health Hospital of Yong Chuan, Chongqing, China, [3]Department of Breast Surgery, Gaozhou People's Hospital, Gaozhou, China, [4]Institute of Life Sciences, Chongqing Medical University, Chongqing, China

Objective: The relationship between macrophages and the gut microbiota in patients with atherosclerosis remains poorly defined, and effective biological markers are lacking. This study aims to elucidate the interplay between gut microbial communities and macrophages, and to identify biomarkers associated with the destabilization of atherosclerotic plaques. The goal is to enhance our understanding of the underlying molecular pathways and to pave new avenues for diagnostic approaches and therapeutic strategies in the disease.

Methods: This study employed Weighted Gene Co-expression Network Analysis (WGCNA) and differential expression analysis on atherosclerosis datasets to identify macrophage-associated genes and quantify the correlation between these genes and gut microbiota gene sets. The Random Forest algorithm was utilized to pinpoint PLEK, IRF8, BTK, CCR1, and CD68 as gut microbiota-related macrophage genes, and a nomogram was constructed. Based on the top five genes, a Non-negative Matrix Factorization (NMF) algorithm was applied to construct gut microbiota-related macrophage clusters and analyze their potential biological alterations. Subsequent single-cell analyses were conducted to observe the expression patterns of the top five genes and the interactions between immune cells. Finally, the expression profiles of key molecules were validated using clinical samples from atherosclerosis patients.

Results: Utilizing the Random Forest algorithm, we ultimately identified PLEK, IRF8, CD68, CCR1, and BTK as gut microbiota-associated macrophage genes that are upregulated in atherosclerotic plaques. A nomogram based on the expression of these five genes was constructed for use as an auxiliary tool in clinical diagnosis. Single-cell analysis confirmed the specific expression of gut microbiota-associated macrophage genes in macrophages. Clinical samples substantiated the high expression of PLEK in unstable atherosclerotic plaques.

Conclusion: Gut microbiota-associated macrophage genes (PLEK, IRF8, CD68, CCR1, and BTK) may be implicated in the pathogenesis of atherosclerotic plaques and could serve as diagnostic markers to aid patients with atherosclerosis.

KEYWORDS

gut microbiota, macrophage, machine learning, atherosclerotic plaques, bioinformatics

1 Introduction

Atherosclerosis is a stealthy vascular disease characterized by lipid accumulation and inflammation within the arterial intima, leading to plaque formation (Camare et al., 2017; Vergallo and Crea, 2020; Alkarithi et al., 2021). This process often progresses asymptomatically, yet when unstable plaques rupture, it can precipitate severe cardiovascular events such as myocardial infarction or stroke (Bailey et al., 2016). Rupture of unstable plaques releases necrotic tissue and structural components into the vasculature, activating the coagulation system and prompting platelet aggregation at the site of injury, forming thrombi (Mangge and Almer, 2019; Sterpetti, 2020). These thrombi may exacerbate arterial narrowing, obstruct blood flow, and cause myocardial ischemia due to oxygen and nutrient deprivation. If not promptly addressed, this ischemia can rapidly deteriorate, leading to life-threatening events. Thus, stabilizing atherosclerotic plaques and preventing their rupture is of paramount clinical importance for preventing acute cardiovascular incidents.

In the progression of atherosclerosis, macrophages within the arterial wall play a complex and pivotal role. They not only contribute to plaque formation by ingesting oxidized low-density lipoprotein (ox-LDL) and transforming into foam cells but also exacerbate local inflammation by releasing pro-inflammatory cytokines such as tumor necrosis factor-α (TNF-α) and interleukin-1β (IL-1β), attracting more immune cells and promoting plaque growth (Libby, 2021a). Macrophage death, particularly through the inflammatory cell death pathway of pyroptosis, releases factors that destabilize plaques, increasing the likelihood of rupture and thrombus formation (Wei et al., 2023). Additionally, macrophages differentiate into various phenotypes based on environmental signals, which play a decisive role in plaque stability and repair (Wolf and Ley, 2019; Libby, 2021b). They also participate in the reverse cholesterol transport, affecting the metabolic balance of plaques. Despite the crucial role of macrophages in atherosclerosis, the identification and clinical application of macrophage-related biomarkers remain challenging.

Recent research suggests a possible connection between the gut microbiota and atherosclerosis. Changes in the composition and metabolic activity of the gut microbiota, which affect host lipid metabolism, inflammation, and immune function, are thought to play a critical role in the formation and development of atherosclerosis. Notably, the gut bacterial metabolite trimethylamine N-oxide (TMAO), derived from the metabolism of choline, has been closely associated with the risk of atherosclerosis. Imbalances in the gut microbiota can also trigger systemic inflammatory responses and metabolic dysfunction, exacerbating the pathological process of atherosclerosis (Jonsson and Backhed, 2017; Ma et al., 2022). Modulating the gut microbiota with probiotics has opened new avenues for the treatment of atherosclerosis. However, the specific mechanisms by which the gut microbiota interacts with the host through its complex metabolic network to influence atherosclerosis require further scientific investigation.

With the ongoing progress of high-throughput sequencing, it's become more common to investigate immune cells and gut microbiota characteristics with single-cell RNA sequencing and transcriptome analysis (Alcazar et al., 2022). In biomedicine, machine learning is increasingly applied to diagnose and predict disease outcomes (Danneskiold-Samsoe et al., 2019). These techniques analyze large data sets to uncover disease mechanisms and guide clinical decisions. This study seeks to identify macrophage genes closely tied to atherosclerotic plaques in relation to gut microbiota. We analyzed gene expression differences between normal carotid artery and atherosclerotic plaque samples, then identified key genes using machine learning algorithms.Finally, our single-cell and clinical sample analyses highlighted these genes' pivotal role in plaque instability, offering novel insights for clinical approaches.

2 Materials and methods

2.1 Data collection

Bulk transcriptome datasets (GSE43292 and GSE120521) and single-cell datasets (GSE155512) were downloaded from the GEO database. GSE43292 contains 32 atheroma plaque and 32 macroscopically intact tissue samples, GSE120521 has four unstable and four stable plaque samples, and GSE155512 includes four atherosclerotic samples.

2.2 Differential expression analysis and WGCNA

Differential expression analysis was performed on the GSE43292 dataset for atheroma plaque and macroscopically intact tissue samples using the limma package, resulting in 188 upregulated genes in atherosclerosis plaques with criteria of |logFC| >0.8 and adjusted P-value <0.05. WGCNA algorithm was used to calculate gene significance (GS) and module membership (MM), confirming a key atherosclerosis module (blue module with 1115 genes) (Wang et al., 2023). Immune infiltration analysis was conducted using the deconvo_tme function from the IOBR package, and CIBERSORT was applied to WGCNA to calculate immune cell-related modules for M0, M1, and M2 macrophages, which were blue, red, and yellow, respectively (Wu et al., 2022). The union of genes from these three modules was defined as macrophage-related genes (a total of 2323 genes).

2.3 Pinpointing crucial macrophage genes

By integrating the 188 differentially expressed genes, the 1115 genes from the disease-related blue module, and the 2323 macrophage-related genes, a Venn diagram was constructed, ultimately yielding 139 genes. STRING database (https://cn.string-db.org/) was used to analyze these 139 genes, identifying key genes with a threshold score of 30 Degrees, and Cytoscape software was employed for visualizing protein-protein interactions (PPI) (Schroeder et al., 2013; Crosara et al., 2018). The cytoHubba plugin was then used to identify important genes, resulting in 24 significant genes. A random forest algorithm from the R package randomForest was applied to feature selection for these 24 genes, with the top 5 results defined as hub genes.

2.4 Collection of gut microbiota-related datasets

Gut microbiota-related gene sets were collected from GSEA (gsea-msigdb.org) using "Gut Microbiota" as the keyword (Supplementary Table S1). After scoring with the ssGSEA algorithm, correlation analysis with the five hub genes was performed to ultimately determine gut microbiota-related macrophage genes.

2.5 Construction of gut microbiota-related macrophage cluster

ConsensusClusterPlus package was used for consistency clustering analysis based on the expression of gut microbiota-related macrophage genes, ensuring the stability of the clustering assessment. The pheatmap package was utilized to visualize the expression differences of the five hub genes between groups, and PCA was visualized according to group and expression levels. GSEABase and GSVA packages were used to calculate immune scores for samples, visualizing differences in immune cell scores between groups and immune cell infiltration between high and low PLEK expression groups.

2.6 Construction of nomogram model for gut microbiota-related macrophage genes

The Nomogram model was constructed using the R package "rms," based on the expression data of the TOP5 gut microbiota-related macrophage genes. The role of macrophage genes associated with gut microbiota in influencing disease outcomes was evaluated, and each gene was assigned a corresponding score. By summing these scores, a total score was obtained, which was used to assess the severity of atherosclerosis in patients.

2.7 Single-cell sequencing analysis

In the single-cell analysis phase, R packages Seurat and SingleR were used to process single-cell RNA sequencing data, with filtering criteria including retaining cells with counts greater than 200 and less than 10,000, and removing cells containing more than 20% mitochondrial genes or ribosomal genes. Data were then normalized, high-variance genes identified, and principal component analysis (PCA) performed for dimensionality reduction. Key principal components were determined through JackStraw analysis, and cell clustering analysis was conducted using the FindNeighbors and FindClusters functions from the "Seurat" package with a resolution of 1.2, followed by further analysis using t-SNE technology. The FindAllMarkers function from the Seurat package was used to identify differentially expressed genes, and cell annotation was based on the Human Primary Cell Atlas. Violin and heat maps were used to display the expression differences of atherosclerosis-related genes across different cell types. Additionally, macrophage sub-group analysis based on PLEK expression and GO and KEGG enrichment analyses were conducted to reveal changes in cell functions and signaling pathways. Finally, cell trajectories and intercellular communication networks were explored using the monocle and CellChat tools.

2.8 Clinical sample collection

After explaining our study to patients set for carotid endarterectomy, we got their approval and they signed consent forms. We collected four samples of stable plaques and five of unstable plaques. The study was approved by the ethics committee at The University-Town Hospital of Chongqing Medical University (Approval No: LL-202213).

2.9 Histology and immunohistochemistry

Fresh carotid atherosclerotic plaques were fixed overnight in 4% formaldehyde, then embedded in paraffin, and continuous 5-micron thick sections were obtained for subsequent experiments.

The specific immunohistochemistry (IHC) protocol followed previously described methods (Jiang et al., 2019). We utilized the PLEK antibody from Proteintech, China. Based on the immunoreactive score method, the intensity of human atherosclerotic plaque tissue staining (protein expression) was scored range from 0-4, indicating negative staining to strong staining.

2.10 Western blot

For the specific Western Blot procedure, please refer to the methods previously described (Jiang et al., 2019). Ultimately, we assessed the expression levels of PLEK, P65, phospho-P65, IkBα, phospho- IkBα and GAPDH. All the aforementioned antibodies were sourced from Proteintech, China.

2.11 Cell culture

The RAW264.7 cell line was cultivated in DMEM (Gibco, USA), enriched with 10% FBS (Gibco, USA), and antibiotics penicillin (100 units/mL) and streptomycin (100 μg/mL). After washing with PBS, the cells were pre-treated with TNF-α (20 ng/mL) and LPS (100 ng/mL) from Abcam, USA, for 24 hours before proceeding with further experiments.

2.12 Lentiviral infection

Design primers, anneal and ligate them, and construct the sh-Plek plasmid with the sh sequence inserted at the AgeI and EcoRI restriction sites in the pLKO.1 vector. Revive normally growing 293T cells. The plasmid sequencing was successful, and lentivirus packaging was carried out at a ratio of 4:3:1 (sh-Plek, PsPAX.2, Pmd2.G) using Lipo3000 (Thermo Fisher, USA) as the transfection reagent. After 60 hours, collect the lentivirus using a 0.45 μm filter (Millipore, USA) and infect cells in six-well plates, with polybrene at a concentration of 8 μg/ml per milliliter. Change the medium 12 hours later, and passage the cells when they grow confluent, followed by antibiotic selection. The knockdown sequences are as follows: sh1- CCGG-GCTGGTTTCTAACAAGCTAGT-CTCGAG-ACTAGCTTGTTAGAAACCAGC-TTTTTT,sh2- CCGG-GGAGAACTCCAGTGATGATGA-CTCGAG-TCATCATCACTGGAGTTCTCC-TTTTTT,sh3- CCGG- GCCTACCTGCACTACTATGAT-CTCGAG- ATCATAGTAGTGCAGGTAGGC-TTTTTT.

2.13 Statistical analysis

In this study, R software version 4.1.2 and GraphPad Prism 7 were utilized for data analysis. We employed t-tests and Wilcoxon tests to assess the differences between the two groups. The significance levels are marked with asterisks: * for p-values below 0.05, ** for p-values less than 0.01, and *** for p-values under 0.001.

3 Results

3.1 Analysis of macrophage-related genes and immune infiltration in atherosclerotic plaques

We conducted a differential expression analysis on the GSE43292 dataset for atheroma plaque and macroscopically intact tissue samples (control group), identifying 142 downregulated and 188 upregulated genes (Figure 1A; Supplementary Table S2). Heatmap illustrates the top 30 genes with the most pronounced upregulation and downregulation (Figure 1B). Pathway enrichment analysis revealed significant enrichment in Neutrophil Extracellular Traps formation, Chemokine signaling pathway, and Lip and atherosclerosis (Figure 1C). Analysis of immune cell infiltration in atheroma plaque and macroscopically intact tissue samples showed a marked increase in inflammatory cell infiltration in the atheroma plaque group (Figure 1D). We employed the CIBERSORT algorithm to score immune cell-related modules, and the WGCNA algorithm to determine key modules related to M0, M1, and M2 macrophages, which were blue, red, and yellow, respectively, totaling 2323 genes (Figure 1E). Using the WGCNA algorithm, we identified a key module of 1115 genes in atherosclerosis (Figure 1F). A Venn diagram was used to identify 139 macrophage-related genes (Figure 1G).

3.2 Functional enrichment analysis of atherosclerotic plaque-related macrophage genes

To explore the potential biological significance of macrophage-related genes, we performed DO/KEGG/GO enrichment analysis. The DO analysis significantly enriched in primary immunodeficiency disease and multiple diseases, the GO analysis significantly enriched in positive regulation of cytokine production and cytokine binding, and the KEGG analysis significantly enriched in cytokine-cytokine receptor interaction and primary immunodeficiency (Figures 2A–C and Supplementary Table S3).

3.3 Identification of gut microbiota-related core macrophage genes

The metabolic products of the gut microbiota can reach the vascular system through the bloodstream and affect macrophages, intervening in the development of atherosclerosis. However, more evidence is needed to deeply understand these complex relationships. Therefore, we compared the gut microbiota-related gene sets of atheroma plaque and macroscopically intact tissue samples. We found that the scores for HP_SMALL_INTESTINAL_DYSMOTILITY, HP_MELENA, HP_INTESTINAL_FISTULA, and GOBP_ENTERIC_NERVOUS_SYSTEM_DEVELOPMENT were significantly higher in the atheroma plaque group than in the control group,while the score for GOMF_N_N_DIMETHYLANILINE_MONOOXYGENASE_ACTIVITY was higher in the control group

10.3389/fcimb.2024.1395716

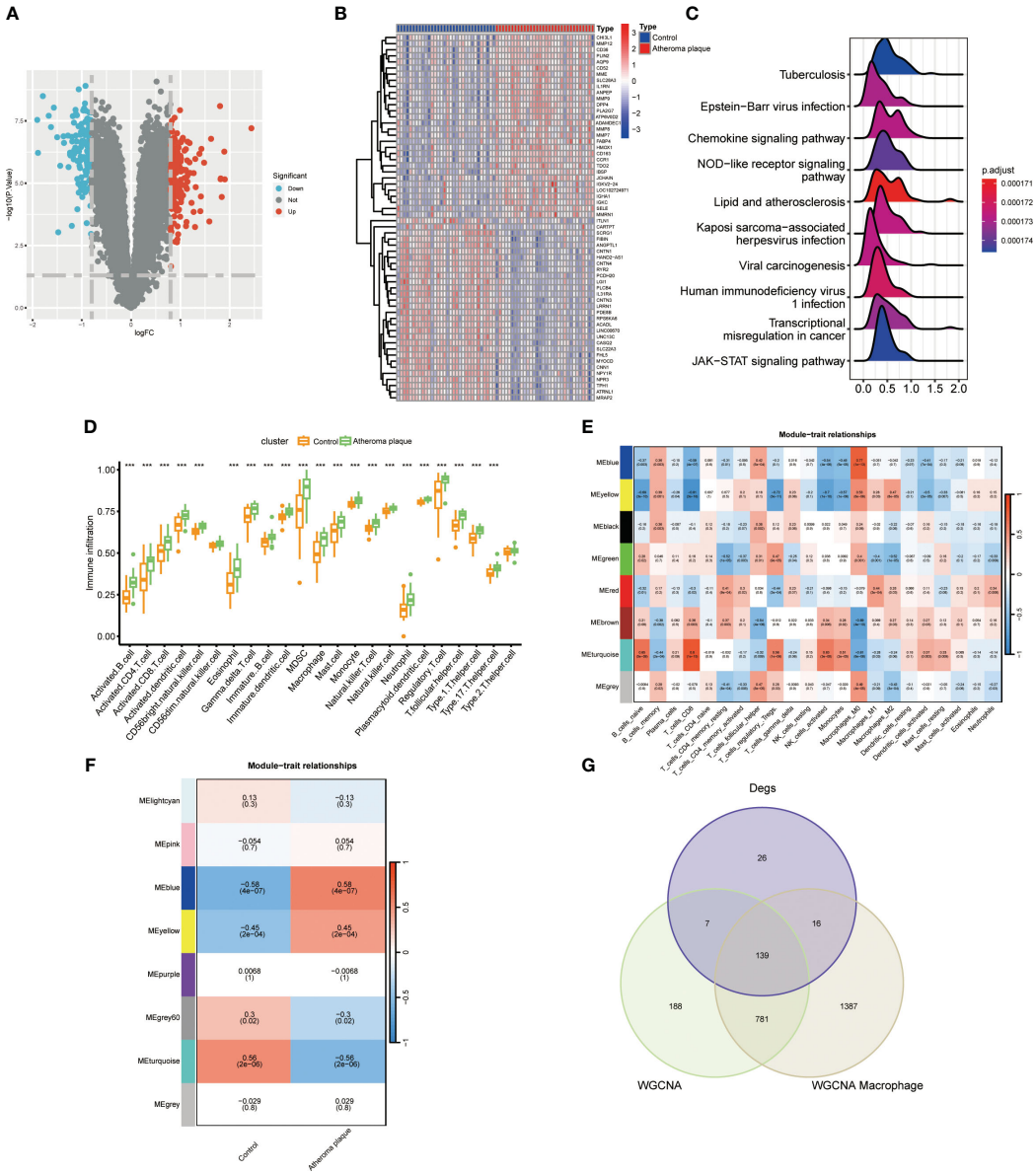

FIGURE 1
Identifyng macrophage genes linked to atherosclerotic plaques. **(A)** Volcano plot showing differentially expressed genes in atherosclerosis. **(B)** Heatmap displaying the top thirty specific differential genes between normal carotid artery and atherosclerotic plaque samples. **(C)** Signaling pathways highly related to atherosclerosis (X-axis: Represents the distribution range of the log2-transformed expression fold changes of core enrichment genes in enriched pathways). **(D)** Immune cell infiltration in normal carotid artery and atherosclerotic plaque samples. **(E)** WGCNA algorithm identifying key macrophage-related modules. **(F)** WGCNA analysis determining key modules in atherosclerosis. **(G)** VENN diagram identifying macrophage genes related to atherosclerotic plaques. (***$P < 0.001$).

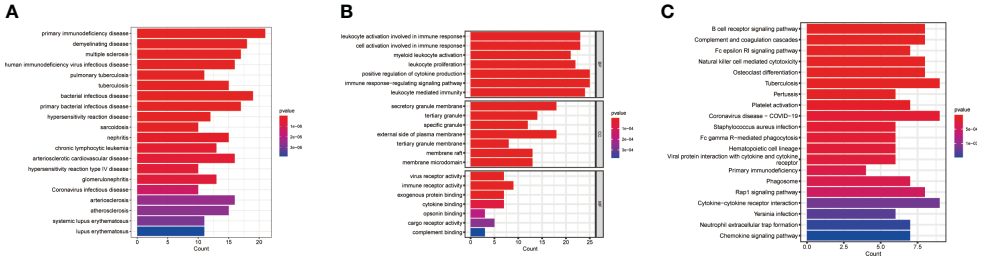

FIGURE 2
Pathway enrichment analysis. **(A)** DO enrichment analysis. **(B)** GO enrichment analysis. **(C)** KEGG enrichment analysis.

(Figure 3A). Subsequently, we performed protein-protein interaction (PPI) analysis on the 139 genes and visualized the results (Figure 3B and Supplementary Table S4). The random forest algorithm identified the top five genes (PLEK, IRF8, BTK, CCR1, and CD68), with PLEK being the most significant (Figures 3C, D). Finally, we conducted a correlation analysis between the top five genes and gut microbiota-related genes, showing that the top five genes were significantly positively correlated with HP_MELENA but significantly negatively correlated with GOBP_ENTERIC_NERVOUS_SYSTEM_DEVELOPMENT (Figure 3E). Ultimately, PLEK, IRF8, BTK, CCR1, and CD68 were confirmed as Gut Microbiota-Related Core Macrophage Genes.

3.4 Constructing a nomogram based on gut microbiota-related core macrophage genes

To provide targeted diagnostic assistance for atherosclerosis patients, we constructed a proprietary Nomogram model based on the expression of PLEK, IRF8, BTK, CCR1, and CD68 (Figure 4A). Calibration curve analysis revealed that the Nomogram model performed well in predictive accuracy, with its predictions closely matching the actual positive rates (Figure 4B). Decision curve analysis (DCA), clinical impact curve analysis (CICA), and ROC analysis further confirmed the significant clinical value of gut microbiota-related core macrophage genes in constructing the Nomogram model for atherosclerosis patients (Figures 4C–I). Analysis results in the GSE120521 dataset also showed that the expression levels of PLEK, IRF8, BTK, CCR1, and CD68 were significantly higher in the atheroma plaque group than in the control group (Supplementary Figure S1).

3.5 Construction and exploration of the biological characteristics of gut microbiota-related core macrophage clusters

To further investigate the potential role of gut microbiota-associated core macrophage genes in atherosclerosis, we applied unsupervised clustering methods based on the expression of PLEK, IRF8, BTK, CCR1, and CD68 to classify atherosclerosis patients into groups A and B (Figures 5A, B). The Principal Component Analysis

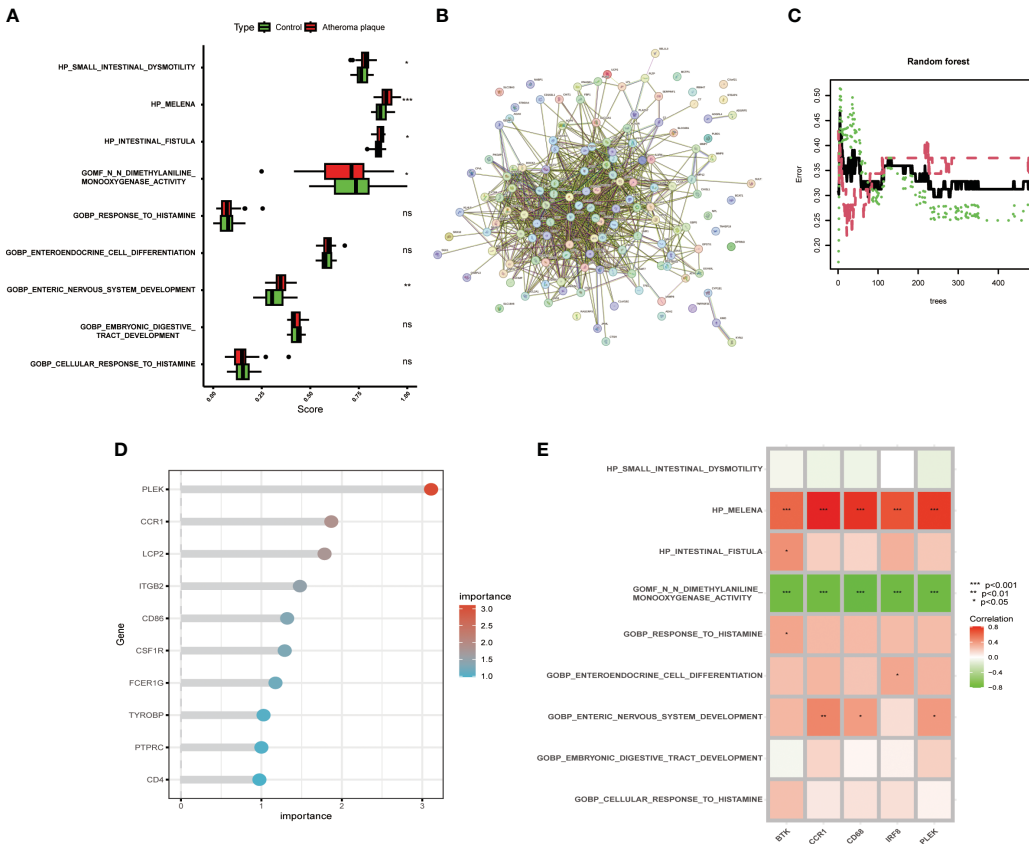

FIGURE 3
Identifying macrophage genes related to gut microbiota. **(A)** Boxplot showing changes in gut microbiota between normal carotid artery and atherosclerotic plaque samples. **(B)** Protein-protein interaction network of macrophage-related genes. **(C)** Random forest plot with red, green, and black dots representing atherosclerotic plaques, normal carotid artery, and all samples, respectively, with the x and y axes representing the number of trees and error rate. **(D)** Lollipop plot showing the top ten important genes. **(E)** Correlation analysis between the top five genes and gut microbiota-related gene sets. (*P < 0.05, **P < 0.01, ***P < 0.001).

10.3389/fcimb.2024.1395716

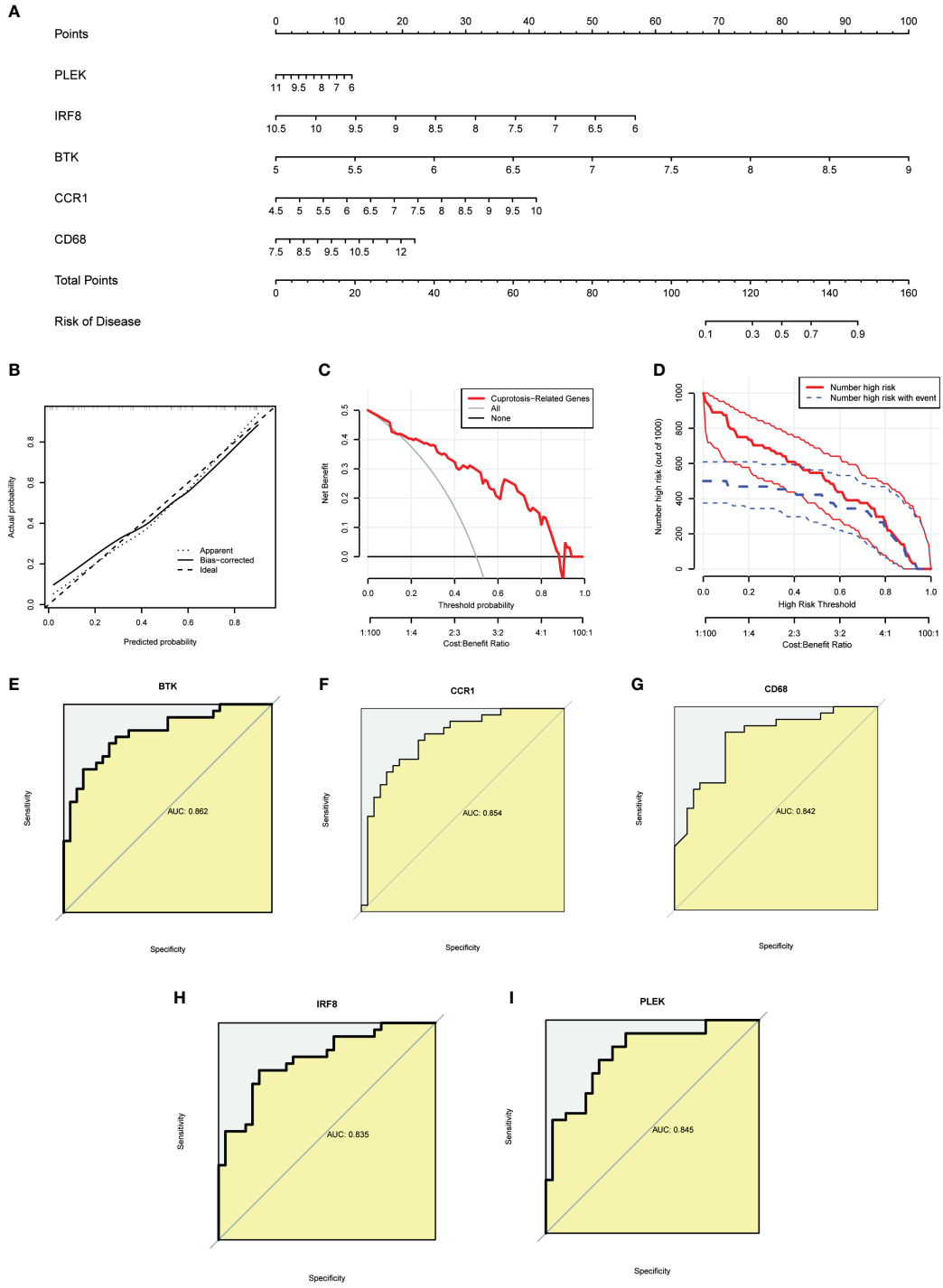

FIGURE 4
Constructing a nomogram related to gut microbiota macrophages to assess clinical value. **(A)** The nomogram demonstrates the prognostic value of the top five gut microbiota-related macrophage genes (PLEK, IRF8, BTK, CCR1, and CD68) for atherosclerosis patients. **(B)** Calibration curves to assess the degree of similarity between the predicted and true results of the gut microbiota-related macrophage nomogram. **(C)** Decision curve analysis to evaluate the sensitivity and specificity of the gut microbiota-related macrophage nomogram. **(D)** Clinical impact curve to assess the clinical impact of the gut microbiota-related macrophage nomogram at different thresholds. **(E–I)** ROC analysis results for the top five gut microbiota-related macrophage genes.

(PCA) results indicated that macrophage genes associated with the gut microbiota could effectively categorize atherosclerosis patients into clusters A and cluster B (Figure 5C). Additionally, PLEK, IRF8, BTK, CCR1, and CD68 were more highly expressed in cluster A than in cluster B, and immune cell infiltration was also significantly higher in cluster A (Figures 5D, E). We then conducted a differential analysis between cluster A and cluster B and displayed the results using heatmaps and volcano plots (Figures 5F, G; Supplementary

Table S5). Finally, we performed pathway enrichment analysis on the upregulated genes in cluster A, which were significantly enriched in pathways such as vascular smooth muscle contraction, regulation of lipolysis in adipocytes, muscle system process, muscle cell development, and muscle cell differentiation (Figures 5H, I).

3.6 Analyze the expression of gut microbiota-related macrophage genes in the atherosclerotic single-cell transcriptome

Using the "FindNeighbors" and "FindClusters" functions in the "Seurat" package for cell clustering analysis, we identified 17 cell clusters (Figure 6A). We used UMAP visualization to divide them into six cell populations: macrophages, monocytes, T cells, endothelial cells, chondrocytes, and smooth muscle cells, with heatmaps showing the marker genes for each subpopulation (Figures 6B, C). Finally, we found that PLEK, IRF8, BTK, CCR1, and CD68 were significantly expressed in monocytes and macrophages, further confirming the reliability of our previous transcriptome analysis (Figures 6D, E).

3.7 Investigating the effects of PLEK expression on macrophages

Since the random forest tree results previously showed that PLEK was the most significant (Figure 3D), we divided macrophagesinto High PLEK Macrophage and Low PLEK Macrophage groups based on the median expression value of PLEK to analyze the biological changes between the two groups (Figures 7A, B). Using the irGSEA.score function for gene set analysis, we found that the TNFA-signaling-via-NFKB pathway was significantly upregulated in the High PLEK Macrophage group, while this pathway was significantly downregulated in the Low PLEK Macrophage group (Figure 7C). Subsequently, we performed

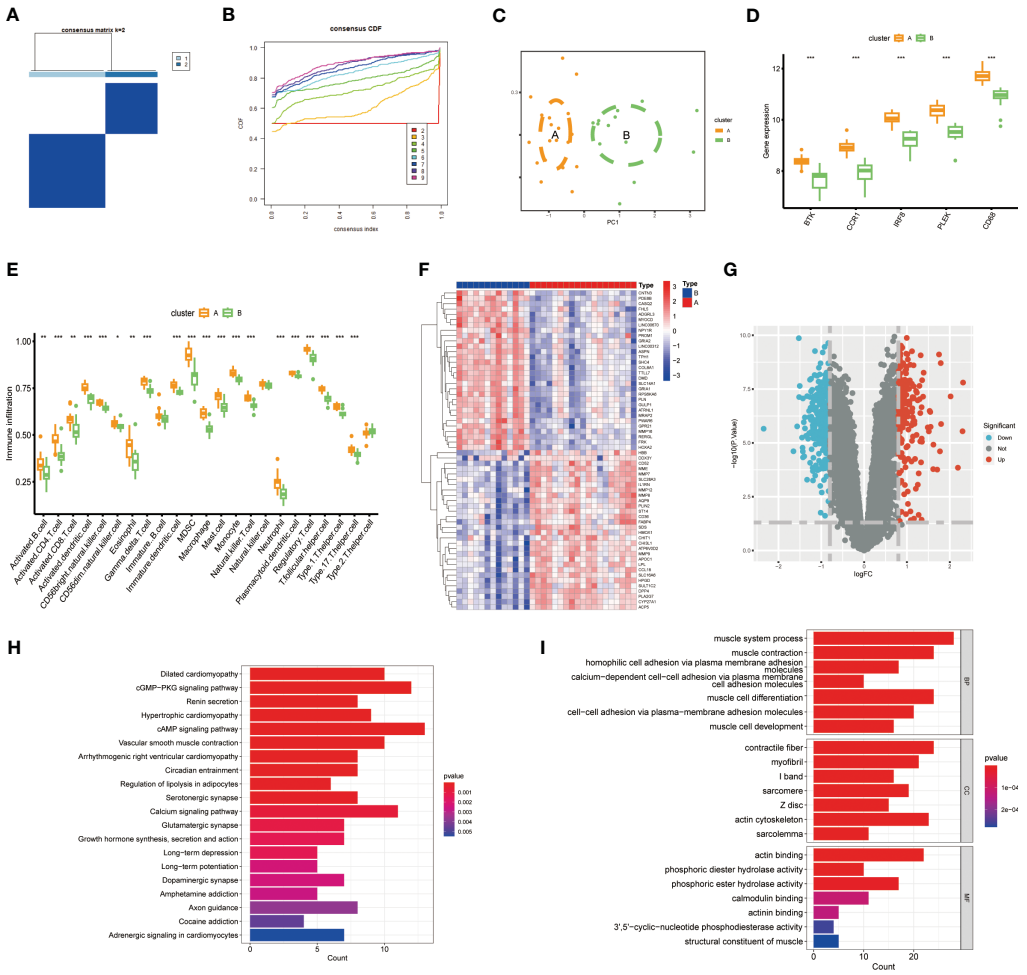

FIGURE 5
Constructing clusters of macrophages related to gut microbiota. **(A, B)** Clusters A and B were established using the NFM algorithm (consensus matrix k=2). **(C)** PCA analysis of Cluster A and Cluster B. **(D)** Expression of the top five genes between the two groups. **(E)** Expression of immune cells in Cluster A and Cluster B. **(F, G)** Results of differential analysis between Cluster A and Cluster B. **(H, I)** Pathway enrichment analysis of Cluster A-specifically expressed genes. (***$P < 0.001$).

10.3389/fcimb.2024.1395716

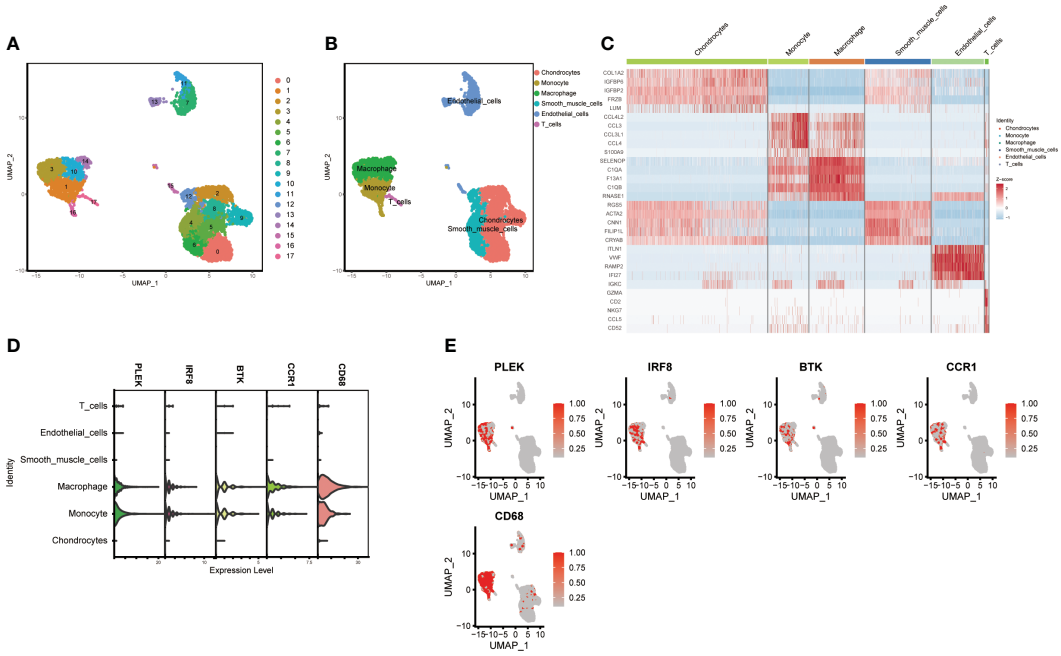

FIGURE 6
Single-cell subgroup annotation of atherosclerosis. **(A, B)** UMAP visualization of subgroup annotations. **(C)** Heatmap showing marker genes. **(D, E)** Expression of the top five gut microbiota-related macrophage genes in immune cells.

pathway enrichment analysis on the differentially expressed genes between the PLEK high and low groups, which significantly enriched in DNA-binding transcription activator activity and DNA-binding transcription factor binding (Figure 7D).

3.8 Validate the expression of PLEK in atherosclerosis samples and investigate its impact on the NFκB pathway

To validate the reliability of PLEK for diagnosing atherosclerosis patients, we collected samples from patients with atherosclerosis, including stable and unstable plaques (Figures 8A, B). PLEK expression was significantly higher in unstable plaques than in stable plaques (Figures 8C–E). Based on the results of Figure 7C, we found that PLEK might affect the NFκB signaling pathway. We stimulated RAW264.7 cells and PLEK-knockdown RAW264.7 cells with LPS and TNF-α to observe whether PLEK would influence the atherosclerosis process through the NFκB signaling pathway (Figure 8F). The results indicated that after the knockdown of PLEK, P65 and IκBα remained unchanged, while there was a significant downregulation of p-P65 expression (Figure 8G).

4 Discussion

Atherosclerosis, a complex and multifaceted disease, is characterized by the accumulation of lipids, inflammation, and fibrous thickening within the arterial walls, leading to vascular stenosis or occlusion and a heightened risk of cardiovascular events. Dysregulation of lipid metabolism, endothelial dysfunction, and infiltration of inflammatory cells synergistically contribute to plaque development. The rupture of an unstable plaque can precipitate thrombosis and trigger acute cardiovascular incidents. Current therapeutic approaches for atherosclerosis encompass pharmacological interventions aimed at mitigating plaque progression and enhancing vascular function. Early diagnosis is pivotal for effective prevention and management of this disease. Our research endeavors to identify and validate early biomarkers of atherosclerosis, facilitating timely interventions and improving patient outcomes. Macrophages, with their dualistic role, are instrumental in the pathogenesis of atherosclerosis, modulating the inflammatory milieu of plaques and thereby influencing disease progression (Tabas and Bornfeldt, 2020). The gut microbiota's intricate relationship with atherosclerosis is increasingly recognized, with dysbiosis potentially exacerbating lipid metabolism disorders and amplifying inflammatory responses. The interplay between the gut microbiota and macrophages is particularly intriguing, yet the specific contributions of gut microbiota-associated macrophage genes to atherosclerosis remain to be fully elucidated.Our study delves into the potential of gut microbiota and macrophages as significant factors in atherosclerosis, aiming to uncover novel insights into the disease's pathophysiology. By identifying and analyzing key genes associated with the gut microbiota and macrophage activity, we seek to unravel the underlying biological mechanisms and chart a course for innovative diagnostic and therapeutic strategies.

In our comparative analysis of gut microbiota-related gene set activities between normal carotid artery and atherosclerotic plaque samples, we discerned a pronounced elevation in the activities of

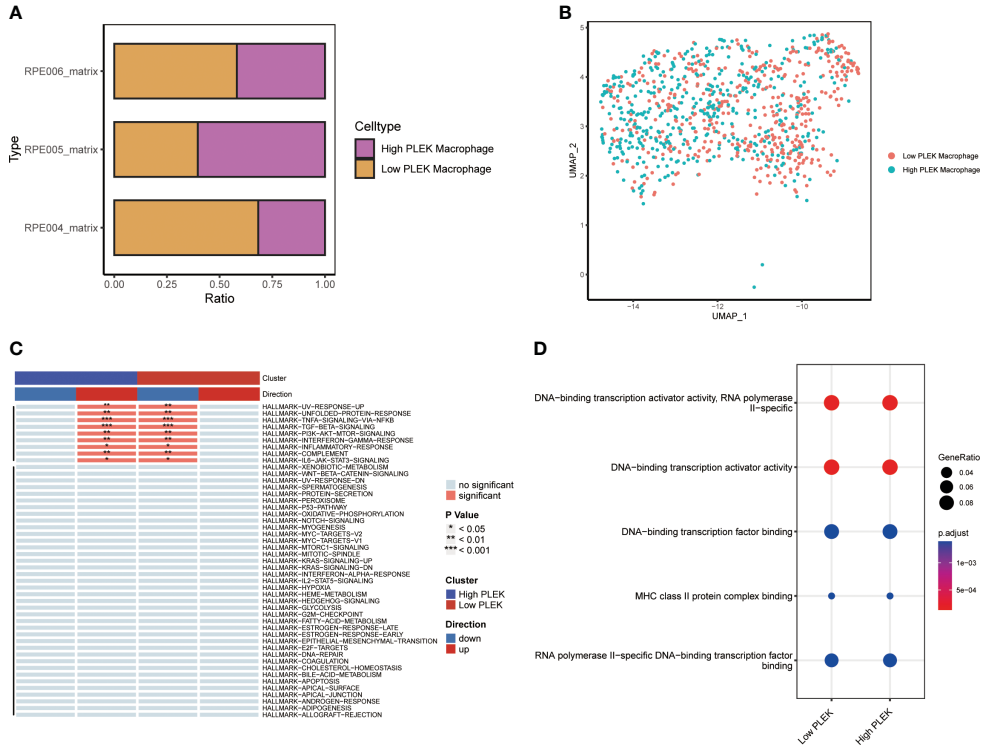

FIGURE 7
Single-cell level analysis of the impact of PLEK on macrophages. **(A, B)** Macrophages were divided into two groups based on PLEK expression and visualized using bar plots and UMAP. **(C)** Gene set enrichment analysis between high PLEK macrophage group and low PLEK macrophage group. **(D)** Pathway enrichment analysis between high PLEK macrophage group and low PLEK macrophage group.

HP_SMALL_INTESTINAL_DYSMOTILITY, HP_MELENA, HP_INTESTINAL_FISTULA, and GOBP_ENTERIC_NERVOUS_SYSTEM_DEVELOPMENT in the cohort with atherosclerotic plaque samples. This finding is corroborated by research highlighting the intimate connection between the progression of non-alcoholic fatty liver disease and disruptions in gut microbiota, as well as intestinal dysfunction (Leung et al., 2016), underscoring the burgeoning research potential in elucidating the interplay between gut microbiota and atherosclerosis. Conversely, the normal carotid artery group exhibited a notable increase in N_N_DIMETHYLANILINE_MONOOXYGENASE_ACTIVITY. Prior studies have posited that plasma TMAO levels do not correlate with the incidence of atherosclerosis but are markedly positively associated with unstable plaques (Koay et al., 2021). This discrepancy may suggest that TMAO within the arterial intima possesses distinct biological implications compared to its plasma counterpart, warranting further exploration into the nuanced roles of TMAO in the arterial wall's pathology.

In recent years, the Nomogram model has emerged as a reliable clinical diagnostic tool, demonstrating exceptional predictive accuracy and offering personalized diagnostic strategies for patients (Tong et al., 2023). Leveraging machine learning algorithms, we have identified PLEK, IRF8, BTK, CCR1, and CD68 as evaluative markers to assist in the diagnosis of atherosclerosis. Studies have reported a significant upregulation of PLEK in ulcerative colitis and rheumatoid arthritis (Chen et al., 2020). Sequence variants near the IRF8 gene have been implicated as key risk factors for inflammatory bowel disease and multiple sclerosis (Salem et al., 2020). BTK inhibitors, approved for the treatment of leukemia and lymphoma (Brullo et al., 2021), raise intriguing questions about their potential role in atherosclerosis patients. Our research has uncovered the specific expression of CCR1 in macrophages, paralleling the observed increase in CCR1 expression on inflammatory cells in patients with severe chronic obstructive pulmonary disease (COPD) (Nakano et al., 2018). CD68, a common macrophage marker, is well-documented in its association with a variety of inflammatory diseases, further substantiating its relevance in the context of atherosclerosis. At the single-cell level, we classified macrophage subpopulations based on the expression levels of the PLEK, dividing them into high PLEK-expression macrophages and low PLEK-expression macrophages around the median value. This stratification revealed a concomitant upregulation of TNFα-signaling-via-NFKB, IFNG response, and inflammatory response pathways in macrophages with heightened PLEK expression. Given the established role of macrophages in orchestrating inflammatory responses, which are critical in the pathophysiology of numerous immune-mediated conditions (Koelwyn et al., 2018), our bioinformatics findings lead us to hypothesize that increased PLEK expression on macrophages may potentiate their inflammatory profile.

In summary, this investigation harnesses a comprehensive suite of bioinformatics tools to uncover the intricate connections between the gut microbiota, macrophage function, and the pathogenesis of atherosclerosis, thereby contributing fresh perspectives to our understanding of this complex disease. Despite these

10.3389/fcimb.2024.1395716

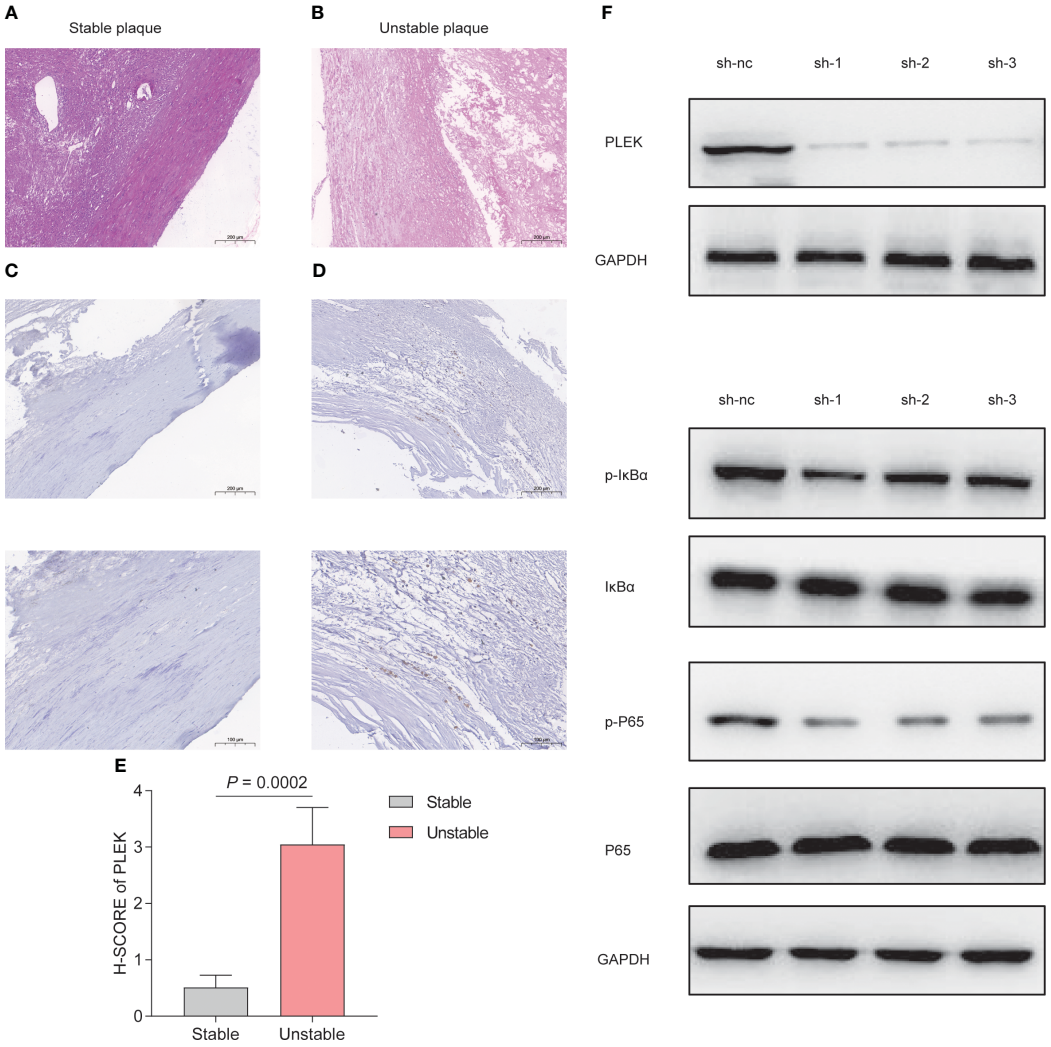

FIGURE 8
Experimental validation of PLEK. **(A, B)** HE staining showing stable atherosclerotic plaques and **(C)** expression of PLEK in stable and unstable atherosclerotic plaques. **(E)** H-SCORE of the two groups (P = 0.0002). **(F)** Validation of PLEK knockdown efficiency in RAW264.7 cells. **(G)** Western Blot detection of changes in p-P65, P65, p-IkBα, IkBα in RAW264.7 cells.

advancements, our study acknowledges limitations, such as the reliance on existing sequencing data, the finite scope of human sample cohorts, and the imperative for more profound exploration into the underlying biological mechanisms.

5 Conclusion

In summary, our study comprehensively examined the relationship between gut microbiota-associated macrophage genes and atherosclerosis, leading to the identification of pivotal genes. Subsequently, these key genes were subjected to an integrated analysis alongside immune cell dynamics, gut microbiota activity, and single-cell profiling. Ultimately, PLEK was revealed as a potential driver in the formation of unstable atherosclerotic plaques.

Data availability statement

The original contributions presented in the study are included in the article/Supplementary Material. Further inquiries can be directed to the corresponding author.

Ethics statement

The studies involving humans were approved by the University-Town Hospital of Chongqing Medical University LL-202213. The studies were conducted in accordance with the local legislation and institutional requirements. The participants provided their written informed consent to participate in this study.

Author contributions

YK: Writing – original draft, Visualization, Validation, Formal analysis, Conceptualization. JY: Writing – original draft, Supervision, Methodology, Conceptualization. HJ: Writing – review & editing, Methodology, Conceptualization. GL: Writing – review & editing, Supervision, Investigation, Conceptualization.

Funding

The author(s) declare that no financial support was received for the research, authorship, and/or publication of this article.

Acknowledgments

All authors acknowledge the contributions from the GEO dataset.

Conflict of interest

The authors declare that the research was conducted in the absence of any commercial or financial relationships that could be construed as a potential conflict of interest.

Publisher's note

Supplementary material

The Supplementary Material for this article can be found online at: https://www.frontiersin.org/articles/10.3389/fcimb.2024.1395716/full#supplementary-material

SUPPLEMENTARY FIGURE 1
GSE120521 validation of the expression of PLEK, IRF8, BTK, CCR1, and CD68.

References

Alcazar, C. G., Paes, V. M., Shao, Y., Oesser, C., Miltz, A., Lawley, T. D., et al. (2022). The association between early-life gut microbiota and childhood respiratory diseases: a systematic review. *Lancet Microbe* 3, e867–e880. doi: 10.1016/S2666-5247(22)00184-7

Alkarithi, G., Duval, C., Shi, Y., Macrae, F. L., and Ariens, R. (2021). Thrombus structural composition in cardiovascular disease. *Arterioscler. Thromb. Vasc. Biol.* 41, 2370–2383. doi: 10.1161/ATVBAHA.120.315754

Bailey, G., Meadows, J., and Morrison, A. R. (2016). Imaging atherosclerotic plaque calcification: translating biology. *Curr. Atheroscler Rep.* 18, 51. doi: 10.1007/s11883-016-0601-6

Brullo, C., Villa, C., Tasso, B., Russo, E., and Spallarossa, A. (2021). Btk inhibitors: A medicinal chemistry and drug delivery perspective. *Int. J. Mol. Sci.* 22. doi: 10.3390/ijms22147641

Camare, C., Pucelle, M., Negre-Salvayre, A., and Salvayre, R. (2017). Angiogenesis in the atherosclerotic plaque. *Redox Biol.* 12, 18–34. doi: 10.1016/j.redox.2017.01.007

Chen, Y., Li, H., Lai, L., Feng, Q., and Shen, J. (2020). Identification of common differentially expressed genes and potential therapeutic targets in ulcerative colitis and rheumatoid arthritis. *Front. Genet.* 11, 572194. doi: 10.3389/fgene.2020.572194

Crosara, K. T. B., Moffa, E. B., Xiao, Y., and Siqueira, W. L. (2018). Merging in-silico and in *vitro* salivary protein complex partners using the STRING database: A tutorial. *J. Proteomics* 171, 87–94. doi: 10.1016/j.jprot.2017.08.002

Danneskiold-Samsoe, N. B., Dias De Freitas Queiroz Barros, H., Santos, R., Bicas, J. L., Cazarin, C. B. B., Madsen, L., et al. (2019). Interplay between food and gut microbiota in health and disease. *Food Res. Int.* 115, 23–31. doi: 10.1016/j.foodres.2018.07.043

Jiang, X., Kuang, G., Gong, X., Jiang, R., Xie, T., Tie, H., et al. (2019). Glycyrrhetinic acid pretreatment attenuates liver ischemia/reperfusion injury via inhibiting TLR4 signaling cascade in mice. *Int. Immunopharmacol* 76, 105870. doi: 10.1016/j.intimp.2019.105870

Jonsson, A. L., and Backhed, F. (2017). Role of gut microbiota in atherosclerosis. *Nat. Rev. Cardiol.* 14, 79–87. doi: 10.1038/nrcardio.2016.183

Koay, Y. C., Chen, Y. C., Wali, J. A., Luk, A. W. S., Li, M., Doma, H., et al. (2021). Plasma levels of trimethylamine-N-oxide can be increased with 'healthy' and 'unhealthy' diets and do not correlate with the extent of atherosclerosis but with plaque instability. *Cardiovasc. Res.* 117, 435–449. doi: 10.1093/cvr/cvaa094

Koelwyn, G. J., Corr, E. M., Erbay, E., and Moore, K. J. (2018). Regulation of macrophage immunometabolism in atherosclerosis. *Nat. Immunol.* 19, 526–537. doi: 10.1038/s41590-018-0113-3

Leung, C., Rivera, L., Furness, J. B., and Angus, P. W. (2016). The role of the gut microbiota in NAFLD. *Nat. Rev. Gastroenterol. Hepatol.* 13, 412–425. doi: 10.1038/nrgastro.2016.85

Libby, P. (2021a). The changing landscape of atherosclerosis. *Nature* 592, 524–533. doi: 10.1038/s41586-021-03392-8

Libby, P. (2021b). Inflammation during the life cycle of the atherosclerotic plaque. *Cardiovasc. Res.* 117, 2525–2536. doi: 10.1093/cvr/cvab303

Ma, S. R., Tong, Q., Lin, Y., Pan, L. B., Fu, J., Peng, R., et al. (2022). Berberine treats atherosclerosis via a vitamine-like effect down-regulating Choline-TMA-TMAO production pathway in gut microbiota. *Signal Transduct Target Ther.* 7, 207. doi: 10.1038/s41392-022-01027-6

Mangge, H., and Almer, G. (2019). Immune-mediated inflammation in vulnerable atherosclerotic plaques. *Molecules* 24. doi: 10.3390/molecules24173072

Nakano, H., Kirino, Y., Takeno, M., Higashitani, K., Nagai, H., Yoshimi, R., et al. (2018). GWAS-identified CCR1 and IL10 loci contribute to M1 macrophage-predominant inflammation in Behcet's disease. *Arthritis Res. Ther.* 20, 124. doi: 10.1186/s13075-018-1613-0

Salem, S., Salem, D., and Gros, P. (2020). Role of IRF8 in immune cells functions, protection against infections, and susceptibility to inflammatory diseases. *Hum. Genet.* 139, 707–721. doi: 10.1007/s00439-020-02154-2

Schroeder, M. P., Gonzalez-Perez, A., and Lopez-Bigas, N. (2013). Visualizing multidimensional cancer genomics data. *Genome Med.* 5, 9. doi: 10.1186/gm413

Sterpetti, A. V. (2020). Inflammatory cytokines and atherosclerotic plaque progression. Therapeutic implications. *Curr. Atheroscler Rep.* 22, 75. doi: 10.1007/s11883-020-00891-3

Tabas, I., and Bornfeldt, K. E. (2020). Intracellular and intercellular aspects of macrophage immunometabolism in atherosclerosis. *Circ. Res.* 126, 1209–1227. doi: 10.1161/CIRCRESAHA.119.315939

Tong, C., Miao, Q., Zheng, J., and Wu, J. (2023). A novel nomogram for predicting the decision to delayed extubation after thoracoscopic lung cancer surgery. *Ann. Med.* 55, 800–807. doi: 10.1080/07853890.2022.2160490

Vergallo, R., and Crea, F. (2020). Atherosclerotic plaque healing. *N Engl. J. Med.* 383, 846–857. doi: 10.1056/NEJMra2000317

Wang, Y., Zhuang, H., Jiang, X. H., Zou, R. H., Wang, H. Y., and Fan, Z. N. (2023). Unveiling the key genes, environmental toxins, and drug exposures in modulating the severity of ulcerative colitis: a comprehensive analysis. *Front. Immunol.* 14, 1162458. doi: 10.3389/fimmu.2023.1162458

Wei, Y., Lan, B., Zheng, T., Yang, L., Zhang, X., Cheng, L., et al. (2023). GSDME-mediated pyroptosis promotes the progression and associated inflammation of atherosclerosis. *Nat. Commun.* 14, 929. doi: 10.1038/s41467-023-36614-w

Wolf, D., and Ley, K. (2019). Immunity and inflammation in atherosclerosis. *Circ. Res.* 124, 315–327. doi: 10.1161/CIRCRESAHA.118.313591

Wu, W., Wang, X., Le, W., Lu, C., Li, H., Zhu, Y., et al. (2022). Immune microenvironment infiltration landscape and immune-related subtypes in prostate cancer. *Front. Immunol.* 13, 1001297. doi: 10.3389/fimmu.2022.1001297

frontiers | Frontiers in Cellular and Infection Microbiology

TYPE Original Research
PUBLISHED 30 April 2024
DOI 10.3389/fcimb.2024.1379831

OPEN ACCESS

EDITED BY
Gang Ye,
Sichuan Agricultural University, China

REVIEWED BY
Dan Yang,
Yibin Vocational and Technical College, China
Jianan Zhao,
Shanghai Guanghua Rheumatology Hospital, China

*CORRESPONDENCE
Xiang Liu
lcyx58214813@163.com

†These authors have contributed equally to this work

RECEIVED 31 January 2024
ACCEPTED 27 March 2024
PUBLISHED 30 April 2024

CITATION
Liu Z, Huang Y, Hu C and Liu X (2024) The impact of Sangju Qingjie Decoction on the pulmonary microbiota in the prevention and treatment of chronic obstructive pulmonary disease.
Front. Cell. Infect. Microbiol. 14:1379831.
doi: 10.3389/fcimb.2024.1379831

The impact of Sangju Qingjie Decoction on the pulmonary microbiota in the prevention and treatment of chronic obstructive pulmonary disease

Zheng Liu[1†], Ying Huang[2†], Chao Hu[3] and Xiang Liu[1*]

[1]Clinical Pharmacy, Xiangtan Center Hospital, Xiangtan, Hunan, China, [2]Pulmonary and Critial Care Medicine, Zhongshan Hospital of Traditional Chinese Medicine, Zhongshan, Guangdong, China, [3]Pulmonary and Critial Care Medicine, Xiangtan Center Hospital, Xiangtan, Hunan, China

Objective: Exploring the effect of SJQJD on the pulmonary microbiota of chronic obstructive pulmonary disease (COPD) rats through 16S ribosomal RNA (rRNA) sequencing.

Methods: A COPD rat model was constructed through smoking and lipopolysaccharide (LPS) stimulation, and the efficacy of SJQJD was evaluated by hematoxylin and eosin (H&E) staining and Enzyme-Linked Immunosorbnent Assay (ELISA). The alveolar lavage fluid of rats was subjected to 16S rRNA sequencing. The diversity of lung microbiota composition and community structure was analyzed and differential microbiota were screened. Additionally, machine learning algorithms were used for screening biomarkers of each group of the microbiota.

Results: SJQJD could improve lung structure and inflammatory response in COPD rats. 16s rRNA sequencing analysis showed that SJQJD could significantly improve the abundance and diversity of bacterial communities in COPD rats. Through differential analysis and machine learning methods, potential microbial biomarkers were identified as *Mycoplasmataceae*, *Bacillaceae*, and *Lachnospiraceae*.

Conclusion: SJQJD could improve tissue morphology and local inflammatory response in COPD rats, and its effect may be related to improve pulmonary microbiota.

KEYWORDS

SJQJD, COPD, pulmonary microbiota, biomarker, machine learning

Abbreviations: SJQJD, Sangju Qingjie Decoction; COPD, Chronic Obstructive Pulmonary Disease; AECOPD, Acute Exacerbation of Chronic Obstructive Pulmonary Diseases; LPS, Lipopolysaccharide; H&E, Hematoxylin and Eosin; IL-6, Interleukin 6; IL-8, Interleukin 8; MMP-2, Matrix Metallopeptidase 2; MMP-3, Matrix Metallopeptidase 3; sIgA, secretory Immunoglobulin A; TNF-α, Tumor Necrosis Factor α; OTUs, Operational Taxonomic Units; LEfSe, Linear discriminant analysis effect size; ELISA, Enzyme-Linked Immunosorbnent Assay; LDA, Linear Discriminant Analysis; FVC, Forced Vital Capacity; FEV1, Forced Expiratory Volume in the 1st second; SCFAs, Short-Chain Fatty Acids.

1 Introduction

COPD is a common respiratory disease in clinical practice, and its risk factors include advancing age, long-term smoke irritation, high incidence, and mortality, with continuous airflow restriction being the main pathological characteristic. Relevant statistics (Fang et al., 2018) show that there are approximately 100 million patients with COPD and increasing incidences of COPD in China. According to the World Health Organization, COPD may become the third leading cause of mortality worldwide by 2030 (Kim et al., 2021). Acute exacerbation of COPD (AECOPD) refers to a clinical event characterized by worsening of respiratory symptoms in patients with COPD, leading to changes in symptoms beyond the daily variation range and drug treatment regimens, which is critical for treating COPD disease. This results in reduced quality of life of patients, accelerated decline of lung function, and increased mortality rate of hospitalized patients (Baqdunes et al., 2021; Celli et al., 2021). Presently, there is no effective treatment for AECOPD; therefore, exploring effective prevention and treatment of COPD is one of the most urgent demands of the medical field worldwide.

The respiratory tract constantly exchanges gases with the environment; hence, it is also a system with bacterial colonization. Studies on respiratory microbiota remain in the initial stages. Reportedly, the pulmonary microbiota is closely related to the host's autoimmune function and participates in the regulation of the immune microenvironment (Cao et al., 2023; Wu et al., 2023). The lungs were presumed to be sterile in healthy individuals; however, owing to the continuous development of medical science and technology, 16S rRNA sequencing has revealed microbial communities detected in the lungs of healthy individuals (Ramsheh et al., 2021; Yagi et al., 2021). The human microbiome includes all forms of microorganisms and their genomes residing within the body of an individual at a specific time, such as in the gut and other mucosal surfaces including the skin, mouth, airways, and vagina (Anand and Mande, 2018, Shi et al., 2021). Ecological imbalance refers to any compositional changes in the microbiome compared with that of healthy individuals (Shi et al., 2021). The low diversity of microbial communities indicates ecological imbalance (Valdes et al., 2018), whereas high diversity is often associated with health and temporal stability (Leitao Filho et al., 2019; Vaughan et al., 2019; Shi et al., 2021).

SJQJD is a medicinal formulation composed of 30 g of *mori cortex*, 15 g of *chrysanthemi indici flos*, 40 g of *semen benincasae*, 20 g of *trichosanthis pericarpium*, 20 g of *pheretima*, 20 g of *fritillariae cirrhosae bulbus*, 50 g of *phragmitis rhizoma*, 150 g of *plantaginis semen*, 20 g of *concretio silicea bambusae*, and 10 g of *glycyrrhizae radix et rhizoma*. SJQJD exerts considerable clinical effects on patients with COPD presenting phlegm-heat obstructing lung (Yee et al., 2022); however, the specific mechanism underlying SJQJD-mediated treatment of COPD remains unclear. Herein, we constructed a COPD rat model and investigated the effects of SJQJD on the pulmonary microbiota of COPD rats through 16S rRNA sequencing. Modern pharmacology indicates that the extract of *mori cortex* has a regulatory effect on oxidative stress (Zhai et al., 2022), *chrysanthemi indici flos, trichosanthis pericarpium, pheretima, fritillariae cirrhosae bulbus, phragmitis rhizoma* all exhibit anti-inflammatory activity (Park et al., 2016; Liu et al., 2020; Tian et al., 2020; Li et al., 2022; Liu et al., 2024), *plantaginis semen* has the function of regulating lipid metabolism and immune response (Sun et al., 2019; Ren et al., 2021), *glycyrrhizae radix et rhizoma* has anti-inflammatory and detoxifying effects (Li et al., 2019; Jiang et al., 2022). These physiological processes are involved in various stages of physiological pathology. However, there is currently limited research by *semen benincaae* and *concretio silicea bambusae*.

2 Methods

2.1 SJQJD preparation

SJQJD is an internal preparation of Zhongshan Traditional Chinese Medicine Hospital (specific lot number: Guangdong Medicine Preparation Z20071015). All traditional Chinese medicine decoction pieces are provided by the Chinese Pharmacy of Zhongshan Traditional Chinese Medicine Hospital, and identified as qualified authentic products by Deputy Chief Pharmacist He Jianhong. The abovementioned 10 herbs were soaked in water for 30 minutes, and the decoction treatment was performed twice for 1.5 hours. Both decoctions were combined, filtered, concentrated, and added with 200 g of sugar, 3 g of sodium benzoate, and 0.5 g of hydroxyethyl ester. The mixture was boiled and brought to a constant volume of 1 L. Following this, it was allowed to stand for 1 day, and the supernatant was isolated and packaged to complete the preparation.

2.2 Animal experiments

Experimental grouping: Specific pathogen free grade 10 week old Wistar male rats (250 ± 20), purchased from Spelford Beijing Biotechnology Co., Ltd. In total, 30 rats were randomly divided into the following five groups (n = 6): control, model, model + SJQJD (high-dose [H]: 1.2 g/mL), model + SJQJD (medium-dose [M]: 0.8 g/mL), and model + SJQJD (low-dose [L]: 0.6 g/mL) groups.

Animal model construction: Both cigarette smoke exposure and lipopolysaccharide (LPS) intratracheal instillation were used to establish the COPD model, as follows: (1) LPS intratracheal instillation: 0.2 mL of LPS solution (1 mg/mL) was instilled into the airway on the 1st and 14th day of modeling; and (2) smoking: from day 2 to 28, rats were transferred to a dedicated disinfection box and exposed to smoke daily (except for day 14), 10 cigarettes per time for 30 minutes, twice a day in the morning and afternoon.

Medication intervention: The control group was not subjected to LPS intratracheal instillation and smoking procedures and was administered 2.5 mL of physiological saline by gavage every day; the model group was administered 2.5 mL of physiological saline by gavage every day; the administration groups were orally administered 2.5 mL of SJQJD (H, M, and L) every day. The alveolar lavage fluids and lung tissues of rats were retrieved after administration for subsequent experiments.

2.3 H&E staining experiment

The retrieved lung tissues were fixed with 10% formaldehyde solution. Following this, the tissues were cut into 2-mm thick tissue blocks, which were then dehydrated using gradient ethanol, made transparent using xylene, and embedded in paraffin. Next, the tissue blocks were cut into 5-μm thick slices, stained with H&E, and sealed with neutral gum. The morphology of the lung tissues was observed under a microscope and their photos were captured.

2.4 ELISA testing

The alveolar lavage fluids of rats were centrifuged at 4°C at 1800 r/min for 5 minutes, and the supernatants were collected for detection. Next, ELISA was performed to detect interleukin (IL)-6, IL-8, matrix metallopeptidase (MMP)-2, MMP-3, secretory immunoglobulin (sIg)A, and tumor necrosis factor (TNF)-α in the supernatant of the alveolar lavage fluid according to the instructions of the kit (JiangLai, China).

2.5 16S rRNA sequencing and bioinformatics analyses

The 16s rRNA sequencing was performed by Shenzhen Weikemeng Technology Group Co., Ltd. using the experimental alveolar lavage fluid, including DNA extraction, polymerase chain reaction-mediated amplification, and Illumina high-throughput sequencing. Bioinformatics analyses were performed using the Wekemo Bioincloud (https://www.bioincloud.tech). Operational taxonomic units (OTUs) were clustered with 97% consistency, and the sequences of OTUs were annotated with species to obtain the corresponding species information and species-based abundance distribution. Additionally, α-diversity analysis was performed utilizing the following evaluation indexes: Chao1 index for evaluating microbial abundance, and Shannon and Simpson indexes for evaluating microbial evenness and abundance. Furthermore, β-diversity was analyzed to compare the diversity among different ecosystems, and cluster analysis was performed on the sample distance matrix to construct a hierarchical visualization of differences among samples. Linear discriminant analysis effect size (LEfSe) analysis was performed to test the significance of differences in species composition and community structure of the grouped samples, further analyzing the microbiome composition of the two groups at the phylum and genus levels, and determining the species abundances with significant differences. Finally, the characteristic microbial communities of each group were screened using machine-learning methods.

2.6 Statistic analyses

The GraphPad Prism 9.0 software was used to process data and visualize the data. The comparison between two groups was conducted using t-test method, the comparison between three groups was conducted using one-way ANOVA test method, and the comparison between three groups that did not follow a normal distribution was conducted using Kruskal Wallis test. The *P*-value of < 0.05 was considered statistically significant.

3 Results

3.1 SJQJD improves the lung tissue morphology in COPD rats

The tissue morphology of the control group was intact with no notable inflammatory cell infiltration (Figure 1); however, that of the COPD model group was disordered, with considerable detectable inflammatory cell infiltration and epithelial goblet cell proliferation, indicating the successful establishment of the model. In the SJQJD-H group of rats, a few inflammatory cells were observed in the lung tissue, along with an enlargement of the alveolar spaces. The SJQJD-M group of rats showed reduced aggregation of inflammatory cells in the lung tissue, with some increase in the alveolar septa and inflammatory cell infiltration. The SJQJD-L group of rats demonstrated moderate interstitial inflammatory changes in the lung tissue, along with the widening of the alveolar septa and inflammatory cell infiltration.

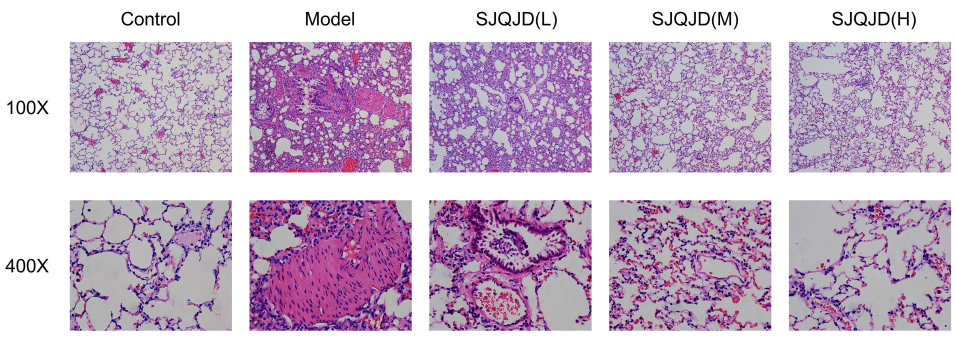

FIGURE 1
SJQJD improved COPD in rats.

3.2 SJQJD inhibited the release of inflammatory factors in COPD rats

ELISA was performed to detect the content of inflammatory factors in the alveolar lavage fluid. The results showed that compared with the control group, the levels of IL-6 ($P < 0.0001$), IL-8 ($P < 0.0001$), MMP-2 ($P < 0.0001$), MMP-3 ($P < 0.0001$), sIgA ($P < 0.0001$), and TNF-α ($P < 0.0001$) in the model group increased considerably, whereas SJQJD (H, M, and L) suppressed their increase in a concentration-dependent manner (Figure 2).

3.3 Analysis of the effects of SJQJD on the pulmonary microbiota

The composition structures of the lung microbiota of each group of rats were analyzed at the phylum and genus levels through 16S RNA high-throughput sequencing to explore the effects of SJQJD. At the phylum level, the composition of *Tenericutes* notably increased in the model group and considerably decreased in the control and SJQJD groups. In contrast, the compositions of *Proteobacteria, Actinobacteria, Unspecified_Bacteria*, and *Firmicutes* considerably decreased in the model group and markedly increased in the control and SJQJD groups (Figures 3A, B). At the genus level, the composition of *Mycoplasmataceae* considerably increased in the model group and markedly decreased in the control and SJQJD groups. In contrast, the composition of *Streptomycetaceae, Enterobacteriaceae, Microbacteriaceae*, and *Bacillaceae* markedly decreased in the model group and notably increased in the control and SJQJD groups (Figures 3C, D).

3.4 Analyses of α- and β-diversities

Compared with the control rats, the α-diversity indexes, namely Chao1 ($P = 0.0397$), Shannon ($P = 0.0030$), and Simpson ($P = 0.0021$) indexes, of COPD rats were markedly reduced (Figures 4A–C), suggesting a decrease in both microbial abundance and diversity under COPD conditions. SJQJD reversed the decrease in the aforementioned three indexes, demonstrating its therapeutic effects on COPD rats. β-diversity distance measurements, performed to study the structural changes of the pulmonary microbiota among samples, showed notable differences in the microbial communities of control and COPD rats (Figure 4D). However, the SJQJD administration reversed this phenomenon.

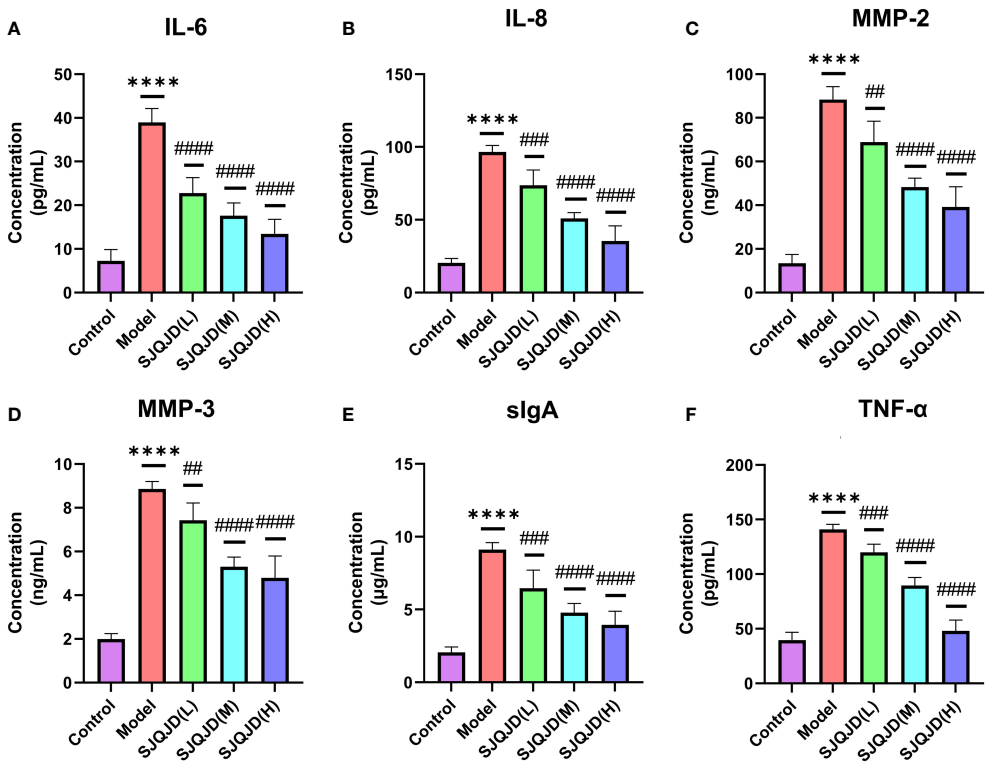

FIGURE 2
SJQJD improved pulmonary inflammatory response. The level of **(A)** IL-6, **(B)** IL-8, **(C)** MMP-2, **(D)** MMP-3, **(E)** sIgA, and **(F)** TNF- α in rat alveolar lavage fluid. The data was displayed as the mean ± SD (n=6). # $P < 0.05$, ## $P < 0.01$, ### $P < 0.001$, #### $P < 0.0001$, * $P < 0.05$, ** $P < 0.01$, *** $P < 0.001$, **** $P < 0.0001$.

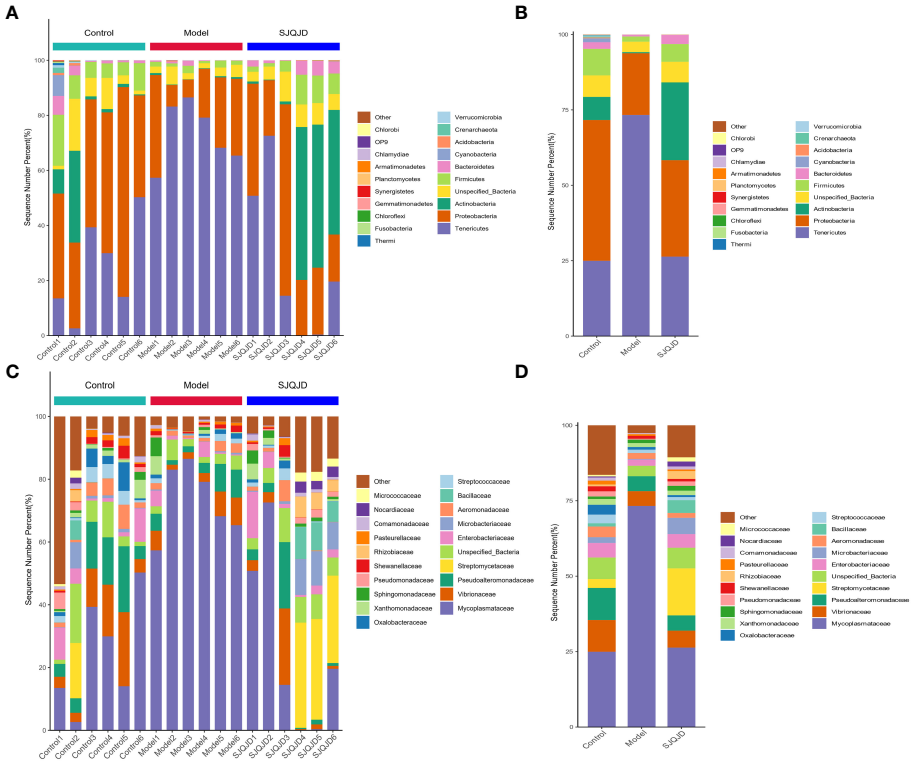

FIGURE 3
Stacking diagram of the relative abundance of microbial communities. **(A)** The relative abundance of microbial communities at the phylum level in each sample. **(B)** The relative abundance of microbial communities at the phylum level in each group. **(C)** The relative abundance of microbial communities at the genus level in each sample. **(D)** The relative abundance of microbial communities at the genus level in each group.

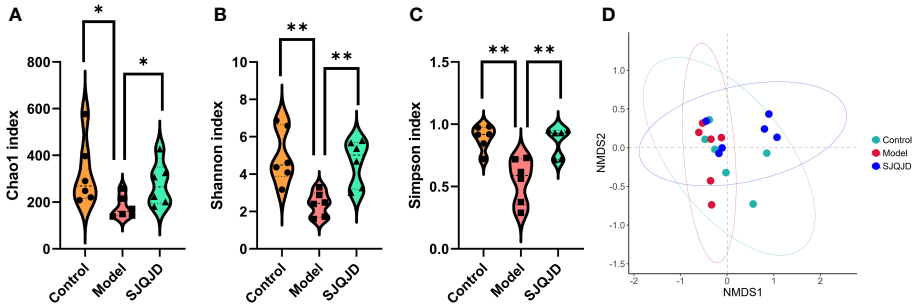

FIGURE 4
SJQJD improved the diversity of lung microbiota. **(A)** Chao1 index. **(B)** Shannon index. **(C)** Simpson index. **(D)** NMDS. * $P < 0.05$, ** $P < 0.01$.

3.5 Analysis of dominant microbial communities in each group

The bacterial taxa with statistically significant differences among the groups were identified based on the Linear Discriminant Analysis (LDA) value, and the results were visualized by creating a LefSe cladogram (Figure 5A) and a histogram of LDA values (Figure 5B). *Actinobacteria*, *Phyllobacteriaceae*, and *Alphaproteobacteria* were the dominant bacterial taxa in the control group, whereas *Mycoplasmatales*, *Mycoplasmataceae*, *Tenericutes*, and *Mollicutes* were the dominant taxa in the model group. *Proteobacteria*, *Gammaproteobacteria*, *Weeksellaceae*, and others were characteristic taxa for the SJQJD group.

3.6 Analysis of species differences in the pulmonary microbiota

The differences in bacterial communities among groups were analyzed at different levels, such as the family level. The results suggest that compared with the control group, the composition of families *Peptostreptococcaceae*, *Mycoplasmataceae*, *Rikenellaceae*, *Listeriaceae*, and *Ruminococcaceae* considerably increased in the

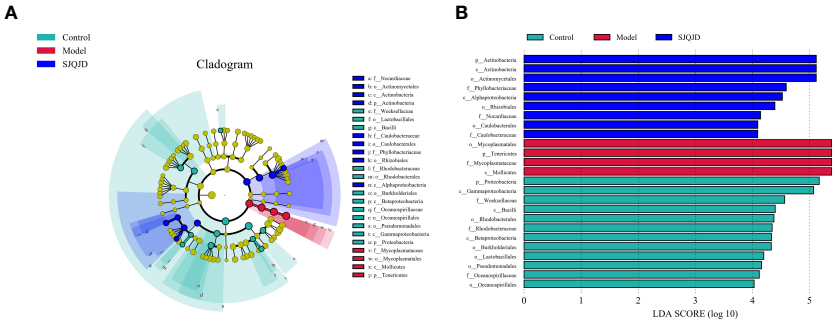

FIGURE 5
Analysis results of the dominant microbial communities in each group. **(A)** The branch diagram was obtained through LEfSe analysis. **(B)** LDA effect size analysis of major biomarker taxonomic groups.

model group, whereas that of *Chthoniobacteraceae, Streptomycetaceae*, and *Enterococcaceae* markedly reduced (Figures 6A, B). Compared with the model group, the composition of families such as *Bacillaceae, Nocardiaceae*, and *Micrococcaceae* notably increased in the SJQJD group, whereas that of *Listeriaceae, Clostridiaceae, Campylobacteraceae*, and *Mycoplasmataceae* considerably reduced (Figures 6A, C). Notably, the abundance of the family *Mycoplasmataceae* (P = 0.0021) was considerably increased in the model group, whereas it remained low in both the control and SJQJD groups, suggesting its potential as a therapeutic marker (Figure 6D). Although there were no statistically significant differences in *Bacillaceae* abundance among the groups, we observed that this family was almost absent in the model group but exhibited high abundances in both the control and SJQJD groups, suggesting its possible protective role in the disease (Figure 6E).

3.7 Machine-learning method-based screening of biomarkers

The markers in the microbiota of each group were further screened through machine learning. The results show that characteristic microbes of the control group obtained using the random forest algorithm included *Lachnospiraceae, Enterococcaceae*, and *Staphylococcaceae*, whereas the model group featured *Mycoplasmataceae, Pasteurellaceae*, and *Aeromonadaceae*. The characteristic microbes of the SJQJD group included Nocardiaceae, Lachnospiraceae, and *Burkholderiaceae* (Figures 7A, B; Table 1). Additionally, the characteristic microbes of the control group obtained using the support vector machine algorithm included *Rhodobacteraceae, Lachnospiraceae*, and *Moraxellaceae*; those of the model group included Campylobacteraceae and *Moraxellaceae*, and

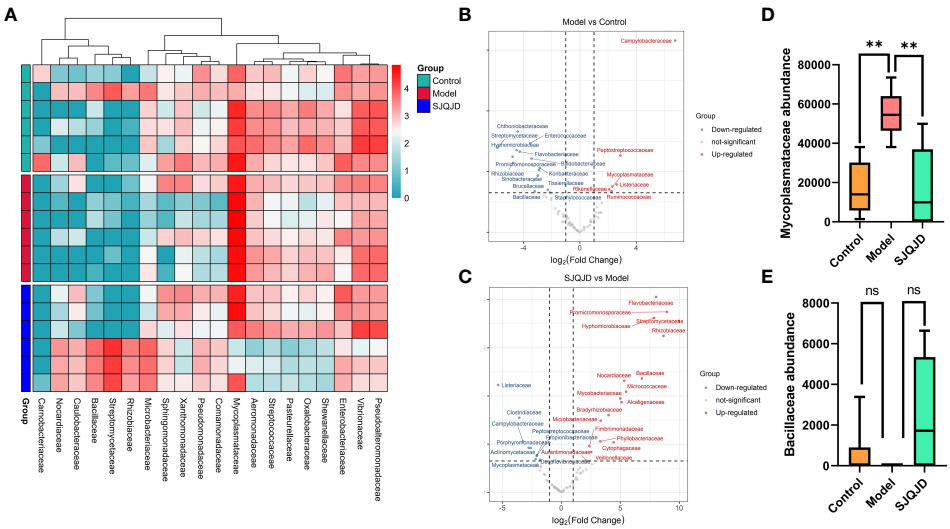

FIGURE 6
Analysis results of species differences in pulmonary microbiota. **(A)** Heatmap of differential microbial communities among groups. **(B)** Volcano diagram of Model vs. Control. **(C)** Volcano diagram of SJQJD vs. Model. **(D)** The abundance of *Mycoplasmataceae* in three groups. **(E)** The abundance of *Bacillaceae* in the three groups. ** P < 0.01, ns, no significant.

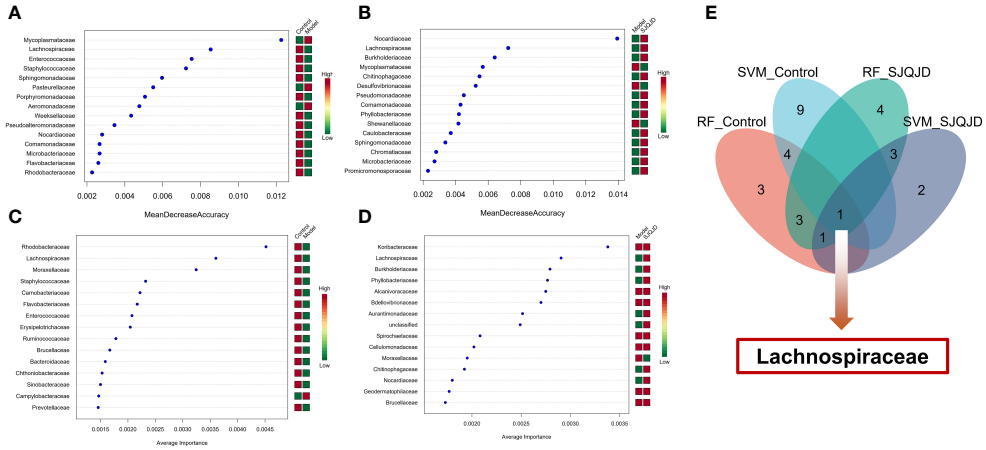

FIGURE 7
Machine learning screening of microbial biomarkers. **(A, B)** The results of RF method screening for characteristic microbial communities. **(C, D)** The results of SVM method screening for characteristic microbial communities. **(E)** Intersection results of feature microbial communities selected by machine learning.

those of the SJQJD group included *Lachnospiraceae, Burkholderiaceae*, and *Phyllobacteriaceae* (Figures 7C, D; Table 1). By intersecting the results, we found the family *Lachnospiraceae* to be a common marker between the control and SJQJD groups (Figure 7E).

TABLE 1 Machine learning screening of characteristic microbial communities in each group.

Group	RF	SVM
Control	*Lachnospiraceae* *Enterococcaceae* *Staphylococcaceae* *Sphingomonadaceae* *Porphyromonadaceae* *Weeksellaceae* *Pseudoalteromonadaceae* *Nocardiaceae* *Comamonadaceae* *Microbacteriaceae* *Flavobacteriaceae* *Rhodobacteraceae*	*Rhodobacteraceae* *Lachnospiraceae* *Moraxellaceae* *Staphylococcaceae* *Carnobacteriaceae* *Flavobacteriaceae* *Enterococcaceae* *Erysipelotrichaceae* *Ruminococcaceae* *Brucellaceae* *Bacteroidaceae* *Chthoniobacteraceae* *Sinobacteraceae* *Prevotellaceae*
Model	*Mycoplasmataceae* *Pasteurellaceae* *Aeromonadaceae* *Desulfovibrionaceae* *Shewanellaceae*	*Campylobacteraceae* *Moraxellaceae*
SJQJD	*Nocardiaceae* *Lachnospiraceae* *Burkholderiaceae* *Chitinophagaceae* *Pseudomonadaceae* *Comamonadaceae* *Phyllobacteriaceae* *Caulobacteraceae* *Sphingomonadaceae* *Chromatiaceae* *Microbacteriaceae* *Promicromonosporaceae*	*Lachnospiraceae* *Burkholderiaceae* *Phyllobacteriaceae* *Aurantimonadaceae* *unclassified* *Chitinophagaceae* *Nocardiaceae*

4 Discussion

COPD is a chronic inflammatory disease characterized by persistent restriction of the small airways, and it often affects multiple systems. Studies predict that because of the increasing number of smokers and population aging, the annual COPD-associated mortality and number of patients may exceed 5.4 million (GBD 2017 Causes of Death Collaborators, 2018) by the 2060s. Acute exacerbation, leading to frequent medical visits, hospitalizations, and changes in medication regimens, is a major cause of mortality in patients with COPD (Wu et al., 2014; Vogelmeier et al., 2017; Hua et al., 2020; Li et al., 2021). Microbial cultures indicate that the lung microbiota is related to COPD pathogenesis (Shi et al., 2021), and the advances in metagenomic technologies have further validated this conclusion (Karakasidis et al., 2023).

SJQJD is a hospital-prepared medication formulation reviewed by the drug regulatory authority. Clinical studies have shown the good therapeutic effects of SJQJD when used in combination with Western medicine to treat phlegm-heat obstructed lung-type community-acquired pneumonia. Reportedly, the combined treatment of SJQJD with Western medicine for bronchiectasis can effectively improve the lung function, forced vital capacity (FVC), forced expiratory volume in the 1st second (FEV1), and FEV1/FVC levels of the patients, with a total effective rate of 97.50%, compared with 85.00% in the control group ($P < 0.05$) (Dong et al., 2018). Additionally, clinical research on patients with phlegm-heat congested lung-type AECOPD has shown (Huang et al., 2021) that after treatment with SJQJD in combination with Western medicine, the T lymphocyte subgroup cluster of differentiation (CD)4$^+$ and the CD4$^+$/CD8$^+$ ratio increased, compared with those before the treatment, and CD8$^+$ reduced, indicating the significantly better optimization in the combined treatment group than that in the Western medicine control group ($P < 0.05$). This suggested that SJQJD might improve the immune function of patients, thereby enhancing their resistance. These findings imply that SJQJD may exert its therapeutic effect on COPD by altering

the lung microenvironment and consequently modulating the lung microbiota.

Herein, a COPD rat model was constructed through a combined approach of cigarette smoke exposure and intratracheal LPS instillation, which is a widely used model for COPD. The COPD model group showed structural disorder with considerable inflammatory cell infiltration and epithelial goblet cell proliferation. However, the SJQJD administration reversed these phenomena, indicating its interventional effects on COPD. Moreover, SJQJD improved pulmonary inflammation.

The lung microbiome plays an important role in maintaining stability within the lungs. The airways of patients with COPD often harbor *Haemophilus influenzae*, *Streptococcus pneumoniae*, and *Moraxella catarrhalis*, which in severe cases can be colonized by *Klebsiella pneumoniae*, *Pseudomonas aeruginosa*, and other *Gram-negative bacteria*. Various factors affect the composition of the respiratory microbiota, including the anatomy of the airways, gender, age, and the immune function of the host (Whiteside et al., 2021). In healthy individuals, the lung microbiota is transient and can be regulated by normal lung defense mechanisms, such as bronchial epithelial cilia movements, coughing, and the immune function of the host. Under healthy conditions, the regional growth conditions generally do not support the extensive proliferation of bacteria, resulting in relatively fewer bacteria. However, inflammatory responses increase the vascular permeability of the airways, providing abundant nutrients, such as amino acids, vitamins, carbon sources, and iron, for bacterial reproduction. Inflammation damages epithelial cells, exposing the basement membrane matrix and promoting bacterial adhesion. Similar to the gut microbiota, dysbiosis of the lung microbiota promotes the persistent progression of COPD (Bowerman et al., 2020). Reduced microbial diversity has been associated with COPD exacerbation events (Sze et al., 2012; Wang et al., 2019; Enaud et al., 2020; Su et al., 2022). Herein, the results showed that the microbial abundance and diversity in the COPD model group were significantly reduced, and SJQJD could considerably reverse this phenomenon, suggesting its role in improving the lung microbiota.

The family *Mycoplasmataceae* includes prokaryotic bacteria such as *Mycoplasma* and *genital Ureaplasma* that are pathogenic to humans (Wood et al., 2021). Reportedly, *mycoplasmas* are one of the common pathogens in patients with COPD (14%) (Lieberman et al., 2001, 2002). *Mycoplasmas* can evade the host immune system, induce apoptosis, generate free radicals, and cause oxidative-reductive imbalance in the cellular glutathione potential through pro-inflammatory cytokines, thus leading to AECOPD (Sessa et al., 2009; Papaetis et al., 2010). The family *Bacillaceae* includes *rod-shaped, endospore-forming, Gram-positive bacteria* (Liu et al., 2015). They are widely found in nature, including both pathogenic and beneficial strains (Hathout et al., 2000). However, their specific role in COPD remains unelucidated. Reportedly, the increase of *Bacillus* in the mouse lungs can aggravate local inflammatory response, resulting in more severe pulmonary emphysema (Richmond et al., 2018), which suggests that *Bacillus* may be a risk factor for COPD. Moreover, a considerably higher population of *Bacillaceae* has been reported in the rat lungs treated with particulate matter 2.5, a COPD-inducing factor, compared with that in the control (Laiman et al., 2023). Furthermore, lower levels of *Bacillus* have been detected in the sputum of patients with COPD (Simpson et al., 2016), indicating that *Bacillus* may play a protective role in COPD. The results of this study indicated a low abundance of *Bacillaceae* in the COPD model, whereas it was considerably higher in the control and SJQJD treatment groups, suggesting that *Bacillaceae* may have a role in combating COPD. Reportedly, most members of the *Lachnospiraceae* family in the gut are associated with decreased lung function; however, the abundances of some members are markedly reduced in COPD (Bowerman et al., 2020; Chiu et al., 2021). To date, only a few studies are on the distribution and role of *Lachnospiraceae* in the lungs. Herein, we discovered *Lachnospiraceae* to be a marker of the microbiota, with a high abundance in the control and SJQJD groups and a low abundance in the model group, suggesting the regulatory role of its members in COPD in the lungs. *Lachnospiraceae* members can metabolize dietary fiber into short-chain fatty acids (SCFAs), and the SCFA levels are positively correlated with the severity of COPD because of their participation in the maturation process of immune cells, which then exert local and systemic anti-inflammatory effects (Jang et al., 2020; Song et al., 2023). The above evidence suggests that *Lachnospiraceae* likely regulate the pulmonary microenvironment and local immune function through their metabolic products.

Furthermore, our study only presented the above results at the animal level. The identification of biomarkers still needs further validation in clinical human specimens. In addition, this article also has certain limitations, as it only observed changes in lung microbiota and did not further verify whether these changes will be involved in the occurrence and development of COPD, as well as the specific mechanisms involved in the process. These are the topics that we need to delve deeper into in the future.

5 Conclusion

The findings of this study show that SJQJD can improve COPD in rats. Pulmonary microbiome analysis combined with machine learning identified *Mycoplasmataceae, Bacillaceae*, and *Lachnospiraceae* as potential key biomarkers for SJQJD intervention in COPD; however, more in-depth studies are required to elucidate their specific mechanisms and clinical significance.

Data availability statement

The 16S sequencing data involved in this article has been uploaded to the figshare database, which can be obtained through the link: https://figshare.com/articles/dataset/16s_sequencing_data_of_Sangju_Qingjie_Detection_SJQJD_on_pulmonary_microbiota_in_COPD_rats/25156670.

Ethics statement

The animal study was approved by Experimental Animal Ethics Committee of Nankai Hospital in Tianjin. The study was conducted in accordance with the local legislation and institutional requirements.

Author contributions

ZL: Conceptualization, Data curation, Visualization, Writing – original draft. YH: Conceptualization, Data curation, Project administration, Writing – review & editing. CH: Writing – original draft. XL: Writing – review & editing.

Funding

The author(s) declare financial support was received for the research, authorship, and/or publication of this article. This work was supported by projects SF-YB20231022 and SF-YB20211018 from the Science and Technology Bureau of Xiangtan City, Scientific Research Program of Health Commission of Hunan Province, (No. B2017166).

Conflict of interest

The authors declare that the research was conducted in the absence of any commercial or financial relationships that could be construed as a potential conflict of interest.

Publisher's note

All claims expressed in this article are solely those of the authors and do not necessarily represent those of their affiliated organizations, or those of the publisher, the editors and the reviewers. Any product that may be evaluated in this article, or claim that may be made by its manufacturer, is not guaranteed or endorsed by the publisher.Abbreviation

References

Anand, S., and Mande, S. S. (2018). Diet, microbiota and gut-lung connection. *Front. Microbiol.* 9. doi: 10.3389/fmicb.2018.02147

Baqdunes, M. W., Leap, J., Young, M., Kaura, A., and Cheema, T. (2021). Acute exacerbation of chronic obstructive pulmonary disease. *Crit. Care Nurs. Q* 44, 74–90. doi: 10.1097/CNQ.0000000000000341

Bowerman, K. L., Rehman, S. F., Vaughan, A., Lachner, N., Budden, K. F., Kim, R. Y., et al. (2020). Disease-associated gut microbiome and metabolome changes in patients with chronic obstructive pulmonary disease. *Nat. Commun.* 11, 5886. doi: 10.1038/s41467-020-19701-0

Cao, Q., Wu, X., Chen, Y., Wei, Q., You, Y., Qiang, Y., et al. (2023). The impact of concurrent bacterial lung infection on immunotherapy in patients with non-small cell lung cancer: a retrospective cohort study. *Front. Cell Infect. Microbiol.* 13. doi: 10.3389/fcimb.2023.1257638

Celli, B. R., Fabbri, L. M., Aaron, S. D., Agusti, A., Brook, R., Criner, G. J., et al. (2021). An updated definition and severity classification of chronic obstructive pulmonary disease exacerbations: the Rome proposal. *Am. J. Respir. Crit. Care Med.* 204, 1251–1258. doi: 10.1164/rccm.202108-1819PP

Chiu, Y. C., Lee, S. W., Liu, C. W., Lin, R. C., Huang, Y. C., Lan, T. Y., et al. (2021). Comprehensive profiling of the gut microbiota in patients with chronic obstructive pulmonary disease of varying severity. *PloS One* 16, e0249944. doi: 10.1371/journal.pone.0249944

Dong, Z. Q., Huang, Y., and Lin, Y. Z. (2018). Clinical observation of Sangju Qingjie soup in treatment of bronchiectasis. *China Med. Pharm.* 8, 60–62. doi: 10.3969/j.issn.2095-0616.2018.07.018

Enaud, R., Prevel, R., Ciarlo, E., Beaufils, F., Wieërs, G., Guery, B., et al. (2020). The gut-lung axis in health and respiratory diseases: A place for inter-organ and inter-kingdom crosstalks. *Front. Cell Infect. Microbiol.* 10. doi: 10.3389/fcimb.2020.00009

Fang, L., Gao, P., Bao, H., Tang, X., Wang, B., Feng, Y., et al. (2018). Chronic obstructive pulmonary disease in China: a nationwide prevalence study. *Lancet Respir. Med.* 6, 421–430. doi: 10.1016/S2213-2600(18)30103-6

GBD 2017 Causes of Death Collaborators. (2018). Global, regional, and national age-sex-specific mortality for 282 causes of death in 195 countries and territories 1980-2017: a systematic analysis for the Global Burden of Disease Study 2017. *Lancet* 392, 1736–1788. doi: 10.1016/s0140-6736(18)32203-7

Hathout, Y., Ho, Y. P., Ryzhov, V., Demirev, P., and Fenselau, C. (2000). Kurstakins: a new class of lipopeptides isolated from Bacillus thuringiensis. *J. Nat. Prod* 63, 1492–1496. doi: 10.1021/np000169q

Hua, J. L., Hu, W. P., Zuo, Y. H., and Zhang, J. (2020). Prevention of acute exacerbation in subjects with moderate-to-very severe COPD by modulating lower respiratory microbiome: protocol of a prospective, multicenter, randomized controlled trial. *Int. J. Chron Obstruct Pulmon Dis.* 15, 2985–2990. doi: 10.2147/COPD.S274005

Huang, Y., Huang, J., Dong, Z. Q., Chen, S. F., Chen, J. F., and Huang, Z. ,. Y. (2021). Effect of sangju qingjie decoction on chronic obstructive pulmonary disease with phlegm-heat accumulation and its influence on immune function. *Chin. Arch. Tradit. Chin. Med.* 39, 184–187. doi: 10.13193/j.issn.1673-7717.2021.07.046

Jang, Y. O., Lee, S. H., Choi, J. J., Kim, D. H., Choi, J. M., Kang, M. J., et al. (2020). Fecal microbial transplantation and a high fiber diet attenuates emphysema development by suppressing inflammation and apoptosis. *Exp. Mol. Med.* 52, 1128–1139. doi: 10.1038/s12276-020-0469-y

Jiang, X., Lin, Y., Wu, Y., Yuan, C., Lang, X., Chen, J., et al. (2022). Identification of potential anti-pneumonia pharmacological components of Glycyrrhizae Radix et Rhizoma after the treatment with Gan An He Ji oral liquid. *J. Pharm. Anal.* 12, 839–851. doi: 10.1016/j.jpha.2022.07.004

Karakasidis, E., Kotsiou, O. S., and Gourgoulianis, K. I. (2023). Lung and gut microbiome in COPD. *J. Pers. Med.* 13, 1–16. doi: 10.3390/jpm13050804

Kim, J., Kim, B., Bak, S. H., Oh, Y. M., and Kim, W. J. (2021). A comparative study of chest CT findings regarding the effects of regional dust exposure on patients with COPD living in urban areas and rural areas near cement plants. *Respir. Res.* 22, 43. doi: 10.1186/s12931-021-01649-4

Laiman, V., Lo, Y. C., Chen, H. C., Yuan, T. H., Hsiao, T. C., Chen, J. K., et al. (2023). Data on lung and intestinal microbiome after air pollution exposure in ageing rats. *Data Brief* 47, 109004. doi: 10.1016/j.dib.2023.109004

Leitao Filho, F. S., Alotaibi, N. M., Ngan, D., Tam, S., Yang, J., Hollander, Z., et al. (2019). Sputum microbiome is associated with 1-year mortality after chronic obstructive pulmonary disease hospitalizations. *Am. J. Respir. Crit. Care Med.* 199, 1205–1213. doi: 10.1164/rccm.201806-1135OC

Li, X., Li, Y., Mao, J., Bian, Q., Xuan, Y., Shen, T., et al. (2021). Combination of chinese and western medicine optimizes the intestinal microbiota of exacerbated chronic obstructive pulmonary disease in rats. *Evid Based Complement Alternat Med.* 2021, 9975407. doi: 10.1155/2021/9975407

Li, S., Yang, Q., Chen, F., Tian, L., Huo, J., Meng, Y., et al. (2022). The antifibrotic effect of pheretima protein is mediated by the TGF-β1/Smad2/3 pathway and attenuates inflammation in bleomycin-induced idiopathic pulmonary fibrosis. *J. Ethnopharmacol* 286, 114901. doi: 10.1016/j.jep.2021.114901

Li, N., Zhou, T., Wu, F., Wang, R., Zhao, Q., Zhang, J. Q., et al. (2019). Pharmacokinetic mechanisms underlying the detoxification effect of Glycyrrhizae Radix et Rhizoma (Gancao): drug metabolizing enzymes, transporters, and beyond. *Expert Opin. Drug Metab. Toxicol.* 15, 167–177. doi: 10.1080/17425255.2019.1563595

Lieberman, D., Lieberman, D., Ben-Yaakov, M., Lazarovich, Z., Hoffman, S., Ohana, B., et al. (2001). Infectious etiologies in acute exacerbation of COPD. *Diagn. Microbiol. Infect. Dis.* 40, 95–102. doi: 10.1016/S0732-8893(01)00255-3

Lieberman, D., Lieberman, D., Ben-Yaakov, M., Shmarkov, O., Gelfer, Y., Varshavsky, R., et al. (2002). Serological evidence of Mycoplasma pneumoniae infection in acute exacerbation of COPD. *Diagn. Microbiol. Infect. Dis.* 44, 1–6. doi: 10.1016/S0732-8893(02)00421-2

Liu, P., Tan, X. Y., Zhang, H. Q., Su, K. L., Shang, E. X., Xiao, Q. L., et al. (2024). Optimal compatibility proportional screening of Trichosanthis Pericarpium – Trichosanthis Radix and its anti – Inflammatory components effect on experimental zebrafish and coughing mice. *J. Ethnopharmacol* 319, 117096. doi: 10.1016/j.jep.2023.117096

Liu, J., Wang, X., Li, M., Du, Q., Li, Q., and Ma, P. (2015). Jilinibacillus soli gen. nov., sp. nov., a novel member of the family Bacillaceae. *Arch. Microbiol.* 197, 11–16. doi: 10.1007/s00203-014-1032-9

Liu, S., Yang, T., Ming, T. W., Gaun, T. K. W., Zhou, T., Wang, S., et al. (2020). Isosteroid alkaloids with different chemical structures from Fritillariae cirrhosae bulbus alleviate LPS-induced inflammatory response in RAW 264.7 cells by MAPK signaling pathway. *Int. Immunopharmacol* 78, 106047. doi: 10.1016/j.intimp.2019.106047

Papaetis, G. S., Anastasakou, E., Tselou, T., Sotiriou, A., Rarra, V. C., Roussou, P., et al. (2010). Serological evidence of Mycoplasma pneumoniae infection in patients with acute exacerbation of COPD: analysis of 100 hospitalizations. *Adv. Med. Sci.* 55, 235–241. doi: 10.2478/v10039-010-0031-6

Park, S. J., Kim, Y. W., Park, M. K., Byun, S. H., Kim, S. C., and Lee, J. R. (2016). Anti-inflammatory steroid from phragmitis rhizoma modulates LPS-mediated signaling through inhibition of NF-κB pathway. *Inflammation* 39, 727–734. doi: 10.1007/s10753-015-0299-6

Ramsheh, M. Y., Haldar, K., Esteve-Codina, A., Purser, L. F., Richardson, M., Müller-Quernheim, J., et al. (2021). Lung microbiome composition and bronchial epithelial gene expression in patients with COPD versus healthy individuals: a bacterial 16S rRNA gene sequencing and host transcriptomic analysis. *Lancet Microbe* 2, e300–e310. doi: 10.1016/S2666-5247(21)00035-5

Ren, Z., Yu, R., Meng, Z., Sun, M., Huang, Y., Xu, T., et al. (2021). Spiky titanium dioxide nanoparticles-loaded Plantaginis Semen polysaccharide as an adjuvant to enhance immune responses. *Int. J. Biol. Macromol* 191, 1096–1104. doi: 10.1016/j.ijbiomac.2021.09.184

Richmond, B. W., Du, R. H., Han, W., Benjamin, J. T., van der Meer, R., Gleaves, L., et al. (2018). Bacterial-derived neutrophilic inflammation drives lung remodeling in a mouse model of chronic obstructive pulmonary disease. *Am. J. Respir. Cell Mol. Biol.* 58, 736–744. doi: 10.1165/rcmb.2017-0329OC

Sessa, R., Di Pietro, M., Schiavoni, G., Macone, A., Maras, B., Fontana, M., et al. (2009). Chlamydia pneumoniae induces T cell apoptosis through glutathione redox imbalance and secretion of TNF-alpha. *Int. J. Immunopathol. Pharmacol.* 22, 659–668. doi: 10.1177/039463200902200311

Shi, C. Y., Yu, C. H., Yu, W. Y., and Ying, H. Z. (2021). Gut-lung microbiota in chronic pulmonary diseases: evolution, pathogenesis, and therapeutics. *Can. J. Infect. Dis. Med. Microbiol.* 2021, 9278441. doi: 10.1155/2021/9278441

Simpson, J. L., Baines, K. J., Horvat, J. C., Essilfie, A. T., Brown, A. C., Tooze, M., et al. (2016). COPD is characterized by increased detection of Haemophilus influenzae, Streptococcus pneumoniae and a deficiency of Bacillus species. *Respirology* 21, 697–704. doi: 10.1111/resp.12734

Song, W., Yue, Y., and Zhang, Q. (2023). Imbalance of gut microbiota is involved in the development of chronic obstructive pulmonary disease: A review. *BioMed. Pharmacother.* 165, 115150. doi: 10.1016/j.biopha.2023.115150

Su, L., Qiao, Y., Luo, J., Huang, R., Li, Z., Zhang, H., et al. (2022). Characteristics of the sputum microbiome in COPD exacerbations and correlations between clinical indices. *J. Transl. Med.* 20, 76. doi: 10.1186/s12967-022-03278-x

Sun, X., Lan, J., Tong, R., Zhang, H., Sun, S., Xiong, A., et al. (2019). An integrative investigation on the efficacy of Plantaginis semen based on UPLC-QTOF-MS metabolomics approach in hyperlipidemic mice. *BioMed. Pharmacother.* 115, 108907. doi: 10.1016/j.biopha.2019.108907

Sze, M. A., Dimitriu, P. A., Hayashi, S., Elliott, W. M., McDonough, J. E., Gosselink, J. V., et al. (2012). The lung tissue microbiome in chronic obstructive pulmonary disease. *Am. J. Respir. Crit. Care Med.* 185, 1073–1080. doi: 10.1164/rccm.201111-2075OC

Tian, D., Yang, Y., Yu, M., Han, Z. Z., Wei, M., Zhang, H. W., et al. (2020). Anti-inflammatory chemical constituents of Flos Chrysanthemi Indici determined by UPLC-MS/MS integrated with network pharmacology. *Food Funct.* 11, 6340–6351. doi: 10.1039/D0FO01000F

Valdes, A. M., Walter, J., Segal, E., and Spector, T. D. (2018). Role of the gut microbiota in nutrition and health. *Bmj* 361, k2179. doi: 10.1136/bmj.k2179

Vaughan, A., Frazer, Z. A., Hansbro, P. M., and Yang, I. A. (2019). COPD and the gut-lung axis: the therapeutic potential of fiber. *J. Thorac. Dis.* 11, S2173–s2180. doi: 10.21037/jtd.2019.10.40

Vogelmeier, C. F., Criner, G. J., Martinez, F. J., Anzueto, A., Barnes, P. J., Bourbeau, J., et al. (2017). Global strategy for the diagnosis, management, and prevention of chronic obstructive lung disease 2017 report. GOLD executive summary. *Am. J. Respir. Crit. Care Med.* 195, 557–582. doi: 10.1164/rccm.201701-0218PP

Wang, Z., Maschera, B., Lea, S., Kolsum, U., Michalovich, D., Van Horn, S., et al. (2019). Airway host-microbiome interactions in chronic obstructive pulmonary disease. *Respir. Res.* 20, 113. doi: 10.1186/s12931-019-1085-z

Whiteside, S. A., McGinniss, J. E., and Collman, R. G. (2021). The lung microbiome: progress and promise. *J. Clin. Invest.* 131, 1–10. doi: 10.1172/JCI150473

Wood, A. M., Tang, M., Truong, T., Feldman, C., Pieper, C., and Murtha, A. P. (2021). Vaginal Mycoplasmataceae colonization and association with immune mediators in pregnancy. *J. Matern Fetal Neonatal Med.* 34, 2295–2302. doi: 10.1080/14767058.2019.1663820

Wu, D., Hou, C., Li, Y., Zhao, Z., Liu, J., Lu, X., et al. (2014). Analysis of the bacterial community in chronic obstructive pulmonary disease sputum samples by denaturing gradient gel electrophoresis and real-time PCR. *BMC Pulm Med.* 14, 179. doi: 10.1186/1471-2466-14-179

Wu, X., Zhou, Z., Cao, Q., Chen, Y., Gong, J., Zhang, Q., et al. (2023). Reprogramming of Treg cells in the inflammatory microenvironment during immunotherapy: a literature review. *Front. Immunol.* 14. doi: 10.3389/fimmu.2023.1268188

Yagi, K., Huffnagle, G. B., Lukacs, N. W., and Asai, N. (2021). The lung microbiome during health and disease. *Int. J. Mol. Sci.* 22, 1–13. doi: 10.3390/ijms221910872

Yee, N., Kim, H., Kim, E., Cha, Y. H., Ma, L., Cho, N. E., et al. (2022). Effects of sangju honey on oral squamous carcinoma cells. *J. Cancer Prev.* 27, 239–246. doi: 10.15430/JCP.2022.27.4.239

Zhai, Y., Li, D., Wang, Z., Shao, L., Yin, N., and Li, W. (2022). Cortex mori radicis attenuates streptozotocin-induced diabetic renal injury in mice via regulation of transient receptor potential canonical channel 6. *Endocr. Metab. Immune Disord. Drug Targets* 22, 862–873. doi: 10.2174/1871530322666220110161458

frontiers | Frontiers in Cellular and Infection Microbiology

TYPE Original Research
PUBLISHED 13 May 2024
DOI 10.3389/fcimb.2024.1350181

OPEN ACCESS

EDITED BY
Wenle Li,
Xiamen University, China

REVIEWED BY
Nitesh Tewari,
All India Institute of Medical Sciences, India
Yan kai Dong,
Jiujiang Maternity and Child Health Care Hospital, China

*CORRESPONDENCE
Jiaqi Wu
525150229@qq.com

†These authors have contributed equally to this work

RECEIVED 05 December 2023
ACCEPTED 10 April 2024
PUBLISHED 13 May 2024

CITATION
Zheng J, Wang X, Zhang T, Jiang J and Wu J (2024) Comparative characterization of supragingival plaque microbiomes in malocclusion adult female patients undergoing orthodontic treatment with removable aligners or fixed appliances: a descriptive cross-sectional study. *Front. Cell. Infect. Microbiol.* 14:1350181. doi: 10.3389/fcimb.2024.1350181

Comparative characterization of supragingival plaque microbiomes in malocclusion adult female patients undergoing orthodontic treatment with removable aligners or fixed appliances: a descriptive cross-sectional study

Jiajia Zheng[1†], Xiujing Wang[1†], Ting Zhang[2], Jiuhui Jiang[2] and Jiaqi Wu[1*]

[1]First Clinical Division, Peking University School and Hospital of Stomatology & National Center for Stomatology & National Clinical Research Center for Oral Diseases & National Engineering Research Center of Oral Biomaterials and Digital Medical Devices, Beijing, China, [2]Department of Orthodontics, Peking University School and Hospital of Stomatology & National Center for Stomatology & National Clinical Research Center for Oral Diseases & National Engineering Research Center of Oral Biomaterials and Digital Medical Devices, Beijing, China

Objectives: This study aimed to explore the effects of removable aligners and fixed appliances on the supragingival bacterial communities in adult female patients undergoing orthodontic treatment.

Methods: Supragingival plaque samples from 48 female individuals underwent microbiome analysis (16S rRNA gene sequencing) using PacBio Sequel sequencing. The study included 13 adults without orthodontic treatment needs as the control group (Group C), and 35 patients with comparable initial orthodontic conditions who received treatment at a university clinic in Beijing, China. The treatment involved either traditional fixed brackets (Group B, n = 17) or Invisalign® aligners (Group AT, n = 18). Bioinformatics methods were used for data analysis.

Results: From the 48 plaque samples, a total of 334,961 valid reads were obtained, averaging 6,978 sequences per sample. The 16S rDNA sequences were classified into 25,727 amplicon sequence variants (ASVs). Significant variances in alpha and beta diversity among the groups were noted. Group B microbiome exhibited an increased presence of Gram-negative bacteria. At the phylum level, *Actinobacteriota* was significantly more prevalent in Group C samples, while *Bacteroidota* was enriched in Group B samples. Family-level relative abundance analysis showed a notable increase in *Saccharibacteria* (formerly TM7) and *Prevotellaceae* in Group B. Genus-level analysis revealed a significant rise in *Lautropia* in Group AT. Fixed orthodontic appliances were linked to oral microbiome changes, notably an enhanced relative abundance of anaerobes, including periodontal pathogens.

Conclusion: The observation points to the impact of orthodontic appliance on the oral microbial community, highlighting the difference between traditional braces (Group B) and clear aligners (Group AT)in terms of the predominance of anaerobic and gram negative bacteria. This emphasizes the importance of considering the microbiological effects when choosing orthodontic appliance and underscores the need for tailored oral hygiene practices for individuals undergoing these treatments. This research might provide insights that could assist in the development of innovative cleaning techniques and antibacterial materials.

KEYWORDS

16S rRNA gene, orthodontic brackets, clear aligners, oral plaque, oral microbiome

Introduction

Developments in materials science have significantly advanced the field of invisible orthodontic technology. This technology has become increasingly popular, particularly among female patients, owing to its aesthetic appeal and comfort (Lucchese et al., 2020). One of the key advantages of these aligners is their removability, which allows for uninterrupted daily oral hygiene practices. However, the way these invisible appliances interact with enamel surface is distinct from that of traditional fixed appliances. This difference is particularly notable because patients can remove the aligners, which may impact the mechanical forces applied to the hard and soft tissues.

Clinical studies have suggested that clear aligners may be more beneficial for periodontal health than fixed appliances, potentially making them a better option for patients at risk of developing gingivitis (Jiang et al., 2018). Teenagers who use removable appliances typically demonstrate better compliance with oral hygiene and tend to accumulate less plaque compared to those wearing fixed appliances (Abbate et al., 2015). Fixed appliances, on the other hand, may facilitate plaque buildup and promote bacterial affinity to metallic surfaces (Ahn et al., 2006).

Although the current findings are informative, there is still a limited amount of research on the comparative analysis of oral microecological changes on the enamel surface environment among different orthodontic treatment method. Specifically, the effect of removable aligners on the oral microflora represents an area that requires further exploration to fully understand its implications.

With the emergence of culture-independent methods, exploring the diversity of the oral microbiota has become more feasible. Besides, the advent of third-generation sequencing (TGS) technologies, particularly those offered by the Pacific Biosciences (PacBio) platform, has simplified genome sequencing processes (Athanasopoulou et al., 2021). Combining these technologies, this study aimed to examine how removable aligners and fixed appliances affect the supragingival bacterial communities in adult female patients.

Since bacteria adhere to enamel, metal, and plastic-coated enamel surfaces in distinct ways, this research hope to offer insights that could aid in the development of innovative cleaning methods and antibacterial materials.

Ethical approval

Ethical approval for this study was granted by the Ethics Committee of Peking University Health Science Center (PKUSSIRB-202054050). Written informed consent was obtained from all participants before their involvement in the study.

Materials and methods

Recruitment

The study recruited all suitable patients from October 2019 to January 2021 at the First Clinical Division, Peking University School and the Hospital of Stomatology. Participants were all female, aged between 18 and 38 years, and free from chronic periodontal disease and active caries.

Inclusion Criteria:

1. Aged above 18 years old.
2. No missing permanent teeth, except the third molars.
3. Essential oral hygiene practices. No untreated caries.
4. Good compliance, with braces worn for at least 6 months and clear aligners for at least 22 hours per day.

Exclusion Criteria:

1. Pregnancy.
2. Medical complications.

3. Lack of cooperation.
4. Chronic periodontitis and untreated dental caries.
5. Antibiotics or analgesics should be used before treatment.

Our study participants consist of 48 female patients, who are categorized into three distinct groups (Table 1).

Control Group (Group C): 13 patients, serving as the control group.

Brackets Group (Group B): 17 patients underwent treatment with self-ligating fixed appliances and nickel-titanium (NiTi) archwires.

Aligners T Group (Group AT): 18 patients treated with Invisalign® aligners, with samples taken from the tooth surface.

The baseline data for age, weight, and height were analyzed using one-way ANOVA tests. The results indicated no statistically significant differences among the three groups for each of these parameters: age (p=0.73), weight (p=0.79), and height (p=0.99).

Sample collection

Supragingival plaque samples were collectedusing a sterile cotton swab. Plaque was collected from the buccal and lingual sides, as well as the occlusal surface, of the teeth ranging from 17 to 47. The orthodontic group refrained eating for 2 hours and from brushing teeth for 4 hours before plaque sampling. Samples were preserved at -80°C for subsequent analysis.

Bacterial DNA extraction, PCR amplification, and PacBio sequel sequencing

Total DNA was extracted from the samples using the PowerSoil® DNA Isolation Kit, following the manufacturer's instructions. The 16S full-length gene was amplified using PCR with the 27F-1492R conservative region primers in a 10 μL reaction system (Solexa PCR). The specific primers used were:

Forward primer 27F: AGRGTTTGATYNTGGCTCAG

Reverse primer 1492R: TASGGHTACCTTGTTASGACTT

After constructing the sequencing library, we performed a quality check, which involved barcode identification and processing the obtained high-quality circular consensus sequencing (CCS) sequences. We then clustered the optimized CCS sequences with a 97% similarity threshold using USEARCH (version 10.0). Species classification was determined by analyzing the amplicon sequence variants (ASVs) based on their sequence composition. For species annotation and taxonomy analysis, as well as to evaluate the oral microbiota's diversity, we employed the 16S Plaque database and the RDP Classifier. Alpha diversity analysis, examining species richness and diversity within each sample, was performed. Beta diversity analysis compared community composition and structure across samples. Metastats analysis identified significant differences at the genus level between groups, and linear discriminant analysis effect size (LEfSe) identified statistically distinct biomarkers between groups (biomarker screening criteria: LDA score>4). Various statistical techniques were utilized to establish a correlation between 16S data and the specific type of orthodontic appliance utilized by the patients.

TABLE 1 Demographic and clinical characteristics.

Group	Age(y)	Weight(kg)	Height(cm)
Control(N=13)	26.0 ± 6.6	58.6 ± 3.6	168.9 ± 1.9
Brackets(N=17)	26.2 ± 6.0	52.0 ± 5.9	163.4 ± 4.1
Aligners T (N=18)	27.9 ± 5.2	52.8 ± 2.3	163.3 ± 5.3

Results

Taxonomic identification and relative abundance

To investigate the composition of the plaque microbial community in the three groups, plaque samples were analyzed through sequencing with the IPacBio Sequel technology A total of 334,961 valid reads were obtained from the 48 plaque samples, averaging 6,978 sequences per sample. These 16S ribosomal DNA sequences were classified into ASVs.

The rarefaction curves (Figure 1) for all groups confirmed the sufficiency of the sampling efforts.

This rank-abundance curve (Figure 1) underscores the variations in microbial community structure that may be attributed to the different conditions or treatments applied to each group.

Bacterial composition

The predominant phyla across all three groups were *Firmicutes* (42.9% in Group AT, 40.4% in Group B, 44.1% in Group C) (Figure 2). The top 10 phylum: *Firmicutes, Proteobacteria, Bacteroidota, Fusobacteriota, Actinobacteriota, Patescibacteria, Campylobacterota, Verrucomicrobiota, unclassified_Bacteria*, and *Spirochaetota*. Notably, the proportion of *Bacteroidota* increased in Group B patients. At the genus level, *Streptococcus* was the most abundant in all groups (32.0% in Group AT, 25.0% in Group B, 29.7% in Group C). Among these genera, *Streptococcus, Haemophilus, Veillonella, Capnocytophaga, Neisseria, Leptotrichia, Fusobacterium, Prevotella, Rothia*, and *Lautropia* were observed.

Microbiome diversity and richness

Alpha-diversity analysis

The alpha-diversity analysis involved calculates species-level ASVs, diversity, and richness estimates for each sample. The Chao1 and ACE indices are measures of species richness, while the Shannon and Simpson index also considers species evenness.

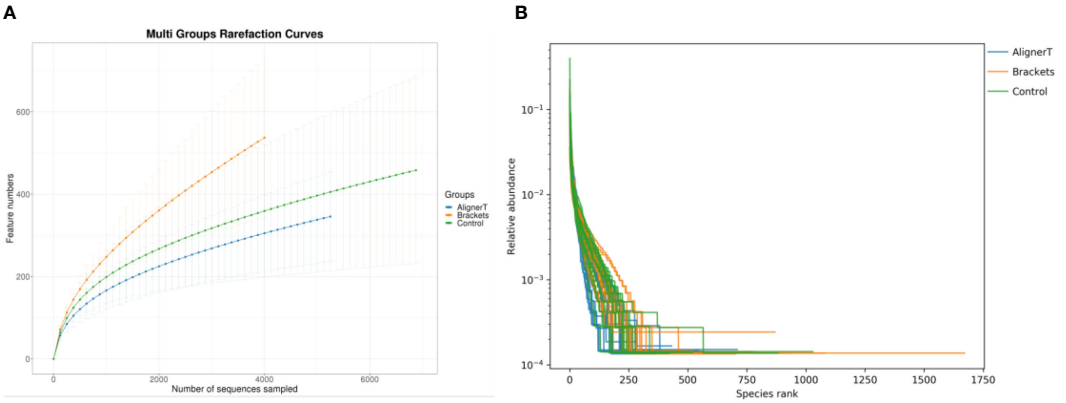

FIGURE 1
(A) Multi-group rarefaction curves, generated based on the number of unique amplicon sequencing variants. **(B)** Rank-Abundance Curves of Microbial Communities Under Different Conditions.

For the Chao1 index, Group C has significantly higher species richness than Group AT. The ACE index reveals significant differences in species richness between all groups, with Group AT having the lowest richness and Group C the highest. The Shannon index shows a significant difference between the AT and B groups, suggesting variance in both the richness and evenness of species between these two treatments. In Simpson index, the presence of a p-value suggests that the difference in diversity between the AT and B groups is statistically significant. The figure does not show any significant difference between the B and C groups or between the AT and C groups (Figure 3).

Beta-diversity analysis

Beta-diversity analysis was employed to examine and compare the community structures among the microbiotas of the three groups. Clustering analysis is presented in Figure 4.

The clustering in the figure displays the similarities and differences in the oral microbial communities of the patients.

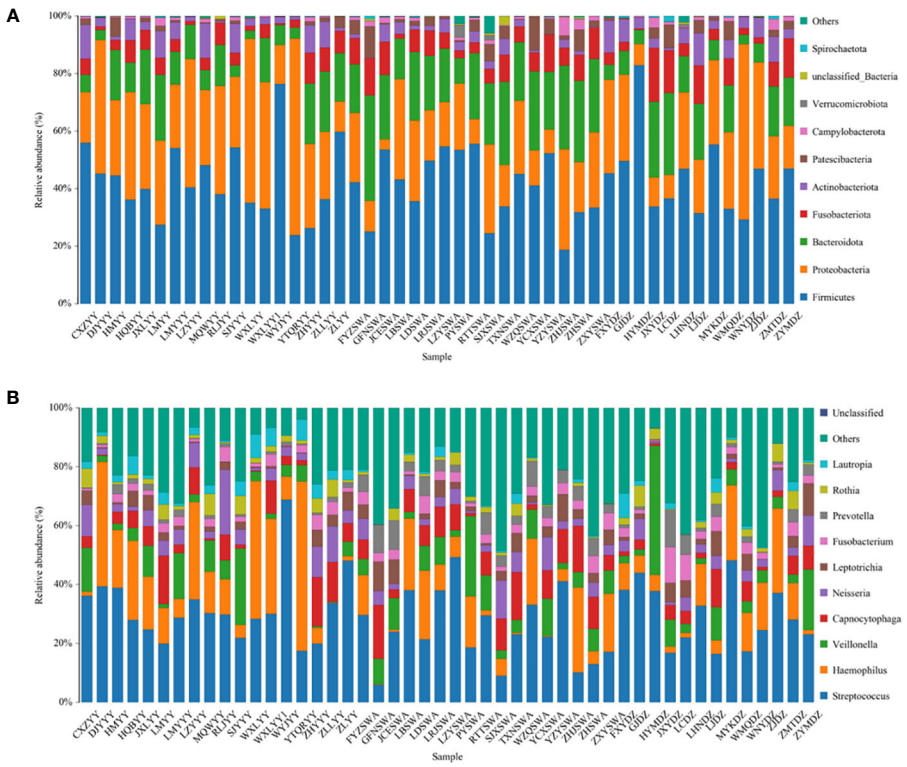

FIGURE 2
Most abundant bacterial phylum **(A)** and genus **(B)** in all samples.

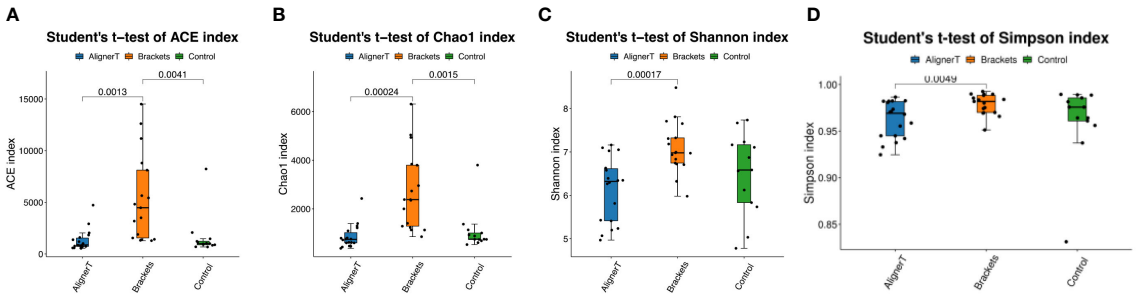

FIGURE 3
Alpha diversity was calculated based on different groups. p-values for each comparison are depicted above the box plots of the groups being compared. **(A)** ACE index. **(B)** Chao 1 index. **(C)** Shannon index. **(D)** Simpson index.

Additionally, a principal component analysis (PCA) plot revealed no distinct separation between these groups (Figure 5). The relative positions of the ellipses and points indicate differences in microbial diversity or the dominance of certain taxa in one group over the other. The analysis of bacterial beta diversity showed no distinct separation between Group B and Group C. We also utilized heatmaps to visually depict the correlation coefficients among the samples (Figure 6).

To further investigate microbial community structure changes, we compared ASV abundance and microbial distribution at the phylum, genus, and species levels.

Figure 7 displays the results of the LEfSe analysis, which was conducted to identify specific microbial communities. This analysis revealed 16 discriminative features (LDA>4, $p<0.05$) at various taxonomic levels: phylum (n=2), family (n=4), order (n=2), class (n=2), genus (n=4), and species (n=2).

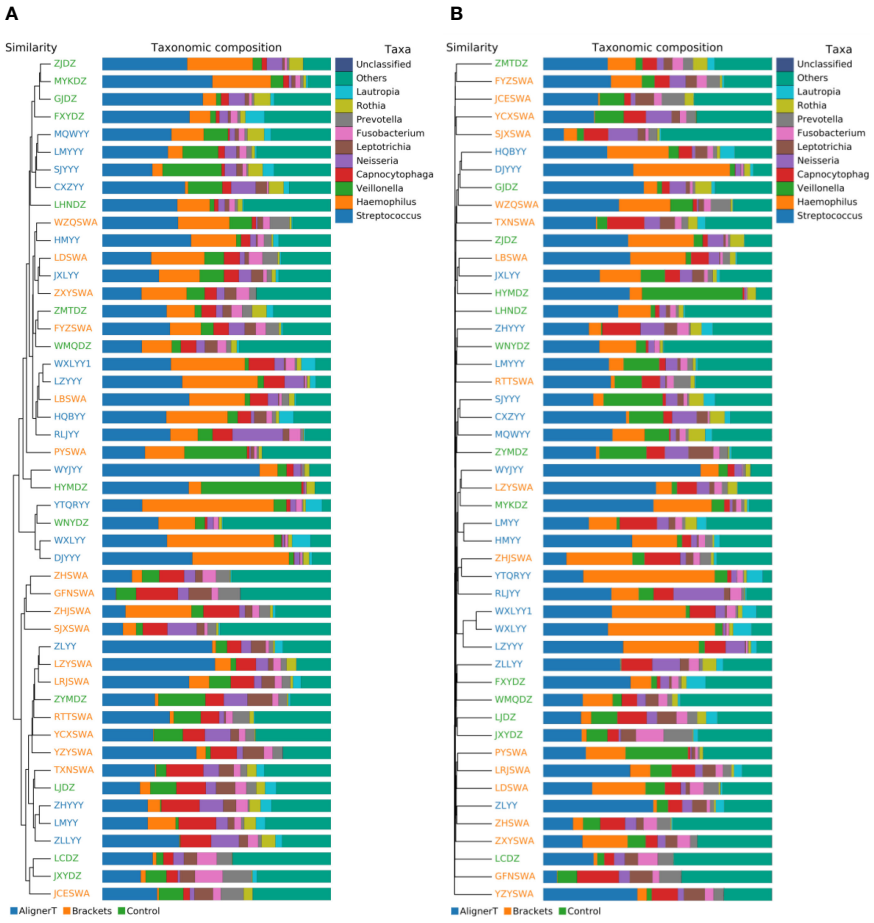

FIGURE 4
Cluster Analysis of Taxonomic Composition in Microbial Communities Across Various Sample Groups. **(A)** Weighted Unifrac. **(B)** Bray-Curtis.

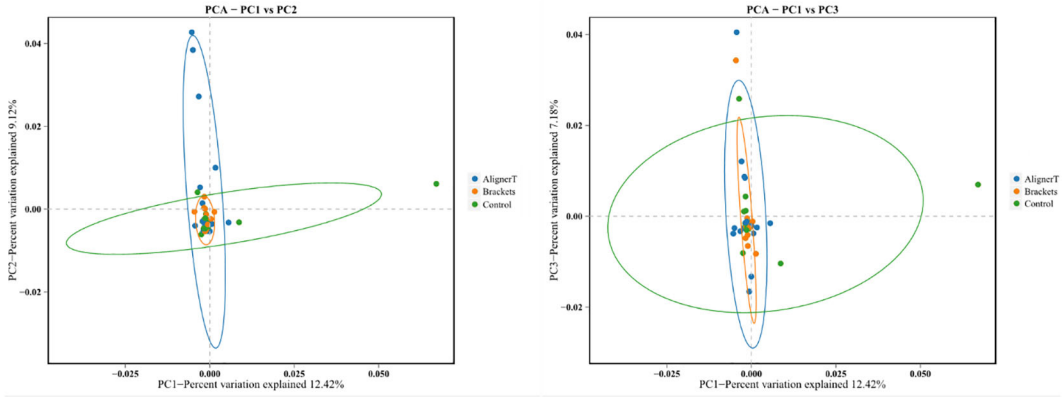

FIGURE 5
Principal components analysis using the weighted UniFrac beta-diversity metric. The ellipses denote the 95% confidence intervals, providing a visual summary of each group's spread and indicating the variability within the groups.

At the phylum level, *Actinobacteriota* was more prevalent in Group C samples, while *Bacteriodota* was predominant in Group B.

Significant variations were noted among the groups in the classes *Actinobacteria* and *Bacteroidia*, families *Burkholderiaceae, Flavobacteriaceae, Saccharimonadaceae*, and *Prevotellaceae*, and genera *Capnocytophaga, Saccharimonadaceae, Lautropia, Prevotella_7*, and *Prevotella*, as depicted in Figures 8, 9.

The functional genes present in the samples were examined using the Kyoto Encyclopedia of Genes and Genomes (KEGG) database. Through differential analysis of the KEGG metabolic pathways, we can understand the differences in the functional genes of the microbial communities among different group samples in terms of metabolic pathways, as well as the extent of these variations (Figure 10).

The microbial communities in Group B displayed significant differences in their polysaccharide biosynthesis, metabolism, and transport when compared to those in Group C. In the case of Group AT, we observed noteworthy distinctions in the metabolism of various amino acids in comparison to Group C. From a microbial functional metabolism standpoint, the effects on the immune system, cardiovascular health, viral infections, and endocrine/metabolic disorders varied between Group AT and Group B.

COGs, or Clusters of Orthologous Groups of proteins, constitute a bioinformatics resource that groups proteins from complete genomes into categories based on orthologous relationships, suggesting a common ancestral gene. We utilized this database to classify and compare the protein profiles of Group AT and Group B, as illustrated in Figure 11.

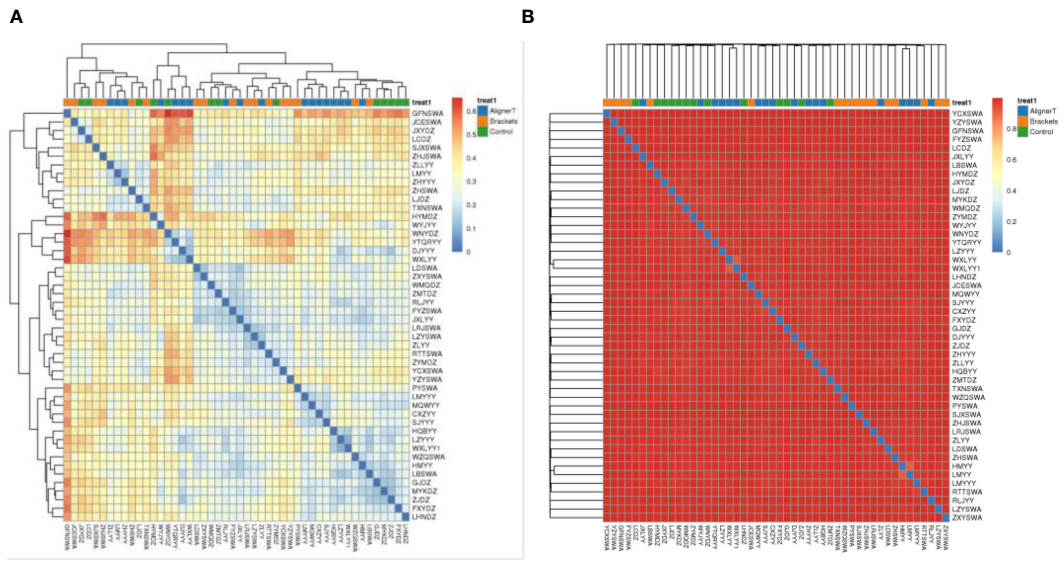

FIGURE 6
Heat map displaying correlations among 48 subjects. In the heatmap, color intensity indicates the magnitude of the correlation, with red representing positive correlations and blue indicating negative correlations. **(A)** Weighted unifrac. **(B)** Bray-Curtis.

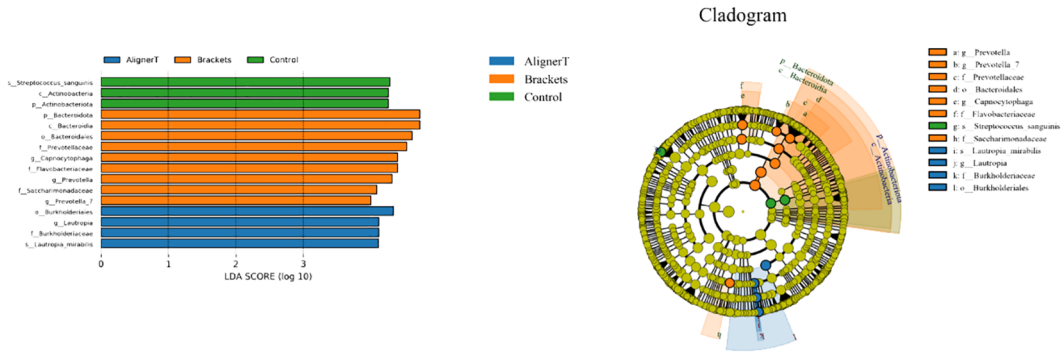

FIGURE 7
Specific taxa associated with orthodontic treatment. Linear discriminant analysis (LDA) effect size analysis of the three groups. Cladogram using LEfSe method indicating the distribution of microbes.

This figure allows for the assessment of the comparative abundance of functional protein categories between experimental conditions, highlighting areas of significant divergence that may warrant further investigation.

Discussion

The composition of the oral microbiome is generally stable under normal conditions. However, microbiome dysbiosis, characterized by a disruption to the stability of the symbiotic microbiota, can adversely affect the host's health status (Duran-Pinedo et al., 2021). Changes in the oral microbial environment are intimately linked to the onset and progression of periodontal diseases and caries. Existing research indicates that the use of orthodontic appliances could modify the oral cavity's status and influence the colonization of oral biofilm by opportunistic/pathogenic strains (Perkowski et al., 2019).

The oral cavity is the entry point to the digestive tract. As such, the oral microbiome can impact the overall health and composition of the gastrointestinal (GI) microbiome (Kitamoto et al., 2020). Microorganisms present in the mouth can be swallowed and integrated into the gut microbiome. Both the oral and digestive tract microbiomes are complex ecosystems, composed of bacteria, viruses, fungi, and other microorganisms. However, the specific composition and diversity vary between these two sites (Kitamoto et al., 2020). The oral microbiome is exposed to different environmental factors (like food, oxygen levels, and oral hygiene practices) compared to the gut microbiome, which is influenced by factors like diet, medication, and intestinal conditions. Changes in the oral microbiome can have repercussions on the gut microbiome and vice versa. The oral and digestive tract microbiomes are deeply interconnected, with implications for overall health, disease, and potential therapeutic strategies.

Full-length 16S sequencing offers advantages such as longer read lengths and more expansive amplification regions, enhancing the comprehensiveness of the analysis (Hong et al., 2024). This approach allows for a more precise species classification and a broader scope of species annotation compared to traditional 16S sequencing methods used in second-generation platforms. In this study, third-generation sequencing technology was utilized to achieve full-length sequencing. To reduce potential biases due to variations in sex hormone levels, the study exclusively included adult female subjects.

It has been shown that the salivary and teeth surface microbiota of patients with invisible braces undergo changes 12 hours post-application of clear aligners (Yan et al., 2021). Saliva and dental plaques are primary sample sources reflecting the oral microbial community. Dental plaque provides a more accurate representation of the bacteria that adhere to tooth surfaces and contribute to dental caries and periodontitis (Campobasso et al., 2021). Studying bacteria within this biofilm environment is crucial for understanding their behavior, and interactions, which differs significantly from their planktonic (free-floating) counterparts in saliva (Jakubovics, 2015). Owing to the difficulty in accessing dental plaques, only a limited number of studies have employed them as sources of samples. Our study used supragingival dental plaque and found an average of 6978 ASVs per patient. We characterized the microbiomes of Groups B and AT patients and compared them to those of orally healthy controls (Group C).

Firmicutes, Planctomycetota, Bacteroidota, and *Cyanobacteria* emerged as dominant bacteria across the three groups. *Firmicutes* are involved in the initial colonization of the tooth surface and the formation of dental plaque. Some species, like *Streptococcus mutans* produce acids from carbohydrate fermentation, contributing to tooth decay (Homayouni Rad et al., 2023). As a key etiological agent of human dental caries, *Streptococcus mutans* primarily resides in dental plaque (Wang et al., 2019). They have a remarkable ability to metabolize fermentable carbohydrates, especially sucrose, to produce lactic acid, which lowers the pH in the mouth and leads to the demineralization of the tooth enamel (Abranches et al., 2018).

For alpha diversity index, Figure 3 collectively suggest that there are differences in microbial diversity associated with the different orthodontic treatments, as indicated by several biodiversity indices. The Group AT consistently shows lower diversity compared to the Group C, and there are noticeable differences between the Group AT and B groups. Clear aligners, made from thermoplastic material, are removable and fit over the teeth. The thermoplastic material itself may influence the oral environment differently than traditional braces, affecting bacterial growth.

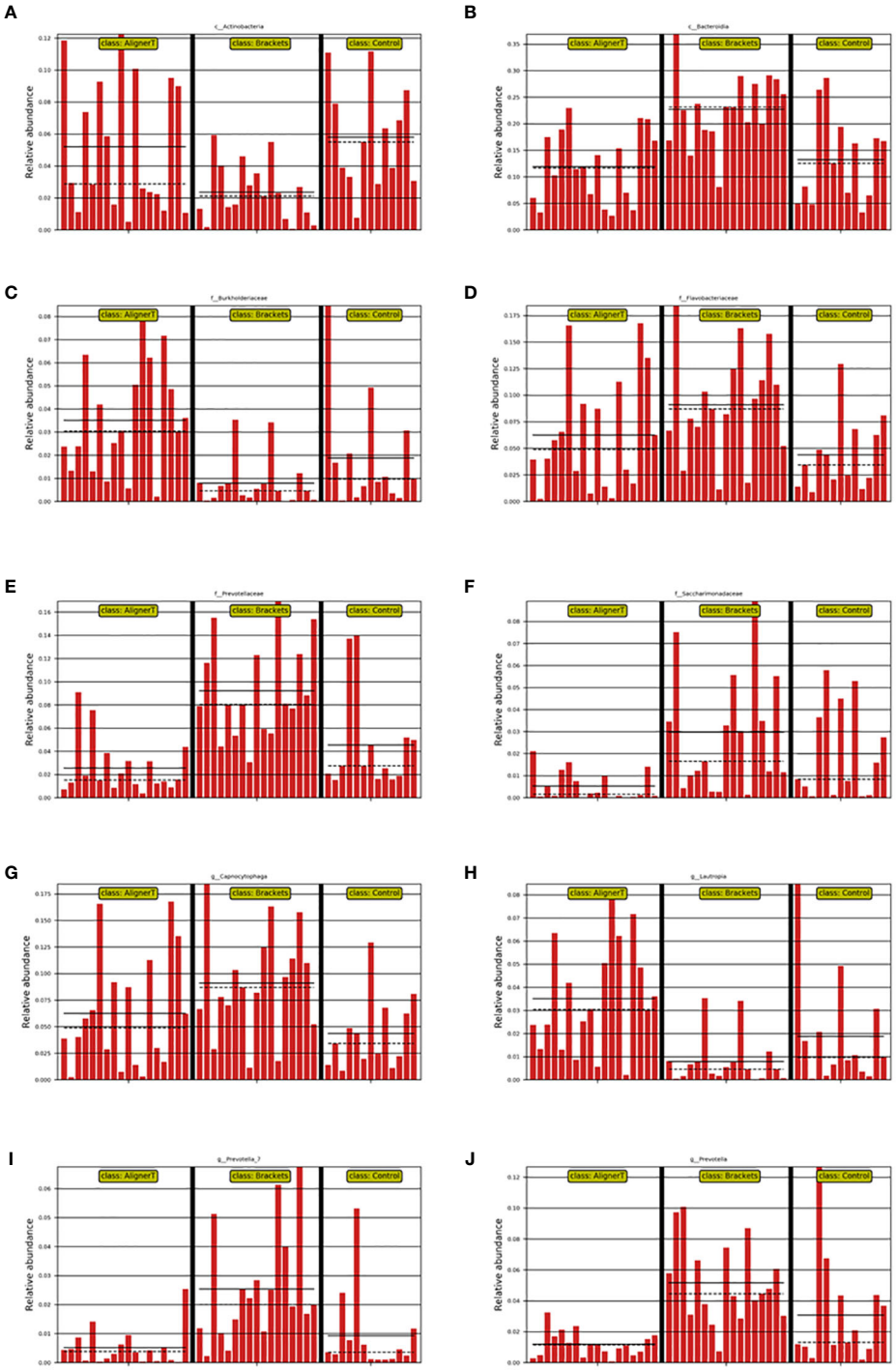

FIGURE 8
Depiction of varied microbial clade abundance in different groups: **(A)** *Actinobacteria*, **(B)** Bacteroidia, **(C)** *Burkholderiacese*, **(D)** *Flavobacteriaceae*. **(E)** *Prevotellaceae*, **(F)** *Saccharimonadaceae*, **(G)** *Capnocytophaga*, **(H)** *Lautropia*, **(I)** *Prevotella_7*, **(J)** *Prevotella*..

The PCA plots function as a means to visualize complex microbial data and simplify the comparison of microbial communities across various treatment groups. In Figure 5, the ellipses that overlap indicate a similarity between the microbial communities in Group AT and Group B. Moreover, the beta diversity—which indicates variation in microbial community structure—reveals no significant differences between Group C and Group B. This may be related to the fact that invisible braces fully envelop the tooth surface. In contrast, the tooth surfaces in the fixed orthodontic group are exposed to the oral environment.

We found the presence of orthodontic brackets can create unique niches and environmental conditions in the oral cavity. The environments where dental plaque forms are different; there is plaque accumulation beneath bracket slot, brackets, and under

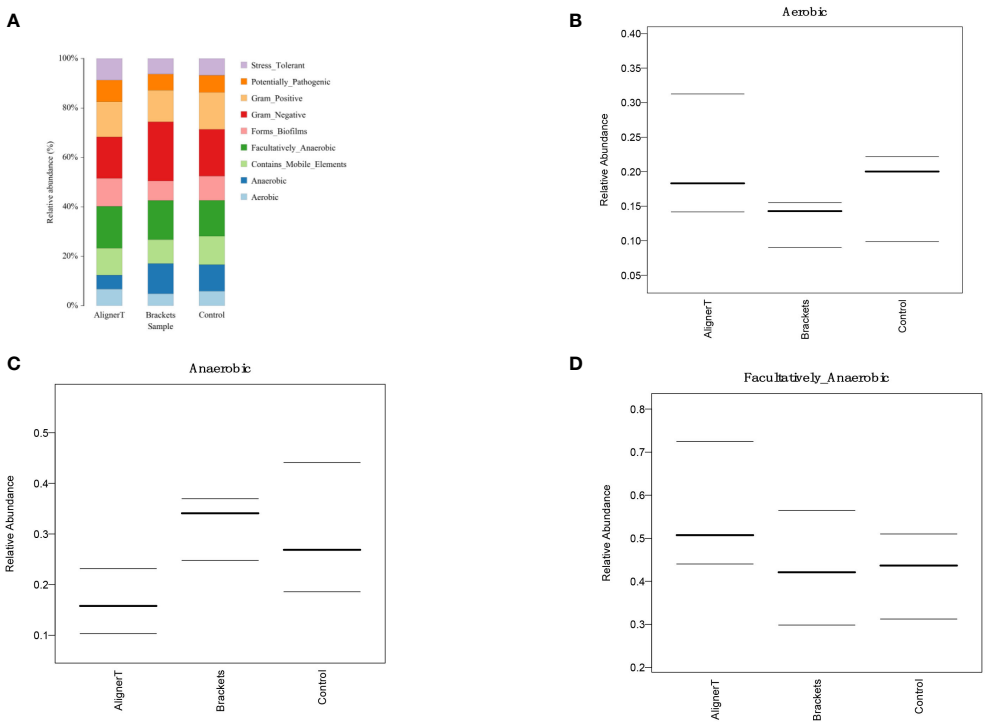

FIGURE 9
Comparative Analysis of Microbial Characteristics Across Three Groups. **(A)** the relative abundance of microbial categories. **(B–D)** plots depicting the relative abundance of aerobic, anaerobic, and facultatively anaerobic bacteria across the three groups.

archwires. According to our research findings, fixed orthodontics may create a more anaerobic environment on the enamel surface.

Fixed orthodontic appliances pose challenges to oral hygiene and may temporarily impact periodontal health (Azaripour et al., 2015). Research indicates increased microbial diversity in patients with fixed orthodontics compared to normal individuals (Sun et al., 2018).These conditions may favor certain bacterial species or alter bacterial behavior. A meta-analysis suggests that patients treated with Invisalign® exhibit better periodontal health than those with traditional fixed appliances (Lu et al., 2018). Previous studies have highlighted that Invisalign® aligner margins are typically designed below the marginal gingiva, and their smooth surface, coupled with a maximum usage duration of 14 days per aligner, results in significantly less biofilm accumulation compared to traditional fixed orthodontic and removable appliances (Zhao et al., 2020).

In Group B, there was a significant reduction in *Actinobacteriota* compared to Groups AT and C. *Actinobacteriota*, formerly known as *Actinobacteria*, is a phylum of Gram-positive bacteria. While certain bacteria within the *Actinobacteriota* phylum may be present in the oral cavity, their direct association with dental caries is not as prominent as that of other bacteria like mutans streptococci (from the *Firmicutes* phylum) (Qudeimat et al., 2021). Brackets can make oral hygiene more challenging, leading to changes in the microbial community. The reduction in *Actinobacteriota* might reflect an imbalance in the oral microbiome due to these changes.

At the family level, higher levels of *Flavobacteriaceae*, *Prevotellaceae*, and *Saccharimonadaceae* were observed in Group B. *Flavobacteriaceae* specific role in oral health is less clear. *Prevotellaceae* is commonly found in the human oral cavity and gut. They are anaerobic and are known to play a role in the breakdown of proteins and carbohydrates. Increased levels of *Prevotellaceae* in the oral microbiome are often associated with periodontal disease (Tian et al., 2021). The alteration in the microbiome composition, particularly the increase in families associated with periodontal pathogens, underscores the importance of enhanced oral hygiene practices for patients with fixed braces. In Group C, because the absence of orthodontic appliances, the natural balance of the oral microbiome, including *Actinobacteriota*, is expected to be maintained.

Within Group AT, elevated levels of the family *Burkholderiaceae* were observed. *Burkholderiaceae* is not commonly associated with the oral cavity (Kerber-Diaz et al., 2022). However, advancements in microbial sequencing have started to reveal a more diverse array of bacteria in dental plaque than previously recognized. Their presence in dental plaque might also indicate a broader diversity in the oral microbiome than traditionally understood. Insights into lesser-known bacterial families in the oral cavity could lead to the development of targeted therapeutic strategies for managing oral health.

Longitudinal studies have identified biofilm maturation and caries lesion progression with an increase in Gram-negative anaerobes, including *Veillonella* and *Prevotella* (da Costa Rosa et al., 2021). Our observation that higher levels of *Prevotella* and *Prevotella_7* were observed at the genus level in Group B suggests a significant shift in the oral microbial community among those wearing fixed orthodontic appliances. These changes in the oral environment can create

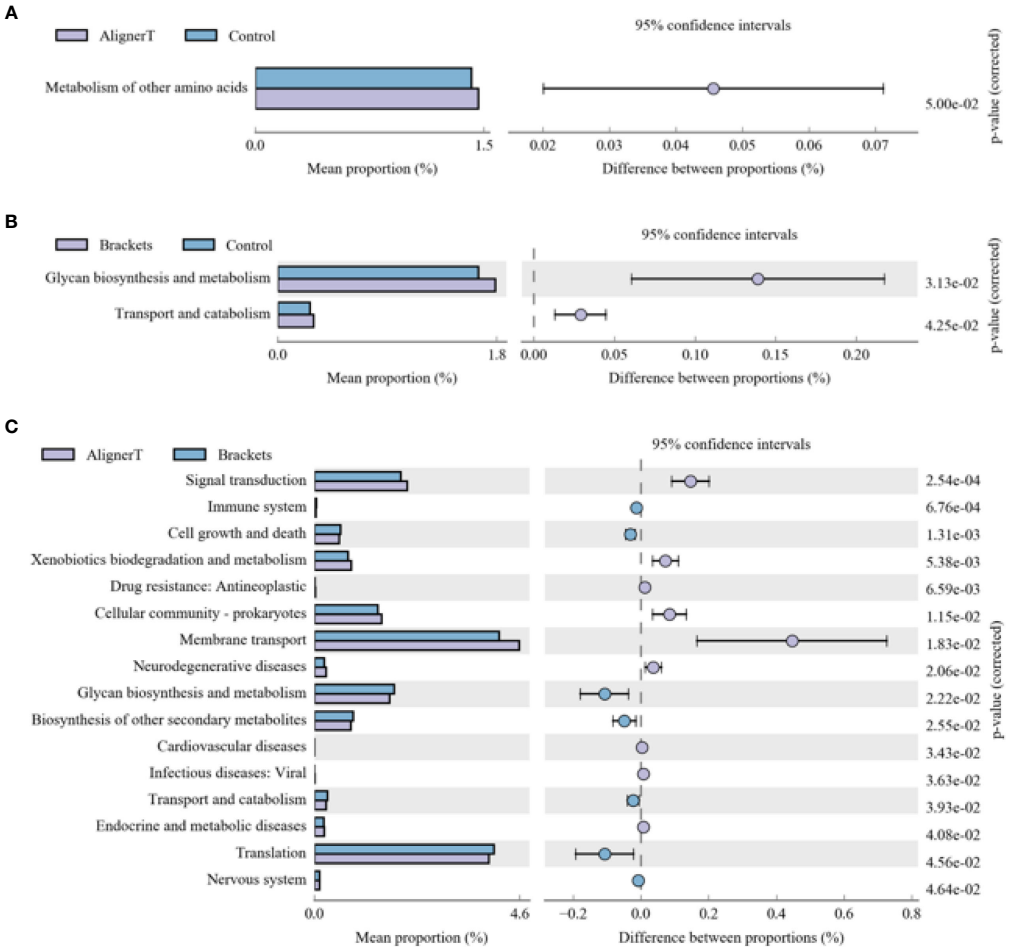

FIGURE 10
KEGG analysis results for the three groups **(A)** Group AT compared with Group C. **(B)** Group B compared with Group C. **(C)** Group AT compared with Group B.

conditions that favor the growth of *Prevotella* species, as they thrive in anaerobic conditions and can utilize the nutrients available in the accumulated dental plaque. An increase in *Prevotella* levels might indicate a higher risk of periodontal disease or caries development (Sharma et al., 2022), making it important for individuals with fixed braces to maintain rigorous oral hygiene and have regular dental check-ups. *Streptococcus, Lactobacillales*, and *Neisseria* cinerea were also noted. This aligns with another study that found Neisseria mucosa had higher levels at sites with orthodontic bands either at (OBM) or below the gingival margin (OBSM) (Kim et al., 2010). The significant increase in *Lautropia* in Group AT suggests that the use of the clear aligners creates an oral environment that favors the growth or proliferation of *Lautropia.* While *Lautropia* is not typically associated with oral diseases (Keijser et al., 2018), its increased prevalence could indicate changes in the oral ecosystem that might have implications for oral health, although these would likely be benign. *Saccharimonadaceae* falls within the realm of bacterial taxonomy. It's part of a more extensive classification that includes various bacteria with differing characteristics and roles. While some families like *Streptococcaceae* and *Actinobacteriota* are well-known for their roles in oral health and disease, the role of *Saccharimonadaceae* in dental plaque might be less clear (Tian et al., 2022). The next-generation sequencing allowed us to

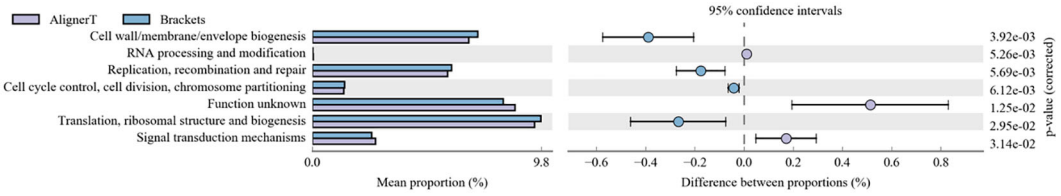

FIGURE 11
Cluster of Orthologus Groups of proteins (COG).

uncover of this previously underexplored microbial resident in the supragingival plaque. Its role in oral health still needs to be further explored.

Changes in polysaccharide biosynthesis, metabolism, and transport suggest a shift in how bacteria process and utilize carbohydrates. This could be due to altered food retention around the brackets, changes in saliva flow, or variations in the oral microbiome composition.

Microecological alterations in the oral environment can lead to detrimental changes in the composition or metabolic activity of the oral microbiome (Nascimento et al., 2019). The specific mention of differences in amino acid metabolism indicates that the bacteria present in Group AT might be processing amino acids differently compared to the normal oral microbiome. This could be due to changes in pH, oxygen levels, or nutrient availability caused by the aligners.

The oral microbiome can modulate the immune response (Hou et al., 2022). A balanced microbiome supports immune function, while dysbiosis (microbial imbalance) can trigger inflammatory responses, potentially leading to systemic effects. Research has suggested connections between oral health and cardiovascular diseases (Carasol et al., 2023). For example, periodontal disease has been associated with an increased risk of heart disease (Priyamvara et al., 2020). The oral microbiome can influence the body's resistance to or susceptibility to viral infections. A healthy microbiome can act as a barrier to infection, while an imbalanced one might increase vulnerability (Di Stefano et al., 2022). It highlights the need for a holistic approach in orthodontics, considering not just dental outcomes but also broader health implications.

These findings highlight the need to understand how orthodontic treatments influence the oral microbial ecosystem. This knowledge can guide dental professionals in recommending appropriate oral hygiene practices for patients with braces or aligners. It also contributes to the development of materials and designs that minimize adverse effects on the oral microbiome.

A notable limitation of this study is its sole focus on adult female patients. This specific demographic inclusion restricts the applicability of the results to a more diverse patient population, potentially affecting the generalizability of the findings.

Limitation

One notable limitation of our study is the exclusion of male subjects, potentially impacting the generalizability of our findings.

Conclusion

The observation points to the impact of orthodontic appliance on the oral microbial community, highlighting the difference between traditional braces (Group B) and clear aligners (Group AT) in terms of the predominance of anaerobic and gram negative bacteria. This emphasizes the importance of considering the microbiological effects when choosing orthodontic appliance and underscores the need for tailored oral hygiene practices for individuals undergoing these treatments. This research might provide insights that could assist in the development of innovative cleaning techniques and antibacterial materials.

Data availability statement

The datasets presented in this study can be found in online repositories. The names of the repository/repositories and accession number(s) can be found below: NCBI, under BioProject PRJNA1064555 (http://www.ncbi.nlm.nih.gov/bioproject/1064555).

Ethics statement

The studies involving humans were approved by Ethics Committee of Peking University Health Science Center (PKUSSIRB-202054050). The studies were conducted in accordance with the local legislation and institutional requirements. The participants provided their written informed consent to participate in this study.

Author contributions

JJ: Investigation, Writing – review & editing, Supervision, Resources. XW: Writing – review & editing, Supervision, Validation. TZ: Writing – review & editing, Methodology, Supervision, Software. JZ: Writing – original draft, Software, Formal analysis, Data curation. JW: Writing – review & editing, Writing – original draft, Supervision, Resources, Project administration, Funding acquisition, Conceptualization.

Funding

The author(s) declare financial support was received for the research, authorship, and/or publication of this article. This research was supported by Beijing Natural Science Foundation (7214274), Program for New Clinical Techniques and Therapies of Peking University School and Hospital of Stomatology (PKUSSNCT-13A11) and Program for New Clinical Techniques and Therapies of Peking University School and Hospital of Stomatology First Clinical Division (YMZXJ-2009).

Conflict of interest

The authors declare that the research was conducted in the absence of any commercial or financial relationships that could be construed as a potential conflict of interest.

Publisher's note

References

Abbate, G. M., Caria, M. P., Montanari, P., Mannu, C., Orru, G., Caprioglio, A., et al. (2015). Periodontal health in teenagers treated with removable aligners and fixed orthodontic appliances. *J. Orofac Orthop* 76, 240–250. doi: 10.1007/s00056-015-0285-5

Abranches, J., Zeng, L., Kajfasz, J. K., Palmer, S. R., Chakraborty, B., Wen, Z. T., et al. (2018). Biology of oral streptococci. *Microbiol. Spectr.* 6 (5), 10. doi: 10.1128/microbiolspec.GPP3-0042-2018

Ahn, S. J., Lim, B. S., Lee, Y. K., and Nahm, D. S. (2006). Quantitative determination of adhesion patterns of cariogenic streptococci to various orthodontic adhesives. *Angle Orthod* 76, 869–875. doi: 10.1043/0003-3219(2006)076[0869:QDOAPO]2.0.CO;2

Athanasopoulou, K., Boti, M. A., Adamopoulos, P. G., Skourou, P. C., and Scorilas, A. (2021). Third-generation sequencing: the spearhead towards the radical transformation of modern genomics. *Life (Basel)* 12 (1), 30. doi: 10.3390/life12010030

Azaripour, A., Weusmann, J., Mahmoodi, B., Peppas, D., Gerhold-Ay, A., Van Noorden, C. J., et al. (2015). Braces versus Invisalign(R): gingival parameters and patients' satisfaction during treatment: a cross-sectional study. *BMC Oral. Health* 15, 69. doi: 10.1186/s12903-015-0060-4

Campobasso, A., Lo Muzio, E., Battista, G., Ciavarella, D., Crincoli, V., and Lo Muzio, L. (2021). Taxonomic analysis of oral microbiome during orthodontic treatment. *Int. J. Dent.* 2021, 8275181. doi: 10.1155/2021/8275181

Carasol, M., Munoz Aguilera, E., and Ruilope, L. M. (2023). Oral health, hypertension and cardiovascular diseases. *Hipertens Riesgo Vasc.* 40, 167–170. doi: 10.1016/j.hipert.2023.04.001

da Costa Rosa, T., de Almeida Neves, A., Azcarate-Peril, M. A., Divaris, K., Wu, D., Cho, H., et al. (2021). The bacterial microbiome and metabolome in caries progression and arrest. *J. Oral. Microbiol.* 13, 1886748. doi: 10.1080/20002297.2021.1886748

Di Stefano, M., Polizzi, A., Santonocito, S., Romano, A., Lombardi, T., and Isola, G. (2022). Impact of oral microbiome in periodontal health and periodontitis: A critical review on prevention and treatment. *Int. J. Mol. Sci.* 23 (9), 5142. doi: 10.3390/ijms23095142

Duran-Pinedo, A., Solbiati, J., Teles, F., Teles, R., Zang, Y., and Frias-Lopez, J. (2021). Long-term dynamics of the human oral microbiome during clinical disease progression. *BMC Biol.* 19, 240. doi: 10.1186/s12915-021-01169-z

Homayouni Rad, A., Pourjafar, H., and Mirzakhani, E. (2023). A comprehensive review of the application of probiotics and postbiotics in oral health. *Front. Cell Infect. Microbiol.* 13, 1120995. doi: 10.3389/fcimb.2023.1120995

Hong, B. Y., Driscoll, M., Gratalo, D., Jarvie, T., and Weinstock, G. M. (2024). Improved DNA extraction and amplification strategy for 16S rRNA gene amplicon-based microbiome studies. *Int. J. Mol. Sci.* 25 (5), 2966. doi: 10.3390/ijms25052966

Hou, K., Wu, Z. X., Chen, X. Y., Wang, J. Q., Zhang, D., Xiao, C., et al. (2022). Microbiota in health and diseases. *Signal Transduct Target Ther.* 7, 135. doi: 10.1038/s41392-022-00974-4

Jakubovics, N. S. (2015). Saliva as the sole nutritional source in the development of multispecies communities in dental plaque. *Microbiol. Spectr.* 3. doi: 10.1128/microbiolspec.MBP-0013-2014

Jiang, Q., Li, J., Mei, L., Du, J., Levrini, L., Abbate, G. M., et al. (2018). Periodontal health during orthodontic treatment with clear aligners and fixed appliances: A meta-analysis. *J. Am. Dent. Assoc.* 149, 712–20 e12. doi: 10.1016/j.adaj.2018.04.010

Keijser, B. J. F., van den Broek, T. J., Slot, D. E., van Twillert, L., Kool, J., Thabuis, C., et al. (2018). The impact of maltitol-sweetened chewing gum on the dental plaque biofilm microbiota composition. *Front. Microbiol.* 9, 381. doi: 10.3389/fmicb.2018.00381

Kerber-Diaz, J. C., Leos-Ramirez, M. A., Flores-Ceron, A. A., Ponce-Mendoza, A., Estrada-de Los Santos, P., and Ibarra, J. A. (2022). Distribution of CRISPR-Cas systems in the Burkholderiaceae family and its biological implications. *Arch. Microbiol.* 204, 703. doi: 10.1007/s00203-022-03312-y

Kim, K., Heimisdottir, K., Gebauer, U., and Persson, G. R. (2010). Clinical and microbiological findings at sites treated with orthodontic fixed appliances in adolescents. *Am. J. Orthod Dentofacial Orthop* 137, 223–228. doi: 10.1016/j.ajodo.2008.03.027

Kitamoto, S., Nagao-Kitamoto, H., Hein, R., Schmidt, T. M., and Kamada, N. (2020). The bacterial connection between the oral cavity and the gut diseases. *J. Dent. Res.* 99, 1021–1029. doi: 10.1177/0022034520924633

Lu, H., Tang, H., Zhou, T., and Kang, N. (2018). Assessment of the periodontal health status in patients undergoing orthodontic treatment with fixed appliances and Invisalign system: A meta-analysis. *Med. (Baltimore)* 97, e0248. doi: 10.1097/MD.0000000000010248

Lucchese, A., Nocini, R., Tacchino, U., Ghislanzoni, L. H., Bertossi, D., Ricciardi, G., et al. (2020). Invisalign appliance: aesthetic and efficiency. *Minerva Stomatol* 69, 329–334. doi: 10.23736/S0026-4970.20.04128-X

Nascimento, M. M., Alvarez, A. J., Huang, X., Browngardt, C., Jenkins, R., Sinhoreti, M. C., et al. (2019). Metabolic profile of supragingival plaque exposed to arginine and fluoride. *J. Dent. Res.* 98, 1245–1252. doi: 10.1177/0022034519869906

Perkowski, K., Baltaza, W., Conn, D. B., Marczynska-Stolarek, M., and Chomicz, L. (2019). Examination of oral biofilm microbiota in patients using fixed orthodontic appliances in order to prevent risk factors for health complications. *Ann. Agric. Environ. Med.* 26, 231–235. doi: 10.26444/aaem/105797

Priyamvara, A., Dey, A. K., Bandyopadhyay, D., Katikineni, V., Zaghlol, R., Basyal, B., et al. (2020). Periodontal inflammation and the risk of cardiovascular disease. *Curr. Atheroscler Rep.* 22, 28. doi: 10.1007/s11883-020-00848-6

Qudeimat, M. A., Alyahya, A., Karched, M., Behbehani, J., and Salako, N. O. (2021). Dental plaque microbiota profiles of children with caries-free and caries-active dentition. *J. Dent.* 104, 103539. doi: 10.1016/j.jdent.2020.103539

Sharma, G., Garg, N., Hasan, S., and Shirodkar, S. (2022). Prevotella: An insight into its characteristics and associated virulence factors. *Microb. Pathog.* 169, 105673. doi: 10.1016/j.micpath.2022.105673

Sun, F., Ahmed, A., Wang, L., Dong, M., and Niu, W. (2018). Comparison of oral microbiota in orthodontic patients and healthy individuals. *Microb. Pathog.* 123, 473–477. doi: 10.1016/j.micpath.2018.08.011

Tian, Y., Sun, L., Qu, H., Yang, Y., and Chen, F. (2021). Removal of nonimpacted third molars alters the periodontal condition of their neighbors clinically, immunologically, and microbiologically. *Int. J. Oral. Sci.* 13, 5. doi: 10.1038/s41368-020-00108-y

Tian, J., Utter, D. R., Cen, L., Dong, P. T., Shi, W., Bor, B., et al. (2022). Acquisition of the arginine deiminase system benefits epiparasitic Saccharibacteria and their host bacteria in a mammalian niche environment. *Proc. Natl. Acad. Sci. U.S.A.* 119. doi: 10.1073/pnas.2114909119

Wang, Q., Ma, J. B., Wang, B., Zhang, X., Yin, Y. L., and Bai, H. (2019). Alterations of the oral microbiome in patients treated with the Invisalign system or with fixed appliances. *Am. J. Orthod Dentofacial Orthop* 156, 633–640. doi: 10.1016/j.ajodo.2018.11.017

Yan, D., Liu, Y., Che, X., Mi, S., Jiao, Y., Guo, L., et al. (2021). Changes in the microbiome of the inner surface of clear aligners after different usage periods. *Curr. Microbiol.* 78, 566–575. doi: 10.1007/s00284-020-02308-5

Zhao, R., Huang, R., Long, H., Li, Y., Gao, M., and Lai, W. (2020). The dynamics of the oral microbiome and oral health among patients receiving clear aligner orthodontic treatment. *Oral. Dis.* 26, 473–483. doi: 10.1111/odi.13175

frontiers | Frontiers in Cellular and Infection Microbiology

TYPE Original Research
PUBLISHED 16 May 2024
DOI 10.3389/fcimb.2024.1395267

OPEN ACCESS

EDITED BY
Gang Ye,
Sichuan Agricultural University, China

REVIEWED BY
Mei-Xue Dong,
Renmin Hospital of Wuhan University, China
Feng Wang,
Xinxiang Medical University, China
Lei Dong,
Southeast University, China, in collaboration with reviewer FW

*CORRESPONDENCE
Lingling Yang
linglingyang@gzucm.edu.cn
Yan Li
janeliyan2002@163.com

†These authors have contributed equally to this work and share first authorship

RECEIVED 03 March 2024
ACCEPTED 26 April 2024
PUBLISHED 16 May 2024

CITATION
Zeng H, Xu J, Zheng L, Zhan Z, Fang Z, Li Y, Zhao C, Xiao R, Zheng Z, Li Y and Yang L (2024) Traditional Chinese herbal formulas modulate gut microbiome and improve insomnia in patients with distinct syndrome types: insights from an interventional clinical study. *Front. Cell. Infect. Microbiol.* 14:1395267. doi: 10.3389/fcimb.2024.1395267

Traditional Chinese herbal formulas modulate gut microbiome and improve insomnia in patients with distinct syndrome types: insights from an interventional clinical study

Huimei Zeng[1†], Jia Xu[2†], Liming Zheng[1], Zhi Zhan[1], Zenan Fang[1], Yunxi Li[1], Chunyi Zhao[3], Rong Xiao[4], Zhuanfang Zheng[5], Yan Li[1*] and Lingling Yang[1*]

[1]Guangdong Provincial Hospital of Chinese Medicine, Guangdong Provincial Academy of Chinese Medical Sciences, and The Second Clinical College, Guangzhou University of Chinese Medicine, Guangzhou, China, [2]Singapore Institute for Clinical Sciences, Agency for Science, Technology and Research, Singapore, Singapore, [3]The Second Clinical Medical College, Guangzhou University of Traditional Chinese Medicine, Guangzhou, China, [4]Department of Rehabilitation, The Eighth People's Hospital of Hefei, Hefei, China, [5]Teaching and research Center, Guangdong Provincial Trade Union Cadre School, Guangzhou, China

Background: Traditional Chinese medicine (TCM) comprising herbal formulas has been used for millennia to treat various diseases, such as insomnia, based on distinct syndrome types. Although TCM has been proposed to be effective in insomnia through gut microbiota modulation in animal models, human studies remain limited. Therefore, this study employs machine learning and integrative network techniques to elucidate the role of the gut microbiome in the efficacies of two TCM formulas — center-supplementing and qi-boosting decoction (CSQBD) and spleen-tonifying and yin heat-clearing decoction (STYHCD) — in treating insomnia patients diagnosed with spleen qi deficiency and spleen qi deficiency with stomach heat.

Methods: Sixty-three insomnia patients with these two specific TCM syndromes were enrolled and treated with CSQBD or STYHCD for 4 weeks. Sleep quality was assessed using the Pittsburgh Sleep Quality Index (PSQI) and Insomnia Severity Index (ISI) every 2 weeks. In addition, variations in gut microbiota were evaluated through 16S rRNA gene sequencing. Stress and inflammatory markers were measured pre- and post-treatment.

Results: At baseline, patients exhibiting only spleen qi deficiency showed slightly lesser severe insomnia, lower IFN-α levels, and higher cortisol levels than those with spleen qi deficiency with stomach heat. Both TCM syndromes displayed distinct gut microbiome profiles despite baseline adjustment of PSQI, ISI, and IFN-α scores. The nested stratified 10-fold cross-validated random forest classifier showed that patients with spleen qi deficiency had a higher abundance of *Bifidobacterium longum* than those with spleen qi deficiency with stomach heat, negatively associated with plasma IFN-α concentration. Both CSQBD and STYHCD treatments significantly improved sleep quality within 2

weeks, which lasted throughout the study. Moreover, the gut microbiome and inflammatory markers were significantly altered post-treatment. The longitudinal integrative network analysis revealed interconnections between sleep quality, gut microbes, such as *Phascolarctobacterium* and Ruminococcaceae, and inflammatory markers.

Conclusion: This study reveals distinct microbiome profiles associated with different TCM syndrome types and underscores the link between the gut microbiome and efficacies of Chinese herbal formulas in improving insomnia. These findings deepen our understanding of the gut-brain axis in relation to insomnia and pave the way for precision treatment approaches leveraging TCM herbal remedies.

KEYWORDS

insomnia, traditional Chinese medicine syndrome, herbal formula, gut microbiome, gut-brain axis, longitudinal integrative network

1 Introduction

Insomnia, a condition marked by dissatisfaction with sleep duration, continuity, and quality, is characterized by persistent difficulties in falling asleep or maintaining sleep, coupled with daytime functional impairment (Perlis et al., 2022). As the most common sleep disorder, insomnia is highly prevalent, affecting approximately 30%–50% of the general population (Brownlow et al., 2020). Often present independently or co-occurring with other medical conditions, such as cardiometabolic diseases, or mental health disorders, such as depression or anxiety, insomnia poses a significant risk of the development and exacerbation of these conditions if left untreated (Perlis et al., 2022).

The first-line recommended treatment for insomnia is cognitive behavioral therapy for insomnia, but access to this therapy is often limited due to high costs and variable response rates (Wilson et al., 2010). As a second-line treatment, pharmacotherapy, particularly hypnotics, is frequently prescribed (Madari et al., 2021; Sutton, 2021; Perlis et al., 2022). Despite their relative safety for long-term use, the long-term adverse effects and varying efficacy of hypnotic medications remain a concern (Yue et al., 2023). There is no global consensus on the most effective pharmacological treatment with the best risk-benefit ratio (Perlis et al., 2022). This complexity underscores the necessity to explore different nonpharmacologic and pharmacologic treatments, especially with the emergence of more effective interventions (Yue et al., 2023).

Current understanding of the neurobiological mechanisms underlying insomnia is still evolving. The central system, which controls the sleep-wake cycle, is influenced by signals from peripheral tissues. Recent research has revealed reciprocal connections between the central nervous system, sleep, and the immune system. This relationship implies that while sleep bolsters immune defenses, afferent signals from immune cells also promote sleep. The homeostatic regulation of sleep is influenced by cytokine responses, neuroendocrine and autonomic pathways, and inflammatory peptides, collectively forging a link between sleep and the immune system (Irwin, 2019; Garbarino et al., 2021). Additionally, emerging studies suggest that the microbiota-gut-brain axis plays a regulatory role in sleep behavior, highlighting its potential significance in understanding sleep disorders (Wang et al., 2022). Notably, sleep deprivation can negatively affect gut microbiome function, and alterations in gut microbiota have been observed in sleep disorders (Feng et al., 2023).

Traditional Chinese medicine (TCM) has been used to treat insomnia for over 2000 years, and it continues to gain attention in modern medical practices (Liu et al., 2017). Historical medical books and recent studies have confirmed the efficacy of various TCM formulas and herbs in enhancing sleep (Singh and Zhao, 2017b). TCM treatments are customized based on individual pattern diagnosis or syndrome differentiation, which involves analyzing an individual's symptoms, signs, pulse form, and tongue appearance. Given the diversity of symptoms and signs, multiple TCM pattern diagnoses can exist for the same disease, leading to varied treatment approaches (World Health Organization, 2007). There are different TCM prescriptions for different TCM syndrome types for insomnia (Yeung et al., 2012). Spleen qi deficiency syndrome, including spleen qi deficiency and spleen qi deficiency with heat stagnation, is a prevalent TCM syndrome type in insomnia cases (Singh and Zhao, 2017a). Previous studies have highlighted a significant correlation between spleen inadequacy and imbalances in gut microbiota

Abbreviations: CSQBD, center-supplementing and qi-boosting decoction; STYHCD, spleen-tonifying and yin heat-clearing decoction; PSQI, Pittsburgh sleep quality index; ISI, insomnia ; severity index; ASV, amplicon sequence variants.

(Qiu et al., 2017; Lin et al., 2018). Recent evidence in animal models suggests that TCM can improve sleep quality by regulating gut microbiota (Si et al., 2022a, Si et al., 2022b).

The center-supplementing and qi-boosting decoction (CSQBD) and spleen-tonifying and yin heat-clearing decoction (STYHCD) are two classic TCM formulas recorded in the "Treatise on Spleen and Stomach" by Li Gao of the Jin dynasty (1115–1234). They have been traditionally used to address the imbalances of qi and yin that are often observed in sleep disorders according to TCM principles. Specifically, CSQBD is used to treat spleen qi deficiency, whereas STYHCD addresses spleen qi deficiency with heat stagnation. However, a critical research gap persists, especially in human studies, regarding the association of different spleen qi deficiency syndrome types with distinct gut microbiome profiles. Moreover, the gut microbiome-modulating efficacy of various herbal formulas to treat different TCM syndrome types in insomnia remains largely unexplored.

In addressing the identified research gap, this study endeavors to elucidate the relationship between different TCM syndrome types and their specific gut microbiome profiles in the context of insomnia through a clinical trial. Additionally, it aims to evaluate the role of the gut microbiome in the treatment of insomnia among patients classified by specific TCM syndromes, utilizing two targeted herbal formulas CSQBD and STYHCD. These investigations aim to deepen our understanding of the interplay between the therapeutic efficacy of TCM for insomnia and the microbiota-gut-brain axis, which could provide novel insights to refine the precision of therapeutic interventions for insomnia.

2 Materials and methods

2.1 Study design

This is a two-arm interventional trial involved 63 patients with insomnia. Patients were recruited and divided into two groups based on their TCM syndromes: 28 patients with spleen qi deficiency-associated insomnia received the CSQBD and 35 patients with spleen qi deficiency and stomach heat-associated insomnia were treated with the STYHCD. This study adhered to the principles of the declaration of Helsinki and received approval from the ethics committee of Guangdong Provincial Hospital of Chinese Medicine (ChiCTR-INR-1701110).

Exclusion criteria for the study included individuals with *Diabetes mellitus*, hypertension, cardiovascular diseases (based on clinical history), those on sleep medications, or those who had used antibiotics in the 6 months preceding the study. Additionally, patients whose insomnia was attributed to mental disorders, physical disorders, or medication use were also excluded from the analysis.

The herbal formulas of STYHCD and CSQBD are demonstrated in Supplementary Tables S1 and S2. They were processed into decocting-free granules according to a standard production process (Supplementary Materials) and administered orally with hot water — two bags/dose, twice a day. Both formulas were supervised by Guangdong Provincial Hospital of Chinese Medicine and produced by Jiangyin Tianjiang Pharmaceutical Co., Ltd., ensuring quality control. The major chemical components of these formulas were identified using high performance liquid chromatography-mass spectrometry, with details provided in the Supplementary Methods and Supplementary Figures S1 and S2.

Fecal samples (>500 mg each) were collected at 0, 2, and 4 weeks post-interventions using microlution (Dayun Gene Technology, Shenzhen, China) stool collection tubes containing stool DNA stabilizer. All samples were processed within the temperature range and timeframe suggested by the manufacturer's instruction. Samples were stored at −80°C for subsequent gut microbiome analysis. Plasma samples were collected at the baseline (week 0) and at the end (week 4) of the study to assess stress, inflammatory, and anti-inflammatory makers by ELISA.

2.2 Sleep quality assessment

To evaluate the sleep quality of patients, we employed two well-established measurement methods: the Pittsburgh Sleep Quality Index (PSQI) and Insomnia Severity Index (ISI). The total global PSQI score, which ranges from 0 to 21, is used to quantify sleep quality, with a score >7 indicating poor sleep quality (Buysse et al., 1989). It is a comprehensive assessment that measures seven dimensions of sleep: subjective sleep quality (good or poor), sleep latency (≤15 to >60 min), sleep duration (≥7 to <5 h), sleep efficiency (≥85% to <65% h sleep/h in bed), sleep disturbances (any kind of sleep disturbance ≥1 time/week), and use of sleeping medications (use of sleep medication ≥1 time/week). The ISI was used to assess the severity of both nighttime and daytime insomnia (Morin et al., 2011). The efficacy of the herbal formulas in treating insomnia was evaluated by comparing these scores before 2 and after 4 weeks of the treatment.

2.3 Fecal DNA extraction and 16S rRNA gene sequencing

The genomic DNA samples of the gut microbiota were extracted using the DNeasy PowerSoil Kit (QIAGEN Inc., Netherlands). The amplification of the V3-V4 region of the 16S rRNA gene was carried out using the 341F forward primer (5'-CCTACGGGNGGCWGCAG-3') and the 806R reverse primer (5'-GGACTACHVGGGTATCTAAT-3') with minor modifications (Tong et al., 2018). The purification of PCR amplicons was carried out using Agencourt AMPure beads (Beckman Coulter, Indianapolis, IN), and the quantification of the PCR amplicons was performed using the PicoGreen dsDNA assay kit (Invitrogen, Carlsbad, CA, USA). Subsequently, the quantified amplicons were pooled in equal amounts. Paired-end sequencing of 2×250 bp was conducted using the Illumina MiSeq platform and the MiSeq reagent kit v3 (Illumina, San Diego, CA, USA) at Shanghai Personal Biotechnology Co., Ltd.

2.4 Microbiome data processing and bioinformatics

Most of enrolled patients provided fecal samples at all the three time points, resulting in a total of 136 fecal samples for gut microbiome analysis. Among these, the CSQBD group contributed 26, 26, and 22 samples at 0, 2, and 4 weeks, respectively, whereas the STYHCD group contributed 21, 20, and 21 samples at 0, 2, and 4 weeks, respectively. The initial raw sequencing data was processed using QIIME2 (v2023.2) (Bolyen et al., 2019; Chen et al., 2020; Xu et al., 2020). The amplicon sequence variants (ASV) were obtained with the DADA2 plugin (Friedman and Alm, 2012). The taxonomic classification of all ASV representative sequences was performed using a Naive Bayes classifier trained on the V3-V4 region of the 16S rRNA gene with the SILVA database v138.1 (Quast et al., 2013; Robeson et al., 2021). The phylogenetic tree was constructed using the SEPP method within the fragment-insertion plugin (Matsen et al., 2010; Eddy, 2011; Matsen et al., 2012; Janssen et al., 2018). Following rigorous data processing and quality control procedures, 6,540,042 high-quality reads were retained, averaging 48,089 ± 7,669 reads/sample. A total of 891 features were subsequently utilized for downstream analysis. To mitigate discrepancies in varying sequencing depths among the samples, the ASV abundance table was rarefied to the same sequencing depth of 33,000 for downstream analysis. The diversity plugin in QIIME2 was used for the generation of alpha-diversity indices, beta-diversity distance matrices, and ordination matrices through the core-metrics-phylogenetic method. The differential gut microbiome resulting from both herbal formulas over time was identified by using random forest regressor with q2-sample-classifier (Bokulich et al., 2018) — a nested stratified 10-fold cross-validation approach with 500 decision trees. The seed used by random number generator was 123.

2.5 Statistical analysis

The demographics and baseline characteristics between the two treatment groups were compared using the Mann-Whitney U test for continuous variables and chi-square test for categorical variables. A linear mixed model was applied to assess the longitudinal changes in PSQI, ISI, inflammatory markers, differential microbes, and alpha-diversity indices in both treatment groups. The subject ID was included as a random effect, whereas time was considered as a fixed effect. This analysis was conducted in R (version 4.3.0) using the lmerTest package (Kuznetsova et al., 2017). To compare the longitudinal effects of the two herbal formulas, the same methodology was applied. The interaction between time and treatment was included as the fixed effect to investigate potential differences in treatment responses. Prior to analysis, all data underwent log10 transformation. To explore the longitudinal association between PSQI, ISI, stress or inflammatory markers, and microbes, we used the rmcorr package in R (version 4.3.0) (Bakdash and Marusich, 2017). The association between alpha-diversity indices/microbial species and drug treatments was recognized with MaAsLin2 (Mallick et al., 2021). The Adonis test was performed with the vegan package in R. Additionally, to address multiple comparisons, the Benjamini-Hochberg method was used to correct p-values. To visualize associated networks, Cytoscape v3.9.1 was used, constructing an informative representation of interrelationships revealed by the data.

3 Results

3.1 Insomnia patients with different TCM syndromes harbored different gut microbiome profiles

Of the 63 insomnia patients, 47 patients completed the 4-week treatment period and were included in the data analysis (Figure 1). Demographic and baseline characteristics indicated slightly more severe insomnia in patients with spleen qi deficiency and stomach heat than in patients with only spleen qi deficiency, as indicated by PSQI and ISI scores. However, this difference became statistically insignificant after adjusting for multiple comparisons (Table 1). Patients with spleen qi deficiency and stomach heat syndrome exhibited significantly higher INF-α levels at the baseline than patients with only spleen qi deficiency. Rest of the demographic and baseline characteristics were comparable between the two treatment groups at the baseline.

Regardless of minor differences in the insomnia levels, striking differences in gut microbiome profiles of patients with the two TCM syndromes (P.adj = 0.001, Figure 2A) were observed. This finding was based on the Unweighted UniFrac distance and adjusted for baseline differences in PSQI, ISI, and IFN-α scores using the Adonis test. Besides, patients with only spleen qi deficiency exhibited greater microbial diversity and evenness than patients with spleen qi deficiency and stomach heat (Supplementary Table S3). These findings suggest a correlation between specific TCM syndrome types in insomnia and gut microbiota profiles.

By using random forest classifier, we identified 22 differential microbial species in insomnia patients with different TCM syndromes (Figure 2B). The classification accuracy was 97.8%.

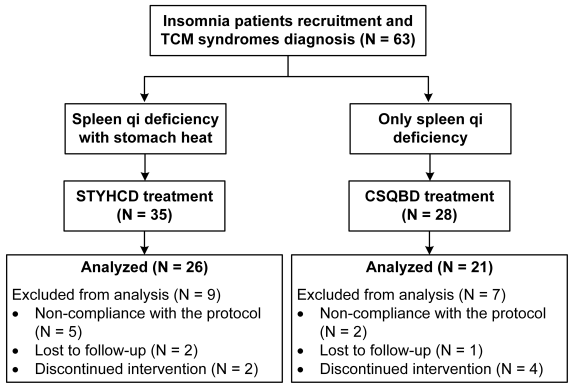

FIGURE 1
Clinical interventional trial flow diagram. STYHCD, spleen-tonifying and yin heat-clearing decoction; CSQBD, center-supplementing and qi-boosting decoction.

10.3389/fcimb.2024.1395267

TABLE 1 Study demographics and baseline characteristics.

Variable		STYHCD (N = 26)	CSQBD (N = 21)	p-value[α]	FDR_BH[β]
Age (year)		36.0 ± 11.3	41.7 ± 11.6	0.1768	0.3789
Gender (N)	Female	18	15	1	1
	Male	8	6		
Education (N)	Below university	12	10	1	1
	University	14	11		
Systolic blood pressure (mmHg)		114.3 ± 13.7	114.5 ± 11.5	0.9896	1
Diastolic blood pressure (mmHg)		70.4 ± 8.2	70.9 ± 7.2	0.6945	0.9470
Heart rate (BPM)		71.9 ± 12.6	76.7 ± 9.7	0.1358	0.3563
PSQI score		13.6 ± 2.4	12.4 ± 2.6	0.0884	0.3315
ISI score		20.6 ± 4.0	17.6 ± 4.8	0.0328	0.2420
Cortisol (ng/mL)		19.3 ± 12.2	29.0 ± 19.7	0.0484	0.2420
IL-1β (pg/mL)		158.3 ± 66.6	185.4 ± 205.9	0.1425	0.3563
IL-6 (pg/mL)		57.2 ± 56.5	50.8 ± 17.4	0.2567	0.4345
TNF-α (pg/mL)		56.7 ± 29.7	65.4 ± 78.9	0.2607	0.4345
TNF-β (pg/mL)		26.5 ± 44.1	41.5 ± 67.3	0.9429	1
IFN-α (pg/mL)		93.0 ± 87.4	36.4 ± 50.2	0.0003	0.0045
IL-10 (pg/mL)		22.1 ± 19.9	14.3 ± 6.8	0.3748	0.5622

The table displayed the number of subjects for each categorical variable — gender and education. The rest of the variables were shown as the mean ± standard deviation.
STYHCD, spleen-tonifying and yin heat-clearing decoction; CSQBD, center-supplementing and qi-boosting decoction.
[α] p-values were obtained with Mann-Whitney U test for continuous variables and chi-square test for categorical variables.
[β]FDR_BH, FDR-corrected p-values were obtained using Benjamini-Hochberg method for adjusting multiple comparisons.

Of these 22 ASVs, 11 species, including *Bifidobacterium longum*, *Bacteroides coprocola*, 2 ASVs of *Bifidobacterium*, 3 ASVs of *Veillonella*, and 1 ASV of *Prevotella*, were more abundant in the patients with only spleen qi deficiency than in patients with spleen qi deficiency and stomach heat. Conversely, 11 variants, including 4 ASVs from the Lachnospiraceae family, 1 ASV of *Eubacterium ruminantium*, *Clostridium butyricum*, *Bacteroides fragilis*, *Succinivibrio*, *Roseburia*, *Bacteroides plebeius*, were less abundant in these patients' gut than in the gut of patients with spleen qi deficiency and stomach heat. A higher abundance of *Bifidobacterium longum* was significantly correlated with lower baseline levels of INF-α in patients with only spleen qi deficiency (FDR_BH < 0.01, Figure 2B). Additionally, the high abundance of other species, such as ASV351-*Bifidobacterium*, ASV32-*Bacteroides coprocola*, and ASV24-*Megamonas*, and the rarity of ASV723-Lachnospiraceae family, ASV96-*Eubacterium ruminantium* group, ASV41-*Bacteroides fragilis*, and ASV76-*Succinivibrio*, showed significant positive correlations with INF-α levels (FDR_BH < 0.05, Figure 2B).

3.2 Insomnia improvement with herbal formula interventions

Following 4 weeks of treatment, both herbal formulas significantly improved PSQI and ISI scores (Figures 3A, B), suggesting consistent longitudinal alleviation of insomnia symptoms. Notably, this improvement was already significant after 2 weeks of treatment and sustained through 4 weeks (Figure 3C). However, the effect sizes of both treatments were more substantial between week 2 and 0 than between week 4 and 0. This pattern may stem from treatment compliance and patient adaptation. Besides, no significant differences in insomnia improvement were observed between the two treatments over time (Figure 3B).

Apart from insomnia measurements, we evaluated the effects of herbal formula interventions on stress and systematic inflammation. At the baseline, insomnia patients exhibiting only spleen qi deficiency displayed elevated cortisol levels — an indication of heightened stress. This elevation, though initially significant, became statistically insignificant after adjustments for multiple comparisons (Table 1). However, CSQBD administration reduced plasma cortisol levels, suggesting its efficacy in mitigating stress in the affected patients. Additionally, after 4-week CSQBD treatment, a marked increase in the levels of anti-inflammatory marker IL-10 along with a reduction in IFN-α levels was observed (Table S4). These findings collectively indicate CSQBD's potential anti-inflammatory and anti-stress effects.

Conversely, patients with combined spleen qi deficiency and stomach heat exhibited significantly higher IFN-α levels than patients with only spleen qi deficiency — a trend that persisted even after FDR correction for multiple tests (Table 1). This pattern

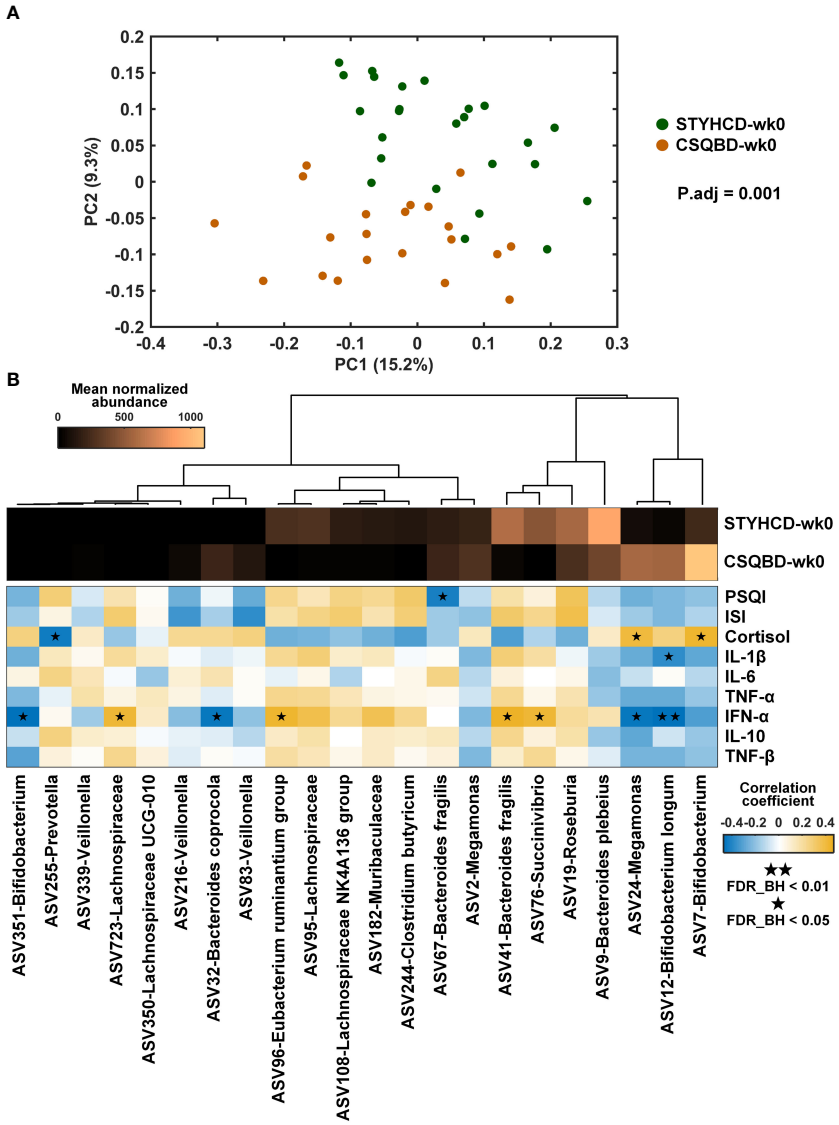

FIGURE 2
Baseline gut microbial profiles in insomnia patients with different TCM syndromes. **(A)** Principal coordinate analysis based on unweighted UniFrac distance. Adjusted P-value (P.adj) was obtained after controlling the baseline scores of PSQI, ISI, and IFN-α using the Adonis test. **(B)** Heatmap of the top 22 differential gut microbial species between the two treatment groups at the baseline and their correlations with clinical measurements. The abundance of each ASV was averaged within each group. Correlation coefficient was obtained with spearman correlation. FDR_BH, FDR-corrected p-value obtained using the Benjamini-Hochberg method to adjust for multiple comparisons. STYHCD, spleen-tonifying and yin heat-clearing decoction; CSQBD, center-supplementing and qi-boosting decoction; ASV, amplicon sequence variant.

underscores a more pronounced inflammatory state in these patients. Four-week STYHCD treatment in these patients resulted in a significant increase in the levels of IL-10. Conversely, the levels of inflammatory markers IL-1β and IL-6 and TNF-α also increased significantly (Table S4), presenting a complex interplay of inflammatory responses post-treatment of STYHCD.

3.3 Impact of herbal formula interventions on gut microbiome

As indicated by unweighted UniFrac PCoA, both CSQBD and STYHCD treatments significantly changed gut microbiome profiles over the intervention period (Figure 4). Similar findings were observed using PCoA of other distance metrics, including Jaccard and Bray-Curtis (Supplementary Figure S3). However, no significant longitudinal effects were detected within each treatment group or between the two treatments in terms of alpha-diversity measures, such as Shannon entropy, Pielou's evenness, and Faith's phylogenetic diversity (Supplementary Table S5).

3.4 Key gut microbial species altered by herbal formulas

Utilizing a nested stratified 10-fold cross-validated random forest regressor, we identified key gut microbial features impacted by each herbal formula treatment over time. Based on the ranking of

10.3389/fcimb.2024.1395267

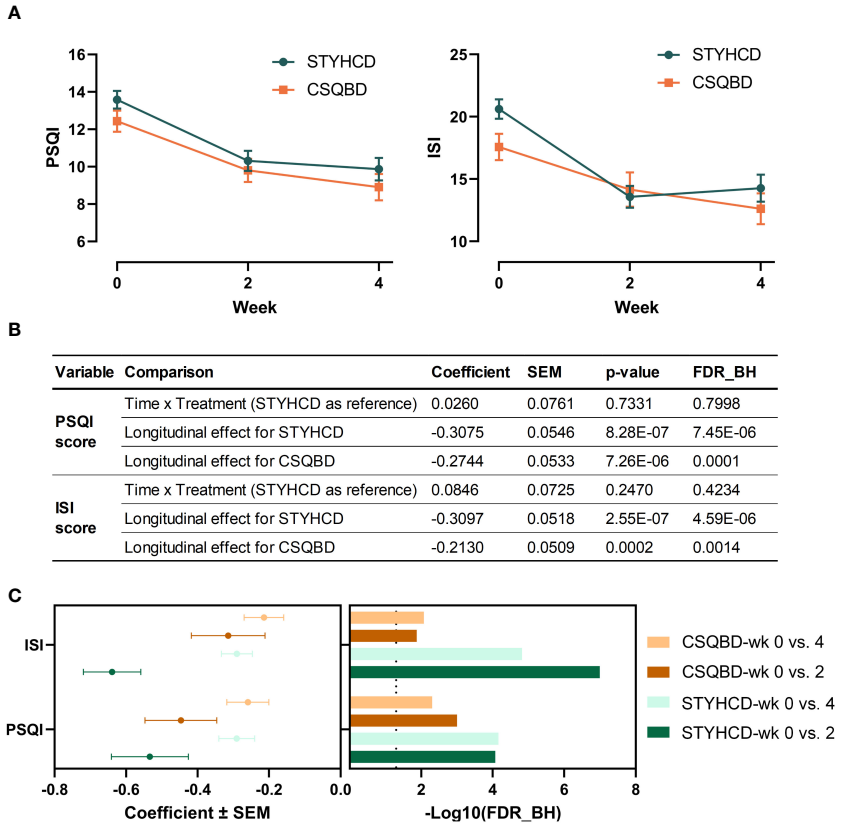

Variable	Comparison	Coefficient	SEM	p-value	FDR_BH
PSQI score	Time x Treatment (STYHCD as reference)	0.0260	0.0761	0.7331	0.7998
	Longitudinal effect for STYHCD	-0.3075	0.0546	8.28E-07	7.45E-06
	Longitudinal effect for CSQBD	-0.2744	0.0533	7.26E-06	0.0001
ISI score	Time x Treatment (STYHCD as reference)	0.0846	0.0725	0.2470	0.4234
	Longitudinal effect for STYHCD	-0.3097	0.0518	2.55E-07	4.59E-06
	Longitudinal effect for CSQBD	-0.2130	0.0509	0.0002	0.0014

FIGURE 3
Both herbal formula interventions significantly improved insomnia. **(A)** Changes in PSQI and ISI scores over time following intervention with two herbal formulas. **(B)** Longitudinal effects on PSQI and ISI scores between two treatments and within each treatment. **(C)** Long-term sustainability of the effectiveness of treatments compared to baseline. FDR_BH, FDR-corrected p-value obtained using the Benjamini-Hochberg method to adjust for multiple comparisons. The vertical dashed line represents the FDR_BH threshold of 0.05. P-values were determined using linear mixed models. PSQI, Pittsburgh Sleep Quality Index; ISI, Insomnia Severity Index; STYHCD, spleen-tonifying and yin heat-clearing decoction; CSQBD, center-supplementing and qi-boosting decoction.

the feature importance of these microbes (Supplementary Figure S4), top 14 and 20 microbial species were identified for further analysis of STYHCD and CSQBD treatments, respectively. Both treatments enriched *Bacteroides coprophilus* (Figure 5).

Among the top 14 microbial species affected by STYHCD (Figure 5A), the abundance of 5 species, namely, ASV134-*Bacteroides coprophilus*, ASV783-*Phascolarctobacterium*, ASV244-*Clostridium butyricum*, ASV68-*Prevotella copri*, and ASV24-*Megamonas*, was enhanced. Conversely, the abundance of 9 species, including 5 species of *Prevotella*, ASV244-*Clostridium butyricum*, ASV2-*Megamonas*, ASV96-*Eubacterium ruminantium* group, and ASV655-*Bacteroides*, was inhibited.

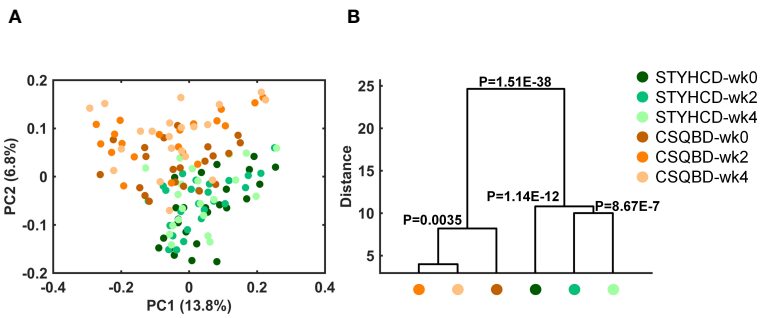

FIGURE 4
Temporal alterations in the gut microbiome of insomnia patients over time after receiving two herbal formula treatments. **(A)** Principal coordinate analysis based on Unweighted UniFrac distance. **(B)** Clustering of gut microbiota based on inter-group distances obtained through MANOVA test using the initial 31 PCs (explained >80% variation) of unweighted UniFrac PCoA. STYHCD, spleen-tonifying and yin heat-clearing decoction; CSQBD, center-supplementing and qi-boosting decoction.

10.3389/fcimb.2024.1395267

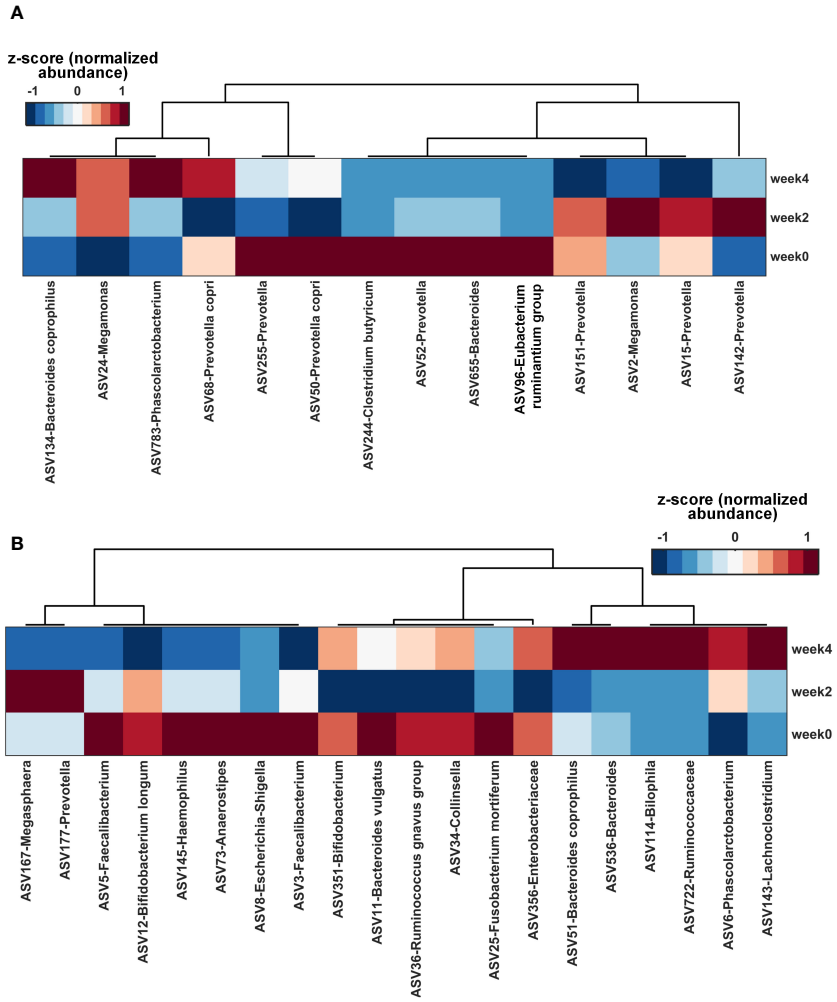

FIGURE 5
Key gut microbial species altered by herbal formula treatments over time. **(A)** Heatmap of the top 14 gut microbial species altered by STYHCD treatment overtime. **(B)** Heatmap of the top 20 gut microbial species altered by CSQBD treatment overtime. STYHCD, spleen-tonifying and yin heat-clearing decoction; CSQBD, center-supplementing and qi-boosting decoction.

Of the top 20 microbial species influenced by CSQBD (Figure 5B), 8 species, including ASV51-*Bacteroides coprophilus*, ASV536-*Bacteroides*, ASV177-*Prevotella*, ASV143-*Lachnoclostridium*, ASV114-*Bilophila*, ASV722-Ruminococcaceae family, ASV34-*Collinsella*, and ASV6-*Phascolarctobacterium*, were enriched. In contrast, 12 species, including ASV167-*Megasphaera*, ASV356-Enterobacteriaceae family, ASV3-*Faecalibacterium*, ASV351-*Bifidobacterium*, ASV145-*Haemophilus*, ASV25-*Fusobacterium mortiferum*, ASV11-*Bacteroides vulgatus*, ASV5-*Faecalibacterium*, ASV12-*Bifidobacterium longum*, ASV73-*Anaerostipes*, ASV8-*Escherichia-Shigella*, and ASV36-*Ruminococcus gnavus* group, were inhibited.

3.5 Longitudinal integrative networks between insomnia improvement, gut microbiome, and systemic inflammation

To explore the comprehensive link between insomnia improvement, modulation of key gut microbial species, and systemic inflammation induced by the herbal formula treatments, we performed longitudinal integrative network analysis (Figure 6). In the patients with spleen qi deficiency and stomach heat (Figure 6A), PSQI and ISI scores were inversely associated with plasma IL-10 levels. ASV783-*Phascolarctobacterium* — enriched by STYHCD treatment — was negatively associated with PSQI and ISI scores, whereas ASV655-*Bacteroides* — inhibited by STYHCD treatment — showed a positive association with PSQI and ISI scores. These findings suggest a link between the change in gut microbiome and improved sleep quality.

In the patients with only spleen qi deficiency (Figure 6B), the stress marker cortisol and ASV34-*Collinsella* — both reduced by CSQBD treatment — showed a positive association with PSQI and ISI scores. The anti-inflammatory marker IL-10 along with ASV114-*Bilophila* and ASV722-Ruminococcaceae family showed negative correlations with PSQI and ISI scores. IL-10 was positively associated with both ASV114-*Bilophila* and ASV722-Ruminococcaceae family. This suggests that CSQBD treatment may bolster the immune system — linked to ASV114-*Bilophila* and ASV722-Ruminococcaceae family

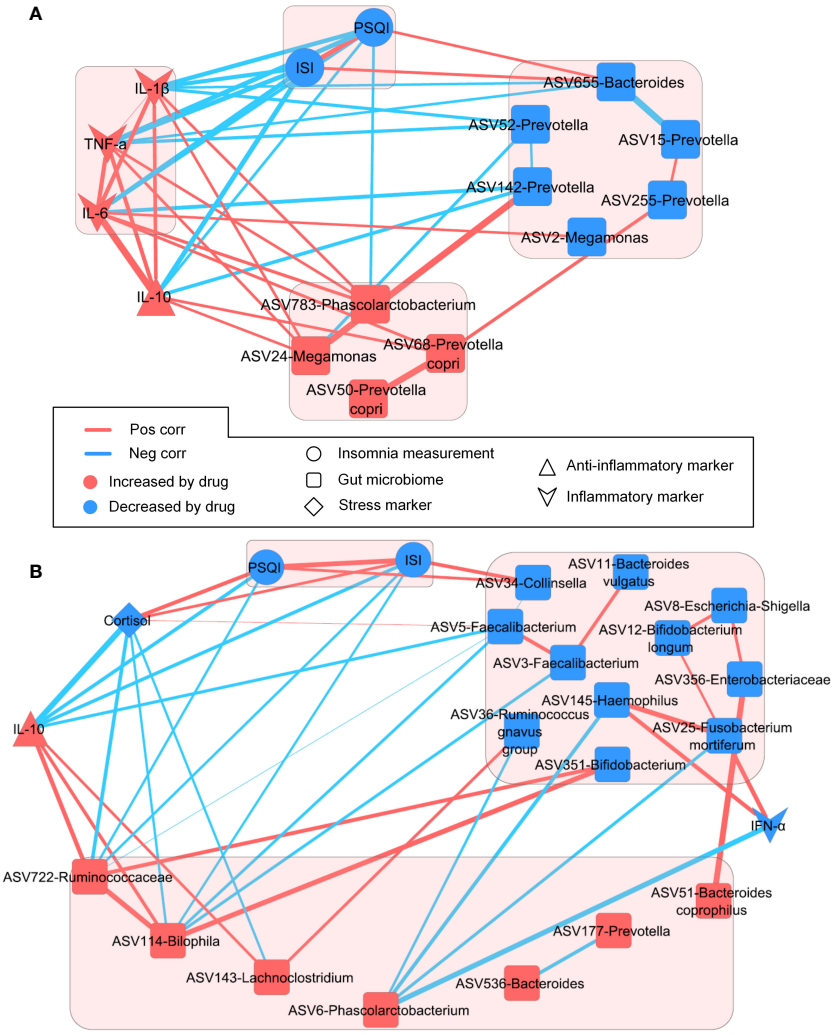

FIGURE 6
Longitudinal networks involved in insomnia improvement, key gut microbial species, and plasma biomarkers. **(A)** Longitudinal integrative network of STYHCD. **(B)** Longitudinal integrative network of CSQBD. STYHCD, spleen-tonifying and yin heat-clearing decoction; CSQBD, center-supplementing and qi-boosting decoction.

enrichment in the gut — and improve sleep quality in patients with spleen qi deficiency.

4 Discussion

Contrary to the uniform treatment approach of Western medicine, TCM tailors therapies to every patient's unique TCM syndrome and diagnosis (Huang et al., 2022; Wu et al., 2022). In this study, we found that distinct TCM syndromes in insomnia patients were mirrored in their gut microbiome composition. The significant microbiome variations observed in patients with spleen qi deficiency and those with spleen qi deficiency coupled with stomach heat underscore the intricate connection between gut microbiota and TCM symptomatology. This association was particularly evident from the differential abundance of specific microbial species, such as *Bifidobacterium longum*. This species showed a notable negative correlation with inflammation markers, such as INF-α. Such gut microbiome distinctions in different TCM syndromes were observed in other conditions, such as intestinal diseases and metabolic syndromes (Zhang et al., 2019; Wang et al., 2020; Shang et al., 2022). Our findings further extend the understanding of insomnia, supporting the biological basis of TCM syndrome differentiation. This insight allows precise treatment selection and medication prescriptions, bridging the TCM theory with precision medicine.

Additionally, our study showed that both CSQBD and STYHCD treatments significantly improved the sleep quality — reflected through PSQI and ISI scores. This finding aligns with TCM's principle of symptom-based treatment and underscores the relevance of personalized approaches in modern medical practice (Janssen et al., 2018; Li et al., 2019). The rapid and sustained improvements in sleep quality highlight the potential efficacy of these herbal formulas. The diminishing effectiveness observed from week 2 to week 4 suggests stabilization in the treatment response — a pattern observed in other herbal intervention studies (Xu et al.,

2015; Tong et al., 2018). The lack of significant differences between the two treatments over time suggests a potential universal mechanism in herbal interventions for insomnia, warranting further investigation.

This study contributes to the growing body of evidence linking gut microbiome alterations to sleep improvement, especially within the context of TCM applications in humans. The significant microbiome changes observed in patients post-treatment provide human data supporting the role of the gut-brain axis in sleep regulation (Sen et al., 2021; Bi et al., 2022; Wang et al., 2022). Our longitudinal integrative network suggests a potential link between specific gut microbes, inflammatory responses, and sleep quality improvement. For example, in insomnia patients with spleen qi deficiency and stomach heat, STYHCD enriched ASV783-*Phascolarctobacterium*, which has been shown to be reduced in patients with obstructive sleep apnea (Szabo et al., 2022). Similarly, CSQBD treatment in the patients exhibiting spleen qi deficiency enriched species, such as ASV114-*Bilophila* and ASV722-Ruminococcaceae, associated with stress and insomnia improvements. The reduction in cortisol levels following CSQBD treatment underscores its potential in stress management — a key factor in insomnia (Zhao et al., 2021; Dressle et al., 2022). Based on our findings, it might be promising to consider the potential beneficial effects of *Phascolarctobacterium* and Ruminococcaceae in the context of insomnia treatment. These bacteria are known as short-chain fatty acids (SCFAs) producers (Wu et al., 2017; Xie et al., 2022). SCFAs, particularly propionate, may influence the gut-brain axis by affecting inflammatory responses, neurotransmitter synthesis, and perhaps even the regulation of stress and circadian rhythms — factors closely linked to the pathophysiology of insomnia (Tahara et al., 2018; Kimura et al., 2020; Cook et al., 2021; Grüter et al., 2023). These findings collectively reinforce the role of TCM in utilizing gut microbiota modulation as a therapeutic pathway for insomnia.

While our study did not directly establish a causative role of the gut microbiome in the effects of TCM formulas on insomnia, it aligns with emerging research suggesting the microbiome's influence on sleep regulation. Notably, a previous study found that depletion of the gut microbiota by antibiotics significantly affects sleep/wake behavior, potentially through disruptions in neurotransmitter balances, such as serotonin, underscoring the microbiome's regulatory capacity on sleep (Ogawa et al., 2020). Additionally, a more recent study proposes a causal link between specific gut microbiotas and insomnia via a Mendelian randomized two-way validation method (Wang et al., 2024). These findings highlight the complexity of the gut-brain axis and its implications for sleep disorders. Given the preliminary nature of these insights and the absence of direct evidence from our study, further investigation into how TCM formulas interact with the gut microbiome to influence sleep is crucial. This includes the need for both animal model studies and clinical trials to elucidate the underlying mechanisms more clearly.

While our study provides valuable insights into precision medicine for insomnia patients with distinct TCM syndromes, it is important to acknowledge its limitations. Future research involving larger clinical trials that include healthy subjects, as well as placebo and positive drug control groups, would facilitate a more comprehensive evaluation of TCM's efficacy in treating insomnia and its link with gut microbiome. Additionally, investigating the molecular mechanisms behind the observed shifts in gut microbiota and sleep quality could unearth deeper insights into how Chinese herbal formulas exert their therapeutic effects on insomnia. Such studies are vital for the seamless integration of traditional herbal formula treatments into modern clinical practices, enhancing the precision of insomnia therapy.

5 Conclusion

This study reveals distinct microbiome profiles associated with different TCM syndromes and underscores the link between the gut microbiome and efficacy of Chinese herbal formulas in improving insomnia. These findings not only enrich our understanding of the gut-brain axis in insomnia but also open new avenues for personalized and holistic insomnia treatments using herbal formulas.

Data availability statement

The sequencing data has been archived to NCBI Sequence Read Archive (BioProject: PRJNA1099612).

Ethics statement

The studies involving humans were approved by Ethnics Committee of Guangdong Provincial Hospital of Chinese Medicine. The studies were conducted in accordance with the local legislation and institutional requirements. The participants provided their written informed consent to participate in this study.

Author contributions

HZ: Formal analysis, Investigation, Methodology, Writing – original draft. JX: Data curation, Formal analysis, Visualization, Writing – original draft, Writing – review & editing. LZ: Supervision, Writing – review & editing. ZZ: Supervision, Writing – review & editing. ZF: Formal analysis, Visualization, Writing – review & editing. YXL: Formal analysis, Visualization, Writing – review & editing. CZ: Formal analysis, Investigation, Writing – review & editing. RX: Formal analysis, Investigation, Writing – review & editing. ZFZ: Investigation, Writing – review & editing. YL: Funding acquisition, Project administration, Writing – review & editing. LY: Funding acquisition, Project administration, Writing – review & editing.

Funding

The author(s) declare financial support was received for the research, authorship, and/or publication of this article. This work

was supported by the Department of Psychology and Sleep Medicine of the Guangdong Provincial Hospital of Traditional Chinese Medicine, and funded by the National Natural Science Foundation of China (Grant Number 82305167) and the Municipality-University Joint Funding Scheme organized by Guangzhou Municipal Science and Technology Bureau (Grant Number 2023A03J0740 and 2023A03J0228).

Conflict of interest

The authors declare that the research was conducted in the absence of any commercial or financial relationships that could be construed as a potential conflict of interest.

Publisher's note

Supplementary material

The Supplementary Material for this article can be found online at: https://www.frontiersin.org/articles/10.3389/fcimb.2024.1395267/full#supplementary-material

References

Bakdash, J. Z., and Marusich, L. R. (2017). Repeated measures correlation. *Front. Psychol.* 8. doi: 10.3389/fpsyg.2017.00456

Bi, C., Guo, S., Hu, S., Chen, J., Ye, M., and Liu, Z. (2022). The microbiota-gut-brain axis and its modulation in the therapy of depression: Comparison of efficacy of conventional drugs and traditional Chinese medicine approaches. *Pharmacol. Res.* 183, 106372. doi: 10.1016/j.phrs.2022.106372

Bokulich, N. A., Dillon, M. R., Bolyen, E., Kaehler, B. D., Huttley, G. A., and Caporaso, J. G. (2018). q2-sample-classifier: machine-learning tools for microbiome classification and regression. *J. Open Res. Softw* 3, 934. doi: 10.21105/joss.00934

Bolyen, E., Rideout, J. R., Dillon, M. R., Bokulich, N. A., Abnet, C. C., Al-Ghalith, G. A., et al. (2019). Reproducible, interactive, scalable and extensible microbiome data science using QIIME 2. *Nat. Biotechnol.* 37, 852–857. doi: 10.1038/s41587-019-0209-9

Brownlow, J. A., Miller, K. E., and Gehrman, P. R. (2020). Insomnia and cognitive performance. *Sleep Med. Clin.* 15, 71–76. doi: 10.1016/j.jsmc.2019.10.002

Buysse, D. J., Reynolds, C. F. 3rd, Monk, T. H., Berman, S. R., and Kupfer, D. J. (1989). The Pittsburgh Sleep Quality Index: a new instrument for psychiatric practice and research. *Psychiatry Res.* 28, 193–213. doi: 10.1016/0165-1781(89)90047-4

Chen, L. W., Xu, J., Soh, S. E., Aris, I. M., Tint, M. T., Gluckman, P. D., et al. (2020). Implication of gut microbiota in the association between infant antibiotic exposure and childhood obesity and adiposity accumulation. *Int. J. Obes. (Lond)* 44, 1508–1520. doi: 10.1038/s41366-020-0572-0

Cook, T. M., Gavini, C. K., Jesse, J., Aubert, G., Gornick, E., Bonomo, R., et al. (2021). Vagal neuron expression of the microbiota-derived metabolite receptor, free fatty acid receptor (FFAR3), is necessary for normal feeding behavior. *Mol. Metab.* 54, 101350. doi: 10.1016/j.molmet.2021.101350

Dressle, R. J., Feige, B., Spiegelhalder, K., Schmucker, C., Benz, F., Mey, N. C., et al. (2022). HPA axis activity in patients with chronic insomnia: A systematic review and meta-analysis of case-control studies. *Sleep Med. Rev.* 62, 101588. doi: 10.1016/j.smrv.2022.101588

Eddy, S. R. (2011). Accelerated profile HMM searches. *PloS Comput. Biol.* 7, e1002195. doi: 10.1371/journal.pcbi.1002195

Feng, W., Yang, Z., Liu, Y., Chen, R., Song, Z., Pan, G., et al. (2023). Gut microbiota: A new target of traditional Chinese medicine for insomnia. *BioMed. Pharmacother.* 160, 114344. doi: 10.1016/j.biopha.2023.114344

Friedman, J., and Alm, E. J. (2012). Inferring correlation networks from genomic survey data. *PloS Comput. Biol.* 8, e1002687. doi: 10.1371/journal.pcbi.1002687

Garbarino, S., Lanteri, P., Bragazzi, N. L., Magnavita, N., and Scoditti, E. (2021). Role of sleep deprivation in immune-related disease risk and outcomes. *Commun. Biol.* 4, 1304. doi: 10.1038/s42003-021-02825-4

Grüter, T., Mohamad, N., Rilke, N., Blusch, A., Sgodzai, M., Demir, S., et al. (2023). Propionate exerts neuroprotective and neuroregenerative effects in the peripheral nervous system. *Proc. Natl. Acad. Sci. U.S.A.* 120, e2216941120. doi: 10.1073/pnas.2216941120

Huang, Z., Miao, J., Chen, J., Zhong, Y., Yang, S., Ma, Y., et al. (2022). A traditional chinese medicine syndrome classification model based on cross-feature generation by convolution neural network: model development and validation. *JMIR Med. Inform* 10, e29290. doi: 10.2196/29290

Irwin, M. R. (2019). Sleep and inflammation: partners in sickness and in health. *Nat. Rev. Immunol.* 19, 702–715. doi: 10.1038/s41577-019-0190-z

Janssen, S., McDonald, D., Gonzalez, A., Navas-Molina, J. A., Jiang, L., Xu, Z. Z., et al. (2018). Phylogenetic placement of exact amplicon sequences improves associations with clinical information. *mSystems* 3. doi: 10.1128/mSystems.00021-18

Kimura, I., Miyamoto, J., Ohue-Kitano, R., Watanabe, K., Yamada, T., Onuki, M., et al. (2020). Maternal gut microbiota in pregnancy influences offspring metabolic phenotype in mice. *Science* 367. doi: 10.1126/science.aaw8429

Kuznetsova, A., Brockhoff, P. B., and Christensen, R. H. B. (2017). lmerTest package: tests in linear mixed effects models. *J. Stat. Software* 82, 1–26. doi: 10.18637/jss.v082.i13

Li, L., Yao, H., Wang, J., Li, Y., and Wang, Q. (2019). The role of chinese medicine in health maintenance and disease prevention: application of constitution theory. *Am. J. Chin. Med.* 47, 495–506. doi: 10.1142/S0192415X19500253

Lin, Z., Ye, W., Zu, X., Xie, H., Li, H., Li, Y., et al. (2018). Integrative metabolic and microbial profiling on patients with Spleen-yang-deficiency syndrome. *Sci. Rep.* 8, 6619. doi: 10.1038/s41598–018-24130–7

Liu, L., Li, C., Yang, Q., Zhang, W., Liu, Y., and Zhu, H. (2017). Clinical and neuroimaging features of a Chinese patient with fatal familial insomnia. *Sleep Med.* 32, 280–281. doi: 10.1016/j.sleep.2016.12.001

Madari, S., Golebiowski, R., Mansukhani, M. P., and Kolla, B. P. (2021). Pharmacological management of insomnia. *Neurotherapeutics* 18, 44–52. doi: 10.1007/s13311-021-01010-z

Mallick, H., Rahnavard, A., McIver, L. J., Ma, S., Zhang, Y., Nguyen, L. H., et al. (2021). Multivariable association discovery in population-scale meta-omics studies. *PloS Comput. Biol.* 17, e1009442. doi: 10.1371/journal.pcbi.1009442

Matsen, F. A., Hoffman, N. G., Gallagher, A., and Stamatakis, A. (2012). A format for phylogenetic placements. *PloS One* 7, e31009. doi: 10.1371/journal.pone.0031009

Matsen, F. A., Kodner, R. B., and Armbrust, E. V. (2010). pplacer: linear time maximum-likelihood and Bayesian phylogenetic placement of sequences onto a fixed reference tree. *BMC Bioinf.* 11, 538. doi: 10.1186/1471-2105-11-538

Morin, C. M., Belleville, G., Bélanger, L., and Ivers, H. (2011). The Insomnia Severity Index: psychometric indicators to detect insomnia cases and evaluate treatment response. *Sleep* 34, 601–608. doi: 10.1093/sleep/34.5.601

Ogawa, Y., Miyoshi, C., Obana, N., Yajima, K., Hotta-Hirashima, N., Ikkyu, A., et al. (2020). Gut microbiota depletion by chronic antibiotic treatment alters the sleep/wake architecture and sleep EEG power spectra in mice. *Sci. Rep.* 10, 19554. doi: 10.1038/s41598–020-76562–9

Perlis, M. L., Posner, D., Riemann, D., Bastien, C. H., Teel, J., and Thase, M. (2022). Insomnia. *Lancet* 400, 1047–1060. doi: 10.1016/S0140-6736(22)00879-0

Qiu, J. J., Liu, Z., Zhao, P., Wang, X. J., Li, Y. C., Sui, H., et al. (2017). Gut microbial diversity analysis using Illumina sequencing for functional dyspepsia with liver depression-spleen deficiency syndrome and the interventional Xiaoyaosan in a rat model. *World J. Gastroenterol.* 23, 810–816. doi: 10.3748/wjg.v23.i5.810

Quast, C., Pruesse, E., Yilmaz, P., Gerken, J., Schweer, T., Yarza, P., et al. (2013). The SILVA ribosomal RNA gene database project: improved data processing and web-based tools. *Nucleic Acids Res.* 41, D590–D596. doi: 10.1093/nar/gks1219

Robeson, M. S.2nd, O'Rourke, D. R., Kaehler, B. D., Ziemski, M., Dillon, M. R., Foster, J. T., et al. (2021). RESCRIPt: Reproducible sequence taxonomy reference database management. *PloS Comput. Biol.* 17, e1009581. doi: 10.1371/journal.pcbi.1009581

Sen, P., Molinero-Perez, A., O'Riordan, K. J., McCafferty, C. P., O'Halloran, K. D., and Cryan, J. F. (2021). Microbiota and sleep: awakening the gut feeling. *Trends Mol. Med.* 27, 935–945. doi: 10.1016/j.molmed.2021.07.004

Shang, H., Zhang, L., Xiao, T., Zhang, L., Ruan, J., Zhang, Q., et al. (2022). Study on the differences of gut microbiota composition between phlegm-dampness syndrome and qi-yin deficiency syndrome in patients with metabolic syndrome. *Front. Endocrinol. (Lausanne)* 13. doi: 10.3389/fendo.2022.1063579

Si, Y., Chen, X., Guo, T., Wei, W., Wang, L., Zhang, F., et al. (2022a). Comprehensive 16S rDNA Sequencing and LC-MS/MS-Based Metabolomics to Investigate Intestinal Flora and Metabolic Profiles of the Serum, Hypothalamus and Hippocampus in p –Chlorophenylalanine-Induced Insomnia Rats Treated with Lilium brownie. *Neurochem. Res.* 47, 574–589. doi: 10.1007/s11064-021-03466-z

Si, Y., Wei, W., Chen, X., Xie, X., Guo, T., Sasaki, Y., et al. (2022b). A comprehensive study on the relieving effect of Lilium brownii on the intestinal flora and metabolic disorder in p-chlorphenylalanine induced insomnia rats. *Pharm. Biol.* 60, 131–143. doi: 10.1080/13880209.2021.2019283

Singh, A., and Zhao, K. (2017a). "Chapter five - treatment of insomnia with traditional chinese herbal medicine," in *International review of neurobiology*. Eds. B. Y. Zeng and K. Zhao (Cambridge, Massachusetts, United States: Academic Press), 97–115. doi: 10.1016/bs.irn.2017.02.006

Singh, A., and Zhao, K. (2017b). Treatment of insomnia with traditional chinese herbal medicine. *Int. Rev. Neurobiol.* 135, 97–115. doi: 10.1016/bs.irn.2017.02.006

Sutton, E. L. (2021). Insomnia. *Ann. Intern. Med.* 174, Itc33–itc48. doi: 10.7326/AITC202103160

Szabo, H., Piroska, M., Hernyes, A., Zoldi, L., Juhasz, J., Ligeti, B., et al. (2022). The relationship between atherosclerosis and gut microbiome in patients with obstructive sleep apnoea. *Appl. Sci.* 12, 11484. doi: 10.3390/app122211484

Tahara, Y., Yamazaki, M., Sukigara, H., Motohashi, H., Sasaki, H., Miyakawa, H., et al. (2018). Gut microbiota-derived short chain fatty acids induce circadian clock entrainment in mouse peripheral tissue. *Sci. Rep.* 8, 1395. doi: 10.1038/s41598–018-19836–7

Tong, X., Xu, J., Lian, F., Yu, X., Zhao, Y., Xu, L., et al. (2018). Structural alteration of gut microbiota during the amelioration of human type 2 diabetes with hyperlipidemia by metformin and a traditional chinese herbal formula: a multicenter, randomized, open label clinical trial. *mBio* 9. doi: 10.1128/mBio.02392-17

Wang, P., Ding, S., Sun, L., Feng, Y., Guo, K., Zhu, Y., et al. (2020). Characteristics and differences of gut microbiota in patients with different Traditional Chinese Medicine Syndromes of Colorectal Cancer and normal population. *J. Cancer* 11, 7357–7367. doi: 10.7150/jca.50318

Wang, Q., Gao, T., Zhang, W., Liu, D., Li, X., Chen, F., et al. (2024). Causal relationship between the gut microbiota and insomnia: a two-sample Mendelian randomization study. *Front. Cell Infect. Microbiol.* 14. doi: 10.3389/fcimb.2024.1279218

Wang, Z., Wang, Z., Lu, T., Chen, W., Yan, W., Yuan, K., et al. (2022). The microbiota-gut-brain axis in sleep disorders. *Sleep Med. Rev.* 65, 101691. doi: 10.1016/j.smrv.2022.101691

Wilson, S. J., Nutt, D. J., Alford, C., Argyropoulos, S. V., Baldwin, D. S., Bateson, A. N., et al. (2010). British Association for Psychopharmacology consensus statement on evidence-based treatment of insomnia, parasomnias and circadian rhythm disorders. *J. Psychopharmacol.* 24, 1577–1601. doi: 10.1177/0269881110379307

World Health Organization (2007). *WHO international standard terminologies on traditional medicine in the western pacific region* (Western Pacific Region: World Health Organization).

Wu, F., Guo, X., Zhang, J., Zhang, M., Ou, Z., and Peng, Y. (2017). Phascolarctobacterium faecium abundant colonization in human gastrointestinal tract. *Exp. Ther. Med.* 14, 3122–3126. doi: 10.3892/etm.2017.4878

Wu, Q., Chen, X., Gan, G., Zhang, Q., Yu, L., Li, C., et al. (2022). Visual analysis and evaluation of clinical research on Traditional Chinese medicine compounds in treating insomnia of Yin deficiency syndrome. *J. Ethnopharmacol* 298, 115669. doi: 10.1016/j.jep.2022.115669

Xie, J., Li, L. F., Dai, T. Y., Qi, X., Wang, Y., Zheng, T. Z., et al. (2022). Short-chain fatty acids produced by ruminococcaceae mediate α-linolenic acid promote intestinal stem cells proliferation. *Mol. Nutr. Food Res.* 66, e2100408. doi: 10.1002/mnfr.202100408

Xu, J., Lawley, B., Wong, G., Otal, A., Chen, L., Ying, T. J., et al. (2020). Ethnic diversity in infant gut microbiota is apparent before the introduction of complementary diets. *Gut Microbes* 11, 1362–1373. doi: 10.1080/19490976.2020.1756150

Xu, J., Lian, F., Zhao, L., Zhao, Y., Chen, X., Zhang, X., et al. (2015). Structural modulation of gut microbiota during alleviation of type 2 diabetes with a Chinese herbal formula. *ISME J.* 9, 552–562. doi: 10.1038/ismej.2014.177

Yeung, W.-F., Chung, K.-F., Poon, M. M.-K., Ho, F. Y.-Y., Zhang, S.-P., Zhang, Z.-J., et al. (2012). Prescription of chinese herbal medicine and selection of acupoints in pattern-based traditional chinese medicine treatment for insomnia: A systematic review. *Evidence-Based Complementary Altern. Med.* 2012, 902578. doi: 10.1155/2012/902578

Yue, J. L., Chang, X. W., Zheng, J. W., Shi, L., Xiang, Y. J., Que, J. Y., et al. (2023). Efficacy and tolerability of pharmacological treatments for insomnia in adults: A systematic review and network meta-analysis. *Sleep Med. Rev.* 68, 101746. doi: 10.1016/j.smrv.2023.101746

Zhang, Y. L., Cai, L. T., Qi, J. Y., Lin, Y. Z., Dai, Y. C., Jiao, N., et al. (2019). Gut microbiota contributes to the distinction between two traditional Chinese medicine syndromes of ulcerative colitis. *World J. Gastroenterol.* 25, 3242–3255. doi: 10.3748/wjg.v25.i25.3242

Zhao, X., Li, J., Ren, X., and Yang, J. (2021). The effect of sleep on the salivary cortisol response to acute stressors: a review and suggestions. *Sleep Med.* 77, 35–44. doi: 10.1016/j.sleep.2020.11.026

Frontiers in
Cellular and Infection Microbiology

Investigates how microorganisms interact with their hosts

Explores bacteria, fungi, parasites, viruses, endosymbionts, prions and all microbial pathogens as well as the microbiota and its effect on health and disease in various hosts.

Discover the latest Research Topics

See more →

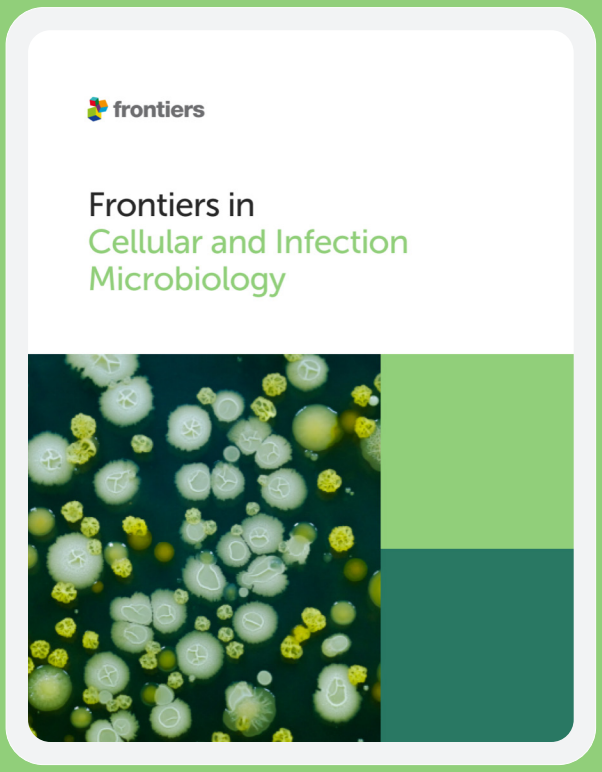

Frontiers

Avenue du Tribunal-Fédéral 34
1005 Lausanne, Switzerland
frontiersin.org

Contact us

+41 (0)21 510 17 00
frontiersin.org/about/contact